

AD-A134372

DTIC

(2)

LJI-LJ-83-252

**LaJolla
INSTITUTE**

P.O. BOX 1434 • LA JOLLA • CALIFORNIA 92038 • PHONE (714) 454-8126

AD A134372

FINAL TECHNICAL REPORT

IDENTIFICATION OF
NEW POTENTIAL SCIENTIFIC AND TECHNOLOGY
AREAS FOR DOD APPLICATION

SUMMARY OF ACTIVITIES
AUGUST 2, 1982 - AUGUST 2, 1983

DTIC
ELECTE
OCT 31 1983
S
B

LA JOLLA INSTITUTE
P. O. Box 1434
La Jolla, CA 92038
(619) 454-3581

CLEARED
FOR OPEN PUBLICATION

OCT 14 1983 3

DIRECTORATE FOR FREEDOM OF INFORMATION
AND SECURITY REVIEW (DASO-PAI)
DEPARTMENT OF DEFENSE

THIS RESEARCH WAS SPONSORED BY THE
DEFENSE ADVANCED RESEARCH PROJECTS
AGENCY UNDER ARPA ORDER NO.: 3710
CONTRACT NO.: MDA-903-82-C-0376

The views and conclusions contained in this document are those of the authors and should not be interpreted as necessarily representing the official policies either express or implied, of the Defense Advanced Research Projects Agency or the United States Government.

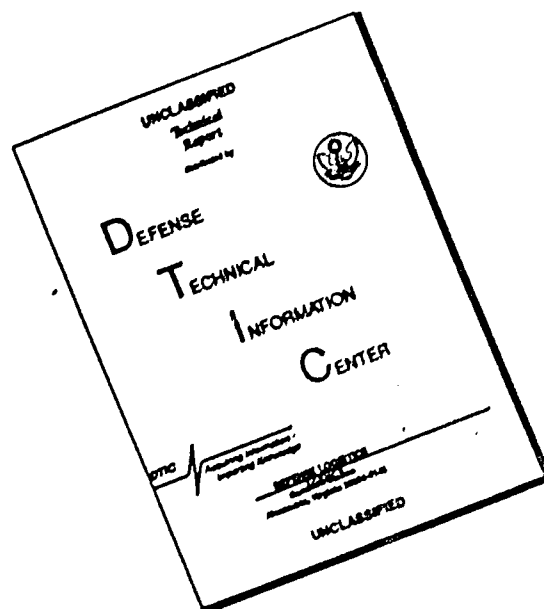
DISTRIBUTION STATEMENT A

Approved for public release
Distribution Unlimited

3611

DTIC FILE COPY

DISCLAIMER NOTICE



THIS DOCUMENT IS BEST QUALITY AVAILABLE. THE COPY FURNISHED TO DTIC CONTAINED A SIGNIFICANT NUMBER OF PAGES WHICH DO NOT REPRODUCE LEGIBLY.

FINAL TECHNICAL REPORT

IDENTIFICATION OF
NEW POTENTIAL SCIENTIFIC AND TECHNOLOGY
AREAS FOR DOD APPLICATION

SUMMARY OF ACTIVITIES
AUGUST 2, 1982 - AUGUST 2, 1983

LA JOLLA INSTITUTE
P. O. Box 1434
La Jolla, CA 92038
(619) 454-3581

THIS RESEARCH WAS SPONSORED BY THE
DEFENSE ADVANCED RESEARCH PROJECTS
AGENCY UNDER ARPA ORDER NO.: 3710
CONTRACT NO.: MDA-903-82-C-0376

The views and conclusions contained in this document are those of the authors and should not be interpreted as necessarily representing the official policies either express or implied, of the Defense Advanced Research Projects Agency or the United States Government.

I. INTRODUCTION

In his statement to the 97th Congress the Director of DARPA gave this motivation for technology search activities as part of the technology base (6.1/6.2) programs:

"With the current emphasis on achieving technological superiority to offset Warsaw Pact weapons and manpower, it is imperative that DOD be cognizant of the military-oriented research and development work that is being conducted by industry and universities that are beyond the purview of DOD. DARPA has, therefore, established a program to aggressively search for and exploit evolving commercial and university research that has military applications. This program, in effect, increases the level of military R&D funding or extends the effect of existing research resources by introducing new and creative ideas into the DOD mainstream--ideas that might have never surfaced without extensive duplicative DOD efforts."

The La Jolla Institute has assisted DARPA in the attainment of the above goal by identifying new scientific and technology areas being pursued at universities that have a potential for DOD applications, and in particular, those that might impact on existing programs or serve as the basis of future programs. This information, prepared by La Jolla Institute staff, Associates, and contacts in universities, is submitted in the form of reviews ("white papers") and presentations. Occasionally such anticipate needs. The latter has been illustrated this year in several respects as outlined below.

One of these, drawing on in-house expertise, discussed matters relevant both to laser propagation in the atmosphere as well as to laser beam clean-up in Raman amplifiers. Another report,



Dist	Avail and/or Special
A-1	

✓
□
□
□
PER
LETTER

requested by the DEO, discussed the status of X-ray laser research and drew attention to some very promising new work done at the University of Illinois at Chicago. The latter work could well serve as the basis of a new program with many defense implications.

With respect to space applications, attention was drawn by the La Jolla Institute to University of California studies on the utilization of the external tanks (ETs) of the space shuttle. The La Jolla Institute pointed out the potential DOD uses of the ETs; DARPA then arranged for a representative to participate in one of the meetings related to ET utilization and helped to support the meeting and follow-on work as well. Deeper study of the military applications of the ET and continuing interaction with the UC group involved were among the recommendations of the DARPA representative.

A briefing for Dr. Cooper, Director of DARPA, on the status of solid-state materials for high-power lasers was organized and presented to him and DARPA staff in May 1983. Contrary to the Soviets, who have a large and continuing effort in this area, the US has had no real program to develop solid-state laser materials since the 1970's. There are now many new solid-state materials suitable for high-power lasers, quite a few of which were first described by Soviet workers. It is possible that a new program will develop in this area as a result of this briefing.

The above touches only on the highlights of this year's program, which is summarized below. Also included are copies of the reports generated.

II. ACTIVITY SUMMARY

1. Utilization of the External Tanks of the Space Shuttle.

Space-based weapon's systems, radar, and E-O surveillance all will require large structures in space. A recent Defense Science Board study¹, in its comments on large structures in space, states:

"There are no DOD programs aimed specifically at this technology outside of adaptive optics."..."In other large structure areas the DOD program is not adequate. There is a need to define a series of demonstrations for future joint NASA/DOD undertaking."..."A key area of concern is the availability of the necessary space transportation capability. A well thought-out plan for the evolution of such structures should be prepared within DOD (six month effort)."

With this in mind, we drew to DARPA's attention some ideas developed by the California Space Institute for NASA relating to first steps towards a low-cost space platform². The concept explored was use in orbit of the external tank (ET) of the shuttle. Currently the ET is ditched with the debris falling into the Indian Ocean. The tanks are very large (50 meters long, 8.4 meters in diameter) structures (mostly aluminum) which additionally contain residual cryogenic liquid oxygen (LOX) and hydrogen (LH₂) after separation from the Space Shuttle. Depending on the mission the amount of residual propellant can be in the range of 10,000-40,000 pounds. Although the ideas on the possible use of the ET arose and

-
1. "Report of the Defense Science Board 1981 Summer Study Panel on Technology Base" (OUSDRE, 1981).
 2. "Workshop on Utilization of the External Tanks of the Space Transportation System" (8-9 March 1982) Unpublished.

were discussed in the context of the NASA and civil applications there are some intriguing potential applications for DOD. A workshop was held at UCSD, August 23-27, 1982 with DARPA representative Dr. Bruno Augenstein in attendance.

The first workshop established that³:

- The ET's can be taken into orbit. Doing so may improve shuttle payload capacity into LEO.
- Provisions must be made to control the ET orbit (either through passive means like tethers, or active means such as using residual propellants) and if desired reenter the ET's in a controlled manner. This is possible at reasonable expense.
- The ET's can serve as strong structures either individually or in groups.
- The ET's can be used as "banks" for orbital energy and momentum and can be used with tethers to assist in inter-orbital transfer with little or no propellant expenditures.
- The ET's should be usable to support observational devices (scientific or military) and provide a very large mass in orbit to use in shielding or eventually to be reworked for other uses in orbit.
- The ET's may have a role in establishing a permanent manned presence in space in several different orbits.

It seems clear that ET's can be modified prelaunch to serve many

3. D. Criswell, Cal. Space Inst., private communication

different functions in space post-launch with minimal (if any) in-space modifications being required.

The second workshop identified several generic problems applicable to large structures in space and manned use thereof:

- 1) EVA is currently limited to about 2 hours limited mostly by physiological considerations. However better suit technology, standardized tools and feedback systems are also required. Apparently NASA views EVA as mostly an emergency operation, but for prolonged or permanent presence in space these problems must be resolved.
- 2) An ET deployed at 500 km will orient itself long-end perpendicular to its trajectory, hence experience drag and decay within a few years. To stabilize it so that it is in a minimum drag configuration the tether concept has been suggested by Columbo.⁴ Further study of the Columbo group's work is required, Draper Labs being an obvious choice. First for the trade-off between deploying at ~500 kilometers with a tether and putting it at ~600 kilometers with no tether, secondly, if stabilization is needed which method looks best, especially in the context of potential DOD requirements. A joint U.S.-Italian experiment is being planned and the group

4. G. Columbo and J. Slowey, "The Use of Tethers for Payload Orbital Transfer", Preprint, Smithsonian Astrophysical Observatory, Sept. 1982.

recommendation will be that NASA consider this for a shuttle flight in the near term.

The military potential of the ET has been summarized by Dr. Augenstein and is included in a document prepared for the Office of Technology Assessment by the California Space Institute⁵. For completeness and ease of reference, the summary viewgraphs of Dr. Augenstein contained therein are reproduced below⁵.

ET: MILITARY APPLICATION POSSIBILITIES

- Need categorization of applications. Examples:
 - By type of application (e.g., war fighting; RECCE; experiment, etc.).
 - By complexity of ET mods, add-ons needed
 - By immediacy of application (Florida, California launch).
 - By added costs (e.g., versus de novo satellite).
 - By DOD needs priority.
 - By classification/compartimentation of proposed applications.
 - By level of new technology needed for implementation.
 - By opportunities presented for exploitation.
 - By possibility for riding on NASA undertakings.

5. "The Process of Space Station Development Using External Tanks" Report by the External Tank Working Group (J.R. Arnold, D.Brin, J.Burke, J.Carroll, D.R.Criswell and S.Nolette) of the California Space Institute of the University of California, Scripps Institution of Oceanography. Report to: Mr. T.F.Rogers, Director of the Space Station Review Project of the Office of Technology Assessment, United States Congress, 11 March 1983.

- By level of on-orbit manned intervention needed.
- First order studies:
 - Develop, flesh-out list of applications.
 - Array applications against categories.
 - Screen candidate applications.
- Reminder:
 - Any ET in orbit can ultimately require some form of controlled disposal.

MILITARY APPLICATIONS OF THE ET

- ET offers:
 - Concealment
 - Pressure capable volume
 - Shielding
 - Bed plate in orbit
 - Momentum
 - Materials, parts
- Military uses of these include:
 - On-orbit asset storage
 - Target proliferation
 - Sensor stage/basing
 - Source of ballistic materials
 - Deep space transport element
- Elaboration of these uses could be a prime defense focus.
- Expansion, elaboration of these uses should be a classified activity parallel to Arnold group work.

MATCH OF ET WITH APPLICATION - EXAMPLE

LAUNCHER NEEDS

- Length
(Minimize launch g's)
- Stiffness
(Minimize guidance of delta-V's)
- Cryogenic cooling
(Superconductor coils)
- High-power needs
(Pulsed power)
- Man-tending
- Low drag orbit
- Environmental control:
attack protection

ET ADAPTABILITY

- Utilize center tunnel
- Rigidity of ET
- HR residual for cooling
- H2-O2 power generation
- ET Habitat
- H2-O2 propulsion to orbit
- ET mass, volume
- attitude control

GENERAL AREAS FOR MILITARY APPLICATIONS OF ETS

- I. GENERIC MISSIONS
 - i.e., broadly applicable applications.
- II. EXPERIMENT BASE
 - e.g., convenient site for experiments running longer than Orbiter mission.
- III. ADJUNCT TO MANNED PRESENCE IN SPACE
 - transition activities between Orbiter and space station.
- IV. OPERATIONS
 - activities supporting forces, other systems.
- V. SPECIAL OPERATIONS
 - operations which we may want to keep specially controlled.
- VI. USE OF ET MATERIALS
 - exploitation of ET for resources in orbit.

POLICY/PROGRAMMATIC ISSUES

- ° ET can appear as low cost prelude/substitute for space station
 - Viewed as a "threat" to space station?
- ° ET uses can ultimately depend on substantial advanced technology
 - Appear as dilution of space station technology effort?
- ° Are ET possibilities sufficiently compelling to proceed independently of space station decisions?
- ° ET military possibilities as independent program:
 - Different/stronger than NASA possibilities?
- ° Military ET interest function of reasonably early uses?
 - Emphasize early payoff efforts in studies, time phase follow-ups.
- ° Decisions to exploit ET possibilities can affect:
 - Image of civil/military shuttle program
 - Broader role of Orbiter in national space program
 - Level of attention of man's role; EVA; space robotics; etc.
- ° In studies, do not underplay policy/programmatic issues.

RECOMMENDATIONS

- ° DOD should pursue studies of ET users.
- ° Study effort should:
 - Focus on development/screening of military applications possible.

- Maintain interactions with Arnold group
- Be conducted under broad access.
- ° Study effort level
 - 5 man years for first year.
 - Continue DOD support for Arnold Group separately.
- ° If studies look promising
 - Consider funding experiment - test plan/program (screened shuttle compatible applications)
 - Consider appropriate broadening of plans for DOD shuttle use.

2. "Bistable Device for Optical Signal Processing", E. Garmire (LJI-R-82-226)

This report discussed a new approach to optical signal processing using a Fabry-Perot resonator with a nonlinear medium to produce a bistable optical device. Emphasis in the report is placed on parallel processing, since these devices have the possibility of processing as many as 10^6 bits in parallel, in nanoseconds. Serial processing is not an application for these devices unless the speed can be increased to 10^8 bits/sec. There is currently a trade-off between speed and required power which causes the psec bistable optical devices to require excessive optical powers and to be impractical. Image processing in an ultra-thin Fabry-Perot with a nonlinear medium was also described as well as parallel processing in a one-dimensional hybrid array. In addition to these devices, the unique nonlinear processing capabilities of the bistable devices were described.

3. "Potential of Very Large Arrays of Semiconductor Laser Sources", E. Garmire (LJI-R-82-217)

The current status of the efficient (approaching 50%) high-power cw and pulsed arrays of semiconductor lasers is summarized and research areas still requiring work identified. Possible application areas include laser designators and communications among others. Another potential application area is the possibility of pumping a YAG laser and frequency doubling its output to get a powerful, efficient, and compact source of $\lambda = 530$ nm radiation.

Applications for semiconductor lasers are expanding rapidly as the importance of opto-electronics increases. These applications extend from optical communications to read-write capability with optical disc data storage to sources for optical image processing. One of the chief limitations to the use of semiconductor lasers in opto-electronics systems is the power emitted by the laser source within a single output beam. It was shown in this report that the output power of semiconductor lasers has some fundamental limitations but that the use of laser arrays can increase the output power within a single beam significantly. Additional advantages of laser arrays are such properties as the possibility of a greater region of linearity, directional tunability, higher efficiency, cooler operating temperatures, and more frequency stability. Also discussed are two regimes of operation of laser arrays, methods of phase-locking the arrays to achieve coherent output, and techniques for output collimation to ensure that the radiation is emitted in a single beam. It is predicted that several watts of output with efficiencies approaching 50% and beam collimations on the order of mrad are obtainable.

4. "The Potential of Using an XeF Laser and Ammonia Raman Cell for Undersea Communication",
P. Hammerling, LJI-R-83-226

This report is related to the Blue-Green Laser submarine communication program. It recalled the advantages of operating at a lower wave-length than the 500 nm obtained using the currently favored XeF laser plus hydrogen Raman cell combination. It is pointed out a wave-length of 460 nm, close to the Jerlov minimum in sea-water, is possible on using an XeF laser plus second Stokes generation in an ammonia Raman cell. This combination has not yet been adequately investigated experimentally but its potential advantage would appear to justify further study.

Some of the outstanding questions are the Raman linewidth of NH_3 , possible photochemical reactions, dimerization, two-photon effects, the influence of trace impurities and whether XeF operating at 351.1 nm can be slightly tuned so that the resulting second Stokes line could be put into exact resonance with the QLORD detector.

5. "Stimulated Phenomena in the High Intensity Laser Interactions: Applications to Raman Amplifiers and Atmospheric Propagation" S. Jorna (LJI-R-83-237).

This report deals with phenomena which can affect both high-power Raman laser amplifiers and the propagation of intense laser radiation in the atmospheres.

The beam quality of an intense laser beam can be affected by various stimulated phenomena in which a property of the medium is changed by the radiation field and in turn changes that field.

Macroscopically the laser-medium coupling changes the dielectric constant through absorption (stimulated thermal Brillouin scattering and stimulated thermal Rayleigh scattering) and through electrostriction (stimulated electrostrictive Brillouin scattering). At sufficiently high irradiances these phenomena can apply to, and hence place limits on usable laser power, Raman amplifiers and laser propagation through the atmosphere.

For pulses which have a duration comparable to the acoustic transit time across the beam, absorption may lead to heating and hence to thermal blooming. As the pulse is shortened thermal blooming is ameliorated and stimulated Brillouin scattering is more likely to affect the beam quality. Stimulated Brillouin scattering may be suppressed in Raman amplifiers by rendering the laser pulse short compared to the vibrational-translational relaxation time of the Raman gas. For hydrogen this relaxation time is $10^{-3}/p$ sec, where p is the gas pressure in atmospheres. Typically, Raman amplifiers using hydrogen operate at 10 atmospheres so that STBS can be largely suppressed by choosing a pulse length much less than 100 μ sec. In this event, SEBS would be expected to dominate.

Their likely significance has been determined from analytic expressions for the steady-state gain of these acousto-optic phenomena. The amplitude equations for the transient phase of instability development have also been solved numerically. Estimates have been obtained for a hydrogen Raman amplifier operating at 10 atmospheres and for the propagation through the atmosphere.

6. May 20, 1983 Briefing to DARPA on

a) "Developing High-Power Solid-State Lasers"
M. Bass

b) "Diode Pumping of Solid-State Lasers", E. Garmire
(LJI-R-83-240)

A briefing organized by LJI was held at DARPA on 20 May for Dr. Cooper, Director, DARPA on "The Status of Solid State Laser Materials". The presentation was by Professor M. Bass of the Center for Laser Studies of the University of Southern California (USC). Following Dr. Bass's briefing, Dr. Elsa Garmire, also of USC, discussed the use of high-power laser diodes as pumps for solid state lasers. The briefing charts and summary are included in the above document.

Developing High Power Solid-State Lasers

Dr. Bass pointed out that apart from private funding for alexandrite laser development there has been no new program in solid-state laser material research in the U.S.A. since the seventies. In contrast there is a strong effort underway in the Soviet Union to study new materials for high-power solid-state lasers. Dr. Bass mentioned some new classes of laser materials and dopings and indicated the broad program required to study and develop such materials for DOD applications. Dr. Bass drew attention to the large Soviet effort directed toward new solid-state laser materials and better variants of existing ones. In the December 1982 Soviet Journal of Quantum Electronics (still untranslated) a group at the Lebedev Institute reported on a variation of the Nd^{3+} laser, a Cr^{3+} - Nd^{3+} gadolinium-scandium-gallium-garnet (GSGG) crystal, reputedly having three

times the slope efficiency of an equivalent Nd:YAG rod. This type of crystal has only just been duplicated in the U. S. and Dr. Bass had an example (loaned by the vendor) of such with him.

The Soviets have also reported at a recent international conference on co-doping with Cr^{3+} in other host crystals besides GS GG, namely gadolinium gallium garnet, lithium gallium garnet, and lanthium-lutetium gallium garnet.

Dr. Cooper asked for an indication of what it might take to put a program together in solid state laser materials. The La Jolla Institute is to coordinate a meeting between Drs. Bass and Garmire, and DARPA staff.

INTEGRATED LASER DIODE ARRAYS FOR PUMPING ND:YAG

Professors M. Bass and E. Garmire have been collaborating on possibilities in waveguide and integrated optics geometries for Nd:YAG lasers. This was inspired by results of Professor Byer at Stanford that slab geometries are better than rod geometries. Indeed, rod geometries were developed because of their compatibility with the geometry of flash-lamps. With the advent of diode-pumped Nd:YAG laser, it is necessary to rethink Nd:YAG geometries. They believe that the waveguide geometry, with transverse diode pumping, holds a great deal of promise in improving the efficiency and reliability, as well as to make Nd:YAG lasers more rugged and compact. Furthermore, the potentialities of integrated optics lasers makes it possible to think of integrated ring lasers or integrated mode-locked lasers.

GaAs laser diode pumping of Nd:YAG lasers is being developed today with discrete laser diodes, packaged in arrays by sandwiching between copper heat sink disks. Diode laser arrays can be fabricated using well-known planar technology. A comparison of the geometry of the integrated array proposed here and the discrete diode arrays currently under development was shown. The integrated laser array replaces the discrete single stripe diode lasers by a mini-array and then utilizes integrated arrays of these mini-arrays rather than a copper-disk sandwich. The advantages of these mini-arrays over single stripe diodes will be outlined below. Packaging these mini-arrays in an integrated array on a single wafer uses planar integrated circuit technology, offering cost saving and efficiency.

Potential advantages of diode mini-arrays over discrete single stripe diodes are:

1. Increased power: A mini-array has been reported in the open literature producing 400 mWatts (cw). This is to be compared to the typically 30 mWatts emitted by the single-stripe discrete diodes. The reason for the higher powers in the mini-arrays is well understood, and occurs because of the ability of the mini-array to control laser filamentation.
2. Longer life: The ability of the mini-arrays to control filamentation in semiconductor lasers ensures the devices will have longer life.

3. Improved efficiency: Design calculations indicate that with simple improvements over devices reported to date, efficiencies as high as 60% may be achieved. This is over twice as high as single stripe discrete diode arrays.
4. Improved wavelength control: Required to optimize pumping of Nd:YAG, all laser wavelengths must be within 3 nm of the absorption frequency. The mini-array technology guarantees this, since all lasers are adjacent on one wafer.
5. Improved power stability: Since the mini-arrays control filamentation, the output from each element has improved stability over single-stripe diodes, offering more stable pumping of Nd:YAG.
6. Reduction in the number of required diodes: Because each mini-array is ten times more powerful than the single-stripe diodes, the same level of pumping can be accomplished with ten times fewer elements, decreasing complexity.

The integrated array technology for packaging the mini-arrays offers a number of advantages over discrete disk packaging:

1. Lower cost. The ability to process the entire linear array on a single wafer makes it possible to use IC fabrication technology.
2. Improved efficiency: The geometry is chosen so that the heat sink is more efficient.

3. Improved reliability: Electrical contact is more reliable with this fabrication technique, and parallel pumping ensures operation even if a few diodes are not working.
4. Possibility of bettering operation: The integrated array technology makes possible parallel pumping of all the diodes, and operation at low voltages, compatible with battery operation. Series operation is also possible with IC technology.
5. Improved stability: Output power and wavelength must be constant, to obtain stable Nd:YAG output. The integrated array geometry increases uniformity in thermal, mechanical and electrical properties, reducing problems with stability.
6. Compatible with advanced Nd:YAG slab and integrated optics geometries.

A university research program is suggested, which is devoted to tailoring the mini-array geometry to optimize efficiency and output power, as well as to develop the integrated array geometry for pumping Nd:YAG. This program will require a dedicated reactor for growth of material appropriate for this application. A three-year effort is anticipated. The payoff would be new diode devices which would provide pumping sources for YAG lasers and could also advanced the state-of-the-art in laser arrays for many other DOD applications.

7. "Recent Laser Studies", Ed. by P. Hammerling
(LJI-LJ-83-249)

i. X-Ray Laser Studies (J. McIver, S. Rockwood,
K. Boyer)

ii. Direct Nuclear Pumped Lasers", M.O.Scully

This report, requested by Dr. L. Marquet of the Directed Energy Office (DEO) at DARPA, gives a critical survey of current laboratory-scale X-ray laser efforts and attempts to parameterize operating regimes. A feature of the report is its research recommendations. The realization of an X-ray laser beam will have very important applications in both the civil and DOD sectors, however its achievement requires overcoming severe technical problems.

The X-Ray laser status and executive summary appears below, the complete document should be consulted for details.

This report presents a broad survey of approaches to X-Ray laser production and laser properties that are relevant to the scaling of X-ray lasers. From this foundation the specific concept of using resonant-line radiation to create an inversion in hydrogenic ions is analyzed in detail. An outline of a research effort on the principal characteristics of the recombination laser is also developed. The conclusions for these specific concepts and required future work are given in (i)-(viii) below. Recommendations (ix) and (x) refer to methods other than resonant-pumping or recombination for producing X-ray or vacuum ultra-violet (VUV) radiation.

(i) To achieve a practical energy per unit volume the laser must operate at as high a density as possible but uniform densities cannot exceed $N = 2 \times 10^{14} z^4$ because of radiation trapping.

(ii) Radiation trapping leads to geometries for the laser medium that are extremely shallow in at least one dimension. This is a major problem that requires innovative structural design for its solution.

(iii) The range of quantum numbers within which the laser may operate is tightly constrained. A lower bound of $p = 3$ is imposed by inversion criteria while an upper bound is set by keeping

$$I - E_p < kT_e$$

to avoid collisional ionization losses from the upper laser level. Also operating efficiency decreases as p^{-3} .

(iv) The maximum efficiency for the radiation-pumped laser is approximately 10^{-6} to 10^{-5} . A major design problem is the inherent inefficiency of the conversion of a broadband light source, such as a plasma, into a narrow emission line for optical pumping.

(v) The recombination-pumped laser, while not analyzed in full detail, shows more promise for efficient operation and scaling than the resonant line radiation-pumped approach. The principal advantages are: (1) better utilization of broad band pump radiation, and (2) a steep density gradient formed in the expanding plasma that facilitates radiative relaxation of the lower laser level.

(vi) Energy level data and line-broadening mechanisms for highly-ionized atoms (over 50 electrons removed) are not known well enough to allow credible laser modeling nor can they be calculated with the present, state-of-the-art codes.

(vii) A laboratory source (or sources) of experimental data for spectroscopy, kinetic rates, and actual X-ray lasing must be established to guide development of the requisite atomic theory and laser models. It is noted that the largest degree of ionization reported to date is 45 times ionized gold obtained with the Helios laser at Los Alamos.

(viii) Amplified spontaneous emission is probably not adequate for practical systems. Beam divergence plays such a strong role in determining the useful range of a laser that investigation of highly nonlinear optical techniques for generating low divergence X-ray sources that might serve for injection of an amplifier should be supported.

(ix) The production of X-rays by other than laser-plasma methods needs consideration, in particular variants of free-electron lasers and other electron-beam plus laser methods need to be looked at in detail.

(x) Multiphotonic Pumping -Very recent work indicates that a new effect in laser-matter interaction may provide an efficient mechanism for multi-photon ionization and pumping. It does not suffer from the defect mentioned in (iv) above and can serve as a source of data required in (viii) above. Although this new area still requires more experimental and theoretical investigation, is considered the one most likely to give both near-and longer-term results with a potential for scaling to larger devices.

8. "Laser Detection of Trace Contaminants in the Atmosphere, J. Wiesenfeld, LJI-LJ-83-251

The above report is related to the problems and methods of detecting complex trace species in the atmosphere, application to CW/BW materials being in mind.

The development of laser-based methods for the detection of trace contaminants in the atmosphere has yielded research tools of great utility. With the introduction of new laser sources, these techniques will become of more general applicability, the eventual goal being the development of a truly "universal" method for routine characterization of trace species. This report includes an assessment of the current state of research in this field as well as a discussion of potential opportunities for further refinement of newly-emerging technologies not yet widely applied to atmospheric measurements.

All methods for atmospheric monitoring of contaminants must contend with the wide variability in such physical characteristics as aerosol content, visibility, and convective activity. While such variability might be of little consequence in certain applications where continuous monitoring is not required, it becomes a matter of intense concern when even intermittent service interruptions are unacceptable. Trace constituents are present even in the pristine atmosphere; when diurnal and meteorological variations in trace composition are convoluted with the potential contamination of this relatively clean environment, the need for high specificity in a monitoring technique is underscored.

An ideal trace contaminant monitor can be imagined as being not only highly selective and sensitive (measurements at or

below the ppm level often being desirable) over a wide dynamic range, but also general in scope and capable of providing a rapid, real-time response when a contaminant is detected. Range and azimuthal information are often of critical importance. Operational simplicity is a must for routine operation.

Of the available techniques for remote detection in the troposphere, Differential Absorption Lidar (DIAL) has been most fully developed. With high sensitivity and ranging capability, this method offers enormous potential for true remote operation. Under ideal conditions, visible/uv probe excitation has enabled the detection of such small molecules as SO_2 , NO_2 , and O_3 . Many other small molecules have been detected in the infrared, although the technique is not so general because intense, continuously tunable infrared sources are not generally available. Further tests of DIAL, especially involving infrared spectroscopy in the fingerprint region, should include evaluation of sensitivity and selectivity under various conditions of atmospheric visibility and aerosol composition. The effectiveness of DIAL in monitoring trace composition in the direction of the sun must also be determined.

Raman spectroscopy was recognized at an early stage in the development of atmospheric sensing methods as having considerable potential for remote characterization of major components and has been successfully applied to the measurement of temperature, etc. Its major limitation is sensitivity, with overlapping weak transitions arising from major constituents overwhelming even strong transitions associated with trace species. No other technique for

laser-based contaminant detection is more general than Raman spectroscopy, excitation at a single frequency being required for full analysis. The utility of Raman spectroscopic methods for atmospheric analysis depends critically upon the required level of detection sensitivity, levels much below 1,000 ppm being relatively difficult to achieve.

Of the local methods, optoacoustic spectroscopy has demonstrated the greatest potential for sensitive detection of trace materials under atmospheric conditions. Because of the exquisite sensitivity of detection afforded by electret microphones, it has proved possible to monitor absorptions as weak as 10^{-7} using routinely available laser sources. The development of broadly tunable laser diode array sources of sub-Doppler width radiation may make optoacoustic spectroscopy even more generally applicable to problems of trace contaminant detection.

Both laser-induced fluorescence (LIF) and photoionization spectroscopies have been employed for wide-ranging laboratory studies of molecular dynamics in the gas phase. LIF has also been applied to the still somewhat controversial detection of ultra-trace quantities of OH radicals in the troposphere. Significant enhancement in selectivity through spectral simplification may be realized by rotationally cooling analytes in supersonic jets prior to analysis. Laser photoionization is of special interest for it is, in principle, capable of detecting single atoms and molecules. Mass selection of photoionized molecules and fragments makes possible what is, in essence, a multidimensional analysis scheme. As is well recognized from mass spectrometry, scrutiny of

fragmentation products makes possible the identification of generic substructure components which cannot be recognized by more standard spectroscopic tools. Thus, laser photoionization spectroscopy seems a highly sensitive especially selective method for trace contaminant detection; its applicability to problems of atmospheric monitoring should be fully explored.

While the feasibility of these various methods for trace analysis have been demonstrated in the laboratory (uniformly) and field (occasionally), relatively little comparative work has been reported. In the near future, trials of these techniques under realistic conditions should be undertaken. Special emphasis should, when appropriate, be placed on ascertaining the reliability of these methods for long-term, uninterrupted analysis. Similarly, increased attention should be paid to refinement pathways, especially with regard to the potential for development of relatively cost-effective integrated packages containing laser sources, detectors, and even perhaps the necessary signal processing electronics. It would be particularly interesting to analyze entire detection systems rather than individual components with a view toward understanding the relative merits of complex remote sensing techniques vs. multiple installations of simpler local field detection methods under the broad range of conditions which would be encountered in a typical application.

9. Miscellaneous Activities

Dr. C. F. Romney (Deputy Director for Research, DARPA) asked us for a technical review of a document. This review was sent to him in letter form at the end of 1982.

We also attended and participated in a DARPA sponsored meeting at SRI International, Washington office, October 25-26, 1982: "DARPA Innovation Search in Electro-Optics" and had consultations at DARPA with Drs. Romney, Mangano, and Reynolds the 27th October 1982.

During this visit Dr. Reynolds (Electronic Science) asked if we could identify any U.S. Groups who would be interested in investigating Langmuir-Blodgett films, a subject mostly pursued in the U. K. Two groups, one at the University of California, San Diego (UCSD) (contact: Professor W. Chang) and another at the University of Southern California (USC) (contact: Professor E. Garmire) indicated interest. By coincidence one of the U.K. scientists involved with this work, Dr. L.M. Walpitta of University College London is spending a year at UCSD. This information was transmitted to Dr. Reynolds by letter in mid-December 1982.

III. REPORTS

BISTABLE OPTICAL DEVICES FOR
OPTICAL SIGNAL PROCESSING

E. GARMIRE*

NOVEMBER 1982

THIS RESEARCH WAS SPONSORED BY
DEFENSE ADVANCED RESEARCH PROJECTS AGENCY
UNDER ARPA ORDER NO.: 3710
CONTRACT NO.: MDA-903-82-C-0376

The views and conclusions contained in this document are those of the authors and should not be interpreted as necessarily representing the official policies, either express or implied, of the Defense Advanced Research Projects Agency of the United States Government.

* Consultant to the La Jolla Institute

TABLE OF CONTENTS

	<u>Page</u>
ABSTRACT	ii
I. INTRODUCTION	1
A. SUMMARY	1
B. OPTICAL PROCESSING WITH BISTABLE DEVICES	3
II. IMAGE PROCESSING WITH BISTABLE DEVICES	10
III. HYBRID ELECTRICAL OPTICAL BISTABLE OPTICAL DEVICES	18

BISTABLE OPTICAL DEVICES FOR
OPTICAL SIGNAL PROCESSING

E. Garmire*

ABSTRACT

In this report, the use of bistable optical devices for optical signal processing is described. Emphasis is placed on parallel processing, since these devices have the possibility of processing as many as 10^6 bits in parallel, in speeds of nanoseconds. Serial processing is not an application for these devices unless the speed can be increased to psec. There is currently a trade-off between speed and required power which causes the psec bistable optical devices to require excessive optical powers and to be impractical.

Image processing in an ultra-thin Fabry-Perot with a nonlinear medium is described, as well as parallel processing in a one-dimensional hybrid array. In addition to these devices, the unique nonlinear processing capabilities of the bistable devices are described (Section I).

* Consultant to the La Jolla Institute

BISTABLE OPTICAL DEVICES FOR OPTICAL SIGNAL PROCESSING

I. INTRODUCTION

A. Summary

The bistable optical device (BOD) is a generic name for a class of nonlinear optical processors which use feedback and optical nonlinearities to achieve a nonlinear transfer curve which may be used to optically process information. The transfer curve (light output as a function of light input) of these devices may be nonlinear, monostable, bistable, multistable, self-pulsing, or chaotic, depending on the characteristics of the system.

Most research to date has emphasized single element bistable devices. However, the bistable optical device shows promise for image processing by using ultra-thin Fabry-Perots as will be described. The ultimate realization of image processing depends on obtaining low power levels for bistability in order to obtain a large number of resolvable spots. Investigations are under way on both new materials and new geometries for use in bistable optical devices with a view toward achieving high speed image processing. We will show that there are image processing and linear array processing geometries for which the bistable optical device holds much promise in optical signal processing.

In this report, we estimate the number of resolvable spots which can be expected from bistable devices which have been demonstrated to date. We show in section II that for image processing, the optimum mode of operation is to use an ultra-thin nonlinear Fabry-Perot. The use of the ultra-thin geometry ensures that diffraction does not blur the pixels. This requires a nonlinear medium (GaAs, InSb, or glass) only 2 μm thick, surrounded by a dielectric reflecting stack. These devices can be fabricated by sputter deposition, a technique well-suited to the needs of the large-area devices desirable for image processing. With this process, a transparent substrate can be used, and all layers, both the dielectric

reflecting stacks and the ultra-thin nonlinear layer, can be deposited. We show that the largest number of bits can be obtained by using InSb at liquid helium temperatures, using a CO laser at 5 μ m. We also show that more convenient operation, although fewer bits, can be obtained using GaAs, or absorbing glass.

In addition to the nonlinear Fabry-Perot, we have studied optical bistability in a hybrid electrical/optical configuration described in section III. This allows the use of the integrated optics format to produce a one-dimensional array of bistable devices for optical signal processing. These hybrid devices require modulators, detectors and amplifiers, all integrated in an array format onto either a combination LiNbO_3 - silicon, or onto GaAs. We will show that, using technology which is available and reported today over 2500 spots in a bistable linear array are possible with hybrid electrical/optical modulation speed which may approach nanoseconds.

E. OPTICAL PROCESSING WITH BISTABLE DEVICES

The classic geometry for the bistable optical device is the nonlinear Fabry-Perot (NLFP) which is shown in Figure 1-1, along with its transmission and transfer curves. An understanding of the nonlinear transfer curve can be obtained in a simple manner from the figure. Consider the device operating at low intensity levels at the point on the transmission curve designated by the arrow. Because of the nonlinear index, an increase in intensity causes a decrease in effective wavelength and a corresponding increase in transmission. The resulting transfer curve shows optical bistability - that is, two possible stable output states for a given input intensity level. In addition to the bistability, the strong nonlinearity of output with respect to input raises the possibility of interesting optical processing methods.

The image processing function of the thin nonlinear Fabry-Perot is shown schematically in Fig. 1-2. If the Fabry-Perot is biased in the nonlinear regime, the weak inputs are only weakly transmitted, while slightly higher inputs are much more strongly transmitted. This represents image enhancement.

The optical processing techniques available with the nonlinear Fabry-Perot are shown in Fig. 1-3. The input is plotted as a function of position going down and the output is plotted as a function of position going left. This particular representation is especially useful to demonstrate the image processing applications of the nonlinear Fabry-Perot. Differential optical gain (Figure 3a) can be used to improve signal-to-noise. This makes possible optical discrimination, background suppression, and contrast enhancement. Optical limiting (Figure 3b), occurs because the flat output of the nonlinear Fabry-Perot as a function of input makes possible level slicing, with clipper action, and saturated output. A multistable Fabry-Perot can be achieved with higher input powers and leads to a digital output for analog input. The level slicing makes possible an optical AND function, shown in Fig. 1-4. For the two additive input signals shown, the

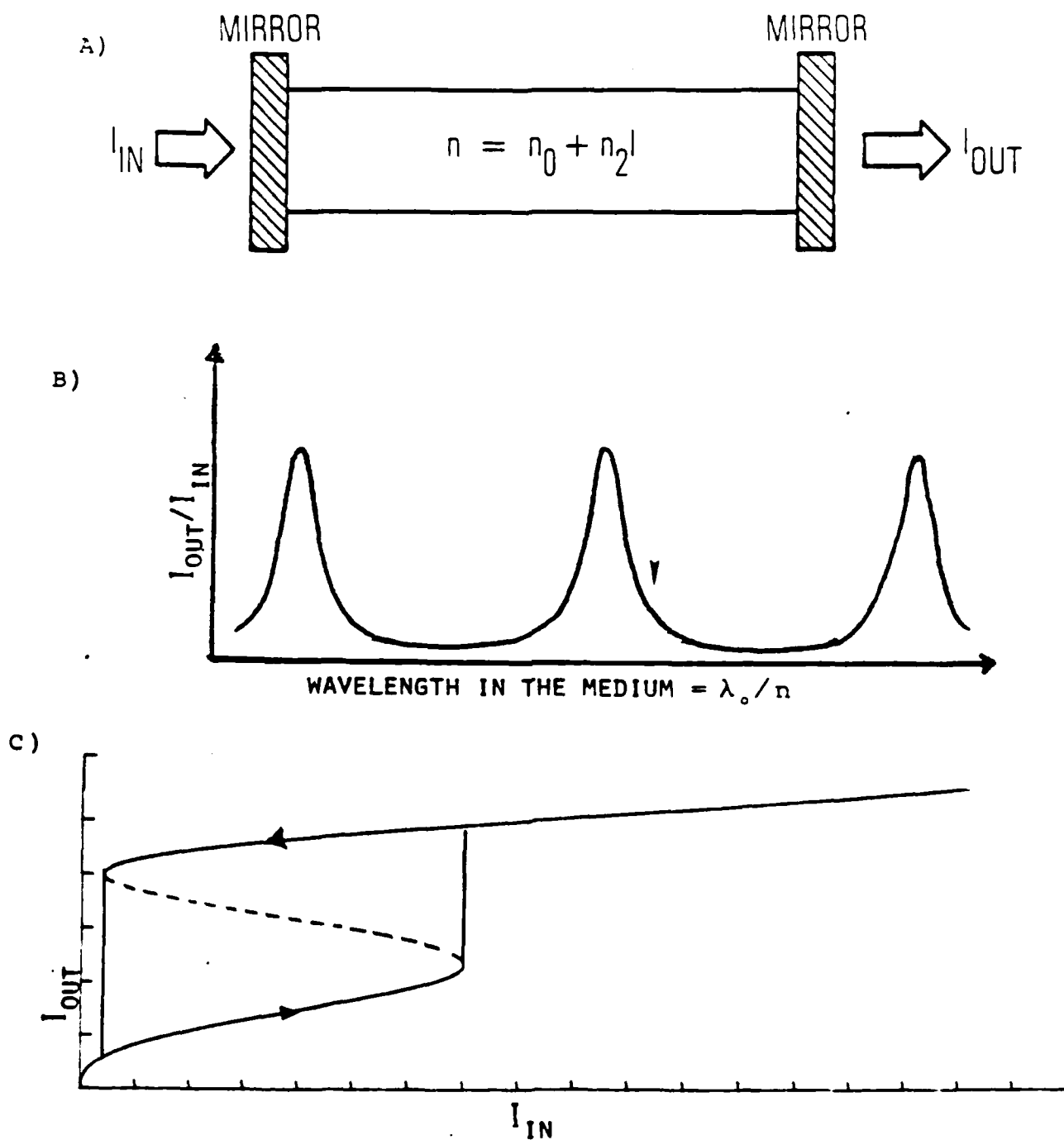
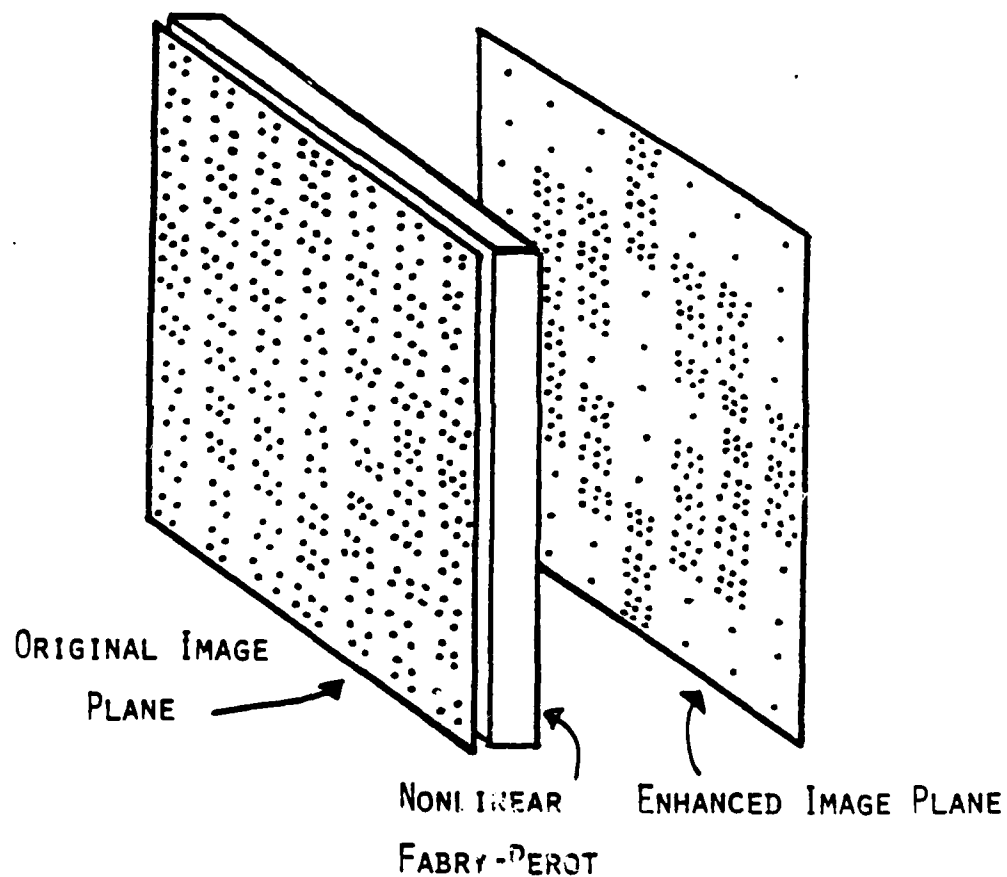


Figure 1-1. Optical bistable nonlinear Fabry-Perot.
 a) Geometry under consideration
 b) Transmission as a function of wavelength in the medium (inversely proportional to refractive index)
 c) Transfer curve (output vs input) showing bistability

Figure 1-2. Image processing in a thin nonlinear Fabry-Perot. Density of dots represents relative intensity. The nonlinear image processing in the Fabry-Perot causes an enhancement of the strong portions and a suppression of the weaker portions of the image.



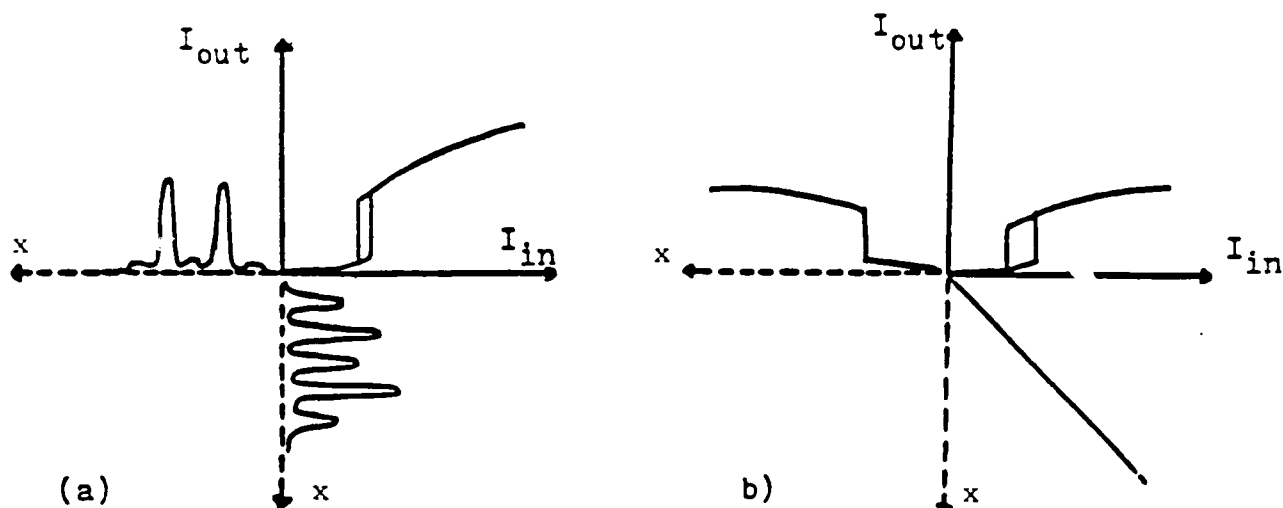


Figure 1-3 Two modes of operation of the nonlinear Fabry-Perot. In each case the functional dependence of the input is shown, running down, while the functional dependence of the output is shown running to the left. The variable can be considered to be the linear distance across the Fabry-Perot describing image information. (a) demonstrates differential optical gain, while (b) demonstrates optical limiting.

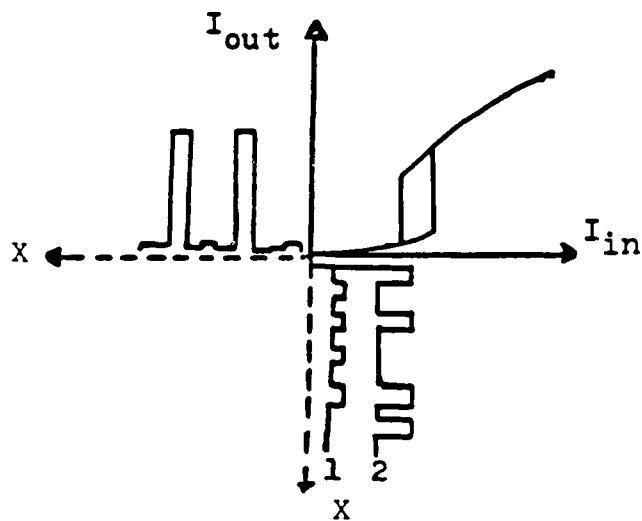


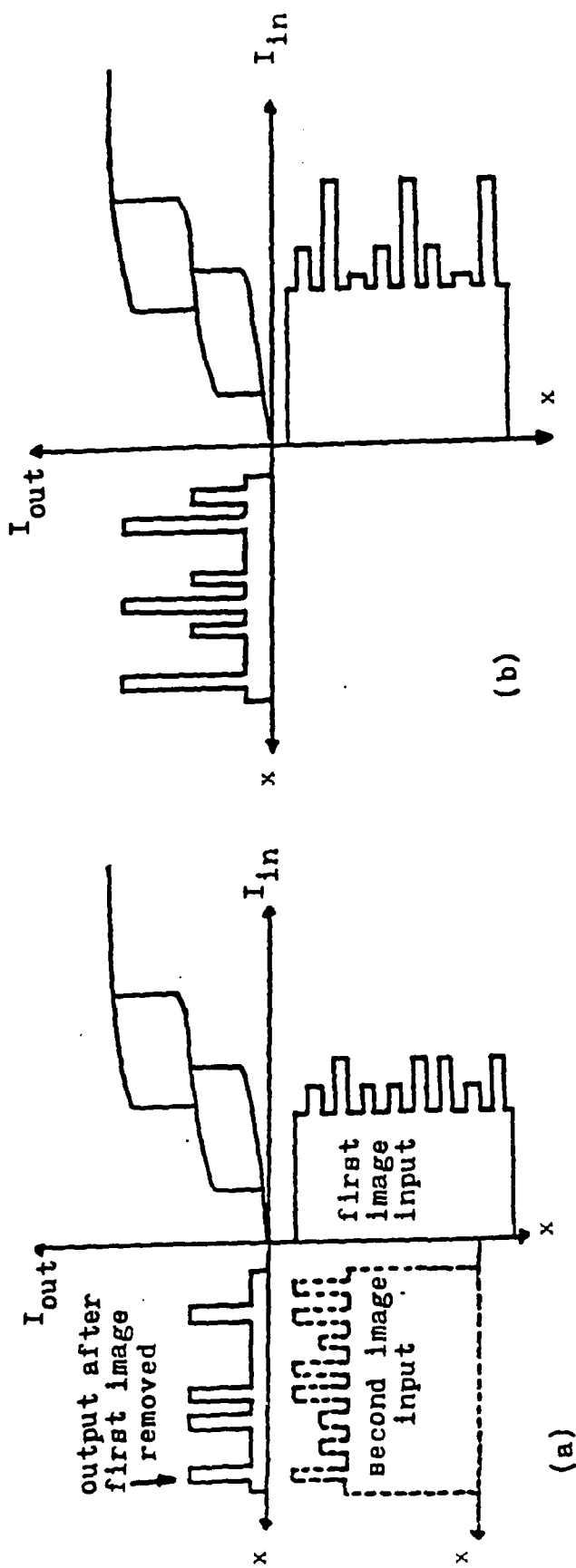
Figure 1-4. Optical AND circuit. a large output results only when both inputs are present.

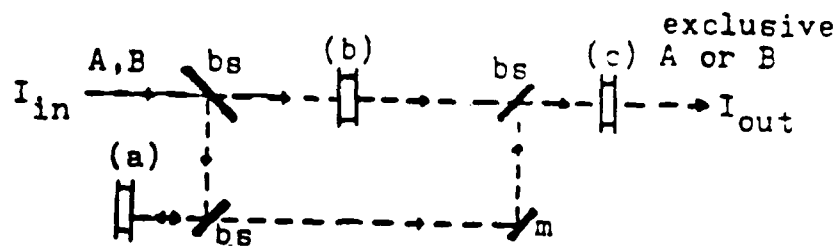
output is large only when both signals are present. Thus two images can be compared and only those features which are in both will be transmitted.

The optical memory function which is available because of the hysteresis requires a certain holding optical power. If this is available, the device retains a memory of its previous signal. This is useful for image retention, allowing one image to be compared to another received later in time. Figure 1-5 shows how a multiple-stable-state Fabry-Perot is used to retain one image, and compare it with another occurring later in time. The device retains information as to positions at which both images are bright, as well as positions at which only one image is bright. The multistable Fabry-Perot is obtained by driving the nonlinear Fabry-Perot at higher input intensities than used to achieve bistability.

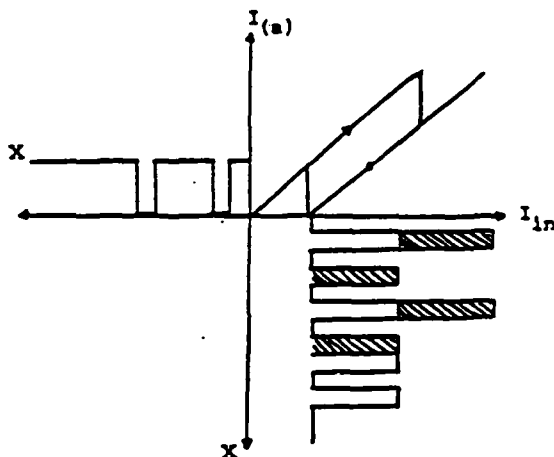
What is not transmitted through a Fabry-Perot is reflected. The reflected transfer curve can be used to develop a device to obtain one of the functions required for optical computing: The exclusive or. To obtain this function requires an output which is periodic in input intensity, so that two "ones" add to a zero. The reflection from a NLFP is such a periodic function. An exclusive or can be constructed as shown in Figure 1-6.

Figure 1-5. Multistable nonlinear Fabry-Perot used for image comparison and retention of matching information: (a) multistable transfer curve, image input and output remaining after first input is removed. Second image input is also shown, dotted. (b) Multistable transfer curve and input of second image summed with the output remaining after the first image is removed. The output has three possible states: the highest is achieved only in areas where both images were bright; the middle intensity level is obtained where one or the other images are bright, but not both; the third is obtained where neither image was bright. The output is shown after both images are removed. In this optical memory is contained the comparison between the two images.

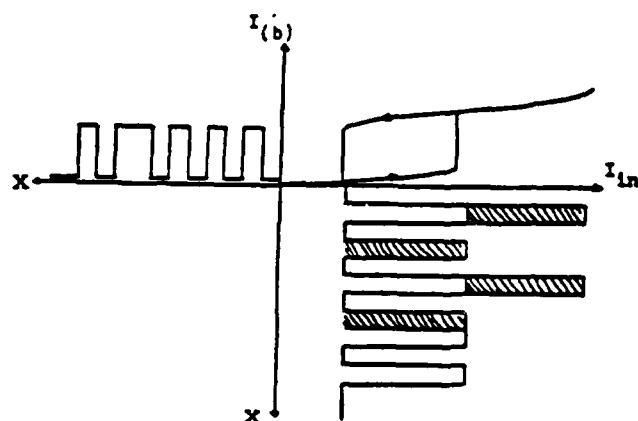




a. Diagram of arrangement of nonlinear Fabry-Perots (a), (b), (c) which combine to yield an exclusive OR. bs is beam splitter, m is mirror. For A,B incident, transmitted light is the exclusive A or B.



b. Signal reflected from nonlinear Fabry-Perot (a) as first step in the exclusive OR



c. Signal transmitted through nonlinear Fabry-Perot (b) as the second step in the exclusive OR.

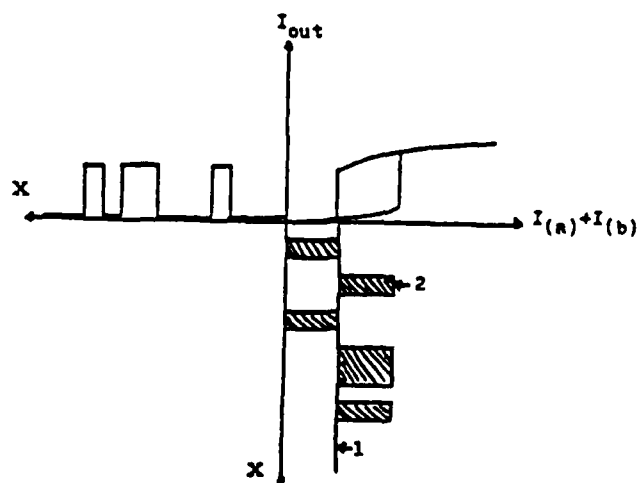


Figure 1-6. Exclusive OR output of the combination of nonlinear Fabry-Perots shown in a. The final signal is obtained by adding the signals from (a) and (b) in a third nonlinear Fabry-Perot, shown as (c).

II. IMAGE PROCESSING WITH BISTABLE DEVICES

Nonlinear optical devices utilize the optical properties of materials to produce nonlinear optical signal processing. In principle these process can be very fast, since they do not require electronics. For example, the nonlinear refractive index of materials like CS_2 have speeds of psec. It is this fact which has spurred research in nonlinear optical signal processing devices such as the bistable devices. Indeed, discussion has been made of the possibility of optical computers utilizing this very fast switching time.

Because nonlinear refractive indices tend to be small, nonlinear optical effects tend to require high incident light levels. The limit on the number of resolvable spots which are useful for optical image processing is determined by the intensity levels necessary for switching and the minimum area which can be achieved for each spot. We examine here the conditions to obtain high resolution image processing with bistable optical devices, and find that under the appropriate conditions, as many as 10^6 resolvable spots with speeds as fast as a nanosecond may be achieved.

The Fabry-Perot has been used for optical image processing by Bartholomew and Lee (Applied Optics 19, 201 (1980)), using a spherical resonator to obtain a large number of resolvable spots. We have considered the possibility of image processing in an ultra-thin Fabry-Perot. These devices have an inherent advantage over the spherical cavity considered by Bartholomew and Lee in not requiring a careful frequency match between laser frequency and the cavity resonance frequency, reducing the cavity stability requirements. An ultra-thin Fabry-Perot is considered to contain a material with a nonlinear refractive index, and some residual linear absorption. The research to date has predominantly involved optical processing of single elements. There are, however, several demonstrated results on bistability in ultra-thin Nonlinear Fabry-Perots (NLFP) which would be useful for image processing. The experimental results are summarized in Table 2-1

Table 2-1

Experimental Results on Single Pixel Signal Processing
Using Bistability in Thin Nonlinear Fabry-Perots.

Medium	Thickness μm	Wavelength μm	Intensity $\text{MW}/\mu\text{m}^2$	Power/ Pixel	Speed
Absorbing glass (refs. 1,2,3)	57	0.63	.08	20 mW	100 μsec
GaAs (refs. 1,2,4)	4	0.82	1	4.2 mW	40 nsec
InSb (ref. 5)	580	5	.01	50 mW	-nsec

References

1. H.M. Gibbs, et.al., Appl. Phys. Lett. 34, 511 (1979).
2. H.M. Gibbs, Et.al., Fourth International Conference on Laser Spectroscopy, West Germany, 1979.
3. McCall, J. Opt. Soc. Am. October, 1978.
4. H.M. Gibbs, et.al., Appl. Phys. Lett. 35, 451 (1979).
5. D. Smith, D.A.B. Miller, Appl. Phys. Lett. 35, 658 (1979).

The limitation on the resolution of the thin Fabry-Perot is diffraction which occurs in the several passes that the light makes through the interferometer. The minimum spot size which can maintain itself at its diameter without diffracting for a distance L_{eff} is given by

$$D = (2 \lambda_0 L_{\text{eff}} / n)^{1/2} \quad (1)$$

where L_{eff} is the effective path length of the beam through the Fabry-Perot, and is given by $L_{\text{eff}} = FL/n$, where F is the finesse.

The number of resolvable spots which may be processed in the image is limited by the available power. since every element must be subject to sufficient intensity to operate in the non-linear regime. D.A.B. Miller (IEEE J. Quantum Electr. QE-17 306 (1981)) has made a theoretical study of the optimization of a NLFP, and found that the critical intensity is given by

$$I_c = \frac{1}{\beta} \frac{1}{\mu_0} \frac{1}{P} \quad (2)$$

where $\beta = \frac{3n_2}{\lambda \alpha}$, proportional to the ratio between the nonlinear index and the linear absorption. P is a parameter which depends on the NLFP reflectivities and can be made close to two and μ_0 is a figure of merit which typically lies between 1 and 10, depending on cavity geometry. The only dependence on cavity length is found in μ_0 , which is close to inversely proportional to cavity length, for a given nonlinear index and absorption coefficient. This means that the shorter the cavity, the better. The shorter cavity has additional advantages of higher spatial resolution, and less stringent tolerances on the bandwidth of the incident light.

Table 2-1 listed the experimental results to date on thin NLFP's. The power per pixel was calculated by including the finite spot size as expressed in Eq. (1), for each device. It can be seen that in several cases, since the length of the Fabry-Perot was relatively large, the power per pixel was rather high - a consequence primarily of diffraction.

The NLFP geometry is optimized by using the thinnest possible cavity lengths, not only to avoid degradation of spatial resolution due to diffraction, but also to obtain lower critical intensities, as expressed in Eq. (2). Since I_0 is inversely proportional to cavity length, within the range of interest, then the critical intensity is directly proportional to cavity length. This means that decreasing the thickness a factor of ten decreases the critical intensity a factor of ten, the critical power per pixel decreases a factor of one hundred. Thus, the optimum NLFP requires using as short a cavity length as possible. There are, of course, limits to this optimization, since decreasing the cavity length to zero is unphysical.

Exact determination of the limits of applicability requires applying the theory of Miller more carefully.

We show in Table 2-2 predicted behavior of ultra-thin NLFP's. For InAs we include the estimated power per pixel based on the above simple arguments, and the estimated power per pixel determined by Miller from a more complete optimization of NLFP parameters in InAs. The fact that he has obtained an additional factor of 25 by more careful optimization indicates that further optimization beyond the values listed in Table 2-2 should be possible with the other devices as well.

Table 2-2

Predicted Theoretical Results for Ultra-Thin Nonlinear
Fabry-Perots For Use With Image Processing

Medium	Thickness μm	Intensity $\mu\text{W}/\mu\text{m}^2$	Power/ pixel μW	Speed	Energy/ Pixel
absorbing glass	2	2.3	25	100 μsec	2.5 nJ
+ heat sink	2	23	250	10 μsec	2.5 nJ
GaAs	2	500	1050	40 nsec	42 pJ
InSb	6	0.1	1	1 nsec	1 fJ
+ further optimization		.004	.04	1 nsec	.04 fJ

A careful look at Table 2-2 allows us to make some very interesting predictions about image processing with a NLFP. Consider first the absorbing glass NLFP. This device relies on the change in refractive index due to localized heating of glass occurring because of optical absorption. The results to date were for a device 57 μm thick. This is as thin as a bulk piece of glass can be polished. Signal processing using an ultra-thin glass NLFP will require obtaining thin glass films $\sim 2 \mu\text{m}$ thick with properties comparable to the thicker films. We suggest that sputter deposition of a thin glass film will be the process by which to obtain the thin film. Good quality glass films have been sputtered, and in fact made into optical waveguides. For the NLFP, dopants will be added during sputtering to ensure the proper amount of absorption in the glass.

In the absorbing glass NLFP, the nonlinearity is effectively dependent on the absorption since it is caused by thermal heating. This means that optimization requires looking at the thermal heating properties of the device. Both the sensitivity and speed of the device are related to the thermal conductivity. We present here a simple modeling of the thermal bistable device.

In order to determine the temperature rise, and therefore the change in refractive index due to the absorption of a given fraction of the incident light intensity, we require that the heat flow into the sample equals the heat flow out of the sample. The relationship equating these two is:

$$\alpha L A I \tau = A L \rho C \Delta T$$

where α is the absorption coefficient, L the length of the Fabry-Perot, I the incident intensity, A its area, and τ the thermal time constant of the particular geometry under consideration, ρ is the density and C the specific heat. The temperature rise ΔT causes the change in refractive index through $\Delta n = (dn/dT)\Delta T$, so that the refractive index rise can be written as

$$\Delta n = \frac{(dn/dT)\tau\alpha}{\rho C} I \equiv n_2 I \quad . \quad (3)$$

Thus the nonlinear index, n_2 , is proportional to the absorption coefficient but does not explicitly depend on the length of the sample. This means that the modeling by Miller which was appropriate for the nonlinear Fabry-Perot is also valid for the thermal nonlinearity.

The nonlinear index does, however, depend on the response time of the sample. The response time may be decreased by heat sinking the sample, but it will be at a cost of a decrease in the nonlinear index.

A related problem is the requirement to reduce the heat flow in the plane of the Fabry-Perot which would decrease the spatial resolution of the image processor. As long as a thin Fabry-Perot is considered, on a heat-sink substrate with conductivity substantially larger than that of the glass, there should be no problem with loss of resolution. As an example, we consider a conductivity sufficient to improve the response time an order of magnitude, causing a related decrease in nonlinear refractive index by an order of magnitude. The results are shown in Table 2-2.

The ultra-thin absorbing glass filter, on an appropriate heat sink (such as sapphire) requires 250 μ W per pixel, so that a 2.5W laser will be able to process 10^4 spots, with a time constant of 10 μ sec. This is considerably better than any spatial light modulator available today. Furthermore, an order of magnitude more pixels can be processed with a time constant of 100 μ sec by eliminating the heat sink. By com-

parison, the GaAs NLFP requires forty times more power, so can process forty times fewer spots, but is at a speed 1000 times faster.

The NLFP with the lowest required power is InSb, in which a power per pixel of 1 μ watt leads to the possibility of processing 10^6 pixels in 1 nsec with a 1 watt laser. The only drawback of this material is the fact that it operates at 5 μ m, with a CO laser, at low temperatures, which is not very convenient for systems applications.

The reference by D.A.B. Miller shows that a complete optimization of all the parameters available in designing a nonlinear Fabry-Perot makes a predicted switching power for the InAs device 6 μ m long of 4 nanowatts rather than the 100 nWatts we predicted from simple arguments above. At this power level, the predicted power per pixel is 40 nWatts, so that a 4 watt laser would produce 10^8 resolvable spots in 1 nsec. Such a device has astounding possibilities for signal processing.

The ultra-thin Fabry-Perot has several other advantages for image processing. Both the frequency and angular acceptance bandwidths are relatively large. Consider, for example, the wavelength acceptance bandwidth of a Fabry-Perot 2 μ m thick. The width of the resonance is given by

$$\Delta\nu = 1/2nLF$$

where L is the length, F is the finesse, and n is the refractive index. We find $\Delta\nu/\nu = .025$, or $\Delta\lambda = 150\text{\AA}$. This wide bandwidth means that no special precautions are required on the light source which is used. In principle, an incoherent light source could be used if it were filtered to 150 \AA . The second consideration is the acceptance angle of the Fabry-Perot. This can be calculated by imagining the Fabry-Perot is on resonance and calculating the angle at which the Fabry-Perot goes out of resonance.

We obtain

$$1 - \cos \theta = n\lambda/2LF.$$

When the Fabry-Perot is 2 μ m thick, with a finesse of ten,

this is 14° . The optical system which most favorably will couple to this NLFP is f4, a perfectly reasonable requirement for an optical system.

The NLFP can be used in image processing in two ways. First, in a cw fashion, in which the image is impressed on the incident laser beam through such means as a photographic plate or other imaging device. The NLFP can also be used in the scanning mode, with the image impressed by intensity modulation on a scan beam. In this mode of operation, the NLFP essentially processes pulses of light, and the processed image will be recorded in suitable fashion, for example, on a detector array or photographic plate. In this case, it is the energy for switching a pixel in a pulse which is important. This information is shown in the last column in Table 2-2. It can be seen that GaAs has a decided advantage over the absorbing glass in this usage, and that InSb is again an optimum material. Assuming that a four watt laser is used, 10^{11} bits can be processed per second using a GaAs NLFP, while only 2×10^9 can be processed in the absorbing glass NLFP. By contrast, at least 10^{15} bits per second can be processed in the InSb NLFP. The very large size of these numbers motivates further research into the NLFP and optical bistability.

III. HYBRID ELECTRICAL OPTICAL BISTABLE OPTICAL DEVICES

In section II we have discussed the nonlinear Fabry-Perot, as a useful bistable device for optical image processing. Another useful device for optical signal processing is hybrid electrical-optical geometries for bistable optical devices (BOD). While these hybrid devices will not be able to have speeds faster than that of electronics, they may be used in a parallel processing fashion thereby providing overall bit rates greater than nanoseconds. It is interesting to note that none of the most useful nonlinear Fabry-Perots discussed in the last section has speeds to date which are larger than nanoseconds. Thus a nanosecond hybrid bistable device may provide a viable alternative to the NLFP for many applications.

The generic concept of a hybrid bistable optical device is shown in Fig. 3-1. This device uses a modulator, detects its output, amplifies it, and feeds it back as a voltage across the modulator with an optional bias voltage applied. The instantaneous output of the modulator is

$$I_{out} = I_{in} T(V), \quad (3-1)$$

where I_{in} is the input light intensity and T is the modulator transmission function, which depends on the control voltage V . Assuming the detector is linear with detectivity factor δ , and fast, the current $i = \delta I_{out}$. Again, assuming the amplifier is linear and fast, with amplification factor γ , the voltage applied to the modulator is given by $V = \delta \gamma I_{out}$. When the detector and amplifier are not negligibly fast, transient effects are observed, as described in Section V. If the detector and amplifier are not linear, Eq. (3-1) applies with appropriate functional relationships to describe the voltage across the modulator in terms of I_{out} .

Bistability comes from relating the input and output through the transmission:

$$I_{in} = I_{out} / T(\delta \gamma I_{out} + V_B) \quad (3-2)$$

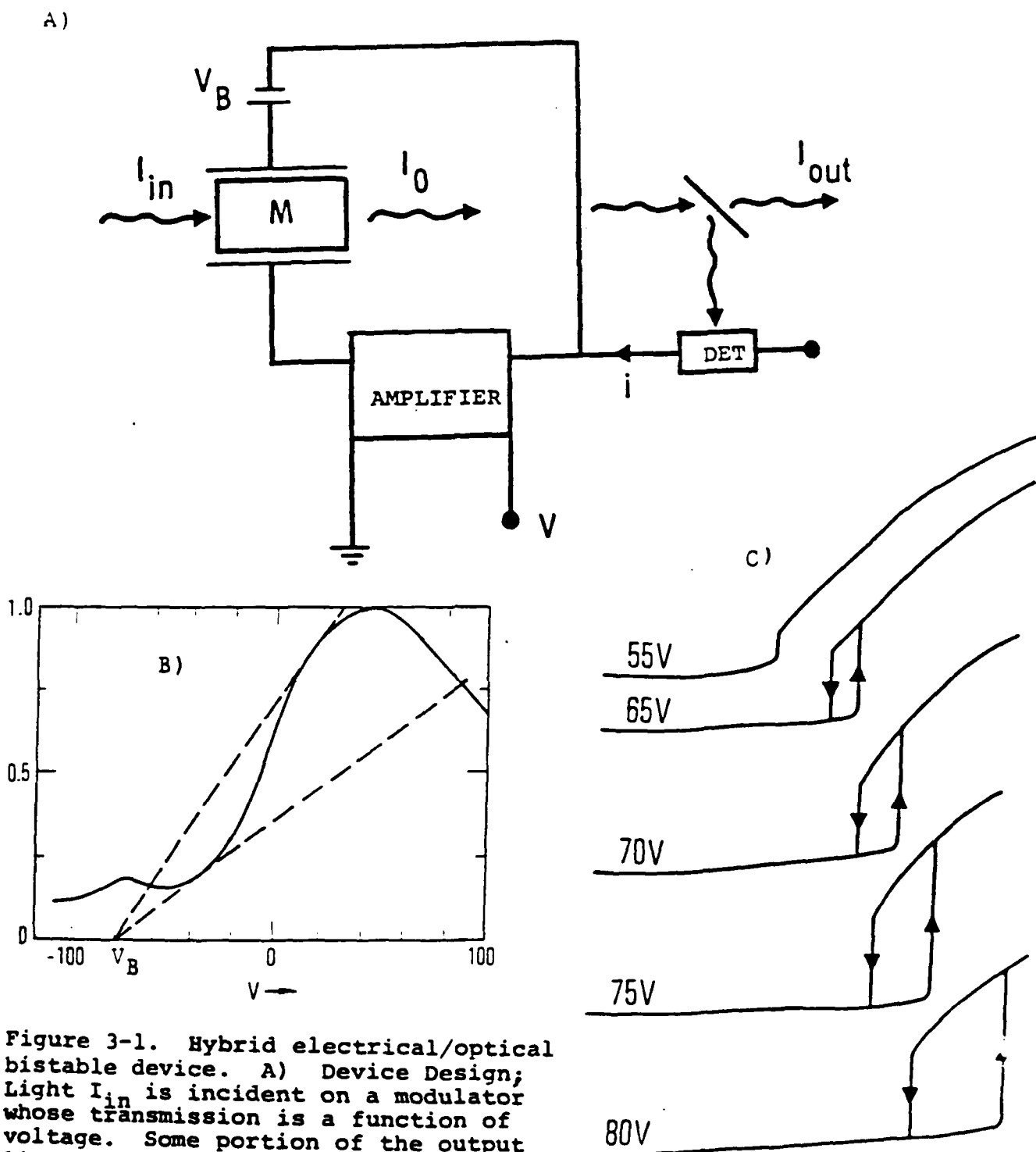


Figure 3-1. Hybrid electrical/optical bistable device. A) Device Design; Light I_{in} is incident on a modulator whose transmission is a function of voltage. Some portion of the output light is detected, amplified and fed back as a voltage on the modulator.

B) Transmission of the experimental modulator as a function of voltage. Regions of bistability lie between two lines (of slope $\sim 1/I_{in}$) originating in V_B which intersect the transmission curve in more than one point. Notice that a monotonic transmission function may still cause bistability. C) Experimental transfer curves (Output vs. Input) for several bias voltages.

Since it is possible for the right hand side of Eq. (3-2) to have the same value for several values of I_{out} , it is possible to have the same value of I_{in} lead to several values of I_{out} . This causes bistability or multi-stability.

We demonstrated experimentally that bistability may occur even if the transmission is a single-valued function of the voltage as shown in Fig. 3-1. This figure also shows the graphical solution of the bistable device, determined by the intersection of a straight line of slope proportional to I_{in}^{-1} and the transmission function. This solution comes from equating both sides of the following equation:

$$\gamma \delta I_{out} \left(\frac{1}{I_{in}} \right) = T (\gamma \delta I_{out} + V_B) \quad (3-3)$$

The existence of bistability in a simple hybrid configuration using a wide variety of transmission functions suggests the versatility of this approach for optical signal processing.

There are a number of modulators and/or switches in which hybrid bistability has been demonstrated. The search for the optimal hybrid bistable device for optical signal processing is a search for a high-speed low-voltage modulator and development of the appropriate high-speed amplifier.

In this section we make a brief review of possible modulators for use with the hybrid bistable device and suggest a device which we believe is the most appropriate for use in hybrid BOD arrays for parallel processing.

The simplest concept for an electro-optic modulator is phase modulation. Kaminow et.al. (Appl. Phys. Lett. 37 555, (1975)) have demonstrated phase modulation with half-wave voltages of less than one volt for y-cut, x-propagating LiNbO_3 waveguides using electrodes 3 cm long and separated by 9 μm . To be useful for bistability, the phase modulator must be converted into intensity modulation, however.

Interference of phase-modulated light with background unmodulated light to achieve hybrid bistability was demonstrated by Garmire et.al. (Opt. Lett. 3 69 (1978)) with electrode spacing of 10 μ m and electrode length of only 2 mm (half-wave voltage of 80V).

Phase modulation is turned into polarization modulation by placing the device between crossed polarizers as demonstrated in the first hybrid BOD without optical feedback (Garmire, et.al., Appl. Phys. Lett. 32 320 (1978)). High speed results of polarization modulation in an integrated optics format were reported by Izutsu et.al., (IEEE J. Quantum Electr. QE-14 394 (1978)) who observed 64% modulation at 2 GHz using electrodes 35 μ m wide and 9 mm long. This device is eminently suitable for a hybrid BOD.

Phase modulation can also be turned into intensity modulation by inserting in a Fabry-Perot resonator. This was used by Smith et.al., to demonstrate the first hybrid BOD (Appl. Phys. Lett. 30 281 (1977)). An integrated optics version was fabricated by cleaving x-cut LiNbO_3 in the appropriate direction (32.75° between z and the cleavage plane). They obtained a half-wave voltage of 1.2V for a 12 mm resonator, using the extra-ordinary ray, and a half-wave voltage of 5.5V for a 8.7 mm resonator using the ordinary ray (Smith et.al., Appl. Phys. Lett. 34 63 (1979)).

The use of a resonator has the advantage that it decreases the voltage which must be applied to the modulator to cause bistability. If the resonator has a finesse F, the required voltage is reduced from the half-wave voltage, $V_{\frac{1}{2}}$, to $V_{\frac{1}{2}}/F$. However, the use of a resonator of reasonable length (required to reduce the half-wave voltage) also increases the alignment problems and requires a narrow-band input source. For this reason, the electro-optic Fabry-Perot is not the most convenient hybrid BOD.

One of the most versatile integrated optics modulators is the directional coupler. This has been used in a hybrid

BOD (Cross, Schmidt, Thornton, Smith IEEE J. Quantum Electr. QE-14 577 (1978)). The reported half-wave voltage was 2 V, with a separation between electrodes of 3 μm and length of 2 cm. The detector was an avalanche photodiode with 30A/Watt, and hysteresis was seen with 10 nanowatts of optical power. However, in order to switch with this low incident signal, it was necessary to integrate the detector charge in order to build up sufficient voltage. Thus the switching time was the order of fractions of milliseconds.

Faster hybrid directional coupler switches require amplifiers. One such device was reported by Tarucha, Minakata and Noda (IEEE, JQE 17 321 (1981)) with switching up to 300 MHz using a Ge avalanche photodiode and wide-band amplifier. This device used z-cut, x-propagation in LiNbO_3 , with a 15 mm interaction length and 4.7 μm separation. A wide variety of directional coupler modulators are currently available to be used in hybrid configuration.

Another modulator type is the interferometric modulator, using branching waveguides such as reported recently by Leonberger (Opt. Lett. 5 312 (1980)), who observed modulation up to 1.4 GHz with 3 mm electrodes separated by 4 μm and a half-wave voltage of 4.5V. Optical bistability has been investigated in a hybrid BOD using an integrated two-arm interferometer (Schnapper, Papuchon, Puech, Opt. Comm. 29 364 (1979)). Using an electrode spacing of width 4 μm and electrode lengths of 5 mm, they observed a half-wave voltage about 10V. They used a photomultiplier to create the voltage sufficient to drive the modulator, and had a response time limited by the RC of the photomultiplier circuit. A similar interferometric modulator was used with a phototransistor and amplifier of bandwidth 25 kHz to obtain a hybrid BOD with 6 μsec time constant. (Ito, Ogawa and Inaba, Electr. Lett. 16 543 (1980)). Both the directional coupler and interferometric modulator represent excellent candidates for fast, single-element hybrid BOD's.

A particularly promising type of electro-optic modulator for use as a BOD is the waveguide-cutoff modulator, reported

in a hybrid configuration (W. Sohler, Appl. Phys. Lett. 36 351 (1980)). This device is a Ti-diffused channel waveguide 2 μ m wide and only 3 mm long. The application of a voltage is chosen to reduce the refractive index and destroy guiding, causing intensity modulation. The half-wave voltage was 25 V, comparable to a phase modulator of the same length. An amplifier was used and a biasing resistor which caused the time constant to be the order of milliseconds. The usual disadvantage of a waveguide cutoff modulator for modulation applications is that its nulls are shallow, and some light is transmitted even in the "off" state. For optical bistability, however, this is not a drawback, since a non-zero null is required to drive the transfer curve. Thus, the waveguide cutoff modulator may be very useful for hybrid optical bistability.

The electro-optic effect is also used in some other geometries for optical modulation. This may be some form of total internal reflection or some electro-optic grating. Bistability has been seen at the total internal reflection interface between electro-optic KDP and a liquid whose index was close to that of the KDP (critical angle 1°). The device had a half-wave voltage of 1200 V, so is not practical in its reported form (Smith, Tomlinson, Maloney, Kaplan, Opt. Lett. 7 57 (1982)). However, integrated optics versions of the total internal reflection modulator have been reported which could be applicable.

There are several hybrid BOD's which have been demonstrated with modulators which are inherently slow, but have useful features. This includes driving a thin Fabry-Perot with a piezo-electric (McCall, Appl. Phys. Lett. 32 384 (1978)), or an electro-strictive (Gomi et.al., J. Appl. Phys. 20 L375 (1981)) transducer. Typically these devices require drive voltages of hundreds of volts and have response times of milliseconds. A magneto-optic bistable device has also been reported by Umegaki et.al., (Appl. Phys. Lett. 38 752 (1981)).

This device has the advantage of operating with current, rather than with voltage, but the switching time of the reported device was still 0.5 msec because of the inductance in the electromagnetic coil. Better design could speed this up.

Finally, an acousto-optic bistable device has been reported by Albert et.al. (Can. J. Phys. 59 1251 (1981)), operating with a photo-diode + lock-in amplifier + voltage-controlled oscillator + broad-band amplifier. This device has the potential of MHz operation, but the reported BOD demonstrated an unexplained slow temporal drift.

The hybrid BOD will be most useful for optical signal processing if an array of devices can be built. In this way, advantage can be taken of parallel processing (if only in one dimension). The modulators discussed above must be investigated in light of the requirements for a high-density array. In this regard, clearly single-channel modulators will have the advantage. The two most promising are the polarization modulator and the waveguide cutoff-modulator.

An array modulator of the sort which would be useful for a hybrid array BOD has been reported by Xerox Company (Flores, et.al., Integ. Opt. Conf. January, 1982). The device reported had several characteristics which make it useful. First, the driving electronics was fabricated in silicon, using VLSI techniques, which was pressed against the LiNbO_3 crystal in close proximity. The fringing fields were the source of electro-optic modulation in the LiNbO_3 . The device reported had 5376 active elements, formed with parallel metal electrodes. The Xerox array modulator does not make use of integrated optics, but uses a single total internal reflection at grazing incidence to achieve a long interaction length. Some aspects of this design will be useful for a hybrid BOD.

The most practical hybrid BOD array would use a waveguide cutoff modulator with electrodes, detector and amplifier all in a silicon VLSI chip which is proximity-coupled to a LiNbO_3 sample. With voltage applied, fringing

fields would create a waveguide, guiding light to the other end of the sample and to the detector array. When no voltage is applied, light would not reach the detector array. Appropriate amplification between the detector and modulator electrodes would be built into the silicon chip using VLSI techniques. Figure 3-2 shows a schematic of such a hybrid BOD array.

Obviously proximity coupling can also be used on other waveguide modulators, such as the polarization modulator. The polarization modulator can be designed to operate at lower voltages than the waveguide cutoff modulator (by fabricating longer devices). However, there is an additional alignment requirements between the modulator electrodes and the channel waveguides.

Another device for a hybrid bistable optical device would be a monolithic construction in GaAs. The modulation, detection and amplifier can all be constructed in GaAs. These techniques have been demonstrated in discrete devices (E. Garmire, Integrated Optics, Ed. Tamir, Springer-Verlag (1975)) and remain to be integrated monolithically.

Two-dimensional hybrid BOD's have been reported using liquid crystal displays, (Sengupta, Gerlach, Collins Opt. Lett. 3 199 (1978), and Athale and Lee, Appl. Opt. 20 1424 (1981)). These devices have the advantage of processing in 2-D, but the slow speed and limited resolution of liquid crystal light valves. The emphasis of our study of hybrid devices has been on developing a high-speed linear array processor.

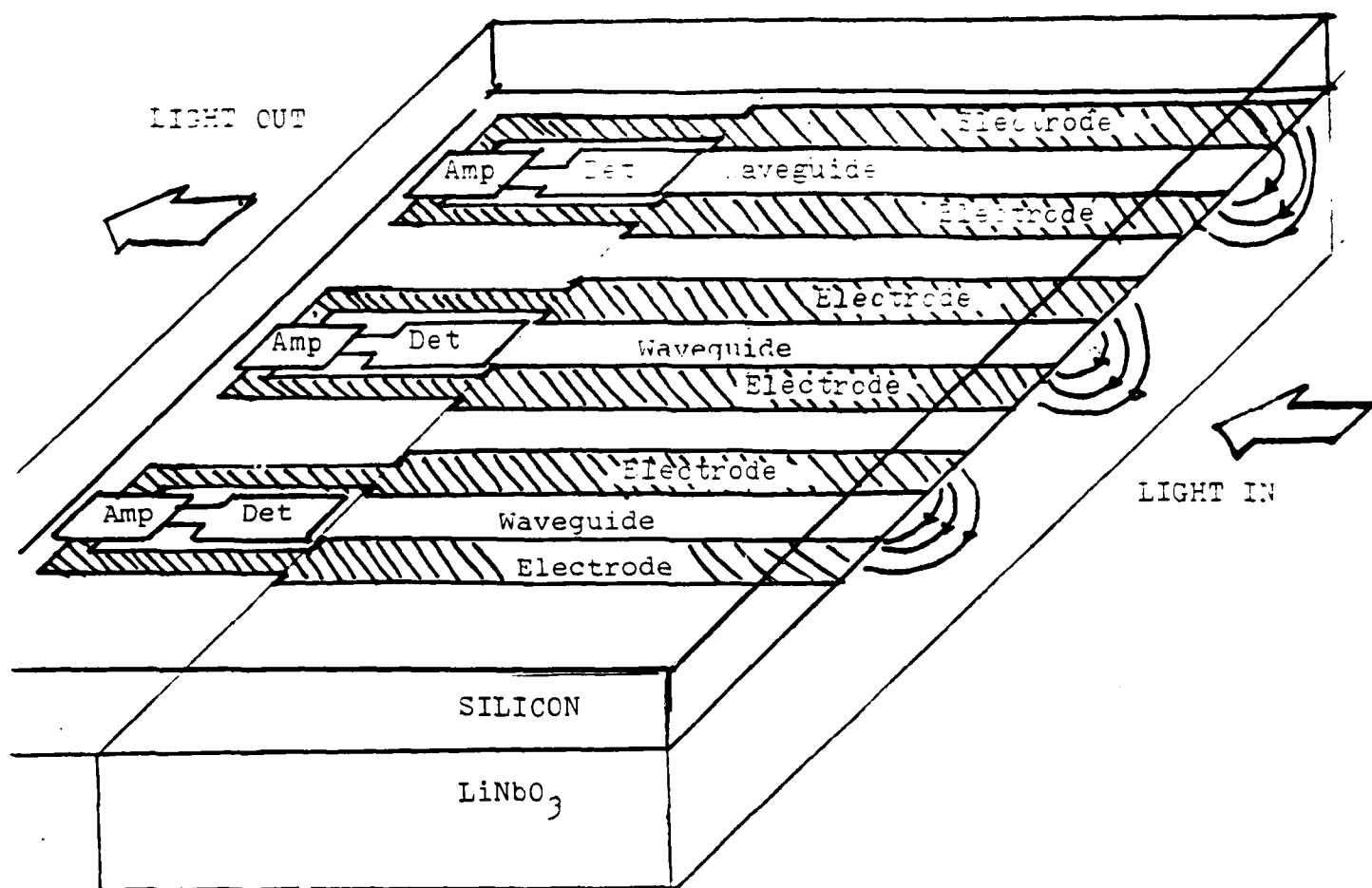


Figure 3-2. Hybrid electrical/optical bistable array. Electronics structure is in silicon, comprised of electrodes, detector and amplifier. Optical waveguide modulator is in LiNbO_3 . Two substrates are placed face-to-face, with a press fit. LiNbO_3 substrate ends before the detector, and some portion of the diffracting light is detected, amplified and fed back. The remaining portion of the light is imaged with a lens (not shown).

POTENTIAL OF VERY LARGE ARRAYS
OF SEMICONDUCTOR LASER SOURCES

ELSA GARMIRE*

NOVEMBER 1982

THIS RESEARCH WAS SPONSORED BY
DEFENSE ADVANCED RESEARCH PROJECTS AGENCY
UNDER ARPA ORDER NO.: 3710
CONTRACT NO.: MDA-903-82-C-0376

The views and conclusions contained in this document are those of the authors and should not be interpreted as necessarily representing the official policies, either express or implied, of the Defense Advanced Research Projects Agency of the United States Government.

* Consultant to the La Jolla Institute

TABLE OF CONTENTS

	<u>Page</u>
I. INTRODUCTION	1
A. <u>Summary</u>	1
B. <u>Limitations to Semiconductor</u>	
<u>Laser Power</u>	1
C. <u>Laser Array Geometries</u>	2
D. <u>Phase-Locking of Arrays</u>	2
E. <u>Coherent Power Combining</u>	3
F. <u>Applications</u>	3
G. <u>State-of-the-Art</u>	3
II. QUASI-BROAD AREA ARRAYS	4
A. <u>Operating Characteristics of</u>	
<u>Reported Devices</u>	4
B. <u>Maximizing the Number of Array Elements</u> ...	6
C. <u>Optimum Array Geometry</u>	10
III. SEPARATE STRIPE LASER ARRAYS OPERATED CW	13
A. <u>Introduction</u>	13
B. <u>Array Design</u>	13
IV. LOCKING OF INDIVIDUAL STRIPES	18
A. <u>Locking by Cross-Coupling</u>	18
B. <u>Injection Locking</u>	20
C. <u>Locking by Phase Selective Reflectivity</u> ...	21

TABLE OF CONTENTS CONTINUED

	<u>Page</u>
V. OUTPUT BEAM FORMING	26
VI. APPLICATIONS	29
VII. STATE-OF-THE-ART	30

I. INTRODUCTION

A. Summary

Applications for semiconductor lasers are expanding rapidly as the importance of opto-electronics increases. These applications extend from optical communications to read-write capability with optical disc data storage to sources for optical image processing. One of the chief limitations to the use of semiconductor lasers in opto-electronic systems is the power emitted by the laser source within a single output beam. It will be shown below that the output power of semiconductor lasers has some fundamental limitations but that the use of laser arrays can increase the output power within a single beam significantly. Additional advantages of laser arrays are such properties as the possibility of a greater region of linearity, directional tunability, higher efficiency, cooler operating temperatures, and more frequency stability. We will discuss two regimes of operation of laser arrays, methods of phase-locking the arrays to achieve coherent output, and techniques for output collimation to ensure that the radiation is emitted in a single beam. We make predictions of several watts of output with efficiencies approaching 50% and beam collimations on the order of m rad. Finally, we will discuss some possible applications.

B. Limitations to Semiconductor Laser Power

The reason that a laser array is required to achieve high power output comes from two facts about semiconductor lasers. First, that a stripe geometry is required in order to avoid filamentation and multimode behavior, and secondly that the small emitting area of the stripe geometry means that relatively low optical powers correspond to very high optical field intensities which can cause catastrophic facet damage.

Filamentation occurs when broad area lasers are used and it has been found that single mode operation requires stripe widths typically less than 10 μm . The reason for this is that the GaAs laser uses cleaved facets as mirrors, so that its optical resonator is theoretically that of two plane mirrors, which is not a stable resonator. This means that sensitive changes to the refractive index of the active region, such as that induced by the existence of gain, are sufficient to change the optical properties of the output. The existence of gain-guiding has been observed in stripe geometry lasers and is described, for example, in Casey and Panish, Heterostructure Lasers, Part B (Academic Press, 1978, p. 240). Models for filamentation in broad area lasers include such effects as spatial hole burning. The universal existence of filamentation in broad area lasers suggests that suitable diffraction-limited

operation may be possible if controlled periodic filamentation is purposely introduced. This is a quasi-broad area emission and is described below. The limitation to the CW output power of such devices will be diode heating.

The ultimate limitation to the output of single stripe-geometry diode lasers is catastrophic facet damage, due to high optical power densities. Because the emitting area is typically about $0.2 \times 5 \text{ } \mu\text{m}$ in area, powers in the tens of milliwatts produce field intensities in the Megawatt/cm² range.

One of the highest reported cw laser powers to date from a single stripe is the CSP laser of Hitachi. They reported an experimental device (M. Nakamura, K. Aiki, N. Chinone, R. Ito and J. Umeda, J. Appl. Phys. 49, 4644, (1978)) with an output power of 30mW/facet, operating at 400mamps. Above this level, facet damage occurred due to the high optical intensities resulting from such large powers being emitted from a small laser area. More typically, commercial lasers are specified at power levels the order of 10mW per facet. This means that diffraction-limited output at higher powers will not be achievable from semiconductor lasers without combining the power from several laser stripes.

C. Laser Array Geometries

It will be shown that the characteristics of laser arrays differ considerably when the stripes are spaced close together compared to far apart. When the distance between the stripes is sufficiently small, the operation is quasi-broad area, with spreading of the injection current from the stripe contact causing a sinusoidal modulation of the gain region. This results in a laser threshold and efficiency which is not much higher than for a single stripe. The output power limitations of the quasi-broad area device are determined by the properties of the heat sink, with the ultimate value predicted to be the order of several watts.

When the stripes are not close enough for the array to operate in the quasi-broad area regime, they must be separated sufficiently far so that the heat sink may cool each element of the array independently. In this case the array may be scaled up in size indefinitely. The chief requirement for the separated stripe array is high efficiency in utilizing the current to each laser stripe. This may require buried heterostructure technology.

D. Phase-locking of Arrays

To obtain the highest power in a single beam, it is necessary that all stripes in the array operate coherently. That is, with the same frequency and with a well-defined phase relation. Two basic technologies to achieve such phase-locking are the use

of cross-coupling and injection locking. The quasi-broad area devices which have been operated to date have shown some degree of cross-coupling and phase-coherence which will be described.

Phase-coherency due either to injection locking or to cross-coupling requires operation on the same wavelength. Analytic estimations for the requirements will be given. This requirement translates to a temperature requirement, since stripes at different temperatures result in different laser wavelengths. Design studies have shown that nonuniform spacing of the laser stripes may yield better phase coherence.

The separated stripe array must be phase-locked either through injection locking or by an external means of cross-coupling. Both techniques will be described, including some numerical estimates on the tolerances required.

E. Coherent Power Combining

Finally, high power output in a single beam requires coherent combining of the power from each of the stripes into a single beam. An efficient integrated optics design will be presented which will achieve this result, and experiments underway will be described. In addition, bulk optics techniques utilizing holography can also serve to coherently combine and collimate the power from each element of the array.

F. Applications

The availability of watts of power in the 0.7 - 1.5 μ m wavelength regime makes possible a wide range of applications, from optical communications to optical signal processing to replacing the Nd:YAG laser in many of its applications. Only a few of the possible applications are discussed in section VI of this report, since the applications seem almost limitless.

G. State-of-the-Art

In section VII, the research required to achieve a fully, collimated, high power laser array is described. Higher power laser arrays should be obtainable in the near future. Apodizing and collimating the output, however, requires further experimentation; from a sophisticated monolithic integrated optics design requiring a major research effort over several years, to the use of holography, also in its infancy for optical elements, to a hybrid integrated optics circuit which may provide a useful collimated powerful output in as little as two years.

II. QUASI-BROAD AREA ARRAYS

A. Operating Characteristics of Reported Devices

This regime of operation is shown schematically in Fig. 1. An array of diodes is closely spaced, so that diffraction coupling locks the adjacent stripes. Current spreading causes the gain in the active region to be periodically modulated, so that the light output is also modulated with the same periodicity. If the overall current threshold can be made sufficiently low, the device can be made to operate cw. Pulsed versions of the quasi-broad area diodes have been reported by Scifres, Burnham and Streifer, (IEEE J. Quantum Electr. QE-15, 917(1979)), and by Ackley and Engelmann (Appl. Phys. Lett. 39 27 (1981)). The lowest threshold was reported by Scifres et.al., as 400mA, for an array of ten stripes 3 μ m wide with a periodicity of 10 μ m. With a drive of 2 amps, they obtained an output of 900mW/facet, with no evidence of output power saturation.

CW operation has been reported by Scifres, Burnham and Streifer, Appl. Phys. Lett. 41 118 (1982) by utilizing quantum well structures fabricated by MOCVD⁺. This structure means that the active region was composed of four 130Å thick GaAlAs wells with 6% aluminum separated by three 40Å thick GaAlAs barriers with 20% aluminum. The advantage of this structure is a lower threshold by almost 25%, even though the differential quantum efficiency is lower. Experimental measurements gave pulsed thresholds on the order of 300-320mamps and cw thresholds of 320-350mA. These diode arrays were fabricated of length 250 μ m and operated pulsed at power levels up to 2.1 Watts per facet before catastrophic damage. CW operation to 410 mWatts was observed before catastrophic damage occurred, with an overall power conversion of 17% and a differential quantum efficiency of 55%.

The cw light output single-stripe was limited to a power per 3 μ m stripe which is comparable to the best devices reported to date indicating that the limitations to the power output may have been optical damage rather than limitations of the heat sink. This means that larger arrays are possible, producing higher output powers. We will discuss in the next section predictions as to limitations on the size of the arrays which should operate in the quasi-broad area regime.

⁺ Metal-Organic Chemical Vapor Deposition (MOCVD)

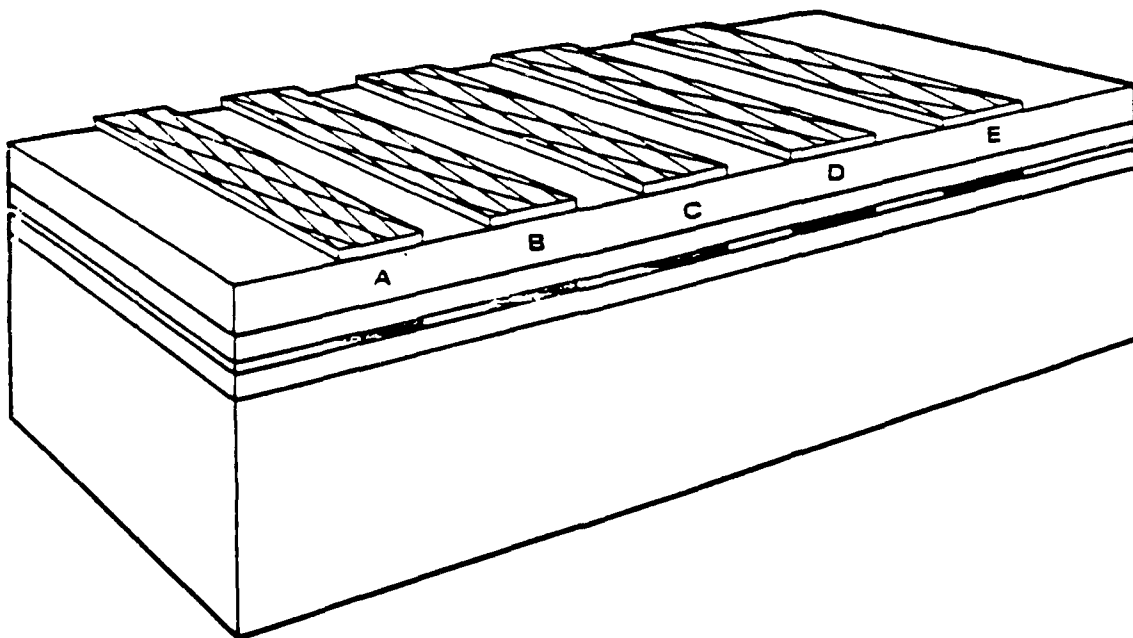


Figure 1. Quasi-broad area laser array. Notice that the separation between the laser stripes is the order of the stripe width. Arrays of ten diodes have been reported operating cw at power levels the order of 400mW/facet. Predictions show that large element arrays may emit many watts .

B. Minimizing the Number of Array Elements

The pulsed quasi-broad area arrays reported by Scifres et.al. had an optical output of 2 watts per facet, when the array was pulsed with 4.5 amps, for an overall power efficiency of about 30%. The dissipation of 70% of this 4.5 amps in an area of 100 x 375 μm caused too much heating for the diode array to operate cw at these power levels. In order to understand the maximum output power levels which will operate cw, it is necessary to model the heat flow in the heat sink and calculate the conditions to ensure the rapid removal of heat. From a theoretical modeling of heat flow in laser diodes, it would appear that it may be possible to achieve cw drive currents as high as 2 amps, with suitable heat sinking. H. C. Casey and M. B. Panish (Heterostructure Lasers, Part B, Academic Press, 1977, p. 234) state that a 250 μm wide broad-area laser should experience about 2°C temperature rise per watt of input power. Assuming the operating voltage is 1.6V and the input current is 2 amps, the temperature rise of the active region would be only 6.5°C, well within the operating regime of the diode, for proper cooling.

To understand the heat sink requirements for the array geometry, it is sufficient to model it as a broad-area laser and to solve Poisson's equation for the heat flow into a heat sink. This can be seen by referring to Figure 2. The analysis assumes that the heat generated in the active region is immediately conducted as a uniform sheet of heat to the diode-heat sink interface, where it is dissipated. This is only an approximation to the amount of heat which can be dissipated in the heat sink. In reality, the finite conductivity of the GaAs/GaAlAs layers and indium solder must be included. Ignoring these latter effects, and referring to W. B. Joyce and R. W. Dixon, (J. Appl. Phys. 46 855, 1975), the temperature at the center of the laser diode can be written as

$$T_0 = \frac{P}{\pi L \sigma} \left\{ \sinh^{-1} \frac{L}{W} + \frac{L}{W} \sinh^{-1} \frac{W}{L} \right\} \quad (1)$$

where P is the power (in watts) dissipated in the active region, L is the length of the laser, W is its width, and σ is the conductivity of the heat sink (in watts/cm²K). Typical numbers for conductivities of interest in this problem are shown in the table.

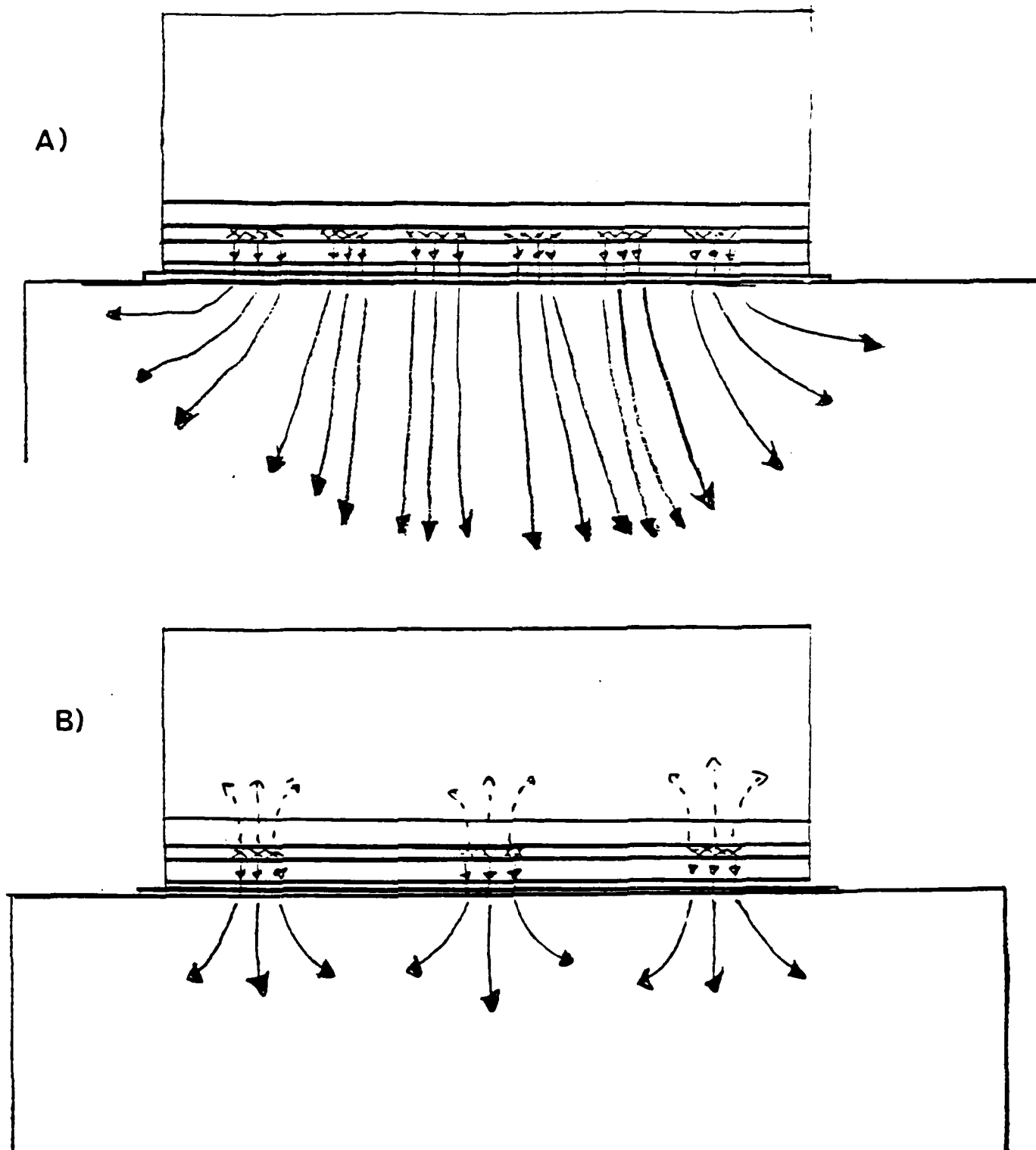


Figure 2. Heat flow in semiconductor laser arrays and their heat sinks

- a) Quasi-broad area array. The heat flow is approximately that of a broad-area device.
- b) Separate laser stripe array. The heat flow is approximately that of individual stripes.

Table I

Thermal Conductivities of Typical Materials Used In Laser Arrays

Material	Conductivity/ (Watts cm°K)
Copper	4
GaAs	0.45
Ga _{.7} Al _{.3} As	.14
Indium	.87
Type II Diamond	20

Considering $L = 250 \text{ } \mu\text{m}$, $W = 100 \text{ } \mu\text{m}$, and using the conductivity of copper, the analysis gives the temperature rise at the center of the array as 8.3°K for each watt dissipated in the active region. Assuming that the array operates at a voltage of 1.6V, an input current of 1.3 amps corresponds to a power input of 2 watts and a predicted temperature rise of 17°K . This temperature rise contributes to the catastrophic damage at current inputs greater than 1.3 amps. The temperature rise may be reduced by using a more effective heat sink. In particular, using type II diamond heat sinks rather than copper should reduce the temperature rise in the active region as much as five times (Table I) and make possible operation at much higher input current levels. The analysis above indicates that with type II diamond, operation at 4.5 amps (sufficient to produce 2 watts per facet) should cause only a temperature rise of 5.7°K . This is, of course, only an approximate analysis, since the thermal impedance of the electrodes and indium solder has been ignored. However, even if these decrease the effective thermal conductivity a factor of two, cw operation should not produce an unacceptable temperature rise.

It is important to point out that the expected improvement in array performance for diamond heat sinks is unique to the array geometry and is not a characteristic of single stripe diodes. Joyce and Dixon showed that for a single stripe-geometry laser there is no real advantage in using a diamond heat sink over copper because of the large amount of heat loss in the GaAlAs. However the array is a very different geometry, in which the heat sink plays a much larger role. The power output of the array relies ultimately on the ability of the heat sink to remove the heat as rapidly as possible. In this case, use of a diamond heat sink is imperative, for maximum power.

In estimating the ultimate power which can be produced from a quasi-broad-area laser array, there are two factors which must be taken into account. First, the ability of the heat sink to remove the heat generated, and secondly, the possibility of catastrophic damage because of the high optical field strengths. Using the results of Scifres et.al., it is possible to calculate that the temperature rise in their devices was about 16° . This is calculated from equation (1) using the fact that at 400 mWatts cw output from each facet, there was a reported total power conversion of 17%, meaning that 1.88 watts was dissipated in the device, which had a length of $250 \text{ } \mu\text{m}$ and a width of $100 \text{ } \mu\text{m}$. These dissipation power levels correspond to 40 mWatts per stripe per facet optical power, which is close to the maximum which can occur before catastrophic damage due to high optical field strengths. The highest cw powers reported are on the order of 80 mWatts for stripes twice as wide (Nakamura, Aiki, Chinone, Ito, Umeda, J. Appl. Phys. 49 4644 (1978)). Higher powers may be achieved, then, only by using more elements in the stripe

array, consistent with obtaining sufficient heat sinking. An estimate may be made using Eq. (1), increasing the array width W , and at the same time increasing the conductivity a factor of five by using diamond.

As an example, by extension of results for 10 diodes, an array of 25 diodes will dissipate $2.5 \times 1.88 = 4.7$ watts in an area of $250 \times 250 \text{ } \mu\text{m}$. This will cause a temperature rise of 25° if a copper heat sink is used. However, if diamond is used, the temperature rise is only -5°C . Using the fact that Scifres et.al. operated devices cw with calculated internal temperature increases of 16° , it is possible to estimate that this same temperature increase would exist for 75 stripes on a diamond heat sink leading to an array which would emit 3 watts out of each facet and which would dissipate 14 watts in an area $250 \times 750 \text{ } \mu\text{m}$. The operating current should be about 6 amps.

In addition, facet coating increases the optical damage level a factor of two and was suggested by Scifres et.al. as a method to increase their output powers a factor of two. The use of facet coatings and a high reflectance mirror on the back face will make it possible to obtain all the output power through the front face, a predicted power level of 6 watts with an overall efficiency of 34%. This same array should operate pulsed with 15 times the pulsed power observed by Scifres et.al. in a ten-diode array. Since they measured 2.1 watts/facet pulsed, pulsed power levels the order of 30 watts out of one face (with a high-reflectance coating on the back face) should be emitted from a 75-stripe array.

Finally, if low-duty-cycle operation is adequate, the limits to the high power operation are not those of the heat sink and the array may be made arbitrarily large, with output powers arbitrarily large. The operative parameter here would be the measured overall efficiency of 17% per facet. Expected improvements should increase the efficiency for light out one facet to perhaps greater than 50%.

C. Optimum Array Geometry

Since these devices operate as quasi-broad area, the stripes should be as close together as possible, consistent with good mode-definition. Scifres et.al. utilized a mask with $3 \text{ } \mu\text{m}$ stripes and a periodicity of $10 \text{ } \mu\text{m}$, and included ten elements in their array. They measured increased threshold and lower efficiency for larger separations between the stripes. The reason for this is the current spreading that occurs around any one stripe, out to distances typically $10 \text{ } \mu\text{m}$. This fact is well known, and is the reason that the most efficient lasers

have stripe widths of 10 μm . These lasers, however, do not operate in a single spatial mode, and therefore have poor brightness. The use of narrower laser stripes ensures single spatial mode operation, but causes the threshold current density to be higher, since current is wasted. An array of narrow stripes with a 10 μm separation utilizes the current which would be wasted for a single stripe, and results in low current thresholds, and high power operation.

Scifres, Burnham and Streifer (IEEE J. Quantum Electr. QE-15 917 (1979)) studied the output power and threshold as a function of stripe separation and their results are summarized in Figure 3. In the region studied, from stripe separations of 10 μm to 30 μm , the threshold increased linearly with separation from 0.45 amps to almost 1.5 amps. Clearly, at both smaller and larger spacings than studied, the threshold must approach constant values. The maximum value would be equal to the threshold for ten separate single stripe lasers. A dotted curve has been introduced to show a saturation of threshold power at 1.6 A corresponding to single stripe lasers with thresholds the order of 160 mAmps. The minimum value would be for the stripe separation to equal the stripe width, in other words, a truly broad-area contact. The broad-area threshold has not been reported, but should be about one third that of the threshold for a single 3 μm stripe, since current spreading causes approximately a factor of 3 decrease in the current density. A dotted line has been introduced at the minimum stripe separation end to show the ultimate broad-area threshold.

This data shows that a decrease in stripe separation below 10 μm will reduce the threshold. However, the area over which the power is emitted will also be decreased as the inter-diode spacing is decreased, so that heat sinking will be less effective. A complete optimization requires choosing the operating power level, determining operating efficiency and calculating the heating which results with cw operation. Such an optimization may increase the power output beyond that predicted in the last section; however, detailed calculations are beyond the scope of this report.

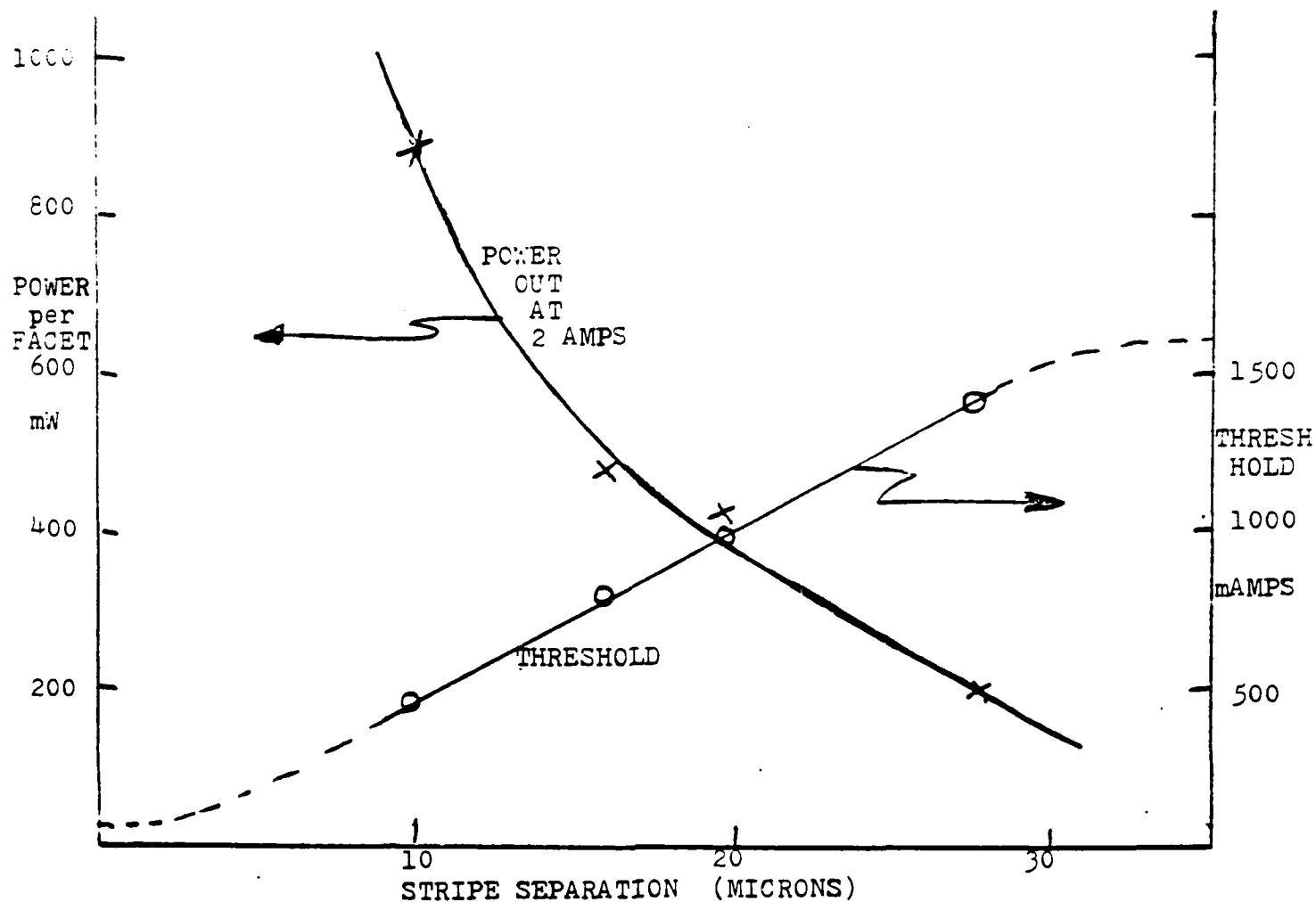


Figure 3. Maximum pulsed output power and threshold current as a function of stripe-separation for ten-element arrays of 3 μ m stripes. Data taken from Scifres, Burnham and Striefer, IEEE J. Quantum Electr. QE-15 917 (1981).

III. SEPARATE STRIPE LASER ARRAYS OPERATED CW

A. Introduction

Scifres, Streifer and Burnham (IEEE J. Quantum Electr. QE-15 917 (1979)) made a study of the output of an array of ten laser diodes, each with a stripe width of 3 μm , separated by differing distances, from 7 to 24 μm . They observed a strong increase of threshold current for increased stripe separation. This somewhat surprising result occurs because the narrow laser stripe geometry suffers current spreading. When the laser stripes are closely spaced, this current spreading causes quasi-broad area emission, with thresholds comparable to broad-area lasers. As the separation between the stripes is increased, a substantial amount of current spreads to inactive regions and is wasted. This means that if a laser array is not operated quasi-broad area, the stripes must be configured so that there is no wasting of current. At the same time they must be sufficiently separated to ensure necessary heat sinking. In this regime, the laser array can be thought of as an array of separate laser diodes. It will be expected that the most efficient laser geometries must be utilized to maximize the output power.

The crucial part of the problem of designing separate stripe laser arrays is the mechanism for optically coupling the lasers to ensure coherent output. The quasi-broad area laser arrays utilize directional coupling between adjacent laser stripes to produce a coherent output. The separate stripe laser arrays require more sophisticated coupling methods, which will be discussed in the next section. In this section we review those laser diodes which have low threshold and efficient operation, making them suitable for laser arrays.

B. Array Design

The ideal laser for a separate stripe array depends on the differential quantum efficiency, threshold current, damage threshold and heat sink characteristics. The output optical power can be written as

$$P = E_{\text{ev}} \eta_D (I - I_{\text{th}})$$

where E_{ev} is the energy of the laser photons in eV, η_D is the differential quantum efficiency, I is the drive current, and I_{th} is the threshold current. Thus, for current levels a few times threshold, both the threshold and quantum efficiencies must be considered.

However, the quantum efficiency must be defined in terms of optical radiation into a single mode, since ultimately in a locked array, only one mode should be oscillating. The best laser reported to date for this purpose appears to be a buried heterostructure reported by Henry, et.al., (IEEE J. Quantum Electronics QE-17 2196 (1981)). They report thresholds of 15 mAmps and differential quantum efficiencies of up to 60%. At a current level of 100 mAmps, the output was 28 mW/facet. An array of ten of these lasers, therefore, would deliver 280 mW/facet at one amp. This is comparable to the power out of the quasi-broad area device reported by Scifres, et.al. (300 mW at one amp).

This buried heterostructure utilizes a very large index change between the guiding region and cladding layers in the transverse direction. Normally, this would result in a highly multimode output because the optical waveguide is highly multimode. The authors attribute the single mode operation to surface roughness of the etched sidewalls causing severe scatter losses to all but the lowest order mode, since the scatter losses are proportional to the mode number squared. It was shown by the authors that widths from 2 to 3 μm are optimum for the operation of these devices.

Assuming that a separated array of these laser stripes can be suitably heat sunk, the only limitation to output power is facet damage. To improve the output power and reduce facet damage, window stripe lasers may be used. A study of such lasers has been recently reported by M. Ueno (IEEE J. Quantum Electr. QE-17, 2113 (1981)). He has shown output optical powers as high as 55 Mw for a stripe 3 μm wide, and 100 mW for 10 μm stripes, with external differential quantum efficiencies of 35 and 45%, respectively. The increase in facet damage threshold is at the slight expense, therefore, of higher threshold and lower differential quantum efficiency. A determination of whether or not it would be practical to pay this price to operate at higher optical power levels awaits more extensive study of the buried heterostructure lasers.

The laser stripes must be separated sufficiently far so that they are essentially thermally isolated. An understanding of this requirement can be seen by applying Poisson's equation to the spread of heat in the heat sink. The result is

$$T = \frac{qW}{\pi K} \sinh^{-1}(L/x) \quad (2)$$

where q is the heat per unit area which is introduced into the heat sink in a laser stripe of width W and length L . K is the

thermal conductivity in Watts/cm°C and x is the distance from the stripe. This expression is valid only for distances much larger than the width of the laser stripe, and midway along the stripe length. When the distance from the laser stripe is much less than the length of the stripe, the temperature rise can be expressed as $T = Q/\pi Kx$, where Q is the total power dissipated in the laser stripe in watts, and x is the distance from the laser stripe in cm. Consider operating individual laser stripes at 50 mW, with an overall efficiency of 30%. This will require an input of 150 mW per laser and then $T = 0.0114/x$. The temperature rise is 1° at 114 μ m from the laser stripe. Thus separations on the order of 100 μ m should be sufficient to allow the lasers to operate independently.

An example of a 100-element separate stripe array is shown in Figure 4; with the 100 μ m separation between elements, this array is 1 cm wide. Assuming that each stripe can be operated cw at 50 mWatts, the power which would be emitted from such an array is 5 watts per facet. If the stripe width can be increased to 10 μ m and single mode operation still be achieved, the measured cw powers of 100 mWatts per facet on the window stripe lasers make it possible to estimate 10 watts out per facet as a possibility for the separate stripe arrays. Estimates of operation at 15 times threshold current and differential quantum efficiencies of 60% indicate that the overall efficiency of operation should be 50%.

A calculation of the operating characteristics of an array of separate laser stripes was performed by R. A. Schmeltzer at The Aerospace Corporation in 1977 and published in four Aerospace Technical Reports (A77-50656, A77-50654, A77-50657 and A78-03553). He considered a 20-element array with spacings from 75 to 250 μ m. In addition, he included the fact that a more uniform temperature distribution between all the laser stripes can be obtained by using a nonuniform spacing between the stripe. Using the optimal spacing which includes bunching the diodes more closely together near the outside of the diode array, the junction temperature spread could be maintained within $\frac{1}{2}$ degree, while a uniform spacing caused a temperature spread range of 3° under the same conditions.

In this model, he found that 100 mW should be achievable per diode for spacings from 75 μ m and larger. However, at the smaller spacing, output power began to decrease when the drive levels were increased above this level. By contrast, however, at spacings of 250 μ m the arrays could be operated at optical output power levels of 200 mW per stripe before saturation took place (ignoring problems with facet damage).

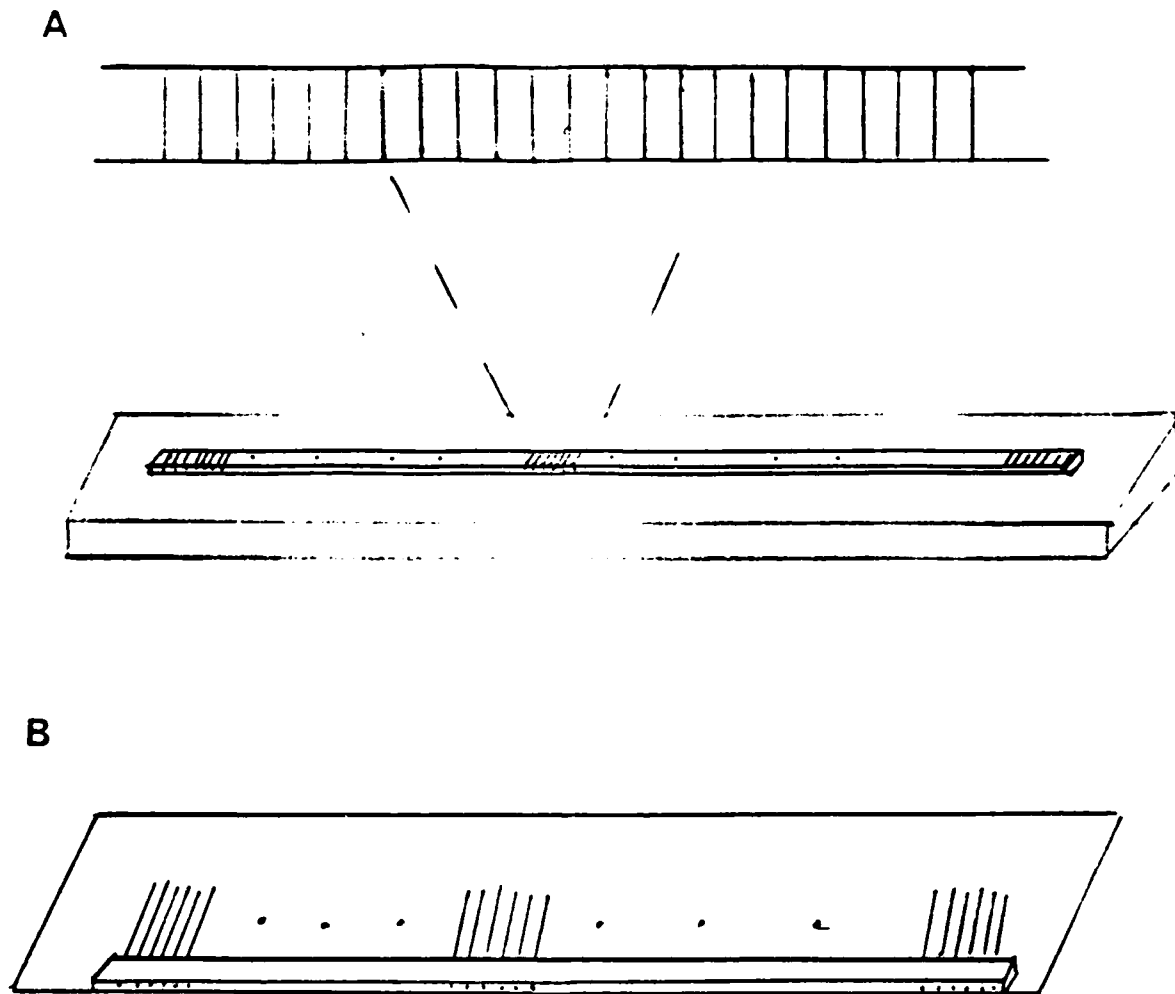


Figure 4. A hundred-element separate-stripe array. This device could utilize buried heterostructure and operate p-side up, so that individual stripes can be separately bonded, as shown in A, or the device could be operated p-side down, contacted to an insulating heat sink, such as diamond, with separate interconnections plated on the heat sink, as shown in B.

The practical limitation to such a diode array is the fact that large separations use up a great deal of real estate and place high requirements on the uniformity of layer fabrication. The extremely low threshold lasers described above require LPE, which is notably nonuniform, although a combination of MOCVD and LPE could be utilized, to minimize these problems. The maximum range of frequency difference which can be tolerated is only the order of 1 Å. In terms of temperature, this requires stabilization to 0.5°C.

Whether the quasi-broad-area or separate stripe array will be the most practical depends on a number of factors. First, the quasi-broad area device has advantages since it utilizes the minimum real-estate and also has internal cross-coupling between stripes which should automatically lock the diodes together. However, separate operation or tuning of the individual stripes is not possible. We will see in the next section that the conditions on locking are very stringent, and may more readily be met if the stripes may be individually pumped. For example, even if one of the stripes has a higher threshold than the others, a uniform optical output can be maintained if it can be separately pumped at a higher current level. When all the stripes are pumped in parallel, that element could not be individually optimized.

The second disadvantage of the quasi-broad area is the severe heat-sink requirements, including the need to use diamond. Reliable operation at optical power levels as high as predicted in the previous section may be difficult to achieve in practice. In addition, separate contacting can be useful to tune the direction of emission of the array or to increase the region of linearity of the output as discussed below. This will not be possible with the quasi-broad-area array.

The separate stripe laser array has neither of these disadvantages; the stripes may be individually contacted and the heat-sink problem is no more severe than for single stripe lasers. However, the penalty for using this technology is the large amount of real-estate and the need for more sophisticated techniques to phase-lock the individual laser stripes.

IV. LOCKING OF INDIVIDUAL STRIPES

In order that the power from the separate stripes of the laser array combine coherently and produce the largest amount of power, it is necessary for the stripes to be phase-locked. That is, to operate at the same frequency and locked in phase. Locking of several lasers requires either cross-coupling, or selection of appropriate phases by an additional mirror.

A. Locking by Cross-Coupling

Cross-coupling is the mechanism of locking the stripes which occurs in the quasi-broad area laser arrays. It was shown many years ago by Bassov that cross-coupled lasers will be locked together if they differ in frequency by less than

$$\frac{\delta\nu}{\nu} < \frac{\lambda\Gamma}{2\pi L}$$

where Γ is the fractional exchange of energy between adjacent lasers. In an Aerospace Corporation Technical Memo 77(7671)-2, Garmire has shown that this equation can be used to estimate the amount of directional coupling between two laser stripes. It is shown that locking requires that the lasers must have a wavelength difference less than

$$\frac{\Delta\lambda}{\lambda} < \frac{0.3\lambda^3 L}{8\pi^3 n^2 S^4} \quad (3)$$

where L is the length of the laser and S is the separation between the laser stripes. It was assumed that the optimum stripe-width was chosen.

Using diode lengths of 250 μm and a separation of 7 μm , corresponding to the experimental parameters of Scifres, the lasers must be within .05 \AA for directional coupling to lock them. This is an unrealistic expectation since the temperature variation of the wavelength is 3 \AA per degree, implying that the individual stripes would have to be within .01 $^\circ\text{C}$ for locking to take place. Scifres, et.al. were aware of the inability of directional coupling to be sufficient to lock the lasers, so they introduced additional coupling with an electrode stripe connecting the two lasers. This geometry is shown in Figure 5. The amount of coupling introduced by this coupling electrode has not been estimated; however, experimental results indicated that it did, indeed, lock the lasers.

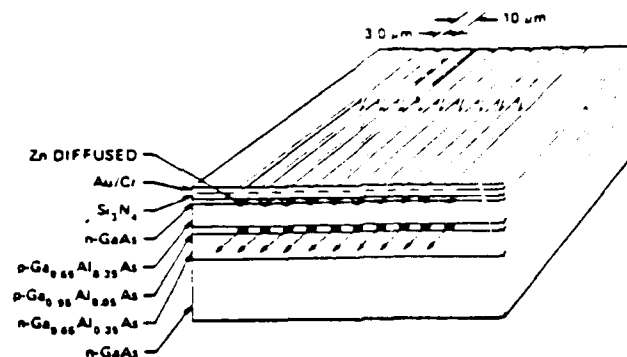


Figure 5. Schematic of a coupled multistripe laser (CMS) reported by Scifres, Burnham and Streifer, IEEE J. Quantum Electr. QE--15, 917 (1979) Notice the connecting current paths to couple light from one stripe into the adjacent one.

Because of the very strong dependence of equation (3) on the separation between the laser stripes, the cross-coupling can be strongly enhanced by decreasing the separation between the stripes to 3 μm . This would result in a structure with 3 μm electrodes separated by 3 μm electrodes. With this geometry laser stripes with a frequency difference of somewhat more than 1 A would lock.

This analysis shows that the choices for locking quasi-broad-area arrays are either to introduce cross-coupling electrodes, as demonstrated by Scifres, et.al., or to fabricate structures with 6 μm periodicities; that is, 3 μm electrodes and 3 μm spacings. These narrow spacings also have the advantage of lower threshold, as shown in Section II.

For the separate stripe laser arrays, other methods must be introduced to lock the lasers together. These include injection locking by a master oscillator, locking by phase-selecting reflectivity and locking by external cross-coupling.

B. Injection Locking

The use of a master laser oscillator to lock an array of slaves has been studied theoretically at The Aerospace Corporation. It was shown by Tavis, ATM 77(7688)-1, that in steady-state the slave lasers could be locked to the injection laser if the frequency difference was less than

$$\frac{\Delta\lambda}{\lambda} < \frac{\sqrt{P_o/P_i}}{2Q}$$

where P_i is the injected power and P_o is the slave free running power returned to the cavity by the mirror at the injection port. Consider the power P from one laser used to injection-lock N lasers each of output power P . The power injected into each diode is $(1-R)P/N$ while the internal power returned to the cavity from the injection cleave is $PR/(1-R)$. Thus the power ratio is

$$P_i/P_o = \frac{(1-R)^2}{NR}$$

and

$$\frac{\Delta\lambda}{\lambda} < \frac{1-R}{2Q\sqrt{NR}}$$

is the requirement for locking. Now, Q is the cold-cavity Q and is given by

$$Q = \frac{2\pi n_o L}{\lambda} (2\alpha L - \ln R)^{-1}$$

Typical numbers give $Q = 2500$. Considering $R = 0.3$, we obtain

$$\frac{\Delta\lambda}{\lambda} = \frac{8 \times 10^{-5}}{\sqrt{N}}$$

It is interesting to notice that even if $N = 1$, the lasers must be within 0.7\AA before the master can lock the slave. This shows that cross-coupling is much more effective than injection locking in producing an array of locked oscillators.

Further studies at The Aerospace Corporation indicate that noise may have a large effect on injection-locked devices (ATR-78(7671-02)-2 by M. T. Tavis, and ATR-78(7671-02)-1 by Tavis and Stoll). For these reasons, and because of the impracticality of fabricating a master-slave geometry, it is expected that cross-coupling and apodization techniques will provide more effective locking for the laser array.

C. Locking by Phase-Selective Reflectivity

This technique utilizes an optical element which reflects light back into the laser array only when all the elements of the array are locked in phase. Such an element was first used in GaAs by placing a three-diode array in an external cavity (E. Phillip-Rutz) and using an output mirror which provided reflectivity only at those positions which ensure phase-locked operation. How this works can be seen by referring to Figure 6. When the laser diodes operate in-phase, the far-field intensity pattern has peaks and nulls, as shown by the solid line in the figure. When the laser diodes are not locked, their power combines, without interference, resulting in the intensity distribution shown by the dotted lines. By using a mirror which reflects only at the maxima of the in-phase diffraction pattern and not where the in-phase intensity pattern is a minimum, the array is forced to operate in-phase to achieve the lowest threshold. The principle is similar to that of mode-locking of a laser to produce short pulses using a saturable absorber. It has been shown that, if the loss is reduced when all modes oscillate in phase, then the laser will choose to oscillate in that manner (Garmire, Yariv, IEEE J. Quantum Electr. QE-3 222 (1967)).

If a many-diode array is used, with each diode separated by $100\text{ }\mu\text{m}$, the diffraction pattern will look like that shown in Figure 6b. By providing reflectivity only at the peaks, in-phase operation will result.

A particularly promising technique for providing selective reflection only to those angles which correspond to in-phase laser emission is the use of holographic optical elements. A hologram can be thought of as a stationary phase-conjugator. That is, when fabricated appropriately, the light can be

Figure 6a. Three-diode array. When phase-locked, the emission pattern looks like that of a three-slit interference pattern. If not phase-locked, the dotted line emission occurs. Reflectivity is provided only for maxima in the phase-locked interference pattern

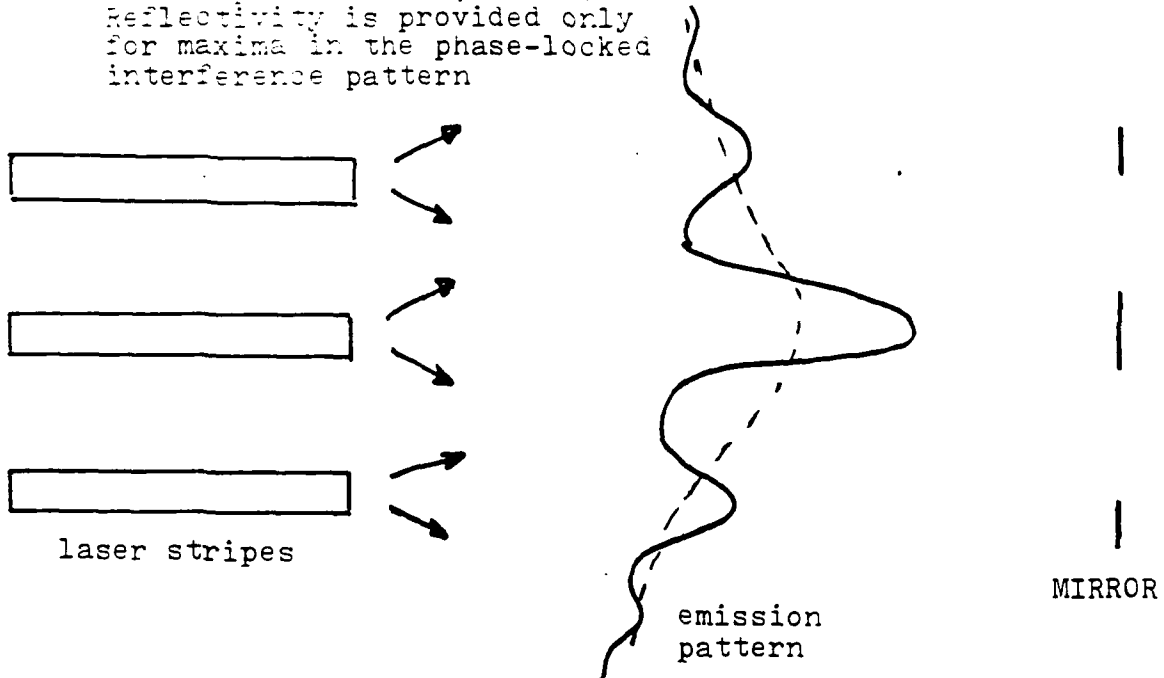
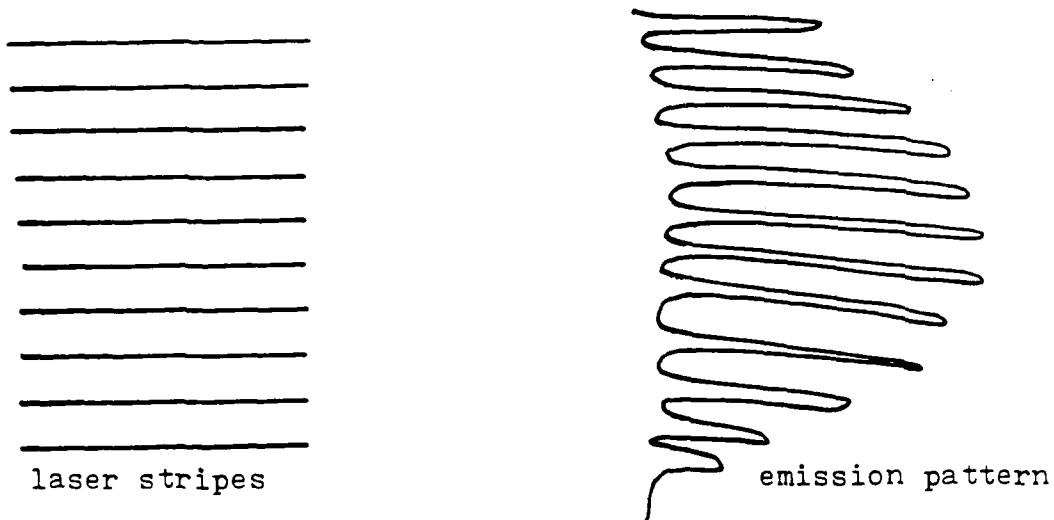


Figure 6b. Multi-diode array with elements spaced 100 μm apart.



retro-reflected exactly back to those elements from which it originated. Thus, if an external mirror is a holographic element, then only in-phase laser oscillation for each element will experience the reflectivity from this third mirror and have low thresholds.

Since the bulk-optics or holographic approach may be relatively awkward to implement, we consider also integrated optics techniques to achieve the same result. One technique which has been developed includes an apodizing element called a Distributed Bragg Deflector, which is shown in Figure 7. This uses a grating to cause a distributed deflection over a distance which may be many times the width of the individual beam. This distributed deflection acts as a collimating beam-expander, and has been discussed both theoretically and experimentally ((Stoll, Soady, IEEE Trans. Integ. Circuits, 1980). The ability of the DBD to assist in phase-locking an array of laser stripes is shown in Figure 7b, in which an array of inputs, a cascade of DBD gratings and an additional grating retro-reflector mirror are appropriately combined. H. Stoll has shown (The Aerospace Corporation, final report on Contract No. 77G-101820-000) that a DBD cascade may be designed which combines each laser stripe into a single well-formed beam. The inverse must also be true, then, using the concepts of reciprocity. This means that when the beam is retro-reflected by the final mirror, it must also be deflected back into the individual laser stripes. Such successful retro-reflection will only occur for the appropriate phase relation between all the laser stripes, and this forms the mechanism for locking the lasers together.

Since the concept under consideration is an integrated optics device, it is necessary to use a DBR laser, rather than cleaved Fabry-Perot lasers. The results of experimentation at The Aerospace Corporation have shown that DBR lasers favor TE polarization, but that the reflectivity of the DBD at 90° is zero for this polarization (E. Garmire, Aerospace Technical Report SD-TR-81-18). This means that the geometry which must be considered will include deflection by a different angle. An example of a possible geometry is shown in Figure 8. In this design, retro-reflection is shown to occur from a grating rather than from a cleave, as the former is more compatible with the planar technology of integrated optics. The retro-reflecting final mirror will be the same period as the retro-reflector used with the DBR laser.

Detailed calculations have not yet been performed on this device, however, the 135° DBD beam expander has been demonstrated. There are no experimental results as yet on the DBD cascade, but work is underway at the Aerospace Corporation at the present time.

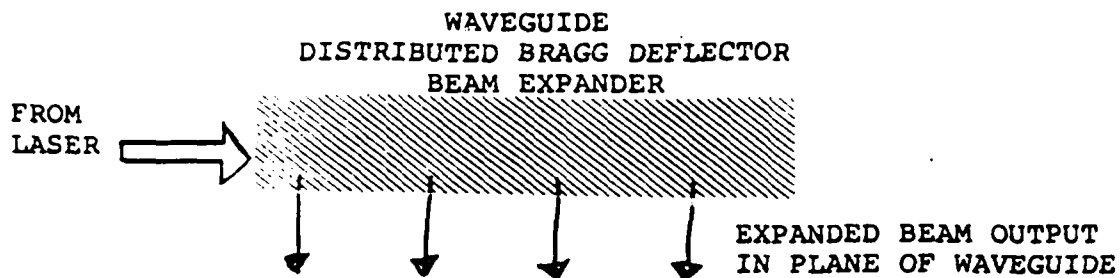


Figure 7a. Distributed Bragg Deflector (DBD), which deflects and expands the beam from a single stripe-geometry laser, within the plane of the waveguide.

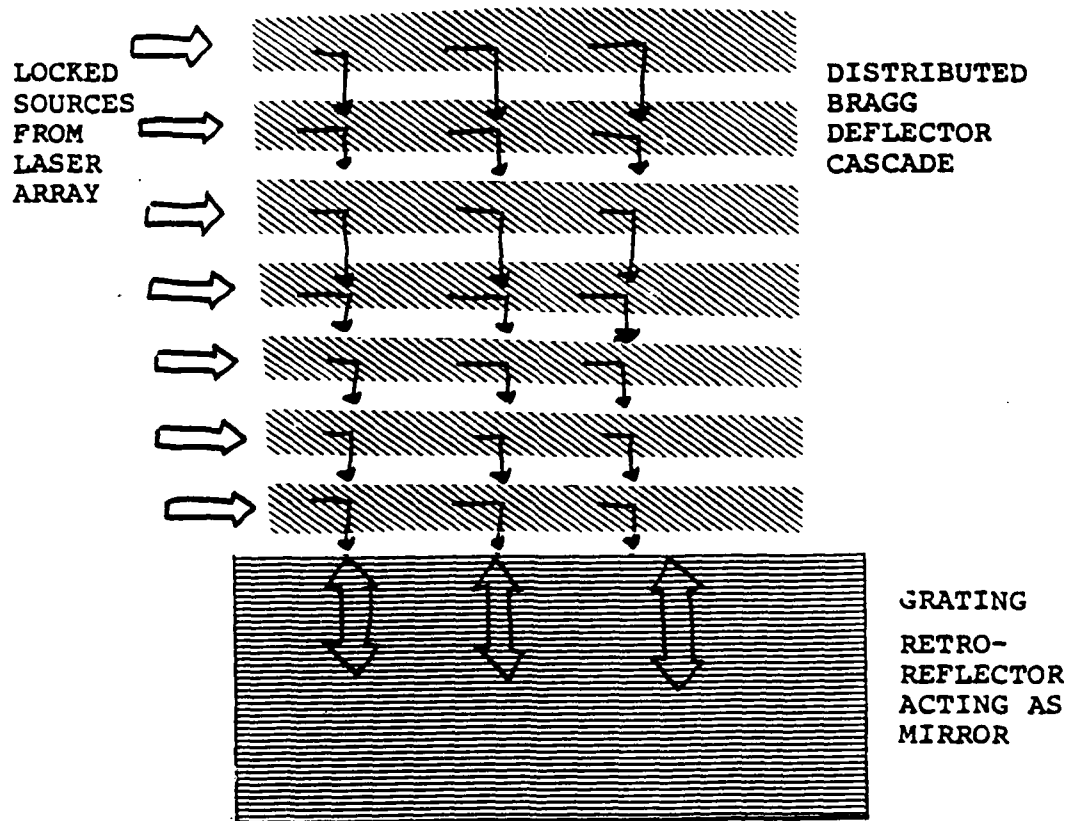


Figure 7b. DBD cascade and grating retro-reflector used to deflect and expand a laser array output. The additional grating mirror is to provide phase-selective reflectivity, in order to phase-lock the array.

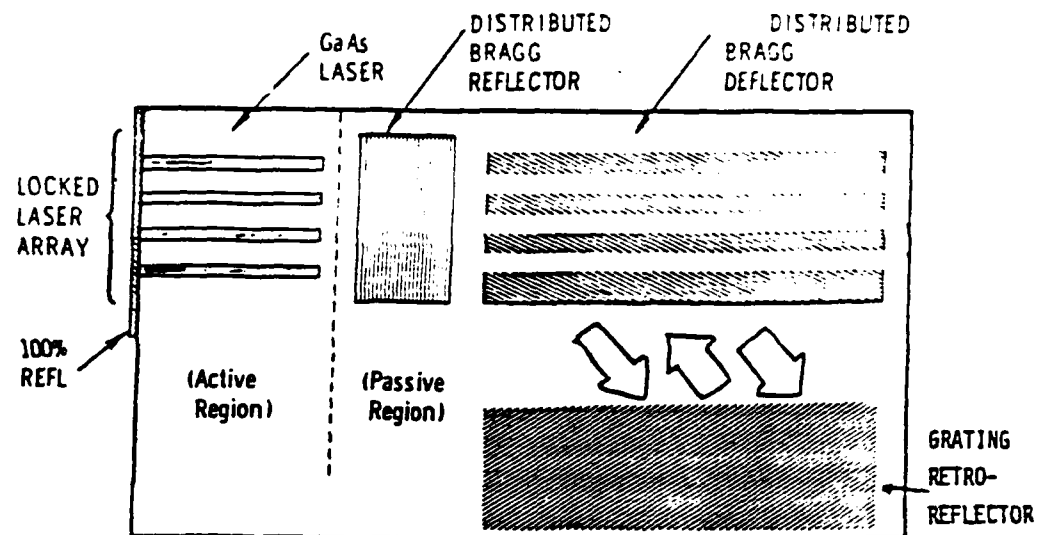


Figure 8. Integrated optics design to phase-lock a laser array. This design consists of a DBR laser array + DBD cascade + phase-locking grating retro-reflector.

V. OUTPUT BEAM FORMING

Even when all elements of the laser array are in phase, the output is not a single beam. In the case of the quasi-broad area devices, the far field patterns had two lobes separated in angle by about 7° , each with a width of about 2° . The farther apart the stripes in the array, the more lobes there will be in the far field. For this reason it is necessary to introduce optical elements to apodize the far-field.

The integrated optics device discussed above already included a beam expander for apodization by utilizing the DBD. In order to have a collimated beam, it is necessary to combine this with a grating output coupler which will reflect light out of the waveguide into free-space. An example of beam forming for a single laser stripe is shown in Figure 9. The output coupler is a well-known device and recent experiments at The Aerospace Corporation (E. Garmire, et.al., in publication) show that close to 100% efficiency can be obtained. Measured divergence angles have been less than 2 mrad. The design shown in Figure 9 can be generalized to produce a collimated output from a high power laser array by including a DBD cascade and a phase-selecting retro-reflector. The final design for the integrated optics high brightness laser source is shown in Figure 10.

A second technique which should be investigated is the use of holographic optical elements to collimate and apodize the multi-directional output of the laser arrays. Preliminary theoretical work by the author indicates that efficient coherent power combining and output beam forming should be possible using holographic techniques.

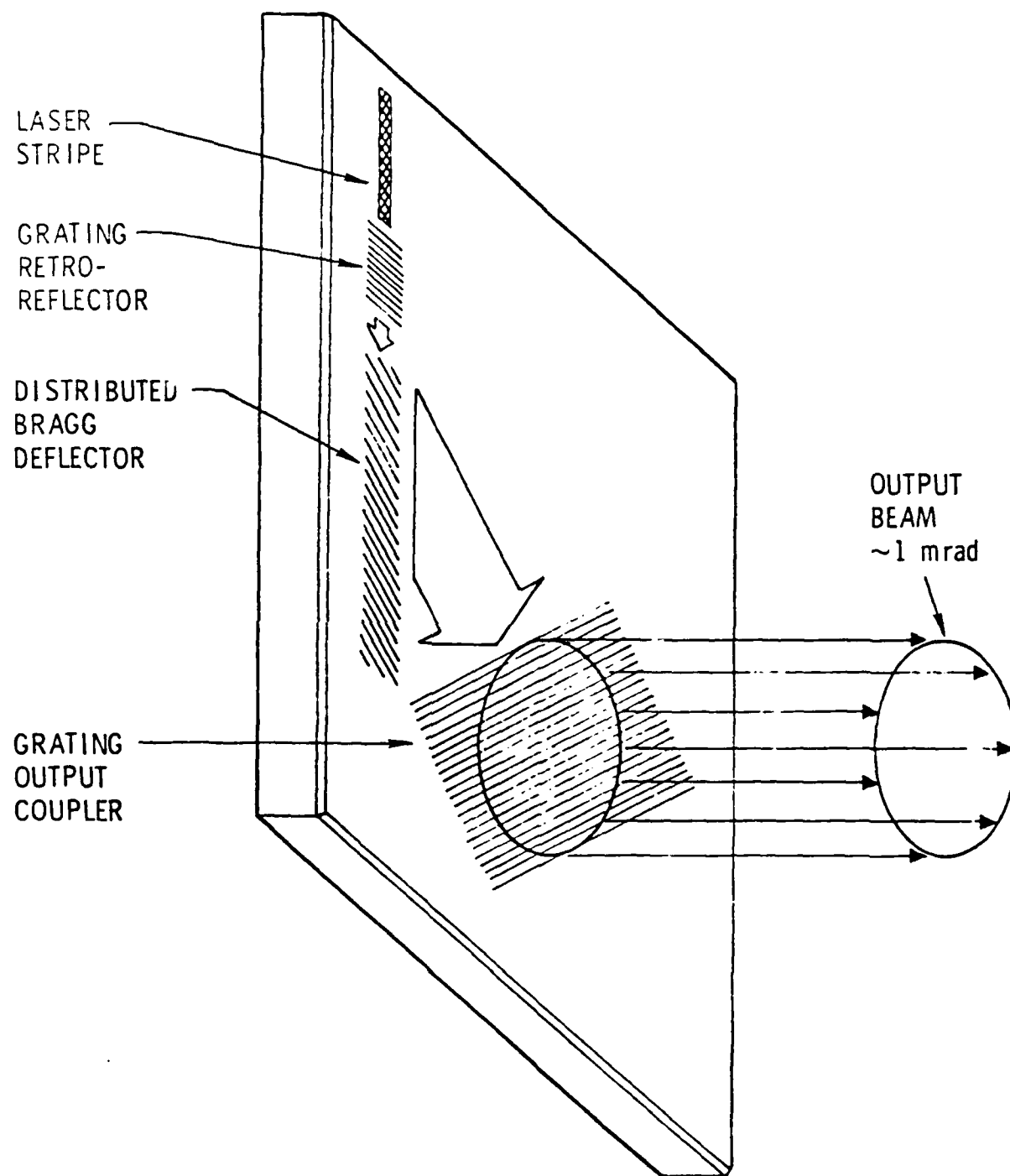


Figure 9 Low beam-divergence laser. The gratings act as an integrated optical spatial filter and telescope.

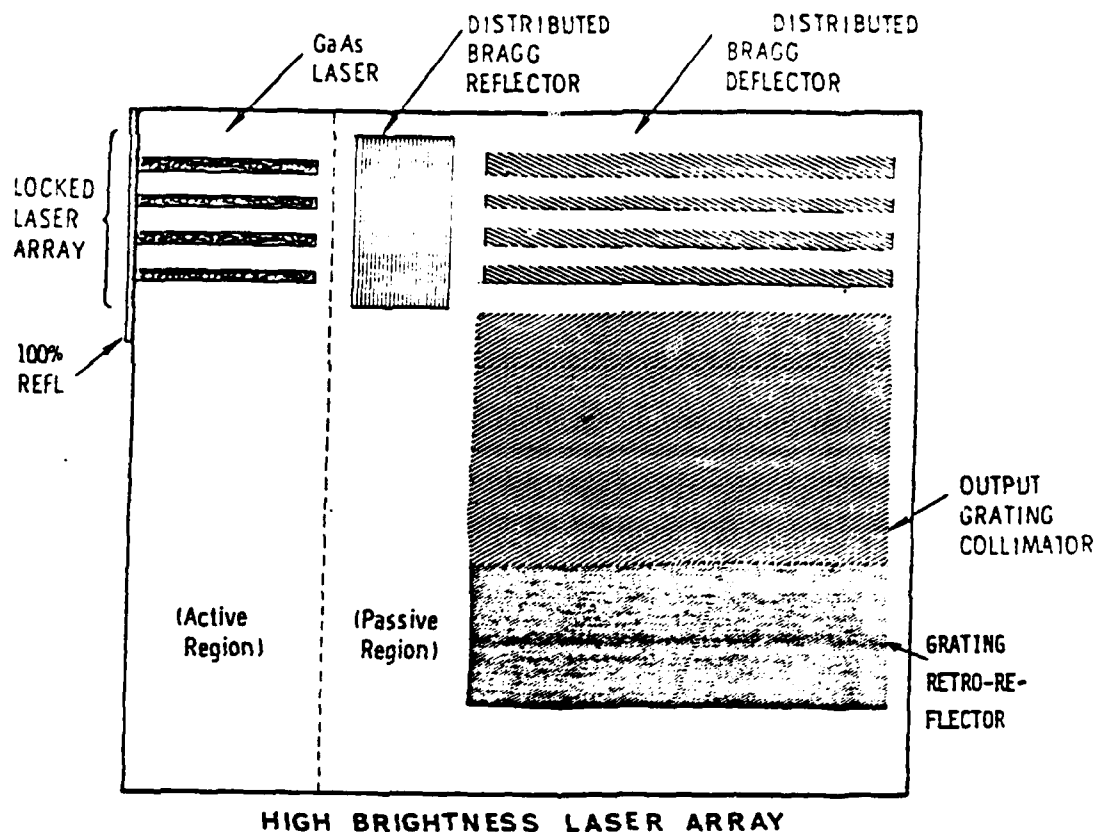


Figure 10. Design for high brightness laser array. Beam is emitted normal to the plane of the figure. Although an array of only four lasers is shown, the design may be scaled up to larger arrays. Design studies have shown estimates of powers in excess of 1 watt in 1 mrad may be produced by such an array.

VI. APPLICATIONS

The previous sections have described the use of multi-element semiconductor laser arrays to achieve cw powers on the order of six watts and pulsed powers on the order of 30 Watts, with efficiencies approaching 50%, and beam collimations on the order of milliradians. Such a source, operating anywhere from 0.75 to 1.55 μm , would have profound applications.

First, it would replace the Nd:YAG laser in many of its uses since the semiconductor laser has much higher efficiencies. This would include laser designators, laser spot welding, etc. In addition, the ability to efficiently modulate the GaAs lasers makes possible a large diversity of applications in optical communications and optical signal processing. For example, satellite-to-satellite space communications in the MBit to GBit regime will be possible with lasers operating in the range of 0.5Watt average power. Indeed, if 10Watts could be provided by a GaAs laser, it may even be possible to have space-to-ground optical communications with high security.

The secure aspects are also important for through-the-atmosphere point-to-point communications where it is not possible to string optical fiber. A milliradian beam divergence laser on the order of a watt will make such communications much more practical.

Optical signal processing applications often require lasers with a wide dynamic range of linearity. While the inherent linear output vs. applied current of a semiconductor laser is usually on the order of a factor of 10, use of a separately contacted laser array can make it possible to multiply the linear range by the number of elements. Thus a hundred-element array should have a linear range of a factor of a thousand. This particular application will require proper apodization so that the beam quality does not depend on the number of elements which are operating.

Optical recording and playback of optical discs uses semiconductor lasers, and places stringent requirements on beam divergence and output power. The use of a laser array, properly apodized, should increase the speed with which optical discs can be played back, and more importantly, a semiconductor laser array may have sufficient power to write, as well as read the optical discs. Thus a single machine could have read/write capability. A related application is that of optical printing, and is one reason that Xerox Corporation is a pioneer in semiconductor laser arrays.

Optical fiber communications will be possible over longer range if more optical power is available at the input to the fiber. This is another application for laser arrays. The higher bandwidth and greater range provided by laser arrays will be useful both for multimode and single mode fiber applications.

VII. STATE-OF-THE-ART

Preliminary demonstrations of laser arrays show their versatility, and relative ease of fabrication. The arrays demonstrated by Xerox Corporation are within the range of a number of research establishments, including University of Southern California, which has available both LPE and MBE laser material, and within a year should have available MOCVD material. Laser array electrodes, with 3 μ m width and 3 μ m separation, are within the current state-of-the-art for electrode fabrication. It should be only a one-to-two year project to demonstrate larger arrays on diamond heat sinks with substantially more power than Xerox has demonstrated.

The locking and apodization techniques require integrated optics or holography and must be developed. Preliminary investigations are underway at The Aerospace Corporation. The development of a full-scale High Brightness Laser will be a multi-investigator project and will probably take several years. Although initial research has been done on LPE material, good quality MOCVD or MBE material is a requirement for the reproducible grating fabrication which is needed to complete the High Brightness Laser.

The integrated optics apodized laser array begins with a DBR laser - a structure which includes both the laser and a grating for retro-reflection - or a distributed feedback laser. Although such structures have been operated cw, they are difficult to make with current technology and are not routinely available. With the new availability of high quality and reproducible material with MOCVD and MBE, it is expected that fabrication of such integrated optics lasers will become routine. Only when this is accomplished will it be possible to fabricate the high brightness laser with any reliability. The first step in research toward the high brightness laser, then, is the development of reproducible cw DBR or DFB lasers, using MBE or MOCVD.

An interesting alternative to a fully integrated high brightness laser is the fabrication of the grating DBD, output coupler and phase-selective reflector all on a glass waveguide, which may be butt-coupled to a laser array. This represents a hybrid integrated optics technology, but has the advantage of short-term payoffs. The development of glass apodization integrated optics could occur in parallel with the development of a laser array, and would result in a powerful, collimated laser output in as little as three years.

Finally, the possibility of holography to provide apodization and phase-selective reflectivity should be pursued experimentally. Very little research has been completed on holographic optical elements. A separate project to study the use of holography to apodize the output of a semiconductor laser would be a valuable addition to the emergence of practical semiconductor laser for opto-electronic applications.

THE POTENTIAL OF USING AN XEF LASER
AND AMMONIA RAMAN CELL
FOR
UNDERSEA COMMUNICATION

28 JANUARY 1983
P. HAMMERLING
PRINCIPAL INVESTIGATOR

THIS RESEARCH WAS SPONSORED BY THE
DEFENSE ADVANCED RESEARCH PROJECTS AGENCY
UNDER ARPA ORDER No.: 3710
CONTRACT No.: MDA-903-82-C-0376

THE VIEWS AND CONCLUSIONS CONTAINED IN THIS DOCUMENT
ARE THOSE OF THE AUTHORS AND SHOULD NOT BE INTERPRE-
TED AS NECESSARILY REPRESENTING THE OFFICIAL POLICIES,
EITHER EXPRESS OR IMPLIED, OF THE DEFENSE ADVANCED
RESEARCH PROJECTS AGENCY OR THE UNITED STATES
GOVERNMENT.

THE POTENTIAL OF USING AN XEF LASER AND AMMONIA RAMAN CELL
FOR
UNDERSEA COMMUNICATION

P. HAMMERLING

Efficient conversion of XeF radiation ($\lambda = 353 \text{ nm}$) by a second Stokes shift in hydrogen into blue-green light ($\lambda \sim 500 \text{ nm}$) has been demonstrated recently.¹⁾ In this note we wish to discuss the potential advantage of using ammonia instead of hydrogen in the Raman cell.

The attenuation of light in various classes of sea water as a function of wave length is given in Jerlov's book.²⁾ Table I compares attenuation factors for various depths at $\lambda = 500 \text{ nm}$ and $\lambda = 460 \text{ nm}$. It is seen that there can be a great advantage for underwater communication or hydrography³⁾ in using the shorter wave length, particularly at depths in excess of 200-300 m. This point has also been discussed at a recent meeting.⁴⁾ Efficient generation of 459.3 nm radiation has been shown using an XeCl ($\lambda = 308 \text{ nm}$) laser and a single Raman shift in a lead vapor.⁵⁾ This latter method has the additional advantage of being in coincidence with the narrow band QLORD (quantum-limited optical resonance) detector.⁶⁾ In order to see whether

similar behavior might be attained with XeF using a different Raman medium, several other candidates were identified from standard references^{7),8)} and are listed in Table I. It is seen that several gases bracket the region of interest, the most practical candidate being ammonia (NH₃).

The cross-section, relative to that of nitrogen, for the Raman scattering of 351 nm radiation from NH₃ has been measured by Hochenbleicher in an unpublished dissertation quoted in Reference 8, which also gives the absolute N₂ cross-section:

$$\frac{d\sigma}{d\Omega} = 6 \times (243 \times 10^{-32}) \text{ cm}^2/\text{sr}$$

The Raman (first Stokes) gain is given by

$$g = \frac{\lambda_s^2}{h\nu_s} \frac{N}{\pi\Delta\nu_R} \left(\frac{d\sigma}{d\Omega} \right)$$

Using $\lambda_s = 397.7 \text{ nm}$ and the above cross-section,

$$g = \frac{0.395}{\Delta\nu_R} P_{\text{atm}} \text{ cm/W}$$

where P_{atm} is the pressure in atmospheres and $2\Delta\nu_R$ is the Raman linewidth (FWHM) of NH₃.

The latter quantity is not well known, as far as can be ascertained.⁹⁾

Assuming, $\Delta\nu_R = 0.10 \text{ cm}^{-1}$ independent of pressure and $P = 10 \text{ atm}$, results in

$$g = 1.3 \times 10^{-9} \text{ cm/W}$$

Thus using a typical value of 10 MW/cm^2 for the incident laser flux and a 10m Raman cell yields an exponential gain of 13. This example is given for

illustrative and motivational purposes only. The Raman gain in ammonia, relative to that in hydrogen is:

$$g_{\text{NH}_3} = 1.5 (\Delta\nu_{\text{R H}_2}) / (\Delta\nu_{\text{R NH}_3}) g_{\text{H}_2}$$

Single photon photochemistry is not expected to be a problem since the XeF photon is about 1.5 ev below the dissociation level of ammonia and does not coincide with any electronic transition.¹⁰⁾ The vibrational relaxation time of NH₃ at ~S.T.P. is 0.4 μsec.¹¹⁾ However, the latter is based on older measurements and needs a more careful look.

In summary, the potential system's advantage of operating with XeF at ~460 nm would appear to justify an experimental and theoretical effort in seeing if NH₃ could be adapted to this purpose.

λ (nm)	$L \equiv e^{-1}$ depth (m)	Attenuation factor, A, at depth l			
		$l = 100$ m	200 m	300 m	500 m
460	55	6	38	234	8,874
500	35	17	303	5,279	1.6×10^6

Table I. Attenuation factor $A \equiv \exp(l/L)$ as a function of depth and wavelength for Jerlov Class I water.^{2),4)}

λ_v (cm ⁻¹)	H ₂	CH ₄	NH ₃	C ₂ H ₂
	4,155	2,917	3,337	3,374
XeF:				
$\lambda = 353$ nm	499.5	444.6	461.8	463.4
$\lambda = 351.1$ nm	495.7	441.5	458.5	460.1

Table 2 Second Stokes wave-lengths in various gases as a function of XeF input wave-length

REFERENCES

- 1) H. Komine, E. Stappaerts, S. J. Brosnan and J. B. West, Appl. Phys. Lett. 40, 551 (1982)
- 2) N. G. Jerlov, Marine Optics (Elsevier, N. Y. 1976) p. 141
- 3) M. B. White, Lasers and Applications, 1, 39 (1982).
- 4) R. N. Keeler and J. B. Marling, "Technological Options for Laser Submarine Communications", presented at the American Optical Society Meeting Eximer Lasers, Lake Tahoe, 12 January 1983.
- 5) S. J. Brosnan, H. Komine, E. Stappaerts, M. J. Plummer, and J. B. West, Opt. Lett. 7, 154 (1982).
- 6) J. B. Marling, J. Nilson, L. C. West, and L. L. Wood, J. Appl. Phys. 50, 610 (1979).
- 7) Physics Vade Mecum, H. L. Anderson, ed. (American Institute of Physics, N. Y., 1981).
- 8) H. W. Schrötter and H. W. Klöckner "Raman Scattering Cross-Sections in Gases and Liquids" in "Raman Spectroscopy of Gases and Liquids", A. Weber, Ed. (Springer-Verlag, Berlin, 1979).
- 9) S. Pinter, Moscow University Physics Bull. #3, 26 (1966) states that in the range 1-16 atm. the NH_3 line width was less than their instrumental resolution of 0.2 cm^{-1} .
- 10) G. Hertzberg, Molecular Spectra and Molecular Structure III Electronic Spectrum and Electronic Structure of Polyatomic Molecules (D. Van Nostrand Co., Inc., N. Y. 1966).
- 11) J. N. Bradley, Shock Waves in Physics and Chemistry, (Methuen and Co., Inc., London 1962) p. 339.

STIMULATED PHENOMENA
IN HIGH INTENSITY LASER INTERACTIONS:
APPLICATIONS TO RAMAN AMPLIFIERS
AND
ATMOSPHERIC PROPAGATION

PREPARED BY

S. JORNA

LA JOLLA INSTITUTE

P. O. BOX 1434

LA JOLLA, CALIFORNIA 92038

MAY 1983

THIS RESEARCH WAS SPONSORED BY THE
DEFENSE ADVANCED RESEARCH PROJECTS AGENCY
UNDER ARPA ORDER NO: 3710
CONTRACT NO.: MDA-903-82-C-0376

THE VIEWS AND CONCLUSIONS CONTAINED IN THIS DOCUMENT ARE THOSE OF
THE AUTHORS AND SHOULD NOT BE INTERPRETED AS NECESSARILY REPRESENTING
THE OFFICIAL POLICIES, EITHER EXPRESS OR IMPLIED, OF THE DEFENSE
ADVANCED RESEARCH PROJECTS AGENCY OR THE UNITED STATES GOVERNMENT.

ABSTRACT

The beam quality of an intense laser beam can be affected by various stimulated phenomena in which a property of the medium is changed by the radiation field and in turn changes that field. Macroscopically the laser-medium coupling changes and the dielectric constant through absorption (stimulated thermal Brillouin scattering and stimulated thermal Rayleigh scattering) and through electrostriction (stimulated electrostrictive Brillouin scattering). At sufficiently high irradiances these phenomena can apply to, and hence place limits on usable laser power, Raman amplifiers and laser propagation through the atmosphere.

For pulses which have a duration comparable to the acoustic transit time across the beam, absorption may lead to heating and hence to thermal blooming. As the pulse is shortened thermal blooming is ameliorated and stimulated Brillouin scattering is more likely to affect the beam quality. Stimulated thermal Brillouin scattering may be suppressed in Raman amplifiers by rendering the laser pulse short compared to the vibrational-translational relaxation time of the Raman gas. For hydrogen this relaxation time, τ_r say, is $\tau_r = 10^{-3}/p$ sec, where p is the gas pressure in atmospheres. Typically Raman amplifiers using hydrogen operate at 10 atmospheres so that STBS can largely be suppressed by choosing a pulse length much less than 100 μ sec. In this event SEBS would be expected to dominate.

To determine their likely significance, analytic expressions are derived for the steady-state gain of these acoustic-optic phenomena. The

amplitude equations for the transient phase of instability development have also been solved. Numerical estimates for a 10 atmosphere hydrogen Raman amplifier and for the propagation through the atmosphere are given in the last section of this report.

TABLE OF CONTENTS

	<u>Page</u>
I. Introduction	
II. Activity Summary	
1. Utilization of the External Tanks of the Space Shuttle	
2. "Bistable Device for Optical Signal Processing", E. Garmire, LJI-R-82-226 . .	
3. "Potential of Very Large Arrays of Semiconductor Laser Sources", E. Garmire, LJI-R-82-217	
4. "The Potential of Using and XeF Laser and Ammonium Raman Cell for Undersea Communication", P. Hammerling, LJI-R-83-226	
5. "Stimulated Phenomena in High-Intensity Laser Interactions: Applications to Raman Amplifiers and Atmospheric Propagation", S. Jorna, LJI-R-83-237	
6. May 20, 1983 Briefing to DARPA on	
a) Developing High-Power Solid-State Lasers", M. Bass	
b) "Diode Pumping of Solid-State Lasers", E. Garmire, LJI-R-83-240	
7. "Recent Laser Studies", Ed. by P. Hammerling LJI-LJ-83-249	
i. X-Ray Laser Studies (J. McIver, S. Rockwood, K. Boyer)	
ii. "Direct Nuclear Pumped Lasers" M. O. Scully	
8. "Laser Detection of Trace Contaminants in the Atmosphere, J. Wiesenfeld, LJI-LJ-83-251	

Page

9.	Miscellaneous Activities	
III.	Reports	
	Items 2-8 Above.	

1. Introduction

To assess the potential problems caused by stimulated phenomena in Raman amplifiers and with laser beam propagation through the atmosphere, we have derived expressions for the gain of the more important of these. We have singled out stimulated Brillouin scattering and stimulated Raman scattering. Stimulated Brillouin scattering is driven by the dependence of the dielectric function on density and temperature through the quantities $(\partial\epsilon/\partial\rho)_T$ and $(\partial\epsilon/\partial T)_\rho$. Thus, heating through absorption and the direct density changes by electrostriction can drive stimulated Brillouin scattering. When the acoustic frequency is small compared to the Brillouin frequency, stimulated Raman scattering can occur driven by absorption.

Solutions are obtained for the transient, or initial value, problem by a novel procedure which is more direct than the cumbersome Riemann method. For laser pulses longer than the relaxation times, expressions are given for the steady-state gain.

2. Formulation of the Basic Equation

In what follows, we assume that the medium's response to the passage of a laser beam occurs through absorption and electrostriction. An acoustic wave is excited which scatters the laser pump wave to produce the Stokes wave. Because of the feedback between the Stokes wave and the medium's density and temperature, there exists the possibility of stimulated processes. We will obtain expressions for stimulated electrostrictive Brillouin scattering (SEBS), stimulated thermal Brillouin scattering (STBS), and stimulated Rayleigh scattering (SRS). These processes are all described by the linearized equations:

$$\nabla^2 E_s(\omega_s, \vec{k}_s) - \frac{\epsilon_s}{c^2} \frac{\partial^2}{\partial t^2} E_s(\omega_s, \vec{k}_s) = \left(\frac{\partial \epsilon}{\partial \rho} \right)_T \frac{1}{c^2} \frac{\partial^2}{\partial t^2} \left[E_L(\omega_L, k_L) \rho_1^*(-\omega, -\vec{k}) \right] + \left(\frac{\partial \epsilon}{\partial T} \right)_\rho \frac{1}{c^2} \frac{\partial^2}{\partial t^2} \left[E_L(\omega_L, k_L) \theta_1^*(-\omega, -\vec{k}) \right] \quad (2.1)$$

$$-\mu \nabla^2 \theta_1^*(-\omega, -\vec{k}) + \frac{\partial}{\partial t} \theta_1^*(-\omega, -\vec{k}) - \frac{(\gamma-1)}{\rho_0 \beta} \frac{\partial}{\partial t} \rho_1^*(-\omega, -\vec{k}) = \frac{\alpha n}{8\pi \rho_0 C_V} E_L^*(-\omega_L, -k_L) E_s(\omega_s, \vec{k}_s) + \frac{1}{4\pi} T_0 \left(\frac{\partial \epsilon}{\partial T} \right)_\rho \frac{\partial}{\partial t} \left(E_L^*(-\omega_L, -k_L) E_s(\omega_s, \vec{k}_s) \right) \quad (2.2)$$

$$\frac{\partial^2 \rho_1^*(-\omega, -\vec{k})}{\partial t^2} - \frac{v_s^2}{\gamma} \nabla^2 \rho_1^*(-\omega, -\vec{k}) - \frac{\eta}{\rho_0} \nabla^2 \frac{\partial}{\partial t} \rho_1^*(-\omega, -\vec{k}) - \frac{8\rho_0 v_s^2}{\gamma} \nabla^2 \theta_1^*(-\omega, -\vec{k}) = \frac{1}{4\pi} \rho_0 \left(\frac{\partial \epsilon}{\partial \rho} \right)_T \nabla^2 \left(E_L^*(-\omega_L, -k_L) E_s(\omega_s, \vec{k}_s) \right), \quad (2.3)$$

where E_s is the Stokes wave Fourier component at frequency ω_s and wave number \vec{k}_s , ϵ_s is the dielectric constant at the Stokes frequency ω_s , $(\partial \epsilon / \partial \rho)_T$ is the variation of ϵ with respect to density at constant temperature, E_L is the pump wave Fourier component at frequency ω_L and wave number k_L , ρ_1^* is the complex conjugate of the perturbed density of frequency $-\omega$ ($=-\omega_L + \omega_s$) and wave number $-\vec{k}$ ($=-\vec{k}_L + \vec{k}_s$), θ_1^* is the perturbed temperature at $-\omega$ and $-\vec{k}$, μ is the thermal diffusivity which can be expressed in terms of the thermal conductivity κ and the specific heat at constant volume, C_V , by $\mu = \kappa / \rho C_V$, γ is the ratio of the specific heats (C_p / C_V), β is the volume expansion coefficient, α is the optical absorption coefficient, v_s is the phonon speed, and η is the viscosity.

For phase matching $\omega = \omega_L - \omega_s$, $\vec{k} = \vec{k}_L - \vec{k}_s$ and $k = 2k_L \sin(\theta/2)$ where $\cos \theta = \vec{k}_s \cdot \vec{k}_L / k_s k_L$.

3. Stimulated Electrostrictive Brillouin Scattering

In this case we set $\mu = 0$ and $\alpha = 0$ and neglect $(\partial \epsilon / \partial T)_\rho$. When combined, Equations (2.2) and (2.3) yield

$$\left[\frac{\partial^2}{\partial t^2} - v_s^2 \nabla^2 - \frac{n}{\rho_0} \nabla^2 \frac{\partial}{\partial t} \right] \rho_1^* = \frac{1}{4\pi} \rho \left(\frac{\partial \epsilon}{\partial \rho} \right)_T \nabla^2 (E_L^* E_s). \quad (3.1)$$

3a. Transient Solution

Express the Stokes field in Equation (2.1) and the density in Equation (3.1) as a slowly-varying amplitude multiplying a phase factor, i.e., for backward scattering ($k=2k_L$, $\theta=\pi$),

$$E_s(\omega_s, \vec{k}_s) = A_1 \exp[i(\omega_s t - k_s z)] + \text{complex conjugate}, \quad (3.2)$$

$$\rho_1^*(-\omega, -\vec{k}) = A_2^* \left[\exp -i(\omega t - k z) \right] + \text{complex conjugate}. \quad (3.3)$$

Retaining only the leading terms, we obtain

$$\frac{\partial A_1}{\partial z} + \frac{1}{c_s} \frac{\partial A_1}{\partial t} + \frac{2}{c_s \tau_s} A_1 = \frac{i \omega_s^2}{2 k_s c_s^2} \left(\frac{\partial \epsilon}{\partial \rho} \right)_T A_L A_2^* \equiv a_1 A_2^*, \quad (3.4)$$

$$\frac{\partial A_2^*}{\partial z} + \frac{1}{v_s} \frac{\partial A_2^*}{\partial t} + \frac{2}{v_s \tau_v} A_1 = \frac{k_0}{8\pi i v_s} \left(\frac{\partial \epsilon}{\partial \rho} \right)_T A_L^* A_1 \equiv \frac{a_2}{v_s} A_1, \quad (3.5)$$

where $2/c_s \tau_s$ is the optical damping coefficient and $2/\tau_v = \eta k \omega / 2 \rho v_s$ is the acoustic damping coefficient.

Assume that the velocity of the phonon wave is negligible, and introduce the new independent variables $y = a_1 a_2 (z + c_s t)$, $t = t$.

Elimination of the exponential factors yields the hyperbolic equation

$$\frac{\partial^2 u}{\partial y \partial t} = u, \quad (3.6)$$

where

$$A_1(y, t) = u(y, t) e^{-2t/\tau_v} e^{-2y/a_1 a_2 c_s \tau_s}. \quad (3.7)$$

Equation (3.6) can be conveniently solved by taking the Laplace transform with respect to t :

$$\bar{u}(y, s) = \int_0^\infty e^{-st} u(y, t) dt, \quad (3.8)$$

so that

$$s \frac{\partial \bar{u}}{\partial y} = \bar{u} + \left(\frac{\partial u}{\partial y} \right)_{t=0}. \quad (3.9)$$

The solution can be written

$$\bar{u}(y, s) = f(s) e^{y/s} - \left(\partial u / \partial y \right)_{t=0}, \quad (3.10)$$

where $f(s)$ is to be determined from $u(0, t)$. Since causality requires $(\partial A_1 / \partial y)_{t=0} = 0$, we obtain from Equation (3.8) that $(b_1 = 2/c_s \tau_s)$

$$\left(\frac{\partial u}{\partial y} \right)_{t=0} = \frac{b_1}{a_1 a_2} u(y, 0) = 0 \text{ for } y > 0. \quad (3.11)$$

Therefore,

$$\bar{u}(0, s) = f(s) - \frac{b_1}{a_1 a_2} u(0, 0), \quad (3.12)$$

and hence

$$f(s) = \frac{b_1}{a_1 a_2} u(0, 0) + \int_0^\infty u(0, t') e^{-st'} dt'. \quad (3.13)$$

Substitution yields

$$u(y,t) = \frac{1}{2\pi i} \frac{b_1}{a_1 a_2} u(0,0) \int_{c-i\infty}^{c+i\infty} ds e^{st} (e^{y/s} - 1) \\ + \frac{1}{2\pi i} \int_{c-i\infty}^{c+i\infty} ds \int_0^\infty dt' u(0,t') e^{s(t-t')} e^{y/s}, \quad (3.14)$$

or

$$u(y,t) = \frac{b_1}{a_1 a_2} u(0,0) (y/t)^{1/2} I_1(2[yt]^{1/2}) \\ + u(0,t) + \int_0^t u(0,t') y \frac{I_1(2[y(t-t')]^{1/2})}{[y(t-t')]^{1/2}} dt'. \quad (3.15)$$

If a different boundary condition is imposed on $(\partial A_1 / \partial y)_{t=0}$, simply replace $b_1 u(0,0)/a_1 a_2$ with $(\partial u / \partial y)_{t=0}$. For a square pulse of duration t_p , the integration can be carried out since $I_1(z) = I_0'(z)$. Thus, if $A_1(0,t) = A_{10}$ for $0 < t < t_p$ and $t_p \ll \tau$, and $c_s \tau_s \gg 1$ (so that b_1 can be ignored)

$$A_1(y,t) = A_1(0,t) + A_{10} I_0(2[yt]^{1/2}) - 1 e^{-t/\tau}, \quad t < t_p. \quad (3.16)$$

For large gain, $yt \gg 1$,

$$A_1(y,t) = \frac{A_{10}}{\sqrt{4\pi}} (yt)^{-1/4} \exp\{2[yt]^{1/2} - t/\tau\}. \quad (3.17)$$

The steady-state gain follows on taking the limit $t \rightarrow \infty$ in Equation (3.15). With u expressed in terms of A_1 through Equation 3.8), we obtain

$$A_1(y,t) \xrightarrow{t \rightarrow \infty} A_1(0,0) (\pi\tau)^{1/2} e^{\frac{1}{2} y\tau} I_{1/2}\left(\frac{1}{2} y\tau\right) \\ \sim A_1(0,0) e^{y\tau} \text{ for } y\tau \gg 1. \quad (3.18)$$

3b. Steady State Spatial Gain

The steady-state gain, and its frequency dependence, follows also from the dispersion relation which is obtained by assuming that $\rho_1 \sim \exp[i(\omega t - kz)]$ and $E_s \sim \exp[i(\omega_s t - k_s z)]$ for backward gain. Substitution into Equations (3.1) and (2.1) yield (we neglect $(\partial\epsilon/\partial T)_\rho$) for ω real

$$\omega^2 - v^2 k^2 + i \frac{\omega \eta}{\rho} k^2 = \frac{k^2}{4\pi c^2} \rho (\partial\epsilon/\partial\rho)_T^2 \frac{\omega_s^2 |E_L|^2}{\left(-k_s^2 + \frac{\epsilon_s}{c^2} \omega_s^2\right)} \quad (3.19)$$

For stimulated Brillouin scattering, the required solution has $\omega = vk_r$ (with $k = k_r + ik_i$). Also, since $k_r = 2k_L$,

$$\begin{aligned} -k_s^2 + \frac{\epsilon_s}{c^2} \omega_s^2 &= -2ik_L k_i + k_i^2 - \frac{2\epsilon_s}{c^2} \omega \omega_L \\ &= \frac{k^2}{4\pi c^2} \rho (\partial\epsilon/\partial\rho)_T^2 \frac{\omega_s^2 |E_L|^2}{\left(\omega^2 - v^2 k_r^2 + i \frac{\omega \eta k_r^2}{\rho}\right)} \end{aligned} \quad (3.20)$$

Equating imaginary parts, we obtain

$$k_i = \frac{k_r k_s (\rho \partial\epsilon/\partial\rho)^2 |E_L|^2}{32\pi n_s v_s \rho} \frac{\tau_v}{\left[(\omega - vk_r)^2 \frac{\tau_v^2}{4} + 1\right]} \quad (3.21)$$

Maximum gain occurs at $\omega = vk_r$, and expressing τ_v in terms of the viscosity η , we obtain

$$(k_i)_{\max} = \frac{(\rho \partial\epsilon/\partial\rho)^2}{2\pi v_s n_s \eta} 10^{-3} P(W/cm^2) \quad (3.22)$$

4. Stimulated Thermal Brillouin Scattering

The appropriate equation is obtained by combining Equations (2.2) and (2.3) and dropping the electrostrictive contribution. Thus,

$$\frac{\partial}{\partial t} \left[\frac{\partial^2}{\partial t^2} - v_s^2 \nabla^2 - \frac{\mu}{\rho} \nabla^2 \frac{\partial}{\partial t} \right] \rho_1^* = \frac{\alpha \text{cn} \beta v_s^2}{8\pi C_p} \nabla^2 (E_L^* E_s). \quad (4.1)$$

4a. Transient Solution

By making the slowly-varying amplitude approximation and adopting Equations (3.2) and (3.3) for the fields, we obtain again coupled equations of the same form as Equations (3.4) and (3.5). The parameter a_1 remains unchanged:

$$a_1 = \frac{i\omega_s^2}{2k_s c^2} \left(\frac{\partial \epsilon}{\partial \rho} \right)_T A_L^*, \quad (4.2)$$

but

$$a_2 = \frac{k^2}{2\omega^2} \frac{\rho_0 v^2 (\gamma-1) \alpha \text{cn}}{8\pi \gamma p_0} A_L^*, \quad (4.3)$$

where we have used the relation between β and the ambient pressure p_0 for gases: $\beta = \rho C_p (\gamma-1) / \beta \gamma$.

The transient gain, for the same initial conditions, is again given by Equation (3.17).

4b. Steady State Spatial Gain

The dispersion relation follows directly from Equations (4.1) and (2.1). We again look for solutions with real ω ($=v_s k_r$)

$$i\omega \left(\omega^2 - v_s^2 k^2 + i \frac{\omega \eta}{\rho} k^2 \right) \left(-k_s^2 + \frac{\epsilon_s \omega_s^2}{c^2} \right) = - \frac{\beta v_s^2 \alpha \text{cn}_s}{8\pi C_p} k^2 \omega_s^2 \left(\frac{\partial \epsilon}{\partial \rho} \right)_T |A_L|^2. \quad (4.4)$$

With $k_r = 2k_L$ and $k = k_r + ik_i$ we obtain on equating imaginary parts

$$k_i = \frac{8\alpha n_s \omega_s}{32\pi C_p} \left(\frac{\partial \epsilon}{\partial \rho} \right) \frac{(\omega - vk_r) (\tau_v^2/4)}{[(\omega - vk_v)^2 (\tau_v^2/4) + 1]} |A_L|^2, \quad (4.5)$$

which is asymmetric with respect to the Brillouin frequency vk_r . Maximum spatial gain occurs for $\omega = vk_r + \frac{2}{\tau}$:

$$(k_i)_{\max} = \frac{\alpha n_s \omega_s (\gamma - 1)}{32\pi \gamma \rho_0} \rho \left(\frac{\partial \epsilon}{\partial \rho} \right) \left(\frac{\tau_v}{4} \right) 8 \times 10^{-3} P_L (W/cm^2) \quad (4.6)$$

5. Stimulated Rayleigh Scattering

When thermal diffusivity is included, an instability can be excited at frequencies $\omega \ll \omega_B = vk_r$. The dispersion relation in this case is ($\mu = k/\rho C_v$)

$$-k_s^2 + \frac{\epsilon_s \omega_s^2}{c^2} = - \frac{\alpha \beta n \omega_s^2}{8\pi C_v C} \left(\frac{\partial \epsilon}{\partial \rho} \right)_T \frac{1}{\mu k^2 - i\gamma \omega} \quad (5.1)$$

with $k_r = 2k_L$ and $k = k_r + ik_i$ this yields the spatial gain

$$k_i = \frac{8\alpha n \omega_s}{16\pi C_p} \left(\frac{\partial \epsilon}{\partial \rho} \right)_T \frac{\omega}{\omega^2 + (\mu k^2/\gamma)^2}, \quad (5.2)$$

and at $\omega = \mu k^2/\gamma \equiv \omega_R$

$$(k_i)_{\max} = \frac{\alpha n \omega_s (\gamma - 1)}{16\pi \gamma \rho_0} \left(\rho \frac{\partial \epsilon}{\partial \rho} \right) \left(\frac{1}{2\omega_R} \right) 8 \times 10^{-3} P (W/cm^2) \quad (5.3)$$

The linewidth ω_R should be replaced with the pump linewidth if this exceeds $\mu k^2/\gamma$.

6. Numerical Estimates

6a. Raman Amplifiers

As an illustration we assume the following parameters for a hydrogen gas at 10 atmospheres, 20° C:

$$\rho \left(\frac{\partial \epsilon}{\partial \rho} \right)_T = 0.0046,$$

$$v_s = 1.3 \times 10^5 \text{ cm/sec},$$

$$\rho = 9 \times 10^{-4} \text{ gm/cm}^3.$$

$$\eta = 87.6 \times 10^{-6} \text{ poises},$$

$$\gamma = 1.4.$$

We further assume a pump wavelength of 5000 Å ($k_L = k_s = 1.26 \times 10^5 \text{ cm}^{-1}$), and for backward scattering $k_r = 2k_L = 2.52 \times 10^5 \text{ cm}^{-1}$.

With these values, y in Equation (3.16) is given by ($z = z + c_s t$)

$$y = 0.9 P(\text{W/cm}^2). \quad (6.1)$$

The Bessel function expansion used to obtain Equation (3.17) is thus valid provided $t \gg 1/P$ after an interaction length l . If $l = 100 \text{ cm}$ and $P = 20 \text{ MW/cm}^2$, this is satisfied for durations lasting at least some nanoseconds. Assuming this to be the case, the transient gain expression applies for an interaction time $t < 4\gamma^2 = 1.5 \times 10^{-18} \zeta P$ or about 3 nanoseconds for an interaction length of 1 meter and $P = 20 \text{ MW/cm}^2$. In typical Raman gain experiments involving H_2 at 10 atm, $P \sim 20\text{--}50 \text{ MW/cm}^2$, the interaction lengths are a meter or more and the pump pulse length exceeds 100 ns, so that we will assume that for most of the pump pulse steady-state conditions prevail.

Equation (3.22) yields for the maximum spatial gain of SEBS:

$$\text{gain} = 3 \times 10^{-10} \text{ cm/Watt}, \quad (6.2)$$

about a factor of 8 less than the steady-state Raman gain of $2.4 \times 10^{-9} \text{ cm/Watt}$.

Equation (4.6) gives for the maximum steady-state spatial of STBS:

$$\text{gain} = 6 \times 10^{-9} \alpha \text{ cm/Watt}, \quad (6.3)$$

which is considerably smaller than that for SEBS since, typically, $\alpha \ll 10^{-2} \text{ cm}^{-1}$.

The gain for SRS follows from Equation (5.1). We obtain the estimate

$$\text{gain} = 40\alpha/\omega_R \text{ cm/Watt}. \quad (6.4)$$

The Rayleigh linewidth ($\mu k^2/\gamma$) for the present case is $5.4 \times 10^9 \text{ sec}^{-1}$, which would yield a gain comparable to that of STBS. For even this gain to be reached, the laser linewidth would have to be less than 0.01 \AA at 5000 \AA !

In summary, therefore, stimulated electrostrictive Brillouin scattering may compete with Raman amplification if the pump bandwidth and pulse spacing are such as to reduce the Raman gain by a factor of 2-4

6b. Atmospheric Propagation

Estimates for laser beam propagation through the atmosphere are obtained by taking:

$$\rho \left(\frac{\partial \epsilon}{\partial \rho} \right)_T = 5.4 \times 10^{-4},$$

$$v_s = 3.33 \times 10^4 \text{ cm/sec},$$

$$\rho = 10^{-3} \text{ gm/sec},$$

$$\eta = 1.8 \times 10^{-4} \text{ poise},$$

$$\gamma = 1.4.$$

Thus, at a pump wavelength of 5000 \AA , the maximum spatial gain of backward SEBS is from Equation (3.16) given by

$$\text{gain} = 7.7 \times 10^{-12} \text{ cm/Watt}. \quad (6.5)$$

This expression predicts an e-folding length of 1 kilometer at a laser irradiance of 1.3 MW/cm^2 .

For STBS we obtain from Equation (4.6) that

$$\text{gain} = 4 \times 10^{-9} \text{ a cm/Watt,}$$

considerably less than that for SEBS in a clear atmosphere ($\alpha \sim 10^{-6} - 10^{-7} \text{ cm}^{-1}$).

MAY 20 1983 BRIEFING
TO DARPA ON

- 1) "DEVELOPING HIGH POWER SOLID STATE LASERS",
M. BASS⁺
- 2) "DIODE PUMPING OF SOLID STATE LASERS",
E. GARMIRE[#]

MAY 1983

THIS RESEARCH WAS SPONSORED BY THE
DEFENSE ADVANCED RESEARCH PROJECTS AGENCY
UNDER ARPA ORDER NO.: 3710
CONTRACT NO.: MDA903-82-C-0376

THE VIEWS AND CONCLUSIONS CONTAINED IN THIS DOCUMENT ARE
THOSE OF THE AUTHORS AND SHOULD NOT BE INTERPRETED AS
NECESSARILY REPRESENTING THE OFFICIAL POLICIES, EITHER
EXPRESS OR IMPLIED, OF THE DEFENSE ADVANCED RESEARCH
PROJECTS AGENCY OR THE UNITED STATES GOVERNMENT.

⁺ Consultant to the La Jolla Institute,
Director, Center for Laser Studies,
University of Southern California

[#] Consultant to the La Jolla Institute,
Center for Laser Studies,
University of Southern California

TABLE OF CONTENTS

Page

1. "Developing High Power Solid State Lasers", M. Bass	1
Appendix: Alexandrite Lasers.	A-13
2. "Diode Pumping of Solid State Lasers",	34
"Direct Use of Semiconductor Laser Arrays",	49
E. Garmire	

Preface

A briefing on May 20, 1983 was held at DARPA on the topic "Developing High Power Solid State Materials", this was given by Dr. M. Bass, Director of the Center for Laser Studies of the University of Southern California (USC). Following Dr. Bass's briefing was a discussion by Dr. E. Garmire of the same institution on "Diode Pumping of Solid State Lasers". Their briefing charts are reproduced herein. Dr. Bass discussed Alexandrite as an example of the development of a new solid state material. Since some of the charts from this part of the briefing do not reproduce too well we have included a reprint of an article by one of those involved in the Alexandrite program.

Dr. Bass drew attention to the large Soviet effort directed toward new solid state laser materials and better variants of existing ones. In the December 1982 Soviet Journal of Quantum Electronics (still untranslated) a group at the Lebedev Institute reported on a variation of the Nd^{3+} laser, a Cr^{3+} - Nd^{3+} gadolinium-scandium-gallium-garnet crystal, reputedly having three times the slope efficiency of an equivalent Nd:YAG rod. This type of crystal has only just been duplicated in the U. S. and Dr. Bass had an example (loaned by the vendor) of such with him.

The Soviets have also reported at a recent international conference on co-doping with Cr^{3+} in other host crystals besides GS GG, namely gadolinium gallium garnet, lithium gallium garnet, and ← lanthium-lutetium gallium garnet.

DEVELOPING HIGH POWER SOLID STATE LASERS

PRESENTED AT D-ARPA

MAY 20, 1983

BY

MICHAEL BASS, DIRECTOR
CENTER FOR LASER STUDIES
UNIVERSITY OF SOUTHERN CALIFORNIA
LOS ANGELES, CA 90089-1112

OUTLINE

1. POTENTIAL ADVANTAGES
2. PROBLEMS TO BE SOLVED
3. WORK TO BE DONE - GENERAL + SPECIFIC
4. CURRENT STATUS OF EXISTING SYSTEMS
5. RECENT DEVELOPMENTS
6. ACTIVITY IN THE U.S.S.R. AND IN THE U.S.A.
7. THE ALEXANDRITE LASER - AN EXAMPLE
8. SUMMARY AND RECOMMENDATIONS

POTENTIAL ADVANTAGES

1. LARGE DENSITY OF LASING IONS COMPARED TO GAS LASERS
2. INTERESTING (SHORTER) WAVELENGTHS
3. OVERALL SYSTEM SIMPLICITY
4. LOWER SYSTEM MASS

THE QUESTIONS ARE,

1. HOW DO WE OBTAIN THESE ADVANTAGES?,
2. WHICH ARE THE MOST IMPORTANT? AND,
3. WHO WILL TAKE PART IN THE WORK?

M. BASS USC
MAY 1983

PROBLEMS TO BE SOLVED

1. MATERIALS DEVELOPMENT AND CHARACTERIZATION.
2. LASER DAMAGE, THERMO-OPTIC AND THERMO-MECHANICAL LIMITATIONS MEASURED AND CIRCUMVENTED.
3. MATERIAL PREPARATION AND PROCESS SCALING FOR SIZE
4. PUMP SOURCE DEVELOPMENT FOR EFFICIENCY AND RELIABILITY.
5. RESONATOR AND AMPLIFIER DESIGN.
6. NONLINEAR DEVICES FOR WAVELENGTH SELECTION.

WORK TO BE DONE

1. SPECTROSCOPY AND MATERIALS PROPERTIES EVALUATION; LASER TESTING
2. MATERIALS PREPARATION - OPTICAL QUALITY AND SIZE CONSIDERATIONS
3. PUMP SOURCES - EXTEND CURRENT FLASHLAMP TECHNOLOGY; DEVELOP NOVEL LAMPS WITH MATCHED SPECTRA; DIODE ARRAY PUMPING
4. SYSTEMS ANALYSIS AND DESIGN
5. HARDWARE FABRICATION AND TESTING

THESE TASKS ARE INTERACTIVE. IF CONDUCTED IN A COORDINATED MANNER THE TECHNOLOGY FOR HIGH POWER SOLID STATE LASERS WILL BE DETERMINED. AN EXAMPLE OF SUCH A PROGRAM IS THE D-ARPA FUNDED IR-WINDOW PROJECT.

BESIDES THE TECHNOLOGY A PREDICTIVE MODEL FOR LASER SYSTEM PERFORMANCE BASED ON SPECTROSCOPIC DATA MAY BE DEVELOPED.

SPECIFICS - MATERIALS

1. OPTICAL PROPERTIES - ABSORPTION AND EMISSION SPECTRA
OPTICAL QUALITY
DAMAGE PROPERTIES
SELF-FOCUSING
2. SPECTROSCOPY - EXCITATION SPECTRA
LIFETIMES
EXCITED STATE ABSORPTION
ROLE OF CO-DOPANTS
QUANTUM EFFICIENCY
3. THERMO-OPTICS - dn/dT
- MECHANICS STRESS OPTIC COEFFICIENT
MECHANICAL STRENGTH
HARDNESS
4. PREPARATION - TEMPERATURE
SCALABILITY-CORE FREE
COMPATIBILITY WITH DOPANTS
MATERIAL PURITY REQUIREMENTS
CRUCIBLE COMPATIBILITY

RECENT PROGRESS:

2 1/2" DIA Nd:YAG BOULES
INITIAL GGG Nd
GScGG Nd,Cr
OTHER XTALS

REASON: NEW "BOMBERS"
LARGE CRUCIBLES
PRACTICE

NOTE: AL GARNETS HAVE CORES!!
GA GARNETS DO NOT!!

M. BASS US
MAY 19

SPECIFICS - LASER TESTING

SYSTEM ANALYSIS

1. LASER TESTING - SMALL SAMPLES WITH LASER PUMPIN
SMALL ROD TESTING
CORRELATE WITH OPTICAL AND
SPECTROSCOPIC PROPERTIES
SCALE UP TO LARGE RODS OR
SLABS
TRUSTWORTHY LASER TO LASER
COMPARISON TESTING
HARDWARE DEVELOPMENT

2. SYSTEM ANALYSIS - IDENTIFY CRITICAL PERFOR-
MANCE PROPERTIES
TRADE-OFF STUDIES (i_r , POWER
-VS- λ ; ENERGY VS t_p)
RESONATOR AND AMPLIFIER
DESIGN CHOICES (ROD VS
SLAB)
EVALUATE DATA AND DEVELOP
PREDICTIVE MODELING

SPECIFICS - PUMP SOURCES

1. EXISTING TECHNOLOGY - TEST FOR HIGHER ENERGIES
AND AVERAGE POWERS
PUMP PULSE DURATION
2. NOVEL GEOMETRIES - MAY BE REQUIRED FOR
DESIRED ROD OR SLAB
CONFIGURATIONS AND
PUMP PULSE DURATION
3. NEW GAS FILLS - TO MATCH EXCITATION
SPECTRUM FOR MAXIMUM
EFFICIENCY
4. DIODE ARRAYS - EVALUATE POTENTIAL
FOR MORE EFFICIENCY
AND LESS HEAT DE-
POSITED

SOLID STATE LASER ACTIVITY

1. U.S.S.R.:

1-A IN THE CRC HANDBOOK OF LASERS THE ARTICLE ON SOLID STATE LASERS HAS 143 OUT OF 307 REFERENCES WHICH SITE SOVIET PUBLICATIONS. THE AUTHOR IS AN AMERICAN.

1-B THE MAJOR BOOKS ON CRYSTALLINE LASERS AND PHOSPHATE GLASS LASERS ARE AUTHORED BY SOVIET SCIENTISTS.

1-C THERE IS AN ENTIRE INSTITUTE IN MOSCOW DEVOTED TO THE SPECTROSCOPY OF TRANSITION METAL IONS.

1-D THERE ARE SEPARATE INSTITUTES FOR CRYSTAL GROWTH AND GLASS PREPARATION WITH MAJOR EMPHASIS ON LASER MATERIALS.

1-E AT SEVERAL INSTITUTES THERE ARE MAJOR LASER DAMAGE RESEARCH EFFORTS.

2. U.S.A.:

2-A ALEXANDRITE DEVELOPED BY ALLIED CORP.

2-B LASER PUMPING OF TUNEABLE LASERS IN THE NEAR IR

2-C DEVELOPMENT OF YLiF BY MIT-SANDERS GROUP

2-D LASER DAMAGE RESEARCH

2-E HIGH PEAK POWER FUSION DRIVERS AT LLL AND LLE (ALSO IN U.S.S.R.)

2-F SOLID STATE LASER BOOK PUBLISHED IN 1974.

RECENT DEVELOPMENTS

1. CO-DOPED Cr, Nd: GGG. REPORTED BY RESEARCHERS IN THE USSR. SPECTROSCOPY AND INITIAL REPORTS SUGGEST 3x OUTPUT OF Nd:YAG. NO WORK IN U.S.A. ON THIS UNTIL SPRING 1983
2. SOVIETS ALSO STUDYING GGG VARIANTS SUCH AS GScGG.
3. HIGH DOPANT DENSITY YAG LASERS: SOVIET WORK ON ER:YAG, 50% ER TAKES ADVANTAGE OF CONCENTRATION QUENCHING. 3% EFF. AT 1.9 μ m. NO WORK IN U.S.A. ON THIS SUBJECT.
4. MULTIPLY DOPED GLASSES: REPORTED BY SOVIET RESEARCHERS ie: Cr, Yb, Er: PHOSPHATE GLASSES. NO WORK IN U.S.A. ON THIS SUBJECT.
5. ALEXANDRITE DEVELOPED BY ALLIED AND DESCRIBED IN DETAIL IN THIS PRESENTATION. BEING STUDIED INTENSLEY IN THE U.S.S.R.

**** CLEARLY THE U.S.S.R. IS NOT NEGLECTING **
THE POTENTIALS OF SOLID STATE LASERS!**

HIGH POWER PERFORMANCE OF CURRENTLY AVAILABLE SOLID STATE LASERS

*LASER ^(OSC/AMP)	λ (μm)	LONG PULSE ENERGY/PULSE (J)	REP. PULSE OR CW AVERAGE POWER (W)
RUBY (O/A)	0.6943	200 (400 max)	200
Nd:YAG (O/A)	1.06	200 (400 max)	1000
Nd:YAG (O)	1.06	50	200
Nd:GLASS (O)	1.06	200 (400 max)	50

PLUS MANY OTHERS WHICH EITHER PRODUCE VERY LOW OUTPUTS OR ARE NOT READILY AVAILABLE.

Nd:YLiF IS AN EXAMPLE OF THE FORMER
AND
Nd:YAlO₃ IS AN EXAMPLE OF THE LATTER

*THESE LASERS HAVE BEEN LISTED BECAUSE THEY ARE AVAILABLE. THERE HAS NOT BEEN A VERY STRONG INCENTIVE TO BUILD HIGHER AVERAGE POWER VERSIONS.

HIGH PEAK POWER LASERS HAVE BEEN BUILT BUT ARE VERY LOW AVERAGE POWER DEVICES. THE O/A EXPERIENCE OF THESE EFFORTS WILL BE USEFUL IN THIS WORK.

THE TECHNOLOGY OF THESE LASERS
SHOULD NOT BE IGNORED !!

POTENTIAL PARTICIPANTS

UNIVERSITIES

SPECTROSCOPY
MATERIALS EVALUATIONS
OPTICAL PROPERTIES
PUMP SOURCE DEVELOPMENT
THEORY

INDUSTRIES

MATERIALS PREPARATION
CHARACTERIZATION
FLASHLAMP AND OTHER PUMP SOURCE
DEVELOPMENT
HARDWARE DESIGN AND BUILDING

LABORATORIES

SPECTROSCOPY
SYSTEMS ANALYSES
TESTING
PROGRAM COORDINATION

SUMMARY

1. SOLID STATE LASERS HAVE THE POTENTIAL TO BE USEFUL HIGH AVERAGE POWER DEVICES.
2. THERE IS MUCH TO BE DONE TO DECIDE THIS ISSUE INCLUDING
 - a. SPECTROSCOPY, MATERIAL PROPERTIES, LASER TESTING
 - b. MATERIAL PREPARATION,
 - c. PUMP SOURCE DEVELOPMENT, AND
 - d. SYSTEM DESIGN AND ANALYSIS.
3. THE WORK INVOLVES PARTICIPANTS IN INDUSTRIES, UNIVERSITIES AND GOVERNMENT AND NOT-FOR-PROFIT LABORATORIES.
4. THERE IS SOME URGENCY SINCE IN 2-A AND 2-B WE ARE BEHIND THE USSR AND WE DON'T KNOW OUR RELATIVE STATUS IN 2-C AND 2-D.

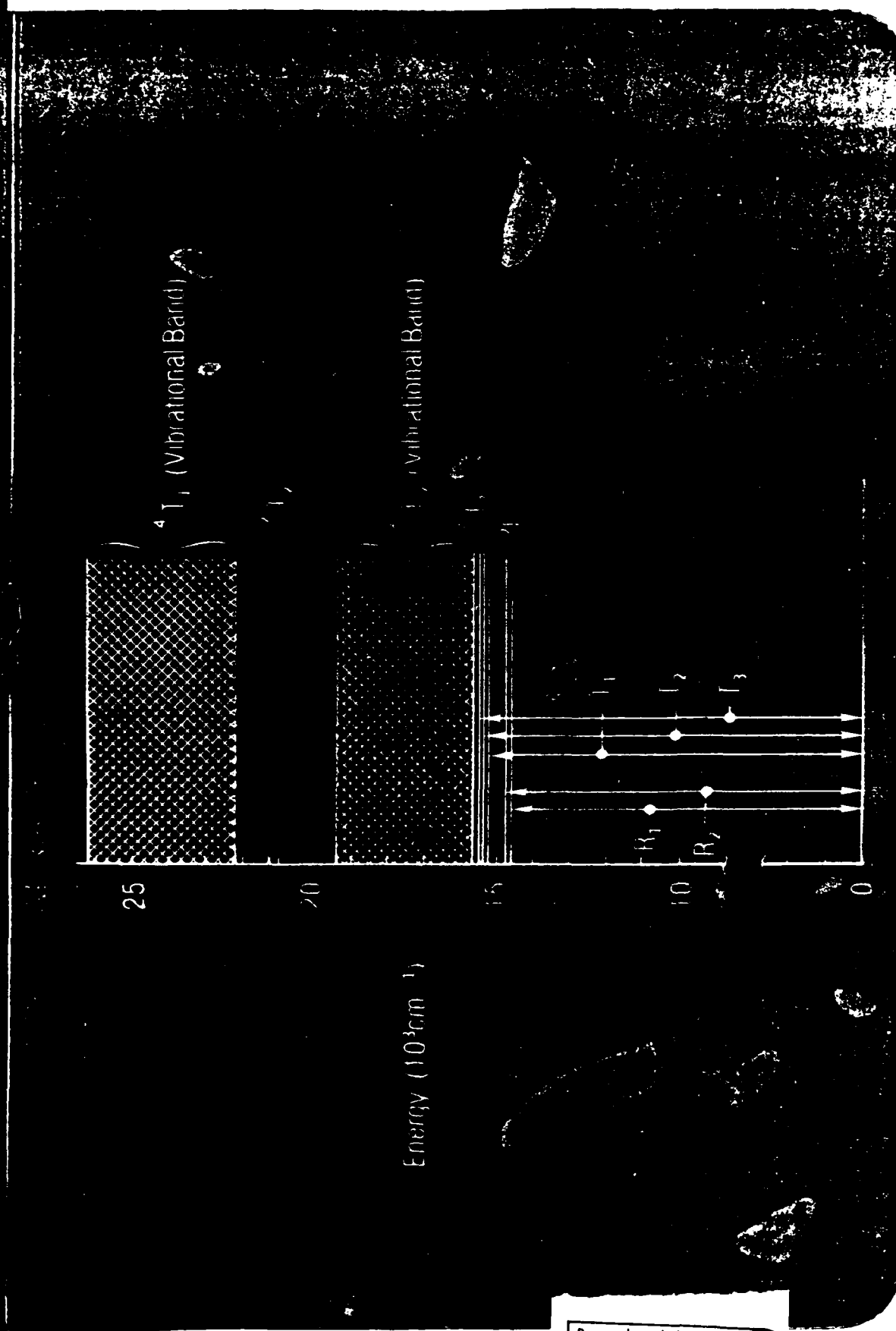
APPENDIX
ALEXANDRITE LASER



Electro-Optical Products
31111 La Tijera Drive
Inglewood, Calif. 90302

FORMULA: $\text{Ba Al}_2 \text{O}_4$
CRYSTAL STRUCTURE: ORTHORHOMBIC
DOPANT: Cr^{3+} SUBSTITUTIONAL FOR Al
DOPANT SITE SYMMETRY: INVERSION & MIRROR
MELTING POINT: 1870 C
HARDNESS: 2000 kg/mm²
INDEX OF REFRACTION: E || a 1.7367
 (750nm) E || b 1.7421
 E || c 1.7346
THERMAL EXPANSION: || a $5.9 \times 10^{-6}/\text{K}$
 || b 6.1
 || c 6.7
THERMAL CONDUCTIVITY: 0.23 W/cm-K
REFRACTIVE INDEX VARIATION: $8 \times 10^{-6}/\text{K}$
NONLINEAR INDEX: $8 \times 10^{-13} \text{ m}^3/\text{J}$

PARAMETERS	DIMENSION
LASER WAVELENGTH (nm)	818
STIMULATED EMISSION CROSS-SECTION (cm^2)	5.0×10^{-20}
SPONTANEOUS LIFETIME (μs)	260 ($T^* = 298^\circ \text{K}$)
DOPING DENSITY (AT. %)	0.05 - 0.3
FLUORESCENT LINEWIDTH (Å)	1000
INVERSION FOR 1% GAIN PER cm (cm^{-3})	$2 - 10 \times 10^{17}$
STORED ENERGY FOR 1% GAIN PER cm (J/cm^3)	0.05 - 0.26
GAIN COEFFICIENT FOR 1 J/cm^3 STORED ENERGY (cm^{-1})	0.038 - 0.19
MAXIMUM STORAGE ENERGY (J/cm^3)	>40
THRESHOLD IN 4 x 100 mm VOLUME (J)	3.5

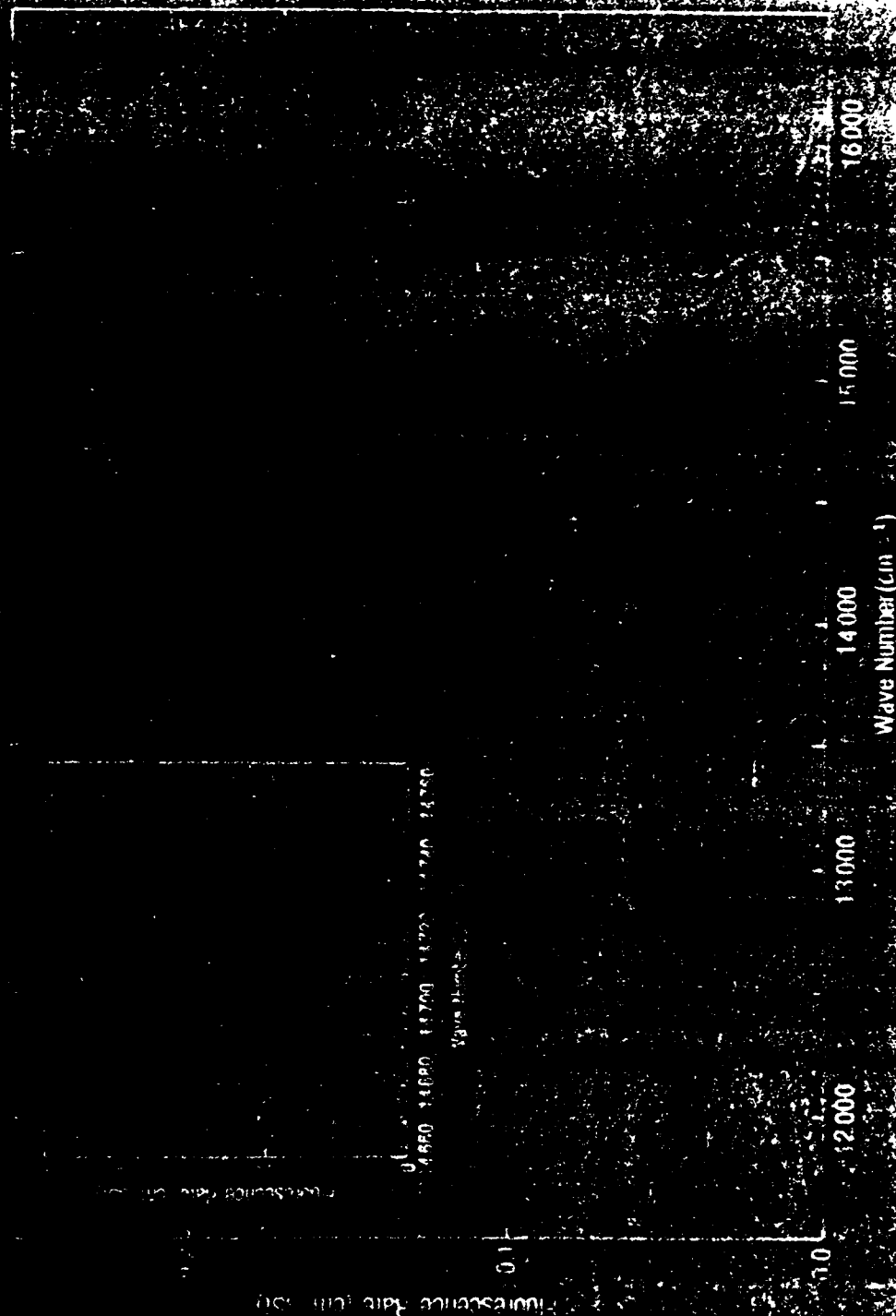


200



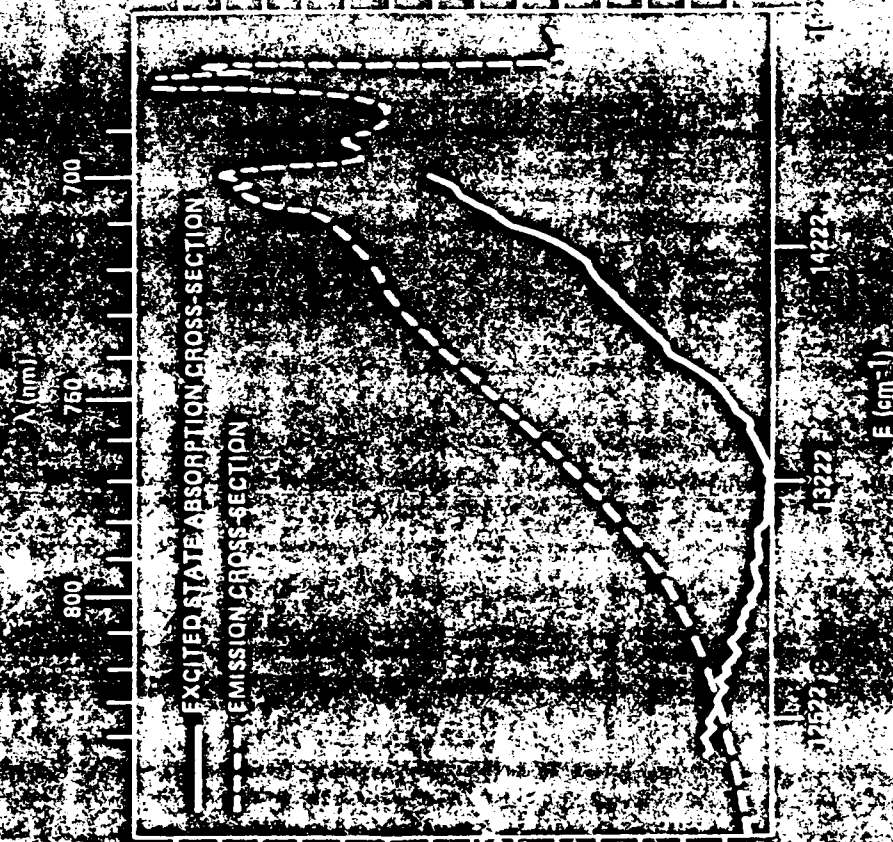
Alexandrite Fluorescence Spectrum

High Quality Products



Reproduced from
best available copy.

EXCITED STATE AND EMISSION CROSS-SECTIONS IN LASING WAVELENGTH REGION



Alexandrite Laser Threshold Dependence On Wavelength



Threshold Energy (J)

0.043 at % Rod A
0.12 at % Rod B

165°C

70.5°C

Wavelength (nm)

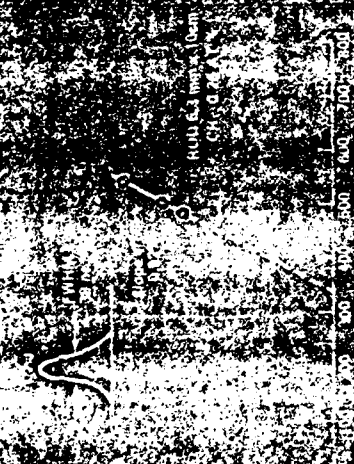
Reproduced from
best available copy.



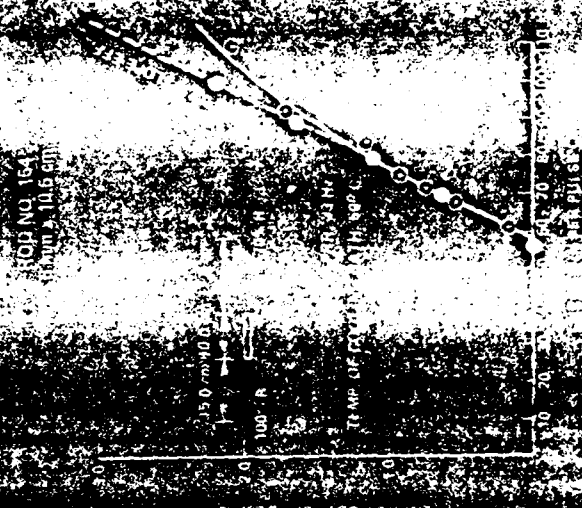
ALEXANDRITE VARIABLE PULSE WIDTH OPERATION



**ALEXANDRITE HIGH ENERGY
NO SWITCHED PERFORMANCE**



LONG PULSE ALEXANDRITE LASER PERFORMANCE



REPRESENTATIVE CW PERFORMANCE



ALFRED

ALEXANDRITE PRODUCTIONS

STANDARD

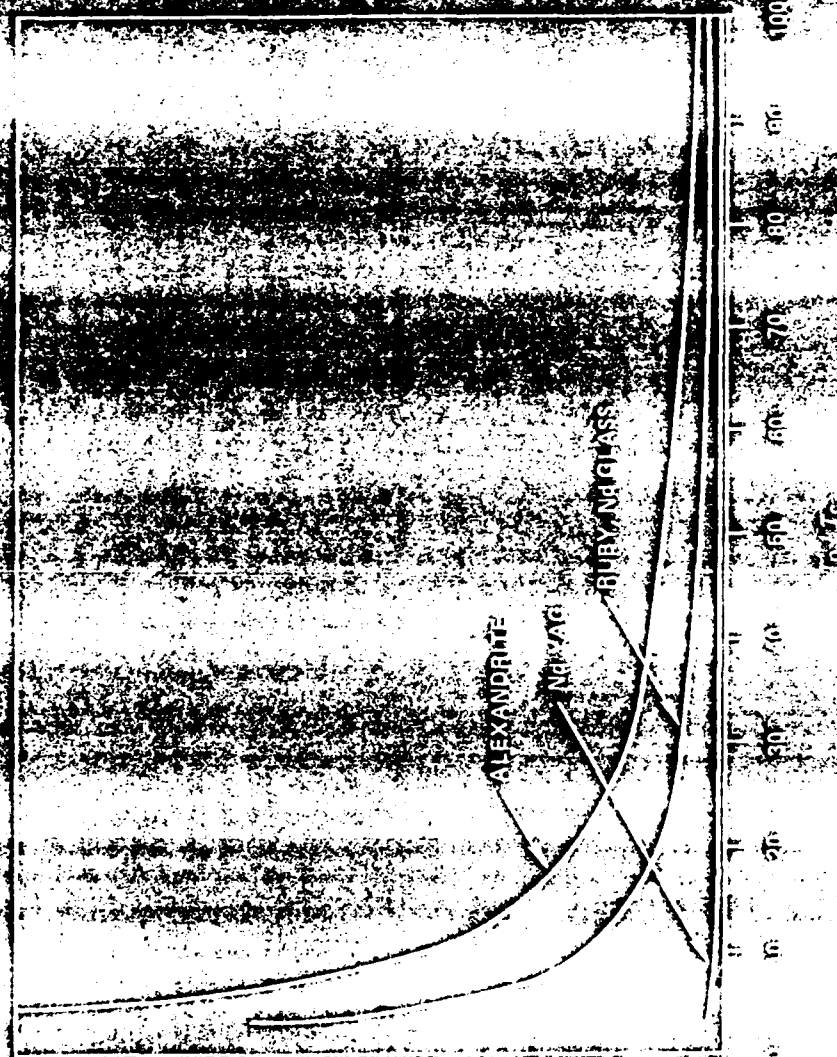
PAV

Reproduced from
best available copy.

INTRINSIC OUTPUT ENERGY PERFORMANCE COMPARISON BETWEEN ALEXANDRITE, Nd:YAG, GLASS AND RUBY

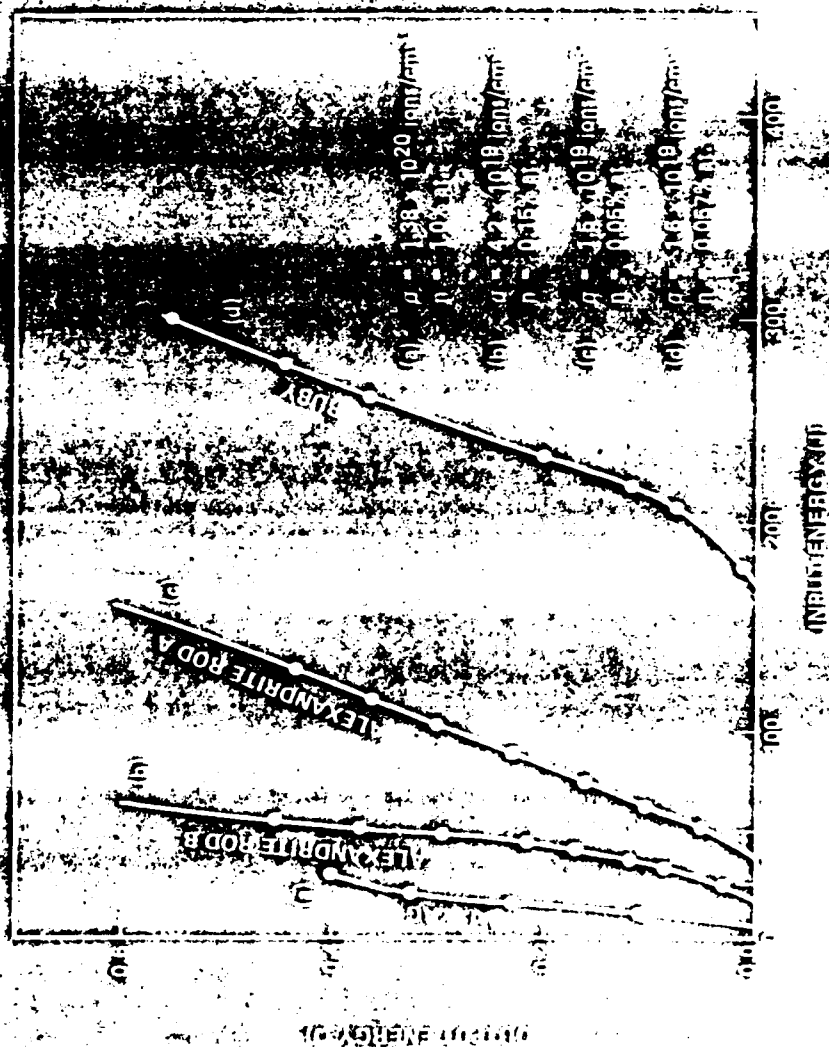


Alameda Optical Products



COMPARATIVE PERFORMANCE BETWEEN ALEXANDRITE, RUBY AND Nd:YAG

ALLIED
Corporation
Electro-Optical Division



LASER INTERCOMPARISON



Electronic Optical Products

Rhodospine
Glass (Nri)

YAG

Organic Dye

Ruby

Alexandrite

Level Type

Wavelength
(nm)

Threshold (J)
(6x 76 mm Volume)

Efficiency (%)
(6x 76 mm Volume)

Storage Time
(min)

Nonlinear Index
(10⁻¹² m³/J)

Thermal Conductivity
(W/cm² K)

Thermal Expansion
(10⁻⁶ K)

4

4

4

3

4

10600

10600

700-800

694

700-818

4

4

10

200

10

3.5

2.5

1.0

0.5

2.5

0.33

0.25

10¹⁶

3.5

0.26

1.5

3.2

2.5

1.1

0.8

0.0007

0.15

0.0006

10.35

0.23

9

7

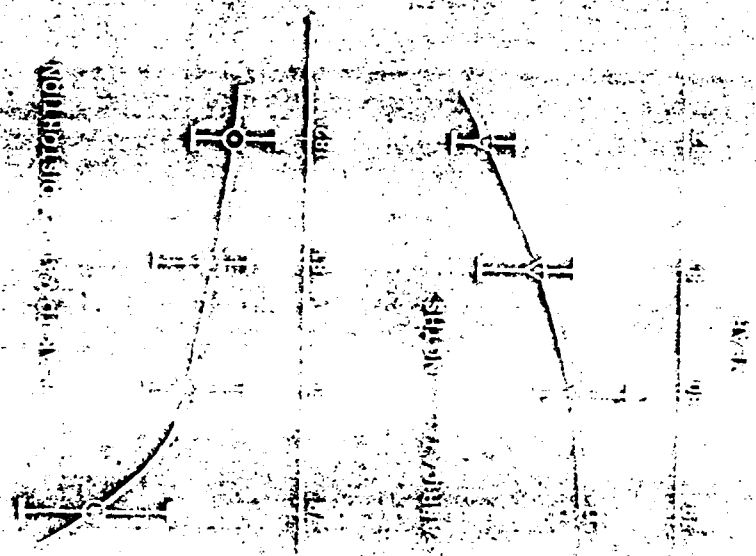
70

15AV

6AV

Reproduced from
best available copy.

ALEXANDRITE ROD QUALITY/PRODUCTION

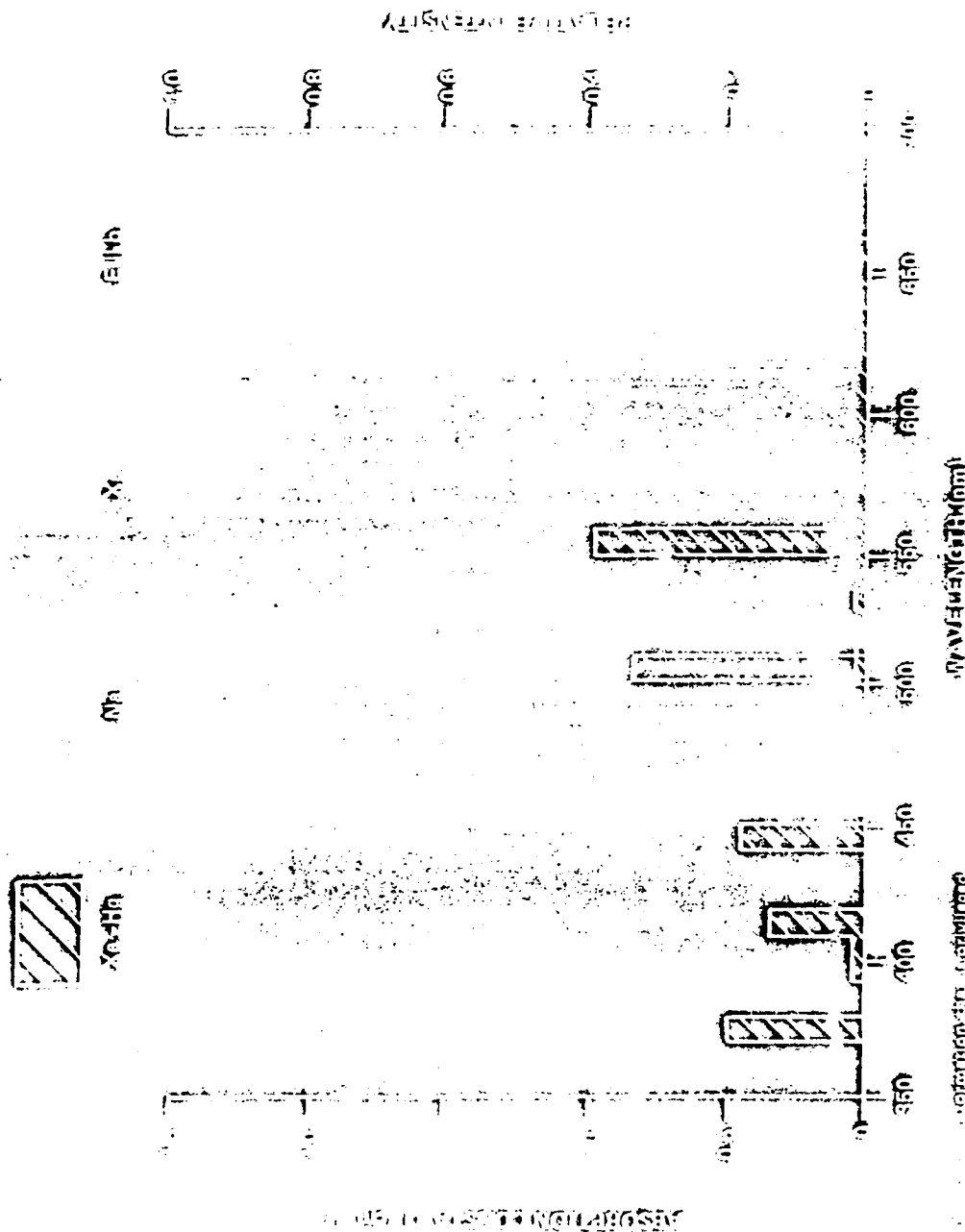


Reproduced from
 best available copy.

ROD ABSORPTION & LAMP INTENSITY VS. WAVELENGTH



AMPER CORPORATION



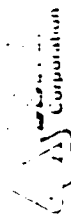
Reproduced from
best available copy.



Electro-Optical Products
31717 La Tijera Drive
Van Nuys, Calif. 91410

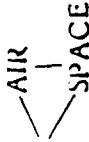
	PRODUCT	DEVELOPED UNDER CONTRACT				EXPERIMENTAL					
		ANNEALING SYSTEM	LOW-DIVERGENCE TUNABLE LASER 1	NARROW BANDWIDTH TUNABLE LASER 2	HIGH POWER LASER 3	HIGH AVERAGE POWER	HIGH PEAK POWER, MODERATE REP RATE	HIGH PEAK POWER, LOW REP RATE	HIGH REP RATE	CW LASER	MODE LOCKED
AVERAGE POWER	(W)	12	1.5	1.0	40	35	70	27	5.8	68	7
PULSE ENERGY	(J)	0.3	0.15	0.1	4	7.0	2	0.9	0.58	0.270	0
O-SWITCHED PULSE WIDTH	(ns)	150	200	100	-	-	-	50	19	-	-
PULSE REPETITION RATE	(Hz)	40	10	10	10	5	35	30	10	250	-
TUNING RANGE	(nm)	-	720-780	750-770	730-803	-	-	740-780	740-765	-	720-770
SPECTRAL BANDWIDTH	(Å)	-	0.03	0.007	4	-	-	0.1	-	-	-
SLOPE EFFICIENCY	(%)	-	-	0.4	2	-	5.2	-	-	-	0.3
OVERALL EFFICIENCY	(%)	0.2	0.16	0.08	1.5	2.5	1.9	0.4	0.2	1.4	0.05
LONG-PULSE DURATION	(μs)	100	100	-	400	200	200	-	-	100	-
MOD SIZE DIAMETER	(cm)	0.5	0.5	0.5	0.5	0.63	0.63	0.63	0.83	0.4	0.3
LENGTH	(cm)	10	7.6	7.6	10	7.6	7.6	7.6	11.0	1.0	7.6

1. DELIVERED TO LOS ALAMOS NATIONAL LABORATORY
2. DELIVERED TO NASA - GODDARD
3. DELIVERED TO NAVAL RESEARCH LABORATORY



Electro-Optical Products
10717 La Tijera Blvd.
Van Nuys, CA 91412

HIGH POWER TUNABLE VISIBLE SOLID STATE LASER APPLICATIONS

- FREQUENCY AGILITY IN OPTICAL AUGMENTATION
- POINTING AND TRACKING IN CONJUNCTION WITH HHEL
- COMMUNICATIONS GROUND 
- INJECTION SOURCE FOR HIGH POWER VISIBLE FEL

ALEXANDRITE LASERS: PHYSICS AND PERFORMANCE

Out of extensive research on numerous 'vibronic' media, only alexandrite — a close cousin of ruby — has emerged as a practical system. A co-developer of the laser reviews its unusual history and projects some near-term applications

JOHN C. WALLING, *Allied Corp., Electro-Optical Products Group*

In most lasers, all of the energy released via stimulated emission by the excited medium is in the form of photons. Recently a new class of solid-state laser materials has emerged in which the stimulated emission of photons is intimately coupled to the emission of vibrational quanta (phonons) in a crystal lattice. In these "vibronic" lasers, the total energy of the lasing transition is fixed, but can be partitioned between photons and phonons in a continuous fashion. The result is broad wavelength tunability of the laser output. This class of lasers — and particularly the alexandrite laser, which this article will describe in detail — offers great potential in numerous applications including spectroscopy, materials working and remote sensing for both civilian and military uses.

Vibronic history

In 1963, Bell Laboratories researchers reported the first vibronic laser, a nickel-doped magnesium fluoride (Ni:MgF_2) device.¹ The same group later built a series of vibronic lasers using nickel, cobalt or vanadium as the dopant and MnF_2 , MgO , MgF_2 , ZnF_2 or KMgF_2 as the host crystal.² Non-continuously tunable in the 1.12- to 2.17-micrometer range, these flashlamp-pumped lasers had a serious drawback: they operated only when cooled to cryogenic temperatures. The first room-temperature vibronic laser, reported by Bell Labs in 1974, was a flashlamp-pumped $\text{Ho:BaY}_2\text{F}_6$ device emitting at 2.17 μm .³ The Bell Labs researchers added Er^{3+} and Tm^{3+} ions to the laser crystal as sensitizers to help absorb and transfer the flashlamp's excitation energy to the Ho^{3+} ions.

The crystal alexandrite (chromium-doped BeAl_2O_4) was first made to lase in 1973 at the Allied Corporation (then Allied Chemical). However for several years researchers assumed that alexandrite could operate only as a three-level laser, like its close cousin ruby. Thus early alexandrite lasers emitted non-tunable red light at 680.4 nm, and were not terribly useful. The first hint that alexandrite might operate as a vibronic system came from the observation that the threshold pumping intensity under certain conditions was much lower than would be expected for a three-level laser. Also, the threshold was found to depend strongly on mirror reflectivity, which is characteristic of a four-level laser.

To resolve the question as to what kind of laser alexandrite really was, the Allied team carried out the

decisive experiment in which the wavelength was measured. In September 1977, the laser was found to be operating at 726 nm — confirming the hypothesis that a vibronic phenomenon was at work.

About a year after the discovery of vibronic alexandrite, a group at MIT's Lincoln Laboratory revived Ni:MgF_2 as a laser medium by replacing the flashlamp pump source of the early Bell Labs work with the 1.33- μm emission from a continuouswave neodymium:YAG laser.⁴ They obtained output powers of 1.7 watts at 200 K, corresponding to a 37% power conversion efficiency. This work later was extended to Co:MgF_2 , where continuous tuning from 1.63 to 2.08 μm was reported, and to Ni:MgO , where 6 W at 1.32 μm was obtained.

While all of the transition-metal vibronic lasers described above involve infrared transitions between energy levels within the $3d$ shell, Lincoln Lab researchers reported in 1979 the generation of tunable ultraviolet vibronic emission at 325 nm and at 309 nm from $5d - 4f$ intershell transitions in Ce^{3+} in YLF (LiYF_4), pumped by the 249-nm light from a krypton-fluoride laser.⁵ They later observed lasing at 286 nm in Ce^{3+} -doped LaF_3 .⁶ The 286-nm line is the shortest wavelength from any solid-state laser to date.

Allied's decision in 1979 to market the alexandrite

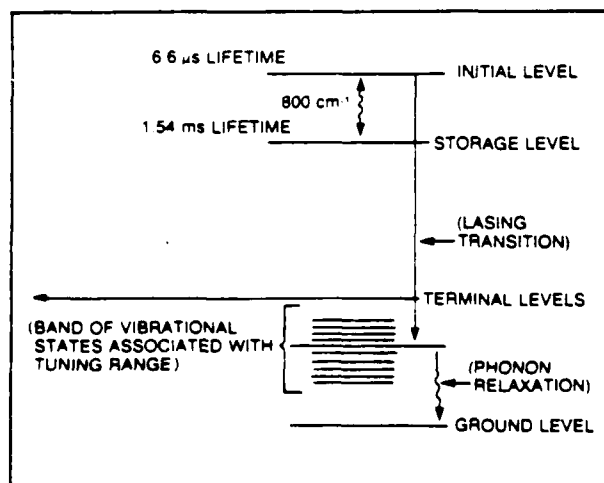


Fig 1 Energy level diagram for chromium ions in alexandrite. The variable partition in de-excitation energy between photons and phonons leads to wavelength tunability

laser marked the beginning of vibronic lasers as a commercial entity. Alexandrite was viewed by corporate management as an important technological discovery in an embryonic industry. The alexandrite laser is now being commercialized by Allied's Electro-Optical Products group in Mt. Bethel, N.J.

Alexandrite kinetics

As noted above, alexandrite can operate both as a four-level vibronic laser and as a three-level system analogous to ruby. As a vibronic laser, it has a low threshold, and is broadly tunable and efficient. As a three-level device, it has a high threshold, fixed output wavelength (680.4 nm at room temperature) and relatively low efficiency. Obviously, the primary interest or allure of alexandrite lies in its vibronic nature.

Fig. 1 shows a model energy-level diagram helpful in describing the essential features of the alexandrite laser kinetics. The "initial" level is the source of the vibronic transitions that are responsible for laser gain. The 6.6-microsecond fluorescence lifetime of this level is much shorter than the 1.5-millisecond life of the "storage" level. The population inversion is formed between the initial level and a set of essentially continuous vibrationally excited terminal levels. The laser wavelength depends on which of these levels acts as the transition terminus; any energy not released by the laser photon will then be carried off by a vibrational phonon, leaving the chromium ion at its ground state.

The fluorescence rate, $F_i(E)$ and laser emission cross section σ are closely related by the expression:

$$\sigma = F_i(E) \left(\frac{h^2 c^2}{E^2 n^2} \right)$$

where h is Planck's constant, c is the speed of light in vacuum, n is the refractive index of the crystal, E is the photon energy and λ gives the polarization. $F_i(E)$ is in units of photons emitted per unit time per unit solid angle per unit energy; σ is in units of area.

As the temperature increases, the population of the initial level increases and consequently the effective emission cross section also increases. However raising the temperature also tends to populate the terminal levels — especially those which lie closest to the ground level and which therefore correspond to the highest-energy (shortest-wavelength) photons. Since laser performance is highest with a maximally populated initial level and a minimally populated terminal level, it can be seen that increasing the temperature has two conflicting effects. The result is that performance is positively affected by temperature increases only for wavelengths above 730 nm.

The alexandrite absorption bands are very similar to those of ruby, and span the region from about 380 to 630 nm. Flashlamp excitation into these pump bands decays to the storage level, as discussed above. The breadth of these pump bands contributes to the alexandrite laser's high efficiency.

A detailed look at salient kinetics properties and their relevance to performance is particularly revealing. In general, the emission cross-section-bandwidth product, summed over all polarizations, is proportional to the total fluorescence rate and hence to the inverse of the storage time. Therefore there's a tradeoff between the wavelength range, ease of energy extraction (which

varies directly with emission cross section) and the storage time. In vibronic lasers (and dye lasers too, for that matter) this tradeoff is inviolate. Fortunately, the balance of these parameters in alexandrite is nearly optimal between room temperature and 100°C where water-based cooling systems can conveniently be used. Within this temperature range the storage time remains above 120 μ s, which is adequate for effective flashlamp pumping. Yet the emission cross section is high enough that the gain dominates parasitic losses in the resonator, leading to efficient operation over a broad wavelength range. In addition, alexandrite emits essentially in one polarization only, thus conserving its photons for polarized laser emission. If alexandrite were an isotropic emitter, as are Ni:MgO and liquid dyes, then there would be a factor-of-three reduction in storage time for the same cross section and tuning range.

Of fundamental importance in the kinetics of alexandrite is the cross-sectional probability σ_{21} that the excited chromium ions will themselves absorb laser photons circulating in the cavity. This probability must be small compared to the effective emission cross section σ , otherwise the excited ions will absorb a significant amount of the emitted laser power before it escapes the resonator. In alexandrite the excited-ion absorption band has a deep broad minimum just where the laser emission gain is maximum. In fact at the band center, σ_{21} is less than 10% of σ . If σ_{21} were greater than σ then lasing could not occur at all. In fact the latter is responsible for the long-wavelength tuning limit in alexandrite, as shown in Fig. 2.

One difficulty with alexandrite (and most other vibronic lasers) is its low emission cross section, 6×10^{-21} cm² at the band center at room temperature — an order of magnitude less than that of typical Nd:glass. To compensate, alexandrite lasers must rely more heavily on oscillator/multipass amplifier configurations for high-power operation. On the other hand, the ability to store energy is not of concern for the alexandrite laser, and at

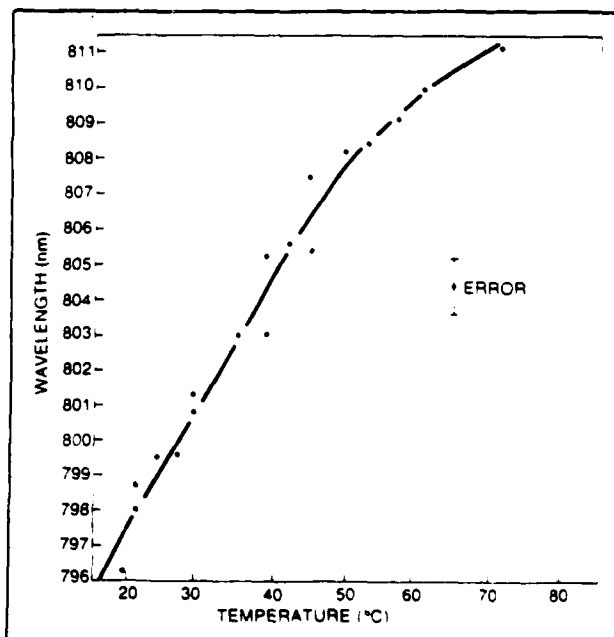


Fig. 2 Long-wavelength tuning limit for alexandrite as a function of temperature. Cut-off wavelengths up to 826 nm have been achieved at higher temperatures

increased temperature the emission cross section can reach a more respectable figure of 2×10^{-17} cm².

Crystal properties and growth

Crystalline alexandrite is optically and mechanically similar to ruby, and possesses many of the physical and chemical properties of a good laser host. Hardness, strength, chemical stability and high thermal conductivity (two-thirds that of ruby and twice that of YAG) enable alexandrite rods to be pumped at high average powers without thermal fracture. In numerical terms the maximum power in kilowatts that can be dissipated per centimeter of length in a laser rod without breaking the rod is 0.8 to 2.8 for ruby, 0.6 to 1.3 for alexandrite and 0.1 to 0.3 for YAG. (The individual variation is the result of the influence of surface roughness on the materials' breaking strengths.) These properties, along with intrinsic high optical damage thresholds (comparable to ruby) combine with the vibronic laser kinetics to give alexandrite unique performance characteristics.

Small alexandrite crystals may be "flux grown" — that is, the crystals slowly develop on the surface of a molten flux in which the alexandrite nutrients are dissolved. However to make laser rods the crystal is grown in large boules by the Czochralski method⁹ much like ruby and YAG. The individual rods are core-drilled from these boules. Although one of alexandrite's constituents, beryllium oxide, is highly toxic, alexandrite itself has no known toxic properties.

The chromium concentration of alexandrite is expressed in terms of the percentage of aluminum ions in the crystal which have been replaced by chromium ions. Alexandrite crystals have been made to lase with Cr concentration of 0.01% to 0.4%. A concentration of 0.1% is equivalent to 3.51×10^{19} ions per cubic centimeter. Of these about 70% fall on the mirror site^{10,11} — one of the two dissimilar crystallographic sites in alexandrite onto which Cr substitutes for aluminum.

The quality of Allied Czochralski-grown alexandrite crystals has progressed steadily throughout the development period. The presence of finely divided indium particles has been entirely eliminated from the material by refinements in the growth technique. Optical quality is well advanced in consideration of the long development time needed to perfect laser-quality crystals of this kind. Typical alexandrite rods 5 mm in diameter and 10 cm long exhibit optical distortion better than one fringe in a Twyman-Green interferometer operating on the 1.15- μ m He-Ne laser line. Alexandrite lasers using these rods have exhibited exceptional performance. Occasionally rods up to 9 mm in diameter and 8 cm long have had distortion less than 2 fringes overall by the same measure.

Alexandrite laser performance

Alexandrite operates long-pulsed or Q-switched both on the R-line and on the vibronic sideband over a very wide temperature range, and CW in the vibronic mode. The operational parameter space to be explored is therefore extensive. The performance obtained at Allied with several laser configurations is summarized in Table 1. Heading the list is the alexandrite annealer, the first alexandrite laser system to be introduced commercially. The next three entries are different types of lasers delivered on a contract basis. The following entries indicate performance achievements of experimental "breadboard" alexandrite lasers.

Long-pulse performance from a 7.6-cm dual lamp ceramic pump chamber is shown in Fig. 3. The characteristic temperature dependence is evident. Note that at 730 nm the temperature dependence of output energy reaches a minimum.

Although in pulsed mode alexandrite can operate either as a 3-level system or a 4-level (vibronic) device, in the continuous mode only vibronic operation has been achieved. To operate any solid-state laser under

TABLE 1: PERFORMANCE OF ALEXANDRITE LASERS

	Product	Developed Under Contract			Experimental						
		Annealing System	Line Narrowed Tunable Laser ¹	High-Power Laser ²	High Average Power	High Peak Power, Moderate Rep Rate	High Peak Power, Low Rep Rate	CW Laser			
Average Power	[W]	10	0.5	1	38	2	35	70	3	4	3
Peak Power	[MW]	1.7	0.6	1	NA	1	—	—	17	5.2	—
Pulse Energy	[J]	0.25	0.1	0.1	3.8	0.2	7.0	3.5	0.6	1.9	—
Q-Switched Pulse Duration	[ns]	150	150	100	—	200	—	—	33	38	—
Pulse Repetition Rate	[Hz]	40	5	10	10	10	5	20	5	2	—
Tuning Range	[nm]	—	780-800	750-770	730-803	730-796	—	—	—	—	—
Line Width	[cm ⁻¹]	—	4	0.015	4	4	—	—	—	—	—
Mode Structure [mm = multimode]		mm Homogenized	mm	mm	mm	Single Mode	mm	mm	mm	mm	Low Order Modes
Slope Efficiency	%	—	—	0.4	2	1.3	—	—	—	0.9	—
Overall Efficiency	%	—	0.1	0.08	1.5	0.2	2.5	1.6	0.2	—	0.05
Long-Pulse Pulse Duration	[μ s]	100	~100	—	400	—	200	200	—	—	—
Rod Size diameter	[cm]	0.5	0.5	0.5	0.5	0.5	0.63	0.63	0.63	0.63	0.3
length	[cm]	10	7.6	7.6	10	10	7.6	7.6	7.6	7.6	7.6

1. Delivered to Los Alamos National Laboratory

2. Delivered to NASA-Goddard for liquid applications

3. Delivered to Naval Research Lab

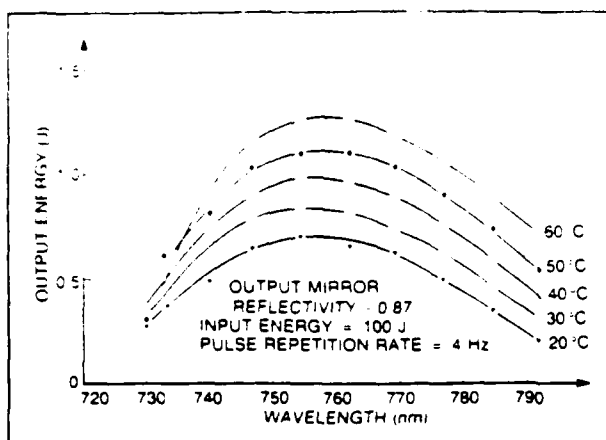


Fig 3 Performance of an alexandrite laser operated in long-pulsed mode. Note that at 730 nm output energy becomes independent of temperature. At shorter wavelengths, output declines with increasing temperature.

the continuous mode only vibronic operation has been achieved. To operate any solid-state laser under the continuous pumping needed for CW output, the material must be able to tolerate depositions of large amounts of heat without fracturing. Because of alexandrite's physical strength and thermal properties, CW operation is possible at room temperature. As with ruby, the most efficient continuous pump source available for alexandrite is a mercury capillary lamp, the output of which matches the material's pump bands.

The first hint that alexandrite might operate as a vibronic system came from the observation that the threshold pumping intensity under certain conditions was much lower than expected

Although alexandrite and ruby lasers have similar CW lasing thresholds, alexandrite has a much greater slope efficiency — that is, its output increases much faster with increased pump power. The reasons for this difference are based on the fundamentally dissimilar kinetics of the two materials.

The threshold in a three-level ruby laser occurs when the pumping has produced the 50% excitation needed for inversion. To achieve this high excitation level the Cr concentration is kept around 0.05%, low enough to permit the pump light to reach the rod center where it becomes concentrated by the focusing action of the rod barrel (which acts as a lens when the rod is in a medium, such as water, with a lower refractive index than itself). For alexandrite, however, threshold is determined more by resonator losses than by the inversion requirement.

Calculations show that the maximum excited ion density for a 3-mm-diameter alexandrite rod in a water bath is achieved when the Cr concentration is 0.4%, a concentration roughly an order of magnitude greater than

used for ruby. As it happens this Cr concentration captures about 50% of the incident energy upon the rod. In the ruby case only about 6% is absorbed. As a result the CW slope efficiency is about an order of magnitude greater in alexandrite than in ruby. Based on the capture probability one would expect also a lower threshold from alexandrite. However, the alexandrite storage time (directly proportional to threshold in CW operation) is an order of magnitude less than ruby's; this compensates for the high capture probability. Consequently, under the same "threshold" pumping conditions, the alexandrite will have about 5% of its ions excited and ruby will have 50%. But 5% excitation in 4-level alexandrite is roughly what is needed to overcome resonator losses. Of course, mirror reflectivities and insertion losses play a major role and the above argument is only qualitative.

Based on mercury lamp pumping, 6 W of quasicontinuous power has been achieved from a 3-mm diameter by 6.4-cm long alexandrite rod, where the slope efficiency is about 0.8%. With CW xenon lamp pumping, a more stable but less efficient 3-W continuous beam has been achieved.

Wavelength extension

Lasers are the ideal light sources for exciting molecules. Their high spectral brightness, short pulse capabilities and other characteristics have led to the evolution of new fields such as laser spectroscopy and photochemistry, and to the generation of a host of new and important application areas including pollutant detection, atmospheric monitoring, isotope separation and materials processing. All of these areas require or prefer high average power and broad wavelength versatility (wide tuning range and narrow bandpass) in addition to high peak power, short pulse duration, efficiency and stability.

Consequently, the advent of CW and pulsed dye lasers has had an enormous impact in most areas where lasers have found a niche. While dye lasers have proven to be excellent laser sources throughout much of the visible, they are relatively inefficient and have other operational drawbacks. At present dye lasers, even when augmented by nonlinear wavelength extension techniques, are least attractive in the near-ultraviolet and the near-infrared. It is in these regions that wavelength-shifted alexandrite lasers have great potential.

As mentioned earlier, alexandrite can provide good output at the joule level and average powers above 100 W in its fundamental tuning region of 700 to 820 nm. Apart from being technically impressive, such power levels are of potential importance in spectroscopic and photochemical research since molecular absorptions in this wavelength region often tend to be extremely weak, arising from forbidden electronic or vibrational overtone transitions. The applications area is no less demanding since average processing power usually translates into process throughput.

Frequency doubling of alexandrite's output into the near UV appears to be particularly promising. Preliminary results, using an angle-tuned KD*P (potassium deuterium phosphate) crystal have demonstrated that 2% conversion can be obtained and that output can be continuously tuned from 360 to 410 nm. Based on dye laser results, 20% to 30% conversion at specific fre-

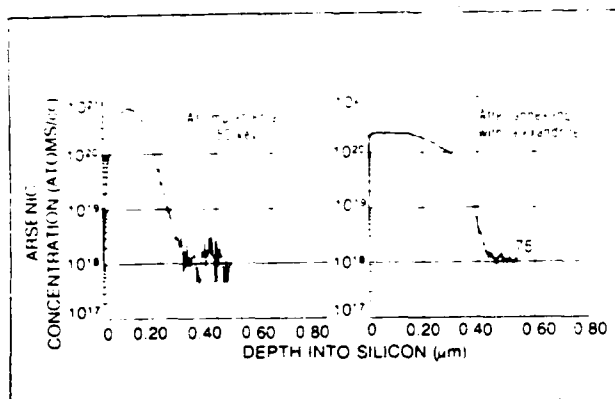


Fig 4 Effect of annealing an arsenic-doped silicon wafer with alexandrite laser light. For this application, the laser's output is fixed at 750 nanometers, where silicon has maximum absorptivity

quencies should be possible. Frequency tripling by nonlinear mixing (sum-frequency generation) of the fundamental and frequency-doubled output in nonlinear crystals should lead to high-power, tunable output at 235 to 270 nm. Through use of stimulated Raman scattering and difference frequency generation it becomes technically feasible to cover the spectrum from 220 nm to 2 μ m starting with high-peak-power laser emission in the alexandrite fundamental wavelength range.

An alexandrite materials processor

Allied's first alexandrite laser product is a system dedicated to laser annealing of silicon wafers, but which serves more generally as a materials processor. The fixed-wavelength (750-nm) system incorporates homogenizing optics which project a flat-profile image a distance of 20 cm to the sample surface, where a 3-mm square area is illuminated uniformly to better than 10%. An xy stage steps the sample so that individual squares overlay 10%. The throughput of the system is two 4-inch-diameter wafers per minute at input intensity of 2J/cm². The wavelength of the alexandrite fundamental is absorbed well by both silicon and gallium arsenide.

Experiments using the system on silicon wafers have produced high quality material as observed by x-ray diffraction and electron and optical microscopy (see Fig. 4). The absence of surface irregularities is characteristic of the anneal; the quality is attributed to the homogenizing optics, the wavelength of operation, and the extended pulse duration of 150 ns.

Conclusion

Vibronic lasers offer tunability together with the high power and stable performance which are characteristic of solid-state lasers based on insulator hosts such as ruby and Nd:YAG. Alexandrite has particular value among vibronic lasers because of its hardness, chemical stability and high thermal conductivity combined with its efficient operation when flashlamp-pumped at room temperature. In addition, alexandrite kinetics can be tailored to specific applications by choice of chromium ion concentration and operating temperature. The high peak power of alexandrite permits its fundamental wavelength range to be shifted by nonlinear methods to

provide full spectral coverage between 200 nm and 2 μ m. This versatility augmented by demonstrated CW operation leads to a broadly based potential in both commercial and military markets.

Now that alexandrite has focused attention on vibronic lasers one might expect that other even better materials would be developed. In the pursuit of new vibronic laser materials, it is difficult to draw many hard and fast rules to narrow the scope. At this point for a new vibronic material to be economically viable, excellent host properties would be needed to compete

In its fundamental tuning region of 700 to 820 nanometers, alexandrite can provide pulsed output at the joule level and average powers above 100 watts

with wavelength shifted tunable alexandrite. Room-temperature operation is important, but cryogenic lasers (such as Ni:MgF₂) that have advanced-design cooling systems would offer potential advantages if the laser could perform more efficiently or powerfully at other wavelength regions than the alexandrite fundamentals for specific applications. The market responds to few contenders, however, and the hurdles of discovery, development, commercialization and market competitors are nontrivial. By and large, it is fair to conclude that alexandrite will play a major role in the future of laser technology.

Acknowledgments

The author thanks J. Pete for the data on long-pulse operation; C. L. Sam for allowing his work on contracted lasers to appear; J. Barrett, H. Jenssen, R. C. Morris, D. Heller and H. Samelson for their helpful comments; and particularly C. Povalski for her assistance in expediting the manuscript's preparation.

References

1. L. F. Johnson, R. E. Dietz and H. J. Guggenheim *Phys Rev Lett* 11 318 (1966)
2. L. F. Johnson, H. J. Guggenheim and R. A. Thomas *Phys Rev* 149 179 (1966)
3. L. F. Johnson, H. J. Guggenheim *IEEE J Quant Electron QE-10* 442 (1974)
4. J. C. Walling, H. P. Jenssen, R. C. Morris, E. W. O'Dell and O. G. Peterson, Annual Meeting of the Optical Society of America (1978)
5. J. C. Walling, O. G. Peterson, H. P. Jenssen, R. C. Morris and E. W. O'Dell *IEEE J Quant Electron QE 16* 1302 (1980)
6. P. F. Moulton, A. Mooradian and T. B. Reed *Appl Phys Lett* 35 838 (1979)
7. D. J. Ehrlich, P. F. Moulton and R. M. Osgood Jr. *Opt Lett* 4 184 (1979)
8. D. J. Ehrlich, P. F. Moulton and R. M. Osgood Jr. *Opt Lett* 5 339 (1980)
9. R. C. Morris and C. Cline, "Chromium-doped Beryllium Aluminate Lasers," U. S. Patent 3,997,853, issued Dec 14, 1976
10. C. E. Forbes, to be published
11. M. Shand and J. C. Walling, to be published

JOHN C. WALLING is manager of research at Allied's Electro-Optical Products Group, 7 Powderhorn Drive, Mt. Bethel, NJ 07060

Reprinted from LASER FOCUS MAGAZINE, February 1982, pages 45-50
Advanced Technology Publications Inc.
1001 Watertown St., Newton, MA 02165
(617) 244-2939

DIODE PUMPING
OF
SOLID STATE LASERS

PROF. E. GARMIRE

W H Y ?

HIGH WALL PLUG EFFICIENCY

DECREASE THERMAL LENSING

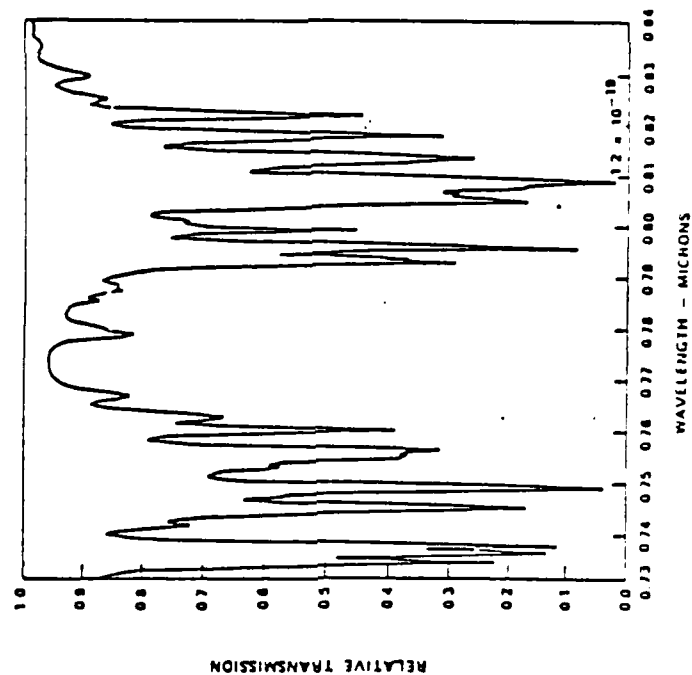
NEW GEOMETRIES POSSIBLE

NEW TIMING SEQUENCES POSSIBLE

SOLID STATE TECHNOLOGY

SPECTRAL MATCH WITH Nd-YAG PUMP BANDS

DEEPEST LINE: $8090 \text{ \AA} \pm 5 \text{ \AA}$
 $\alpha = 20 \text{ cm}^{-1}$
 BAND: $8080 \text{ \AA} \pm 20 \text{ \AA}$
 $\langle \alpha \rangle = 3 \text{ cm}^{-1}$



TRANSMISSION OF 2MM THICK Nd-YAG 1% DOPING

EFFICIENCY

$$\frac{P_{OUT}}{P_{IN}} = \eta_D \left[1 - \frac{I_{TH}}{I} - \frac{R_S I}{eV} \right] = \eta$$

DIFFERENTIAL QUANTUM EFFICIENCY

HITACHI BOG (BURIED OPTICAL GUIDE)

HIGHEST EFFICIENCY:

$$60\% < \eta_D < 85\%$$

THRESHOLD: $I_{TH} = 20 \text{ mA}$

ACTIVE REGION

4 μm WIDE, 1 μm THICK

PULSED OUTPUT: $I = 200 \text{ mA}$, $0.2 \text{ OHM} < R_S < 0.4 \text{ OHM}$

$$53\% < \eta < 75\%$$

$$P_{OUT} = 100 \text{ mW} / \text{FACET}$$

C W OUTPUT: 25 mW / FACET

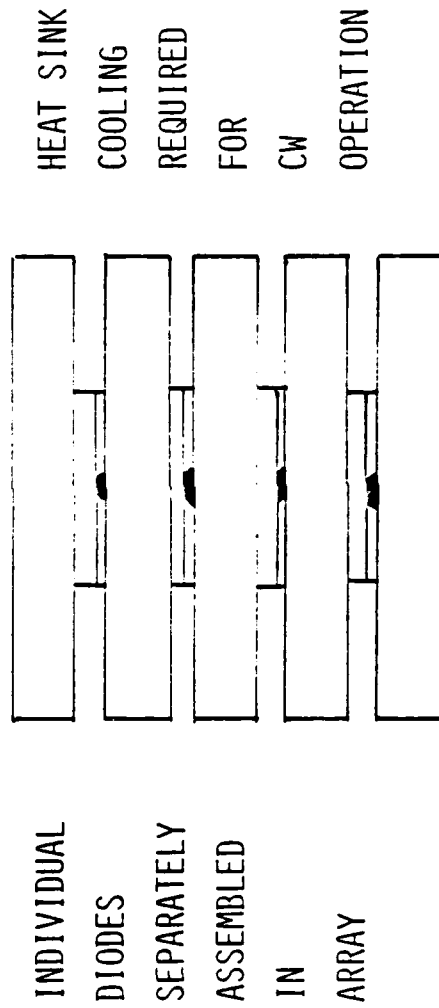
H I G H E R P O W E R

O B T A I N E D W I T H W I D E R S T R I P E S

D S P P R O G R A M : 60 μ m S T R I P E S

E N G I N E E R I N G R E Q U I R E M E N T : 50 mW / D I O D E

S T A C K E D A R R A Y S



D S P P E R F O R M A N C E

AVERAGE 35 mW / DIODE

EFFICIENCY : 12% IN STACK

25 DIODES IN EACH STACK --- 3 STACKS

TOTAL POWER : 2.6 W INTO GAAS LIGHT

OUTPUT Nd-YAG POWER : 0.18 W

ROD SIZE : 1.2 MM DIA. X 12 MM

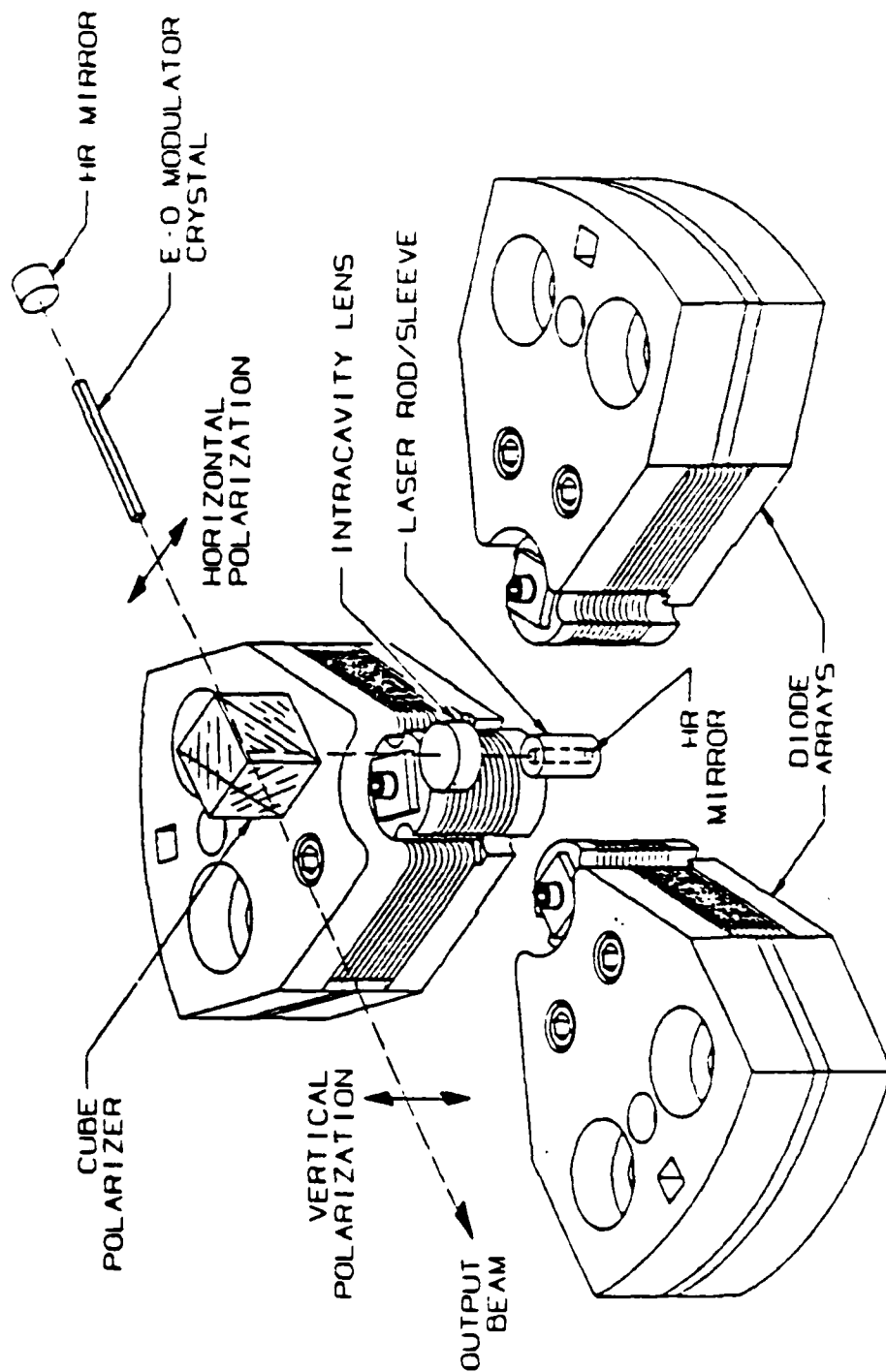
ULTIMATE GOAL : 0.9 W GAAS LIGHT

TO PRODUCE 0.18 W, GAAS LIGHT

20% EFFICIENCY	X	12% EFFICIENCY	=	2.4% WALL-PLUG
Nd-YAG		DIODE		EFFICIENCY

DSP Laser Crosslink

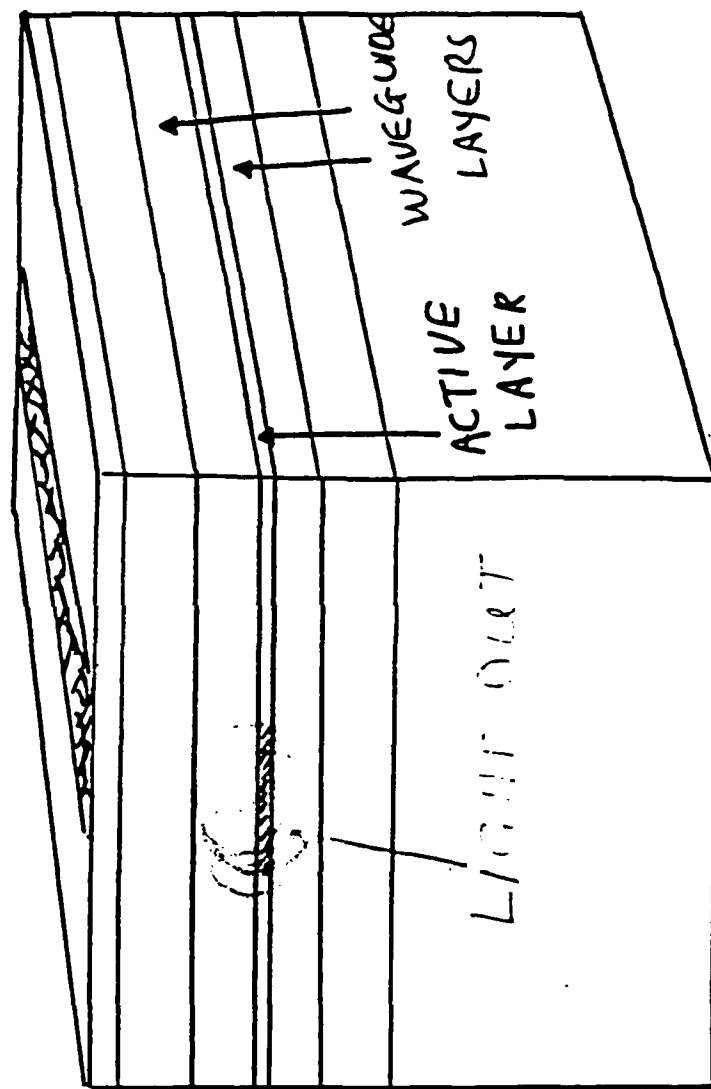
LASER RESONATOR AND DIODE PUMP ARRAYS



HIGH POWER LASERS

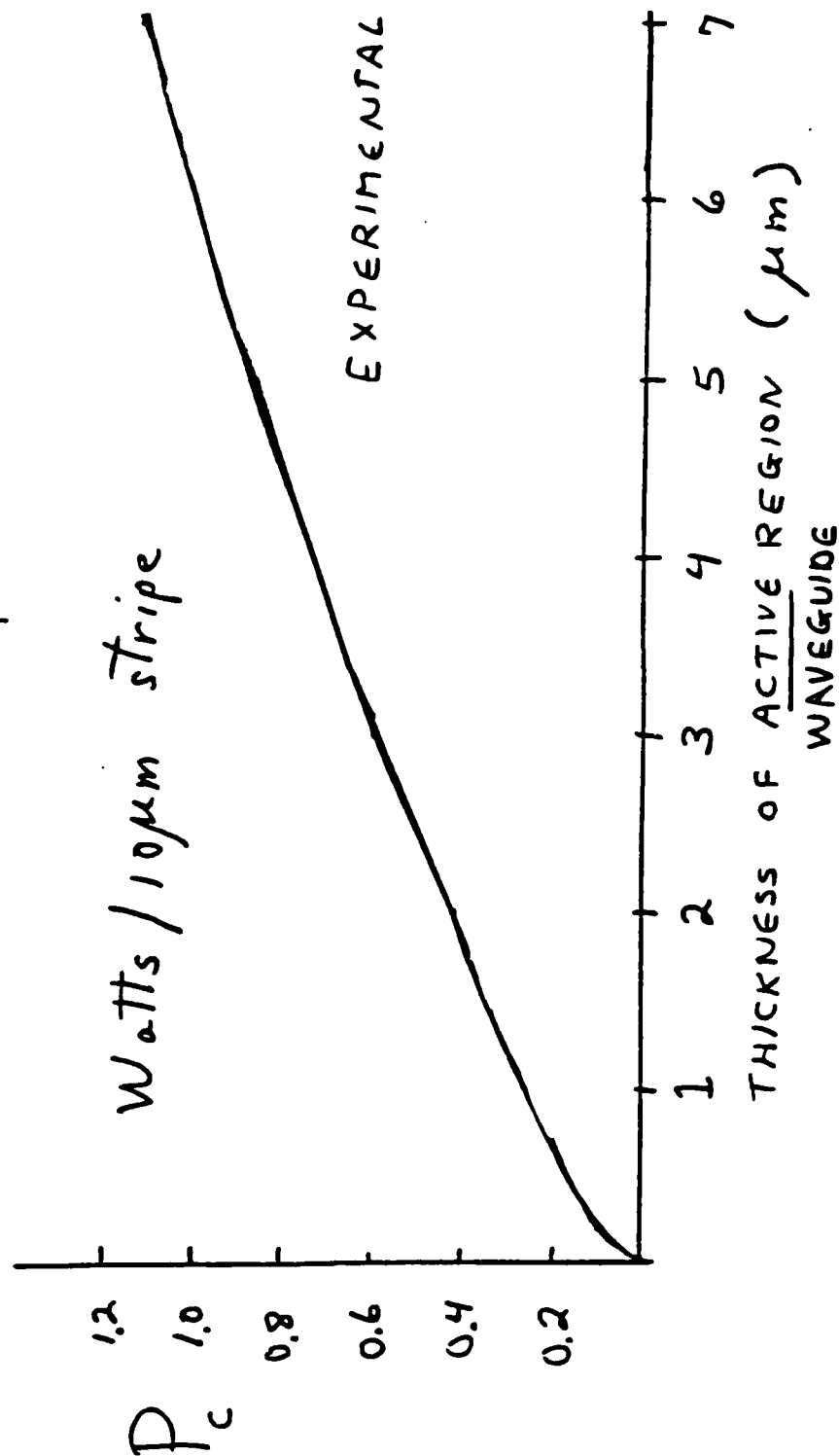
LIMITS ARE FACET DAMAGE

USE LARGE OPTICAL CAVITY (LOC)



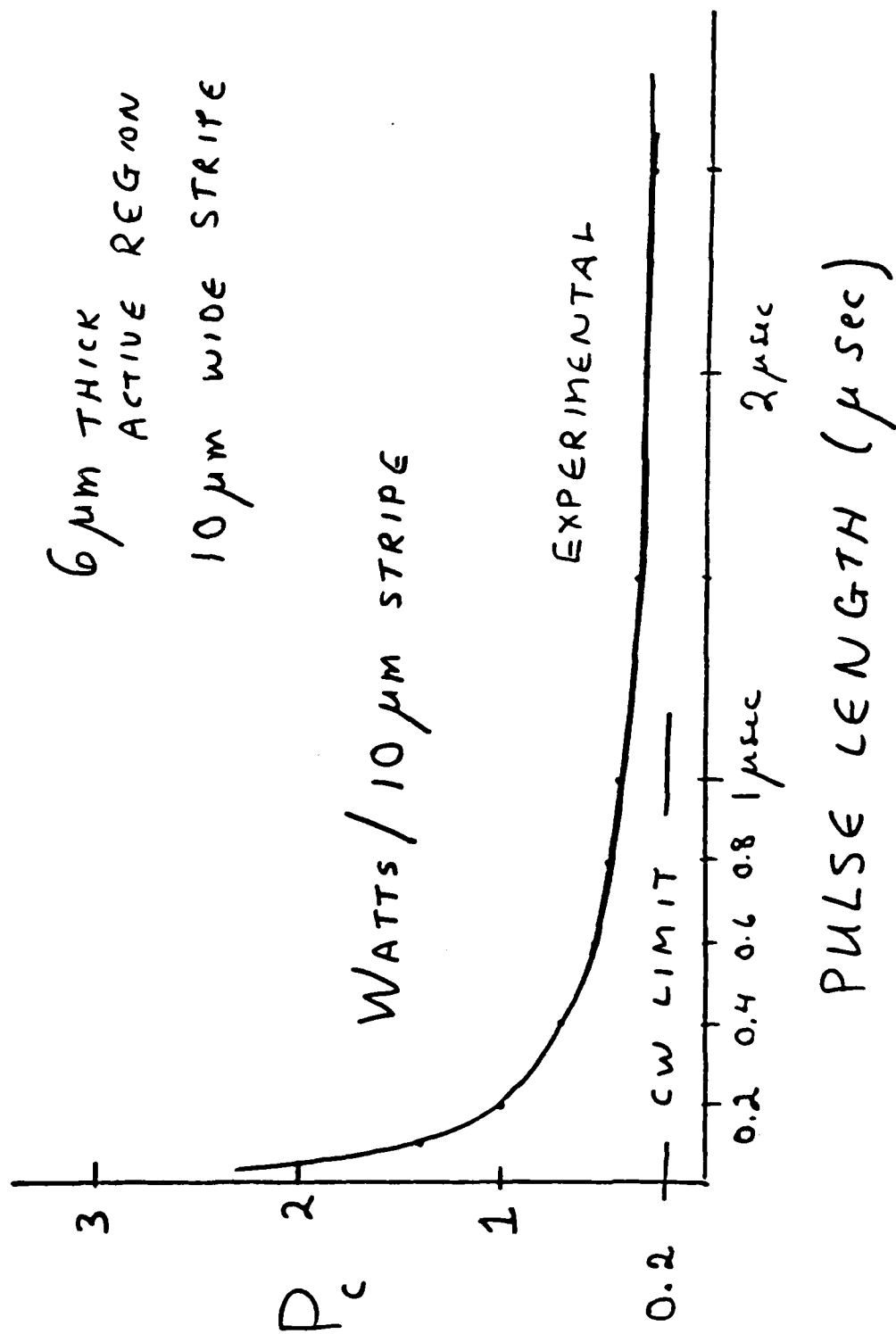
PEAK POWER FROM GaAlAs LASER (LOC)

200 nsec pulse



LIMITATION: OPTICAL DAMAGE

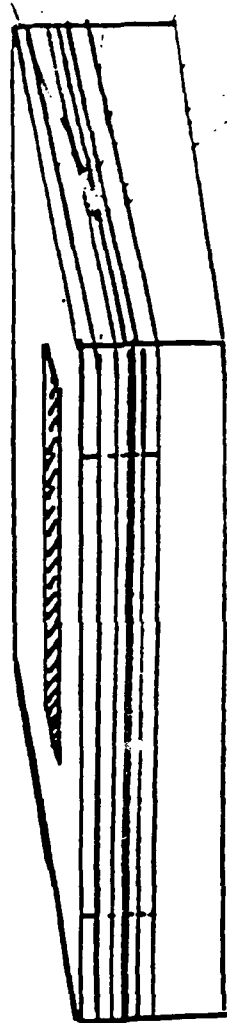
PEAK POWER FROM GaAs LASER AS A FUNCTION OF PULSE WIDTH



FURTHER POWER INCREASES

FROM

WINDOW STRIPE LASERS



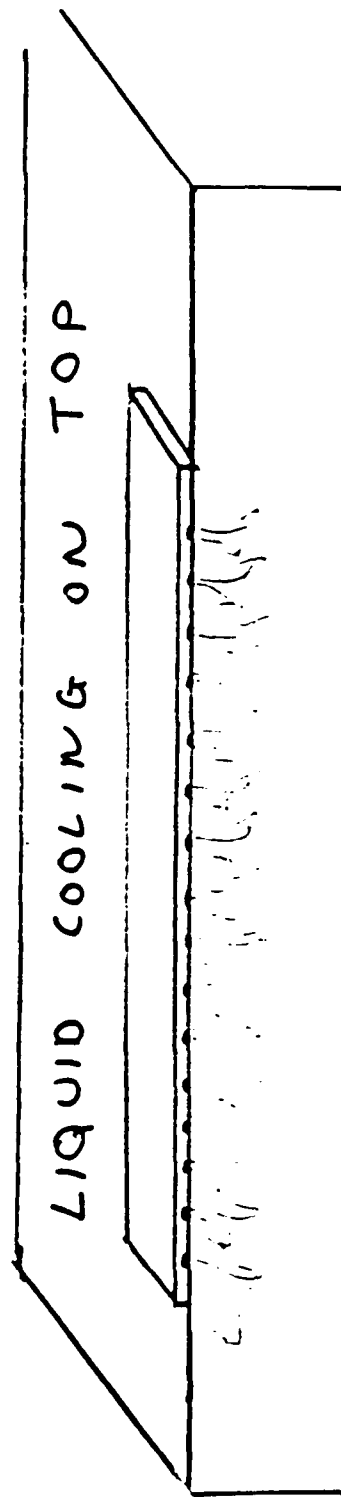
ALLOWS 4 x MORE POWER
OUT

POSSIBILITY: 1 WATT / STRIPE

LOC + WINDOW

ULTIMATE POWER PREDICTIONS

1 WATT / $10\ \mu\text{m}$ STRIPE PLACED
 $50\ \mu\text{m}$ APART ON HEAT SINK



$10\ \text{cm} = 2000\ \text{DIODES} = 2\ \text{kWATTS}$

BEST CURRENTLY AVAILABLE EXPERIMENTAL RESULTS

1.5 WATTS IN $15\mu\text{m}$ STRIPE, PULSED
EFFICIENCY : 30-40% (JAPAN)

0.4 WATTS IN $80\mu\text{m}$ STRIPE, CW
(JAPAN)

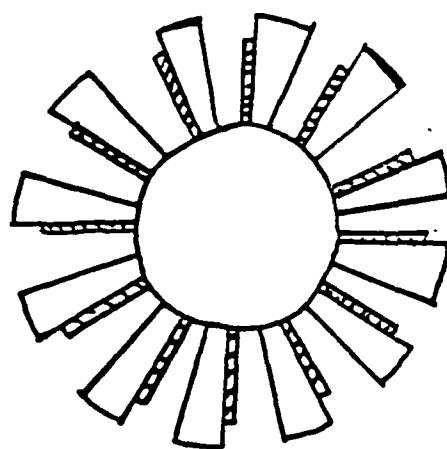
0.4 WATTS IN $100\mu\text{m}$ STRIPE ARRAY
CW, 17% EFFICIENCY (XEROX)

2.1 WATTS IN $100\mu\text{m}$ STRIPE, PULSED
EFFICIENCY APPROACHING 50% (XEROX)

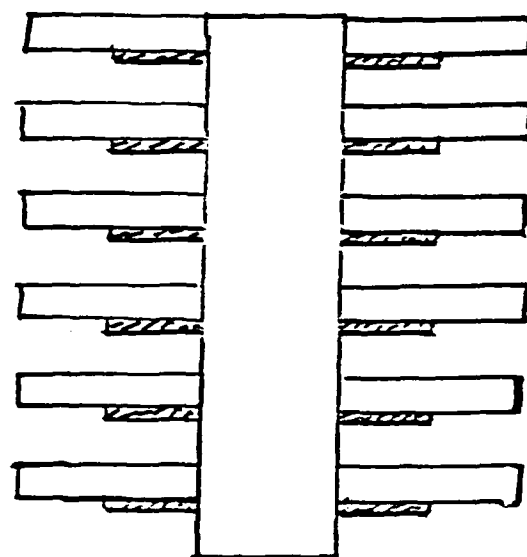
18 WATTS IN $200\mu\text{m}$ STRIPE, PULSED
SINGLE HETEROSTRUCTURE : ~35% EFFICIENCY
CW NOT POSSIBLE (ENGLAND)

PUMPING GEOMETRIES

CROSS-SECTION



ROD



SLAB

NEW TIMING SEQUENCES

200 nsec PULSES / CW

CURRENTLY STUDIED

POSSIBILITIES:

msec

sec

nanosecond

psec

RESEARCH INTO PUMPING OF SOLID STATE
LASERS WITH DIFFERENT TIMING

SOLID STATE TECHNOLOGY

MOCVD LASER FABRICATION

FOR HIGH UNIFORMITY - LARGE ARRAYS

RESEARCH REQUIRED TO DEVELOP

HIGH-POWER ARRAYS BY MOCVD

IC PROCESSING ADVANTAGES

RIGID, DURABLE

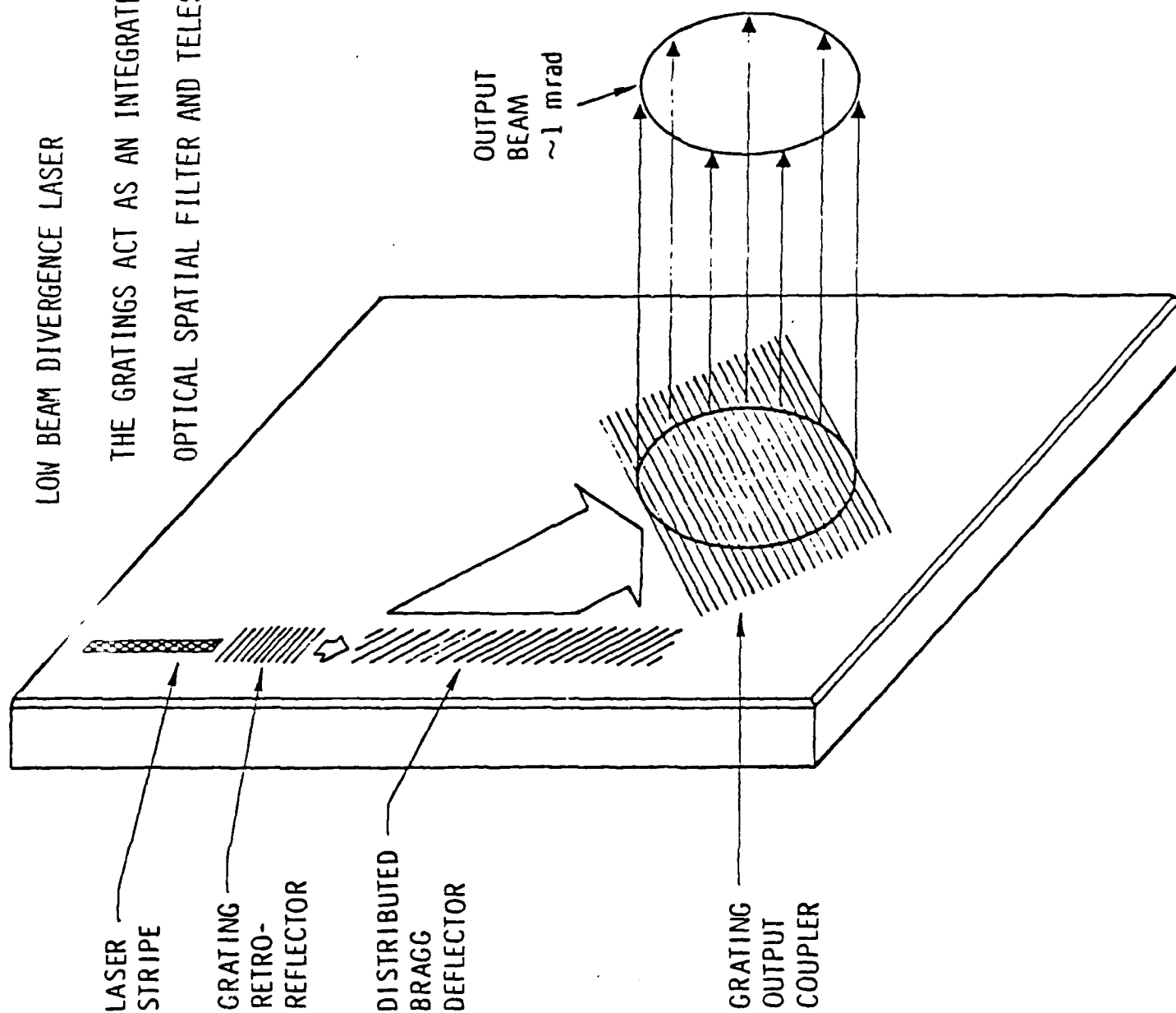
DIRECT USE OF SEMICONDUCTOR LASER ARRAY

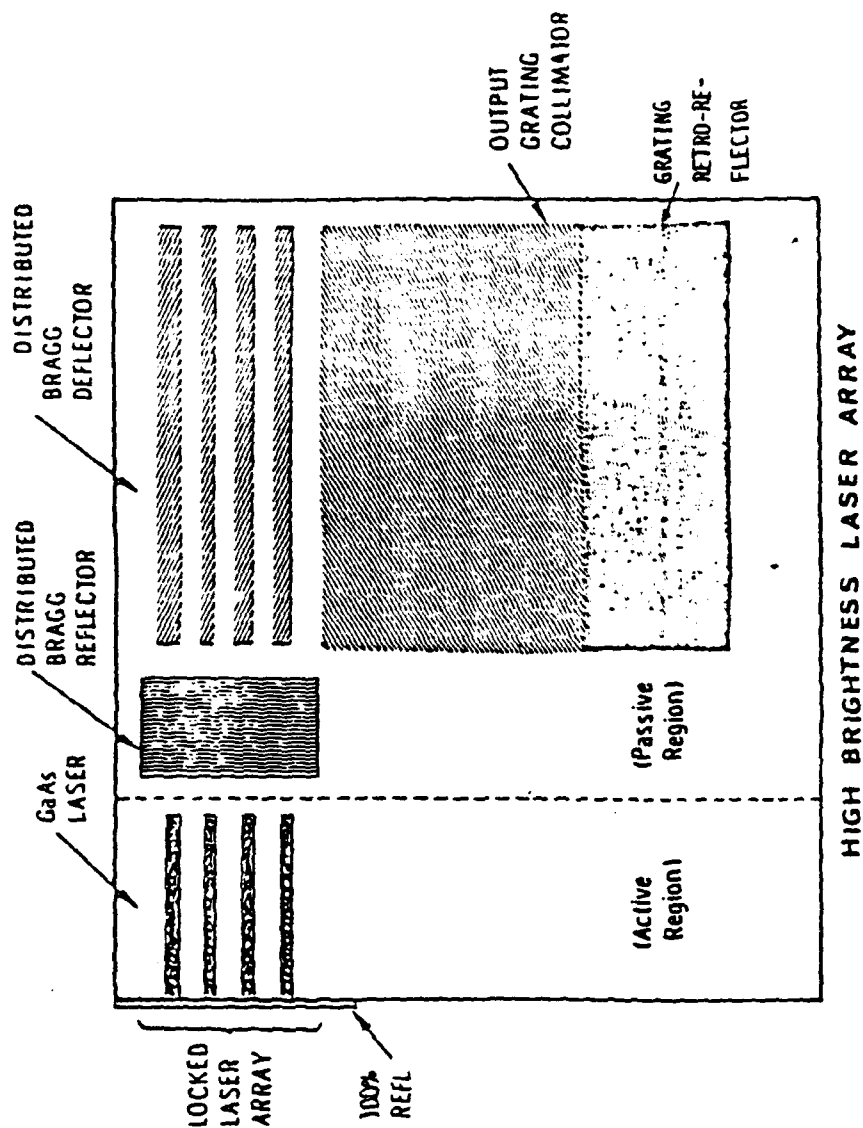
REQUIREMENT :
COHERENTLY COMBINE AND
COLLIMATE POWER

SOLUTION:
USE INTEGRATED OPTICS
DISTRIBUTED BRAGG DEFLECTOR
ACTS TO PHASE-LOCK, COHERENTLY
COMBINE AND COLLIMATE

LOW BEAM DIVERGENCE LASER

THE GRATINGS ACT AS AN INTEGRATED
OPTICAL SPATIAL FILTER AND TELESCOPE.





Design for high brightness laser array. Beam is emitted normal to the plane of the figure. Although an array of only four lasers is shown, the design may be scaled up to larger arrays. Design studies have shown estimates of powers in excess of 1 watt in 1 mrad may be produced by such an array.

RECENT LASER STUDIES

I. X-RAY LASER STATUS

J. McIVER#, S. ROCKWOOD*, K. BOYER**

II. DIRECT NUCLEAR PUMPED LASERS

M. O. SCULLY#

JULY 1983

EDITED BY

P. HAMMERLING

LA JOLLA INSTITUTE

P. O. Box 1434

La Jolla, CA 92038

(619) 454-3581

THIS RESEARCH WAS SPONSORED BY THE
DEFENSE ADVANCED RESEARCH PROJECTS
AGENCY UNDER ARPA ORDER NO.: 3710
CONTRACT NO.: MDA-903-82-C-0376

The views and conclusions contained in this document are those of the authors and should not be interpreted as necessarily representing the official policies either express or implied, of the Defense Advanced Research Projects Agency or the United States Government.

University of New Mexico

Associate of the La Jolla Institute (Max Planck Institute)

* Independent Consultant

** University of Illinois at Chicago

TABLE OF CONTENTS

	<u>Page</u>
I. X-RAY LASER STATUS	1
EXECUTIVE SUMMARY	2
1. Survey of X-Ray Laser Schemes (J. McIver)	5
2. X-Ray Laser Scaling Considerations (S. Rockwood)	21
A) Resonantly Pumped	27
B) Recombination Lasers	36
3. Multiphoton Pumping (K. Boyer)	42
Appendix	
II. DIRECT NUCLEAR PUMPED LASERS (M. O. Scully)	47
Appendix	

I. X-RAY LASER STATUS

EXECUTIVE SUMMARY

This the report presents a broad survey of approaches to X-Ray laser production and laser properties that are relevant to the scaling of X-ray lasers. From this foundation the specific concept of using resonant-line radiation to create an inversion in hydrogenic ions is analyzed in detail. An outline of a research effort on the principal characteristics of the recombination laser is also developed. The conclusions for these specific concepts and required future work are given in (i)-(viii) below. Recommendations (ix) and (x) refer to methods other than resonant-pumping or recombination for producing X-ray or vacuum ultra-violet (VUV) radiation.

(i) To achieve a practical energy per unit volume the laser must operate at as high a density as possible but uniform densities cannot exceed $N = 2 \times 10^{14} z^4$ because of radiation trapping.

(ii) Radiation trapping leads to geometries for the laser medium that are extremely shallow in at least one dimension. This is a major problem that requires innovative structural design for its solution.

(iii) The range of quantum numbers within which the laser may operate is tightly constrained. A lower bound of $p = 3$ is imposed by inversion criteria while an upper bound is set by keeping

$$I - E_p < kT_e$$

to avoid collisional ionization losses from the upper laser level. Also operating efficiency decreases as p^{-3} .

(iv) The maximum efficiency for the radiation-pumped laser is approximately 10^{-6} to 10^{-5} . A major design problem is the inherent inefficiency of the conversion of a broadband light source, such as a plasma, into a narrow emission line for optical pumping.

(v) The recombination-pumped laser, while not analyzed in full detail, shows more promise for efficient operation and scaling than the resonant line radiation-pumped approach. The principal advantages are: (1) better utilization of broad band pump radiation, and (2) a steep density gradient formed in the expanding plasma that facilitates radiative relaxation of the lower laser level.

(vi) Energy level data and line-broadening mechanisms for highly-ionized atoms (over 50 electrons removed) are not known well enough to allow credible laser modeling nor can they be calculated with the present, state-of-the-art codes.

(vii) A laboratory source (or sources) of experimental data for spectroscopy, kinetic rates, and actual X-ray lasing must be established to guide development of the requisite atomic theory and laser models. It is noted that the largest degree of ionization reported to date is 45 times ionized gold obtained with the Helios laser at Los Alamos.

(viii) Amplified spontaneous emission is probably not adequate for practical systems. Beam divergence plays such a strong role in determining the useful range of a laser that investigation of highly nonlinear optical techniques for generating low divergence X-ray sources that might serve for injection of an amplifier should be supported.

(ix) The production of X-rays by other than laser-plasma methods needs consideration, in particular variants of free-electron lasers and other electron-beam plus laser methods need to be looked at in detail.

(x) Multiphotonic Pumping - Very recent work indicates that a new effect in laser-matter interaction involving collective effects in high Z atoms may provide an efficient mechanism for multi-photon ionization and pumping. It does not suffer from the defect mentioned in (iv) above and can serve as a source of data required in (viii) above. Although this new area still requires more experimental and theoretical investigation, it is considered the one most likely to give both near-and longer-term results with a potential for scaling to larger devices.

1. SURVEY OF X-RAY LASER SCHEMES

J. MCIVER

I. INTRODUCTION

In this part of the report, the proposed methods for generating coherent soft X-ray and vacuum ultraviolet radiation are reviewed. For our purposes, the wavelengths of interest are assumed to lie in the range of .1 - 100 nm, i.e. photon energies between roughly 10 KeV and 10 eV. The emphasis will be on the manner in which coherent short wavelength radiation can be generated. The question of resonators for such a laser will not be discussed in any detail.

In the first section, methods for obtaining population inversions in the outer shells of multiply-charged ions in plasmas are discussed. The advantages and disadvantages of several schemes are presented along with a review of the present experimental situation. In the next section generation of X-rays by the interaction of relativistic-charged particles with a periodic potential is reviewed. Schemes that fall in this category are free-electron lasers, Compton lasers, charged particles channeled in crystals, etc. The fourth section deals with those phenomena that do not fall into the other two categories. In the last section, the results of the paper are summarized.

II. TRANSITIONS IN THE MULTIPLE-CHARGED IONS

The vast majority of the published literature that is concerned with VUV lasers considers methods for creating population inversions in multiply-charged ions. As will be shown in this section, theoretical considerations indicate that with existing technical means amplification down to wavelengths of 1 nm can be achieved. The major problem with these systems is not the pumping

energy requirements but rather the preparation of the correct conditions in the plasma.

In order to discuss various pumping schemes it is useful to have in mind a simple model. We will be concerned with the transition between an upper electronic state u in a multiply-charged ion and some lower state L . The difference in energy between the two states determine the wavelength λ of the laser through the relation $E_u - E_L = hc/\lambda$ where E_u and E_L are the energies of the upper and lower states. The populations N_u and N_L of the electrons in the upper and lower states are determined by the rates at which electrons are pumped into them from other states, the rates at which electrons decay from these states and transitions between the two states. In most areas of interest, these transitions are either radiative or caused by collisions with plasma electrons.

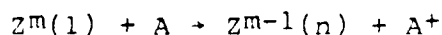
In order to have amplification it is necessary to achieve populations N_u and N_L such that the gain coefficient

$$G = N_u \sigma_i - N_L \sigma_a$$

is positive. Here σ_i and σ_a are cross sections for induced emission and resonant absorption. The most logical way to achieve this condition is to preferentially pump electrons into the upper state. This can be achieved in one of four general ways.

A. Charge-Transfer Pumping [1-5]

The basic idea of charge-transfer pumping is based on the fact that an ion of an element Z and ionization m can in a collision with an atom A be preferentially scattered into an excited state n with a reduction in the degree of ionization:



Therefore, by mixing fluxes of Z^M ions and A atoms a population inversion between the state n and some lower state can in principle be formed. At first glance, this is an attractive scheme because the charge-transfer cross sections are fairly high [5] [$\sigma=10^{-15}$ cm² for collision velocities $v \sim 10^7$ cm/sec]. Unfortunately, the proposed mixing schemes have problems of their own that limit the usefulness of this technique in the VUV range.

Two general schemes have been proposed for mixing the two components. In one case an ion beam is passed through a gas [2,5]. While in the other, a moving plasma collides with a gas [3,5]. Lasing can then occur either along the direction of motion of the ions or transverse to it.

Each method of pumping has its drawbacks. One problem is the instabilities that occur in mixing the ions and gas. The characteristic length scale of the instability and its formation time limit both the duration of the lasing and the region over which it can occur. These constraints in essence limit the wavelength for which this method of pumping is useful to something on the order of $\lambda > 100$ nm. [5]. The plasma/gas system has the further problem that electrons escaping from the plasma to distances of the order of a Debye length can preionize the cold gas. Nevertheless, charge exchange has been reported as producing conditions for amplification of radiation [4]. The charge transfer occurred between natural sodium atoms and protons. Optical gain was measured for the Lyman α line ($\lambda = 121.57$ nm) to be 1.4 cm⁻¹.

B. Excitation From the Ground State [5,6,7]

In this case, it is necessary to achieve a situation where specific levels of the lasing ion are predominantly populated by excitation. The appropriate conditions can be created under pulsed pumping (with a laser or electron beam) if the electron temperature rises rapidly or under steady state conditions (in electron density and temperature) if the recombination by passes the active level. In either case, the electron temperature must be sufficiently high and the ion density sufficiently low to ensure that radiative recombination predominates since this decay preferentially populates the ground state.

Although these systems are conceptually neat, the few practical calculations [6,7] indicate that they will be difficult to implement because of their sensitivities to reabsorption of resonant lines. This in turn implies tight constraints on the transverse dimensions of the medium [6] (10^{-2} - 10^{-4} cm) and the ratio of the diameter to the length [7] (10^{-3} - 10^{-4}). Needless to say, maintaining a long narrow strip without distortion is very difficult in a plasma.

The second problem with these systems is the difficulty of the analysis. These methods require the use of ions with complex spectra thus making both the theoretical and experimental investigations unreliable. Such things as the relaxation kinetics and various cross sections are simply not known very accurately.

C. Resonant Photo-Pumping [8-15]

This method is similar to the method of collisional excitation discussed in the previous section. The difference is

that in this case line radiation from a second ion in the plasma is used to pump the lasing ion. The pumping species could be the same element as the lasant but in a different ionization stage or an entirely different element. As example that has been investigated experimentally [10,11] is the inversion of $n = 4$ and $n = 3$ levels in Mg XII which were pumped by resonant Lyman radiation from C VI. The lasing transition occurs at ~ 13 nm. Other schemes that have been proposed [12] are pumping of Al XII by Si XIII with emission at 4.4 nm and pumping of Ne XI by Na X with emission at 5.8, 8.2 and 23 nm.

A variety of methods to achieve inversion have been reviewed and discussed by Hagelstein of Lawrence Livermore National Laboratory (LLNL) [13-15]. It is proposed to use the Novette laser in either the $1.06 \mu\text{m}$ or $0.53 \mu\text{m}$ mode to both strip and excite via transitions in an exterior target directly illuminated by the laser, an interior neon plasma. Ionization of the neon is to be achieved by means of continuum X-rays while the excited-state population is produced via resonant line pumping from the exterior target. Inversion in Ne^{2+} is predicted at 23.1 nm among other transitions. As noted below, radiation trapping may seriously affect this type of pumping scheme.

Because of the similarity between this method and the previously-discussed one, they have the same problems with their implementation. For example, radiation trapping is a problem in both cases. Likewise, the density at which these schemes give maximum gain are bounded above by the tendency of collisional process to bring the state densities into local thermodynamic equilibrium and below by the domination of radiative pumping and

depletion [12]. In addition to these problems resonant photo-pumping is optimized if the temperature of the pumped plasma is lower than the pumping plasma [12]. Although it is possible to achieve this condition in a laser - or electron beam - produced plasma it is not easy.

D. Recombination Pumping [5,13]

Recombination pumping is based upon the fact that electrons in a neutral plasma of nearly fully-stripped ions recombine predominately into highly excited states as the plasma cools. Thus, in contrast to the previous two methods of pumping, this scheme occurs after the heating pulse has reached its peak since it is necessary for the plasma to cool before large scale recombinations occurs. In principal, this is all that is necessary to create a population inversion. For instance, if we start with a neutral plasma of fully-stripped ions and then rapidly cool it so that the electrons recombine into highly excited states, a population inversion exists with respect to the ground state. The drawback of this method is the plasma must be cooled rapidly with respect to the spontaneous lifetime of the excited state which is typically $< 10^{-11}$ sec. Since this is not feasible at the present time, other methods are used.

Once an electron is in a highly-excited state it decays by a chain of transitions to the ground state. If one of the lower states has a higher decay rate than the state or states above it then a population inversion can exist. The object is then to prepare the plasma so that collisional or radiative recombination predominantly depopulates some lower state or states. Of these two

de-excitation mechanisms radiative recombination is the most useful since the radiative rate increases as Z^4 whereas the collisional rate as Z^{-3} for increasing atomic number z . This scaling along with other considerations limits the wavelength range in which collisional recombination can be used to $\lambda > 40$ nm [5] whereas radiative recombination is good for $\lambda > 1$ nm [13].

As with other pumping methods, this scheme is not restricted so much by the pump power but by the experimentalist's ability to prepare the initial state of the plasma. For instance, a detailed calculation [13] of the pumping requirements has estimated that if the gain coefficient $G \approx 5$ cm $^{-1}$ and an $n = 3 \rightarrow 2$ transition is assumed, then for $\lambda = 1$ nm the plasma power density should be 10^{15} W/cm 2 . This is well within the range of current lasers used in fusion experiments.

The condition on the electron temperature and density as well as the cooling rate are more difficult to achieve. For example, the electron density is bounded from above by the requirement that collisional depopulation from the upper to lower level not be dominant over the radiative decay [13]. This usually requires that electron densities are of two orders of magnitude below solid densities. The cooling time is obviously limited by the requirement that it be short in comparison the recombination time [5].

Nevertheless, these conditions can be met in the laboratory in a limited volume. For example, a laser-produced plasma that is free to expand can satisfy these conditions. Electron beam heated plasmas are another possibility.

Population inversions have been seen in a number of laser-produced plasmas. For example, population inversions in carbon have been reported by groups at Hull University [17,18], Culham Laboratory [19] and the Naval Research Laboratory [20] and in aluminium by the University of Rochester group [21] and the Orsay group [22-25]. The wavelength for these transitions are in the range of 10 nm to 50 nm.

The University of Hull experiments observed inversion in hydrogenic carbon ions on the Balmer- α transition at 18.2 nm. These experiments employed a Nd³⁺-glass laser (1.06 μ m) emitting about 5j in a 100 ps pulse focused onto a carbon fiber. Similar experiments are planned at the Rutherford-Appleton Laboratory for this summer using their laser facility with an especially designed optical system [26]. The Rutherford-Appleton facility can also operate in the frequency-doubled (0.53 μ m) mode.

Jaegle's group at Orsay, using the laser facility of the Ecole Polytechnique, report inversion in Al³⁺ on several lines when illuminated by a 1.06 μ m laser focused to form a line plasma on a planar target. With an incident energy of 30j in a 3 ns pulse, inversion was seen at 10.56 nm and with a 30 ns pulse at 11.74 nm [22-25].

Radiation trapping is again a problem since the lower level is generally given by $n = 2$ or 3 . Therefore depletion of the inversion by populating the lower level due to radiation trapping is a problem [16]. Augmenting recombination pumping by charge transfer or by photo-excitation may alleviate this problem [13].

Scaling considerations to resonantly-pumped and recombination lasers are given in detail in part II of this report below.

III. CHARGED PARTICLES IN PERIODIC POTENTIALS

One of the newest methods for generating coherent radiation is through the interaction of a relativistic charged particle with a periodic electromagnetic potential. These potentials could be a periodic magnetic field as in the standard free-electron-laser [27], the potential of a crystal as in channeling radiation [28], an oppositely directed laser field as in the Compton laser [29], etc. In point of fact, the periodic potential is not needed. A medium with an index of refraction greater than one will do. From the point of view of generation of VUV and X-ray radiation, the devices with a periodic field are more promising so we will confine our discussion to these.

In order to understand how these devices work, it is more convenient to view the interaction from the rest-frame of the particle. In this frame the particle appears to stand still while the potential appears to move past the particle as if it were an electromagnetic wave with a Doppler-shifted wavelength (this is only approximately true if the potential in the lab frame is static). When the particle interacts with this wave, the electromagnetic field "reflects" from the particle while imparting a small momentum (recoil) to the particle. If we now return to the lab frame and ask what is the frequency of this emitted wave we find that the initial period of the potential has been Doppler shifted twice to give a new wavelength

$$\lambda = \frac{1}{2} \left(\frac{mc^2}{E} \right)^2 \lambda_0$$

where λ_0 is the period of the potential, E is the energy of the particle and mc^2 is its rest energy. We therefore see that if the particle's energy is high enough and the period of the potential small enough then, in principle, any wavelength radiation can be generated. Unfortunately, as the energy of the incoming particles is increased for a given device, the gain per unit length per particle decreases. It is therefore necessary to increase the interactions length and/or the strength of the potential and/or increase the particle current in order to keep the output intensity constant.

Of the three types of potentials mentioned at the beginning of the section each has its drawbacks, particularly at the shorter wavelengths. The standard free-electron beam configuration of a static, periodic magnetic field is limited to magnetic periods of greater than few millimeter. Thus, if the most energetic electron accelerators are used it is possible to generate 1 nm radiation. On the other hand, recent estimates have shown that the magnetic structure will have to be hundreds of meters of even kilometers in length to produce interesting amounts of radiation [27].

Crystal potentials already have periods that are at most several angstroms in length restricting their usefulness to the shorter end of the range we are investigating [5]. It is possible to extend this range into longer wavelengths if a different type of radiation is considered, the so called channeling radiation [28]. Even in this case, the emitted radiation will typically have wavelengths shorter than 10 nm. This seems to be about the upper

limit in wavelength that one can get from channeling radiation. Even the consideration of artificial lattices such as superlattices does not appreciably change this number. The usefulness of these devices is limited by the amount of current a crystal can tolerate without being damaged [28].

The remaining device that was mentioned at the beginning of the section is the Compton laser. In this system the potential is an electromagnetic wave travelling in the opposite direction to the charged particle. Here again, the period of the potential is not the limiting factor. The problem seems to be in maintaining a sufficient potential strength over a reasonable interaction length [29].

Although these devices have their drawbacks, they are still very interesting as possible X-ray lasers and amplifiers. This is particularly true for hard X-rays and gamma rays where channeling radiation is now the brightest source of narrow line radiation.

MISCELLANEOUS

Although not truly an X-ray laser, great success has been achieved in generating coherent radiation in the VUV range through creation of harmonics from a laser in a nonlinear medium [30,31]. As an example, this technique has been used to generate radiation between 38 and 76 nm from a 1.06 μm laser. The power of such a system is limited by the conversion efficiencies of the process and the damage threshold of the medium.

CONCLUSIONS

We have attempted to give a brief review of the most common methods for generating coherent radiation with a wavelength between

.1 nm and 100 nm. The list of topics is by no means exhaustive, nor are the discussions of the physical mechanisms and the advantages and disadvantages complete. What is given are what are thought to be the most important points.

All of the above experiments require irradiances of $\sim 10^{11}$ - 10^{14} W/cm² and are characterized by relatively small plasma regions wherein inversion may be reached. Without mirrors to form a cavity or sufficient length for superradiance, the number of X-ray photons emitted per mode is necessarily limited.

Unless pumping schemes are devised so that a traveling-wave excitation can be produced [32], very intense collimated sources of X-rays will be hard to produce via laser-plasma interactions, especially at small facilities.

The above schemes are still very energy inefficient. The Novette experiment anticipated [33] an output of 0.1 mJ in the X-ray region or an efficiency of 10^{-7} , comparable to that obtained by multi-harmonic production [31].

Very recently some new experimental results related to multi-photon pumping and ionization have been obtained [34-35]. The results and their implications for X-ray laser production will be summarized below in the section by K. Boyer.

The first results on the efficiency of multiphotonic excitation of inner shell transitions are very encouraging. In addition the method could provide spectroscopic information for high-Z materials unobtainable by conventional techniques. For these reasons we feel that this new method, involving as it does a

fundamentally new mechanism (see discussion below), is the most promising of the methods discussed in this report.

ACKNOWLEDGEMENT

We are very grateful to Dr. C. Rhodes for material in advance of publication.

REFERENCES

- [1] J. Perel and H. L. Daley, Phys. Rev. A 4, 162 (1971).
- [2] W. H. Louisell, M. O. Scully and W. B. McKnight, Phys. Rev. A 11, 989 (1975).
- [3] D. Anderson, J. McCullen, M. O. Scully and J. F. Seely, Opt. Comm. 17, 226 (1976).
- [4] R. Tkach, H. Mahr, C. L. Tang and P. L. Hartman, Phys. Rev. Lett. 45, 542 (1980).
- [5] F. V. Bunkin, V. I. Derzhiev and V. I. Yakovlenko, Sov. J. Quantum Electron, 11, 981 (1981).
- [6] A. V. Vinogradov, I. Yu. Skobelev, I. I. Sobel'man and E. A. Yukov, Sov. J. Quantum Electron, 5, 1192 (1975).
- [7] A. V. Vinogradov, I. I. Sobelman and E. A. Yukov, Sov. J. Quantum Electron, 10, 754 (1980).
- [8] A. V. Vinogradov, I. I. Sobelman and E. A. Yukov, Sov. J. Quantum Electron, 5, 59 (1975).
- [9] V. A. Bhagavatula, J. Appl. Phys. 47, 4535 (1976).
- [10] V. A. Bhagavatula, IEEE J. Quantum Electron, 16, 603 (1980).
- [11] K. G. Whitney, J. Davis and J. P. Apruzese, Phys. Rev. A 22, 2196 (1980).
- [12] J. P. Apruzese, J. Davis and K. G. Whitney, J. Appl. Phys. 53, 4020 (1982).
- [13] P. L. Hagelstein, "Physics of Short Wavelength Laser Design," NCRL-53130, Jan. 1981.
- [14] P. L. Hagelstein, "Short Wavelength Laser Design," UCRL-86376, July 1981.
- [15] P. L. Hagelstein, "Resonantly-Pumped Soft X-Ray Laser Using ICF Drivers," UCRL-87122, Dec. 1982.
- [16] R. C. Elton, Optical Eng. 21, 307 (1982).
- [17] D. Jacoby, G. J. Pert, S. A. Ramsden, L. D. Shorrock and G. J. Tallents, Opt. Comm. 37, 193 (1981).
- [18] D. Jacoby, G. J. Pert, S. A. Ramsden, L. D. Shorrock and G. J. Tallents, J. Phys. B: At. Mol. Phys., 15, 3557 (1982).
- [19] F. E. Irons and J. J. Peacock, J. Phys. B, 7, 1109 (1974).

- [20] R. H. Dixon and R. C. Elton, Phys. Rev. Lett. 38, 1072 (1977); R. H. Dixon, J. F. Seely and R. C. Elton, Phys. Rev. Lett., 40, 122 (1978).
- [21] V. A. Bhagavatula and B. Yaakobi, Opt. Comm. 24, 331 (1978).
- [22] G. Jamelot, P. Jaegle, A. Carillon, and C. Wehenkel, J. Phys. (Paris) Colloque C1. Suppl. #2, 40 C1-91 (1979).
- [23] P. Jaegle, A. Carillon, C. Wehenkel, A. Surreau, and H. Guennou, J. Phys. (Paris) Colloque C3. Suppl. #4, 41, C3-191 (1980).
- [24] Rapport D'Activite 1981, GRECO, Ecole Polytechnique (Palaiseau, 1982) p. 167.
- [25] G. Jamelot, P. Jaegle, A. Carillon, A. Bideau, C. Moller, H. Guennou, and A. Surreau, Proceedings of the International Conference on Lasers -1981, p. 178.
- [26] D. Nicholas, Private communication.
- [27] G. Moore, Private communication.
- [28] N. P. Kalashnikov and M. N. Srikhonov., Sov. J. Quantum Electron 11, 1405 (1981).
- [29] P. Meystre, Private communication.
- [30] J. Reintjes, C. Y. She and R. C. Eckhardt, IEEE J. Quantum Electron, QE-14, 581 (1978).
- [31] A. L. Robinson, Science, 220, 1259 (June 17, 1983).
- [32] G. Chapline and L. Wood, Physics Today, 28, p. 40 (June 1975).
- [33] Lasers and Applic. 2, 48 (April 1982).
- [34] T. S. Luk, H. Pummer, K. Boyer, M. Shahidi, H. Egger, and C. K. Rhodes, "Anomalous Collision-Free Multiple Ionization of Atoms with Intense Picosecond Ultraviolet Radiation", Phys. Rev. Lett., 51, 110 (1983).
- [35] T. Srinivasan, H. Egger, T. S. Luk, H. Pummer and C. K. Rhodes, "Stimulated Extreme Ultraviolet Emission at 93 nm in Krypton. To be published in Laser Spectroscopy VI. Proc. 6th Intl. Conf. Interlaken (1983), Springer Series in Optical Sciences, Ed. H. P. Weber and W. Luthry (Springer-Verlag).

2. X-RAY LASER SCALING CONSIDERATIONS

S. ROCKWOOD

X-RAY LASER SCALING CONSIDERATIONS

I. INTRODUCTION

If energy is delivered to a target at a rate much greater than the rate at which it can be carried away by a thermal diffusion wave into the target, then a thin layer of the material is vaporized and ejected at a high velocity. In this case, the resulting impulse to the target is the principal cause of damage. And, for this short pulse limit, the damage inflicted is a function of the fluence (energy/area) absorbed by the target. To a good approximation the impulse is given by

$$J = (2\phi_T/K_v)^{1/2} \quad (1)$$

where K_v is the mass absorption coefficient. Further details of the optimization of the impulse are given in Section IV.

The fluence, ϕ_T , absorbed by a target by a beam of light having divergence $\Delta\theta$ is given simply by

$$\phi_T = \alpha \eta E_{\text{pump}} / \pi R^2 (\Delta\theta)^2, \quad (2)$$

where R is the range to the target, α is the absorption coefficient of the target, and η is the conversion efficiency from the pump energy, E_{pump} , to directed energy. Because a certain value of ϕ_T must be achieved to damage the target, the useful range of the weapon is determined by Equation (2) in terms of the parameters η , E_{pump} , and $\Delta\theta$ that are under the control of the attacker. The parameter α depends on the wavelength of the light but is not properly chosen as a free parameter of the attacker since it may be changed by the defender's choice of construction materials.

Thus, the task of scoping a directed energy system's useful range involves examining η and $\Delta\theta$. The remainder of this paper

outlines the basic physical mechanisms that may limit these parameters.

The philosophy of this "first cut" is to ignore engineering constraints and search various laser concepts for the limits imposed upon η and $\Delta\theta$ by fundamental physics considerations. If, even under these best of conditions, the range is not usefully large the concept under consideration will be discarded.

II. ATOMIC CONFIGURATIONS OF X-RAY LASERS

The energy of atomic transitions increases as Z^2 , where Z is the atomic number. As a consequence, most proposals for X-ray lasers use highly ionized atoms as the lasing medium. This adds the complication of preparing the ions in the desired state of ionization as well as creating an inversion within the appropriate energy levels of the chosen ion.

Figure 1 displays the ionization potential of Xe as a function of the number of electrons, $X < Z$, removed from the neutral atom.⁽¹⁾ Note that the energy required to remove successive electrons is relatively small $(E_{X+1} - E_X)/E_X \ll 1$ except at closed shell configurations. As a consequence, the number of ions in a particular charge state will be maximized near a fully-stripped nucleus ($X=Z$) or the closed shells $X = Z-2$ and $X = Z-8$.

This study will thus consider the atomic physics of hydrogen-like ions, ions in He- and Ne-like closed shells, and their adjacent charge states, namely, alkaline or halogenic ions. Section III will consider specific concepts for X-ray lasers. However, before beginning any one concept in detail, a few general features of all X-ray lasers will be outlined.

It is noted that the spontaneous transition rate for a dipole-allowed transition between a level p and the ground state is(2)

$$A(p) = \frac{1.6 \times 10^{10} Z^4}{p^3(p^2-1)} \approx \frac{1.6 \times 10^{10} Z^4}{p^5} \quad (3)$$

so that the spontaneous loss of energy from the lasing medium is

$$P > A_p(E_p - E_1)N_p = 3.5 \times 10^{-8} \frac{N_p Z^6}{p^5} \text{ (W/cm}^3\text{)} \quad (4)$$

where N_p is the number of ions in the upper laser level. Equation (4) defines a lower bound on the pumping power that must be supplied to an X-ray laser to compensate radiative losses. Notice that an increase of Z^2 in photon energy of the laser requires an increase of Z^6 in input power. It also follows that because of the rapid increase in $A(p)$ with Z one should select an upper laser level that is not connected radiatively to the ground state by a dipole-allowed transition. For example, using a D angular momentum state as the upper level in an atom with a S ground state allows, in principle, D→P lasing followed by P→S relaxation of the lower level.

Because of the short lifetime of X-ray transitions given by Equation (3) all X-ray lasers will behave in a quasi-cw mode of operation. Thus, energy extraction will be determined by the saturation power. The saturation power for a laser is defined by

$$I_s = h\nu/\sigma\tau \quad (5)$$

where τ is the lifetime of the lower laser level given by

$$\tau^{-1} = \tau_{\text{rad}}^{-1} + \tau_{\text{coll}}^{-1} \quad (6)$$

and the stimulated emission cross section is

$$\sigma = \lambda^2 A S(\lambda) / 8\pi \quad , \quad (7)$$

where $S(\lambda)$ is the line shape factor.

For the conditions of X-ray lasers, the line broadening will arise primarily from three sources:

A. Doppler broadening with

$$\Delta\omega_D = 7.7 \times 10^{-5} \omega \left[\frac{T(\text{ev})}{M(\text{amu})} \right]^{1/2} ; \quad (8)$$

B. Stark broadening (3) with

$$\Delta\omega = 5 (p^2 h / z m) N^{2/3} ; \quad (9)$$

C. Radiative (uncertainty) broadening

$$\Delta\omega = 2 \pi A(p) \quad , \quad (10)$$

where $A(p)$ is given in Equation (3). In Ref. (3) it is shown that Stark broadening equals Doppler broadening of a transition from p to q for plasma densities

$$N_S = 3 \times 10^{16} z^{21/4} / p^3 q^3 \quad (11)$$

By comparing Equations (10) and (8) one can also find that radiative broadening exceeds Doppler broadening for

$$z > 3.5 p^{5/2} (T/M)^{1/4} \quad (12)$$

If it is assumed that most X-ray lasers will operate at large Z under conditions where τ_{rad}^{-1} is the dominant broadening term, then using equations (3), (7), and (5)

$$I_S (\text{W/cm}^2) = 2.6 \times 10^{10} [h\nu (\text{keV})]^3 z^4 / p^5 \quad (13)$$

where p is the principal quantum number of the lower laser level.

For all laser systems, if an optical resonator can be used to define beam quality, then

$$\Delta\theta = \lambda / D \quad . \quad (14)$$

If, on the other hand, there is no resonator, and the device output is amplified spontaneous emission (ASE) along a preferred axis, then

$$\Delta\theta \approx D/L \quad (15)$$

where D is the transverse dimension of the device and L is the length along the optical axis. Because certain X-ray laser concepts discussed later are found to invert only a very shallow depth of material, it is appropriate to note a lower limit to D. If the laser output is at a wavelength λ , then the aperture must satisfy

$$D > \sqrt{\lambda L} \quad (16)$$

or diffraction will scatter energy out of the optical path before it can travel a distance L.

One may also ask what gain length is required to achieve efficient energy extraction by amplified spontaneous emission. This length, defined as the gain length needed to have ASE into the $(D/L)^2$ solid angle of the amplifier exceed spontaneous emission is found to be

$$g_0 l > \ln [4\pi (L/D)^2] \quad (17)$$

where

$$g_0 = \sigma(N_p - N_q) \quad (18)$$

is the small signal gain. Thus, the output power of the amplifier is

$$I_{out} \approx (1/2) g_0 (L-l) I_{sat} \quad (19)$$

where I_{sat} is given by Equation (13) and the factor of 1/2 arises because energy is escaping from both ends of the amplifier. This factor of two can be recovered if an adequate mirror can be placed on one end of the amplifier. The practical problem of X-ray mirrors will not be addressed in this study.

III-A. Specific X-Ray Laser Concepts

Three mechanisms for creating an inversion in highly-ionized atoms have received most of the attention to date. The mechanisms are: resonant excitation by line radiation, three-body recombination, and resonant charge transfer. The remainder of this interim report is devoted to the scoping of limits on energy extraction and scaling for the first of these mechanisms.

A. Resonant Radiation Excitation

The basic concept is to find a strong emission line of one dominant ion that is resonant with an excited state transition in a different ion of the same element or a different element. As discussed in Sec. II, it is easy to maximize ion populations in hydrogenic-like states, and, because the transition probability is large for transitions to the ground state (Eq. (3)), a typical choice of pump photons is Lyman α $1s^2-1s2p$ radiation. In fact, for hydrogenic ions it has been observed that⁽⁴⁾, to a first approximation, Lyman α radiation in species z_{pump} will always be resonant with $p = 2$ to 4 transitions in an ionic species z_{laser} if

$$z_{\text{laser}} = 2z_{\text{pump}} .$$

This has led to experimental attempts at producing lasing in Mg XI pumped by C V.⁽⁴⁾

In Reference (5) a detailed model for predicting plasma conditions leading to the production of gain in Al XII and Ne IX is discussed. In these cases the pump radiation is L_{α} of Si XIII and Na X to excite the $1s^2-1s3p$ transition of Al XII and $1s^2-1s4p$ of Ne

IX, respectively. The latter approach differs from that of Ref. (3) by employing excitation directly from the ground state of the lasing species as opposed to the first excited state.

One of the major difficulties with the resonant pumping technique is photon trapping that limits pumping depths as well as contributes to overpopulation of the lower laser level. For example, in the Al XII ion, lasing is predicted for the $p = 3$ to 2 levels, but trapping of $1s^2-1s2p$ radiation can retain population in the $p = 2$ lower level and spoil the inversion. It is suggested that optical depths of greater than 3 will generally ruin the inversion.(6)

To evaluate the effect of this limit on laser scaling observe that, if

$$DN_I\sigma_R < 3 \quad (20)$$

where N_I is the ground state density of lasing ions and σ_R is the resonant cross-section for radiation from the lower laser level, then using Equation (16)

$$L < \frac{D^2}{\lambda} < \frac{9}{(N_I\sigma_R)^2\lambda} \quad (21)$$

The maximum stored energy of the laser will be

$$E_{\max} = h\nu_L N_I D^2 L, \quad (22)$$

which, using the limits on L and D , gives

$$E_{\max} = 81 h\nu_L / N_I^3 \sigma_R^4 \lambda_p \quad (23)$$

Taking the special case of a hydrogenic ion lasing on $p = 3 \rightarrow 2$ with trapping of $p = 2 \rightarrow 1$ and using Equation (7) for a σ in the Doppler broadened limit, Equation (23) yields

$$E_{\max}(\text{Joules}) = \left[\frac{2.2 \times 10^{14} z^4}{N_I (\text{cm}^{-3})} \right]^3 \left(\frac{T(\text{ev})}{M(\text{a.m.u.})} \right)^2 \quad (24)$$

The beam divergence in this case has been optimized to $\Delta\theta \approx \lambda/D$ so that fluence on a target at a range R is

$$\begin{aligned} \phi_T &< \frac{E_{\max} D^2}{\pi R^2 \lambda} \\ &= \frac{9 \times 10^8}{R(\text{cm})^2} \left(\frac{T}{M} \right)^3 \left[\frac{2.2 \times 10^{14} z^4}{N_I} \right]^5 \end{aligned} \quad (25)$$

which, when evaluated at a range of 1000 km and noting $A \approx 2z$, yields

$$\phi_T (\text{J/cm}^2) \approx 10^{-8} (T/z)^3 \left[\frac{2.2 \times 10^{14} z^4}{N_I} \right]^5 \quad (26)$$

Finally, assuming a desired fluence on target of 10^3 J/cm^2 and noting that for a hydrogenic ion dominated plasma $T(\text{ev}) \approx z^2$, Equation (26) gives an upper bound for the ion density

$$N < 1.4 \times 10^{12} z^{23/5} \quad (27)$$

The scaling with z is favorable because operation at low density dictates very large physical dimensions for the laser. Even with the z scaling of Equation (25), at $z = 90$, $N < 1.4 \times 10^{21} \text{ cm}^{-3}$ (and ignoring the limits observed in Reference (5) of approximately 10^{20} on N imposed by collisions) the limits for D and L yield

$$\begin{aligned} D &< \frac{3}{N\sigma} = \frac{2.1 \times 10^{-21}}{\sigma} (\text{cm}^3) \\ &\approx 10^{-7} z^2 (T/A)^{1/2} \\ &\approx 5 \times 10^{-3} \text{ cm, (with } z=90, T=z^2, A=2z) \\ L &< D^2/\lambda \approx 2.4 z^2 \rightarrow 200 \text{ m} \end{aligned}$$

As an alternative, one can relax the aperture requirements from a cross section $D \times D$ into a sheet of depth D with width $W > D$. However, this increases beam divergence as $\Delta\theta \approx W/L$. From Equation (2) one observes that the energy on target will then decrease as

$$\phi_T \sim \frac{1}{(\Delta\theta)^2} \sim \frac{L^2}{W^2} < \frac{L^2}{D^2}$$

and, since the energy of the device can only increase as the volume (LWD), with D limited by Equation (20), it is found that

$$\phi_T \sim \frac{L^3}{W} < \frac{L^3}{D}$$

will decrease from the optimum case of Equation (24) and thus require even larger values of L .

Thus, the scaling of radiation pumped devices requires an innovative architectural solution to the radiation trapping problem just described. It is also clear that to reduce size one should try to design a system than can operate in a quasi-cw mode to "reuse" the ions that are lasing. A self-terminating laser will not scale effectively. Quasi-cw operation will require a rapid deactivation rate of the lower level by either collisions (moderate density) or radiation without trapping (low density).

It is also possible to estimate the maximum efficiency, η , of the laser by again noting that most of the energy in ionization comes from the removal of the K electrons. Thus, to reach an excited state p of a hydrogenic ions requires an input energy of

$$E_{in}(\text{eV/cm}^3) < 13.6z^2 \left(1 + \frac{p^2-1}{p^2} \right) N_I \quad (28)$$

where the first term is for ionization and the second term for excitation to the upper laser level.

If the laser operates on a transition $p \rightarrow p-1$, then

$$E_{\text{out}}(\text{eV/cm}^3) < 13.6z^2 \left(\frac{1}{(p-1)^2} - \frac{1}{p^2} \right) N_I \quad (29)$$

so that the ideal or quantum efficiency is found to be

$$\eta_Q = \frac{E_{\text{out}}}{E_{\text{in}}} < \left[\frac{2p-1}{(p-1)^2(2p^2-1)} \right] \approx \frac{1}{p^3} \quad (30)$$

Since it is very unlikely that an inversion will be created relative to the ground state it will generally be true that $p > 3$ so that the quantum efficiency $\eta_Q < 0.1$.

The quantum efficiency must also be multiplied by the efficiency of using the pump energy to produce the desired level of ionization and the desired excited state of this ion. This section on radiation pumped lasers will conclude with an estimate of this pumping efficiency η_p so that the total efficiency

$$\eta = \eta_p \eta_Q \quad (31)$$

can be estimated assuming total coupling of source radiation to the laser plasma.

A blackbody pump source with a temperature T_p is assumed to be the initial source of energy. This blackbody source must ionize the lasant species to the correct charge state and similarly ionize the resonant line radiation source to the charge state appropriate to generating the correct $L\alpha$ line.

To provide flexibility of operating parameters it is assumed that the two plasmas are not contiguous so that the electron

temperature $T_e = z_L^2$, of the lasant plasma does not have to equal T_p in the source plasma.

We consider first the efficiency of using the blackbody radiation to produce hydrogenic nuclei of the lasant ion, z_L . The cross section for photoionization of a hydrogenic ion from quantum level p is given by the Kramers' formula (7)

$$\begin{aligned}\sigma_i(\nu, p) &= \frac{32\pi^2 e^6 R z^4}{3\sqrt{3} (h\nu)^3 p^5} \\ &= 2.0 \times 10^{-23} z^4 / [h\nu (\text{keV})]^3\end{aligned}\tag{32}$$

In this particular case we are in fact concerned with the photoionization of a helium-like ion, and, in general, the use of Equation (32) can lead to serious errors for multi-electron systems.(8) However, in the case of He and the He-like system Li^+ , Reference (8) shows reasonable agreement with hydrogenic ions so it is assumed Equation (32) is accurate enough for present estimates.

The energy deposited by plane wave radiation at frequency ν in a material with an ionization cross section $\sigma_i(\nu)$ is

$$E_D(\nu) = E_{in} (1 - e^{-N_I \sigma_i(\nu) D})\tag{33}$$

where N_I is the ion density and D is the depth of the material. Now recall that to avoid radiation trapping in the lasant plasma Equation (20) limits the product $N_I D$ to the reciprocal of the resonant cross section from Equation (7). A comparison of Equation (33) evaluated at its largest value, the photoionization threshold, to the resonant cross section from Equation (7) shows that for any z the resonant cross section exceeds σ_i by at least 10^2 . Hence, in

the laser plasma the product $N_I \sigma_i D$ in Equation (33) is much less than unity.

The efficiency of using blackbody radiation for ionization is defined by

$$\eta_i = \int_{\nu_{Th}}^{\infty} \frac{2\pi h \nu^3}{c^2} \left[\frac{E_p(\nu)}{e^{h\nu/hT} - 1} \frac{d\nu}{bT_p^4} \right] \quad (34)$$

where E_p is given by Equation (33) with Equation (32) substituted for $\sigma_i(\nu)$ and b is the Stefan-Boltzmann constant. In the optically thin limit that is justified for this case, as discussed above, Equation (33) may be expanded to first order in $N\sigma D$ and the integral in Equation (34) solved to yield

$$\eta_i = \left[\frac{NDZ^4}{3.1 \times 10^{23}} \right] \frac{e^{-x_T}}{T_p^3 (\text{keV})} \quad (35)$$

where $x_T = h\nu_{Th}/kT_p$ is the ratio of threshold energy for photoionization to the pump temperature. For cases of interest, $x_T > 1$.

Now, since $ND = 3/\sigma_R$ from Equation (20) and using Equation (7) in the Doppler limit, $\sigma_R = 3.5 \times 10^{-15}/Z^{5/2}$, the factor ND in Equation (35) may be replaced to yield

$$\eta_i = (1.2 \times 10^{-9} Z^{13/2}) e^{-x/T_p^3} (\text{keV}) \quad (36)$$

Finally, approximating the photoionization threshold energy by its hydrogenic value

$$x = 1.36 \times 10^{-2} Z^2 / T_p (\text{keV})$$

Equation (36) may be written as

$$\eta_i = (4.8 \times 10^{-4} Z^{1/2}) x^3 e^{-x} \quad (37)$$

The function $x^3 e^{-x}$ has an optimum value of 1.34 at $x = 3$, so the optimum efficiency for producing the lasing species by blackbody pumping is

$$n_i(\text{opt}) \approx 6.4 \times 10^{-4} z_L^{1/2} \quad (38)$$

at an optimum pump temperature of

$$T_p(\text{opt}) \approx 4.5 \times 10^{-3} z_L^2 \text{ (keV)} \quad (39)$$

A similar analysis may be performed for the efficiency of producing the hydrogenic ions that generate the resonant line radiation. However, since the line radiation source may be physically separated from the laser plasma, it need not be optically thin to the blackbody radiation at the photoionization threshold. As a consequence, the efficiency of producing a line radiation source may be higher, and the upper bound on the total laser efficiency is set by Equation (38).

This value of 10^{-4} to 10^{-3} must be multiplied by a laser extraction efficiency, η_{ex} , that depends on the degree of saturation of the laser. If it is assumed that the laser is highly saturated so that in Equation (19) $L \gg 1$, then the extraction efficiency will approach 0.5 in the absence of nonsaturable losses. An analysis of nonsaturable losses in the X-ray region is beyond the scope of this study. However, it is unreasonable to believe there will not be significant nonsaturable losses. Thus, η_{ex} will probably be 0.1 or less and the overall efficiency of converting a continuum of radiation into directed laser radiation

$$\eta = \eta_{\text{in}} \eta_{\text{ex}} \approx 10^{-4} \frac{1}{3} \eta_{\text{ex}} < 10^{-5} \quad (40)$$

is found to be quite small for the resonant pumping concept even for $z_L \sim 100$.

In summary, the following observations are made concerning the resonant radiation pump X-ray laser:

(i) To achieve a practical energy per unit volume the laser must operate at as high a density as possible but cannot exceed $N = 2.2 \times 10^{14} z^4$ because of radiation trapping. Equation (24).

(ii) radiation trapping leads to geometries for the laser medium that are extremely shallow in at least one dimension (Equation (20)). This is a major problem that requires innovative structural design for the laser.

(iii) The range of quantum numbers within which the laser may operate is tightly constrained. A lower bound of $p = 3$ is imposed by inversion criteria while an upper bound is set by keeping

$$I - E_p < kT_e$$

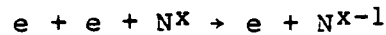
to avoid collisional ionization losses from the upper laser level. Also operating efficiency decreases as p^{-3} . Equation (30).

(iv) The maximum efficiency for the radiation pumped laser is approximately 10^{-6} to 10^{-5} as shown in Equation (40). A major design problem is the inefficient conversion of a broadband light source, such as a plasma, into a narrow emission light for optical pumping.

(v) As a research issue, energy level data accurate enough to predict resonant line overlaps in high-Z ions does not exist nor can it be calculated even with the state-of-the-art in present codes.(1)

III-B. RECOMBINATION LASERS

This approach to creating a laser exploits the physical fact that three-body recombination



preferentially populates high lying states where $E_p \approx kT_e$. This section will develop a scaling model for this inversion process using the atomic physics data of References (9) and (10) as well as a similarity solution for the expansion and heating of a plasma with uniform energy deposition as discussed in Reference (11).

It will be shown that for the case of a one-dimensional expansion of a plasma under conditions where energy is being added at the rate of W watts/cm² and thermal conduction is large enough that $dT/dx \approx 0$, similarity solutions exist for the hydrodynamic variables of the form:

$$\rho(x) = \frac{\mu_0}{\sqrt{\pi} \xi_0} e^{-(x/\xi_0)^2} \quad (41)$$

$$u = u_0 x / \xi_0 \quad (42)$$

$$T = T_0(t/t_0) \quad (43)$$

where the scale length

$$\xi_0 = \sqrt{\frac{32}{45}} (W / \mu_0)^{1/2} t^{3/2} \quad (44)$$

and μ_0 is the mass per unit area.

The study will find a region of space in the parameters (ρ , ρ , T , T) for which nonequilibrium conditions leading to an inversion may occur. Equations (41-44) will then define trajectories into this lasing space as a function of initial conditions. The

objective will be the determination of the optimum efficiency for laser operation and inherent beam divergence as was done in Section III-A.

The problem of calculating excited state populations in hydrogenic plasmas was first addressed in Reference (10). In this study photoionization of atoms and ions was neglected with relation to collisional ionization. For X-ray lasers, however, the plasma containing the lasing species should have as high a number density as possible in order to present a useful stored energy per unit volume. Thus, it is appropriate to consider for what values of electron temperature, radiation temperature and plasma density the neglect of photoionization is justified.

The rate of photoionization from level n is

$$R_n = N_n \int_n^{\infty} \frac{\mu_{\nu T}}{h\nu} d\nu c\sigma_{\nu n} \left(1 - e^{-h\nu/kT_p}\right) \quad (45)$$

where the last term compensates for induced emission and T_p is the temperature of the incident radiation field. From Reference (7) the photoionization cross section is approximated by

$$\sigma_{\nu n} = 2.8 \times 10^{29} z^4 / \nu^3 n^5 \quad (46)$$

and for emission from a planar surface

$$\frac{cU_{\nu T}}{h\nu} d\nu = \frac{2\pi\nu^2}{c^2} \frac{d\nu}{e^{h\nu/kT} - 1} \quad (47)$$

so that Eq. (45) yields

$$\frac{R_n}{N_n} = 1.9 \times 10^9 \frac{z^4}{n^5} E_i\left(\frac{13.6}{n^2}\right) \quad (48)$$

where

$$\theta = kT/z^2 \quad (49)$$

is the reduced radiation temperature in electron volts, and $Ei(x)$ is the exponential integral.

The rate of electron collisional ionization from level n used in Reference (7) yields

$$\frac{R_n^e}{N_n} = n_e \frac{1.3 \times 10^{-7} n^2}{z^3 \theta^{1/2}} \exp\left(\frac{-13.6}{n^2 \theta}\right) \quad (50)$$

where

$$\theta = kT_e/z^2 \quad (51)$$

is the reduced electron temperature. Notice that if collisional ionization (Equation (50)) exceeds photoionization (Equation (48)) for $n = 1$, then it exceeds photoionization for all levels of $n > 1$. Thus comparing Equation (50) with Equation (48) for $n = 1$ yields

$$\left(\frac{n_e}{z}\right) \frac{e^{-13.6/\theta}}{\sqrt{\theta}} > 1.5 \times 10^{16} Ei\left(\frac{13.6}{\theta}\right) \quad (52)$$

as the plasma condition necessary to assure the assumptions of Reference (9) are valid. As noted in Section III-A, for hydrogenic plasmas $\theta \sim 1.0$ and for most cases of interest $\theta < 1.0$ so that the asymptotic expansion

$$Ei(x) \sim e^{-x}/x$$

may be used. (12) Thus, Equation (52) may be simplified to find the electron density for which collisional ionization will dominate photoionization at some temperature Θ

$$\left(\frac{n_e}{z^7}\right) > 9 \times 10^{20} \Theta e^{-13.6/\Theta} \quad (53)$$

For $\Theta = 0.1$, Equation (53) is easily satisfied, but for $\Theta > 0.5$ Equation (53) is not generally satisfied for plasmas where Equation (27) obtains. Thus, in modeling a photo-driven plasma the results of Reference (10) can only be assumed valid if the radiation temperature is less than about $z^2/2$ (eV).

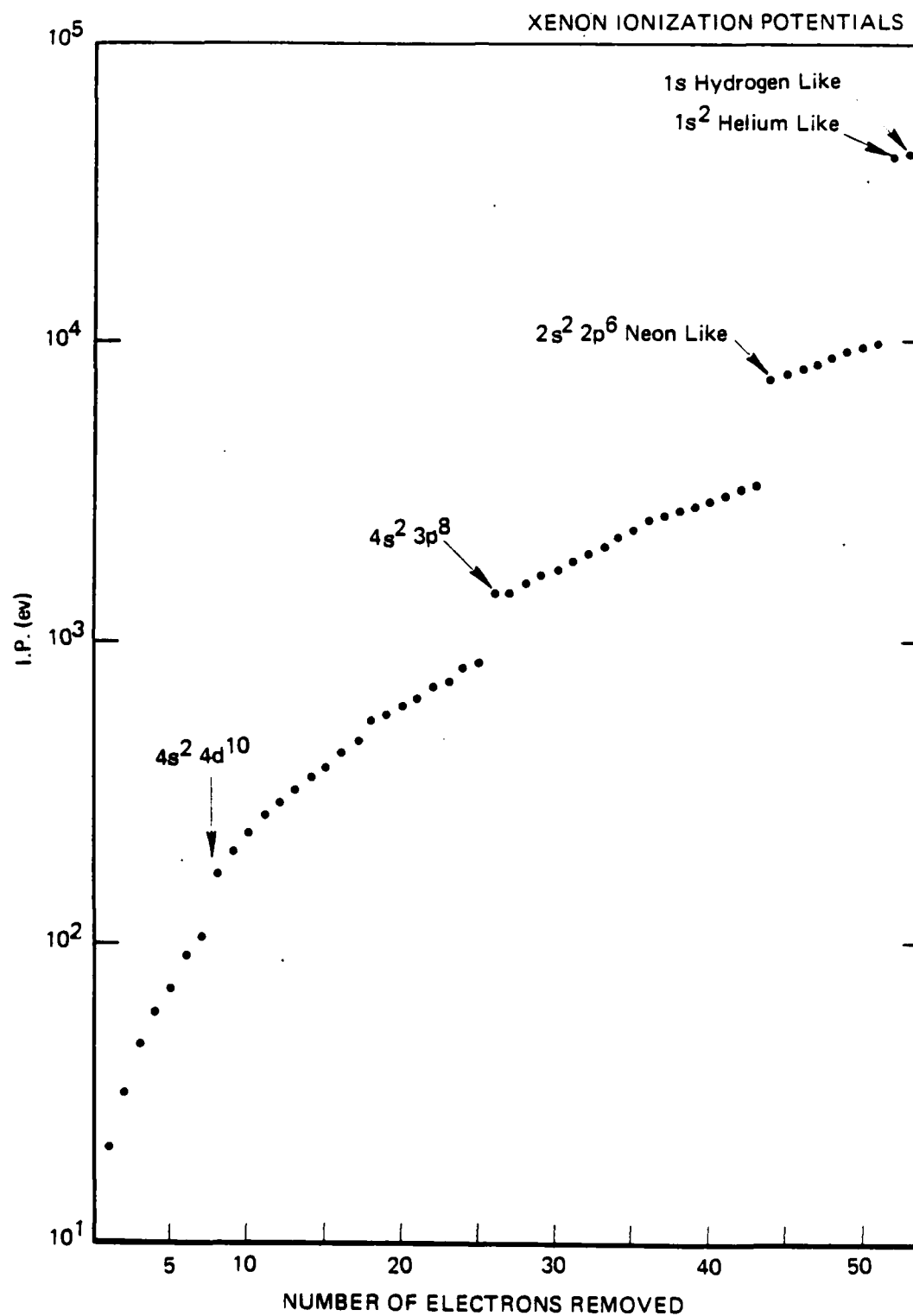


Figure 1

REFERENCES

- (1) R.D. Cowan, "Theory of Atomic Structure and Spectra," (University of California Press, Berkeley 1981, pp. 12-15).
- (2) Ya B. Zeldovich and Yu. P. Raizer "Physics of Shock Waves and High-Temperature Phenomenon" (Ed. by W. D. Hages and R. F. Probstern) (Academic Press, N. Y., 1966. V. I., pp. 289, 291, 393)
- (3) H. R. Griem and K. Y. Shen, Phys. Rev. 122, 1490 (1961).
- (4) V. A. Bhagavatula, IEEE J. Quantum Electronics 16, 603 (1980).
- (5) J. P. Apruzese, J. Davis and K. G. Whitney, J. Appl. Phys. 53, 4020 (1982).
- (6) R. C. Elton, Opt. Eng. 21, 309 (1982).
- (7) "Atomic and Molecular Processes," D. R. Bates, Ed., Academic Press, 1962.
- (8) D. R. Bates, Monthly Nat. Roy. Astr. Soc. 106, 432 (1946).
- (9) D. R. Bates, A. E. Kingston, and R. W. P. McWhirter, Proc. Roy. Soc. A 267, 297 (1962).
- (10) R. W. P. McWhirter and A. G. Hearn, Proc. Phys. Soc. 82, 641 (1963).
- (11) S. D. Rockwood, Los Alamos Report LA-5532-MS (1974).
- (12) M. Abramowitz and B. Stegun, "Handbook of Mathematical Functions," (NBS AMS-55, p. 228.)

MULTIPHOTONIC PUMPING

KEITH BOYER

Recent work at the University of Illinois at Chicago under the direction of Charles Rhodes could represent one of the most important developments in laser-matter interaction physics in the last decade. It also may have the potential for realizing a family of high intensity tunable XUV and soft X-ray lasers in the 100 to 1 nm region. (1,2)

The goal of this program(3) was to pursue the generation of coherent XUV and soft X-ray radiation by utilizing the extraordinary brightness of UV sources made possible by recent developments in noble gas halide excimer laser technology (to which Dr. Rhodes was a substantial contributor). The first attempt in this direction was harmonic generation of KrF* and ArF* radiation to produce high intensity sources of coherent radiation as short as 38.5 nm. The second attempt was to explore high-order multiphoton processes in the UV using ArF* radiation at 193.5 nm in 10 picosecond pulses. Here it was found that multiple ionization states could readily be produced with large cross sections and strong shell effects. The highest ionization state, 10^+ , was obtained for Uranium and required 99 photons of 193.5 nm (≈ 633 eV) radiation to be absorbed coherently. Subsequent experiments with krypton in which 4 photons were absorbed produced efficient laser action at 93 nm from inner-shell transitions which also proved to be moderately tunable. This represents the shortest wavelength for which stimulated emission has been observed. In order to produce lasing from neutral krypton this process had to compete successfully against photoionization and the Auger process indicating that appreciable

time was required to couple energy from the inner to the outer shell where electrons could be released.

Conventional theoretical models of multiquantum absorption and ionization do not seem capable of describing either the Z dependence of the observations nor the magnitude of the observed charge states for atoms heavier than argon. The authors (1-3) have ascribed the anomalous enhanced coupling strength to a collective response of the atom to the radiation depending on the shell structure of the atom.

From these results it seems likely that by going to shorter pumping pulses and higher intensities (≤ 1 picosecond and $> 10^{15}$ Watts/cm²) achievable with modest modifications of the existing equipment, lasing transitions may be discovered throughout the 10 eV to one keV region or beyond with good conversion efficiencies.

The present experiments permit the exploration of collective excitation of inner atomic shells by multiphoton processes and the determination of precise wavelengths and transition probabilities in Ne-like and possibly He-like high z atoms. These could be important to other X-ray laser concepts as well as providing new understandings of atomic systems. The importance of obtaining such data was stressed earlier in this report.

The collective response of higher z atoms to high intensity laser radiation represents a completely new mechanism in laser matter interaction. It is important both for its own inherent interest and as the possible basis for a whole new device technology.

If the shortwave length tunable lasers postulated here can be realized, they will make possible holography of living biological systems as well as biological molecules at or near the atomic level of resolution. Given atomic species could be emphasized by tuning to atomic resonances and chemical reaction dynamics frozen. Certainly such a development would revolutionize the field of biological research. The high temporal resolution and high spectral brightness would also permit studies of processes in semiconductors, surface physics, and the action of catalysts which are not accessible to synchrotron light sources.

Such a promising new development certainly deserves adequate funding and support. The present level of support while substantial for a typical university laboratory is definitely limiting the rate of progress. Theoretical efforts aimed at understanding this new phenomenon are also needed.

The appendix to this section reprints References 1-3. We are indebted to Dr. Rhodes for making them available in advance of publication.

REFERENCES

1. T. S. Luk, H. Pummer, K. Boyer, M. Shahidi, H. Egger, and C. K. Rhodes, "Anomalous Collision-Free Multiple Ionization of Atoms with Intense Picosecond Ultraviolet Radiation", Phys. Rev. Lett. 51, 110 (1983).
2. T. Srinivasan, H. Egger, T. S. Luk, H. Pummer, C. K. Rhodes, "Stimulated Extreme Ultraviolet Emission at 93 nm in Krypton" to be published in Laser Spectroscopy VI Proc. 6th Intl. Conference, Interlaken (1983), Springer Series in Optical Sciences, Eds. H. P. Weber and W. Luthy (Springer-Verlag).
3. C. K. Rhodes, "Vacuum Ultraviolet and Extreme Ultraviolet Generation with Excimer Lasers" Invited presentation Laser 83 Opto-Elektrnik 6th Intl. Conference, Munich 27 June -1 July 1983 (Unpublished).

APPENDIX A

Anomalous Collision-Free Multiple Ionization of Atoms with Intense Picosecond Ultraviolet Radiation

T. S. Luk, H. Pummer, K. Boyer, M. Shahidi, H. Egger, and C. K. Rhodes

Department of Physics, University of Illinois at Chicago, Chicago, Illinois 60680

(Received 27 April 1983)

Collisionless multiphoton absorption, resulting in multiple atomic ionization and exhibiting anomalously strong coupling, has been studied in the region spanning atomic number $Z = 2$ (He) to $Z = 92$ (U). The highest ion state identified is U^{10+} , corresponding to absorption of 99 quanta (~ 633 eV). Models of stepwise ionization using standard theoretical techniques are incapable of describing these results. A mode of interaction involving radiative coupling to a collective motion of an atomic shell is proposed.

PACS numbers: 32.80.Kf, 32.80.Fb, 33.80.Kn

The availability of spectrally bright picosecond ultraviolet light sources enables the study of nonlinear coupling mechanisms in that spectral range under experimental circumstances unaffected by collisional perturbations. In this Letter, the results of the first experiments examining the atomic-number dependence of processes of multiple ionization of atoms X with intense ($\leq 10^{14}$ W/cm²) picosecond 193-nm radiation under *collision-free* conditions are reported.

The general physical process studied is

$$N\gamma + X = X^{q+} + qe^- \quad (1)$$

for which observed values of N and q range as high as 99 and 10, respectively. Of particular significance is the behavior of the amplitude for Reaction (1) as a function of atomic number (Z). Accordingly, the response of materials spanning the range in atomic number from He ($Z=2$) to U ($Z=92$) has been measured. Similar processes involving the irradiation of Kr at 1.06 μ m have recently been described by L'Huillier *et al.*,¹ in addition to other studies concerning the characteristics² of Xe and Hg.

The experiments reported herein exhibit two salient features. These are (1) an unexpectedly strong coupling for extraordinarily high-order processes, and (2) a coupling strength which is dramatically enhanced at higher Z values.

The experimental arrangement used to detect the production of the highly ionized species consists of a double-focusing electrostatic energy analyzer (Comstock) operated as a time-of-flight mass spectrometer. The analyzer is positioned in a vacuum vessel which is evacuated to a background pressure of $\sim 10^{-7}$ Torr. The materials to be investigated are introduced into the chamber in a controlled manner at pressures typically from $\sim 3 \times 10^{-7}$ to 10^{-4} Torr. The 193-nm ArF⁺ laser used for irradiation³ (~ 10 psec, ~ 4 GW) is

focused by a $f=50$ -cm lens in front of the entrance iris of the electrostatic analyzer, producing an intensity of $\leq 10^{14}$ W/cm² in the experimental volume. The number of atoms in the focal volume is estimated to be $\sim 10^4$ at 10^{-3} Torr. Therefore, any ion produced with a probability less than $\sim 10^{-4}$ cannot be detected without extensive signal averaging. Ions formed in the focal region are collected by the analyzer with an extraction field in the range of 50–500 V/cm and detected with a microchannel plate at the exit of the electrostatic device.

Representations of the experimental results are given in Figs. 1(a) and 1(b) and Table I. Figure 1(a) shows a sample of typical time-of-flight ion current data for Xe. Table I contains the normalized relative abundances of the observed ion charge states for Xe, derived from Fig. 1(a) and uncorrected for detector sensitivity. Experiments indicate that the detector is about four times as sensitive for Xe⁺. Similar data have been recorded for He, Ne, Ar, Kr, I, Hg, and U. In Fig. 1(b), the observed ions and the total energies required for their generation in the electronic ground state are given.

A remarkable feature of the data is the magnitude of the total energy which can be communicated to the atomic systems, especially for high- Z materials. The total energy investment^{4,5} of ~ 633 eV, a value equivalent to 99 quanta, needed to generate U^{10+} from the neutral atom, with neglect of the small contribution associated with molecular binding³ in the experimental material UF₆, represents the highest energy value reported for a collision-free nonlinear process. The removal of the tenth electron from uranium, which requires⁶ ~ 133 eV if viewed as an independent process, requires a minimum of 21 quanta. The coupling strength implied by this scale of energy transfer at an intensity of $\sim 10^{14}$ W/cm² very sub-

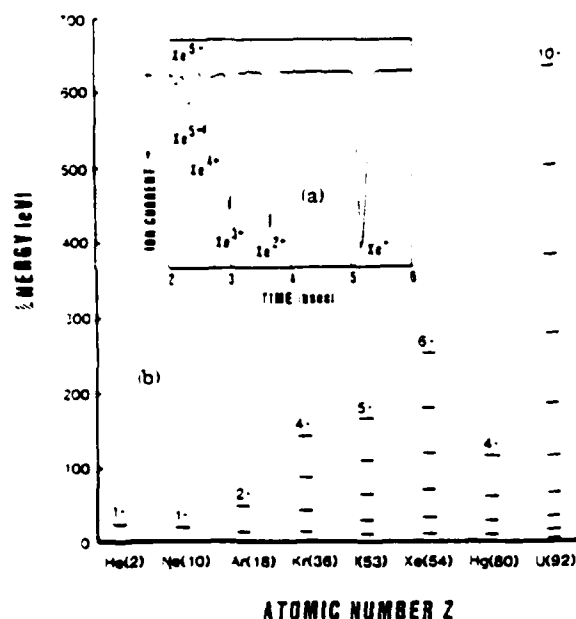


FIG. 1. Data concerning multiple ionization of atoms for 193-nm irradiation at $\sim 10^{-4}$ W/cm². (a) Inset: typical time-of-flight ion current signal for xenon. (b) Plot of total ionization energies of the observed charge states as a function of atomic number (Z).

stantially exceeds that anticipated from conventional theoretical formulations describing multi-quantum ionization.

Aside from the magnitude of the observed excitation energies, the general and strong tendency for increased coupling for materials heavier than argon and the similarity in the response of I and Xe, for which the maximum charge state observed in both cases corresponds to complete loss of the 5p shell, are significant. An examination of the ionization energies^{4,5} for the species involved fails to suggest any consistent picture for this behavior. For example, the ionization of the second electron from He, which is not detected, requires an energy of ~ 54.4 eV, a value less than that necessary to remove the fifth electron from Xe. We are led to the conclusion that some factor other than the magnitude of the ionization potentials corresponding to the different species, or equivalently, the order of the non-linear process, governs the strength of the coupling.

An explanation based simply on the density of states is also unconvincing. A comparison of the excited-state structures^{6,7} for He and Ne quickly shows that the density of levels for Ne is very large in comparison to that for He, but only singly

TABLE I. Charge-state distribution of xenon derived from Fig. 1(a).

Charge state	Relative abundance
1+	44
2+	26
3+	20
4+	7
5+	5
6+	1

ionized species are observed for both materials. Likewise, the comparison of Xe and Hg leads to the conclusion that the density of states is not a key factor in determining the coupling strength.

Conversely, all the conspicuous characteristics of Fig. 1(b) can be consolidated if the shell structure of the atom is the principal physical property determining the magnitude of the coupling. The considerable change seen in the atomic response observed between Ar and Kr implicates a role for the 3d shell which is filled in that region. A very similar variation between Ar and Kr, that has been observed in the amplitude for single-quantum multiple photoionization,¹¹ has been attributed to correlation effects arising from the d shell. A significant shell-dependent effect is also suggested by the comparative behavior of I and Xe, since complete removal of the valence 5p shell is observed in both cases although the total energies required differ substantially. We note that I and Xe exhibit similar and unusually intense 4d absorptions^{12,13} in the region ~ 100 eV, strongly implicating correlated¹⁴⁻¹⁶ motions in that shell.

The most elementary mechanism that could lead to the production of the observed ionic charge states is the stepwise removal of the individual electrons by conventionally described multiphoton ionization. A given charge state (e.g., Xe⁵⁺) then requires the generation of all lower charge states, thereby linking the probability for its occurrence directly to the rates of production of these other species. The appearance of Xe⁵⁺ would require a sequence of 2-, 4-, 6-, 8-, 10-, and 12-photon processes of ionization.

The probabilities for multiphoton transitions calculated with standard perturbative approaches⁷ and procedures valid in the high-field limit¹⁸ have been discussed for single-electron systems. From these calculations, it can be shown that, at the 193-nm intensity of $\sim 10^{-4}$ W/cm² used in these experiments, the transition rates for A-

photon processes decrease very rapidly with increasing N . An estimate shows that for $N=3, 5, 7$, the relative transition probabilities scale as $1:10^{-2}:10^{-3}$. On this basis, the expected ionic distributions should decrease very sharply towards higher charge states. Indeed, the abundances of ions in charge states $q > 3$ would fall below the detection limit of the apparatus used. It follows that the results obtained from single-electron models for multiquantum processes of this nature do not represent the observed experimental findings involving charge states $q > 3$. This conclusion holds for all materials studied that are heavier than Ar. Conversely, inspection of the experimental data indicates that the low- Z materials, essentially up to Ar, exhibit behavior in reasonable accord with that predicted by conventional theory. This interpretation can be reconciled with the presence of two different coupling mechanisms, one dominating in the low- Z region and the other providing enhanced coupling in the higher- Z materials. From our data, the division between these two regimes appears to occur between Ar and Kr.

The very substantial underestimate provided by standard theoretical models of the coupling strength observed and the envelope of the Z dependence both conspire to support an interpretation involving an alternative mode of coupling. The enhanced and anomalous strength of the radiative interaction points to a collective response of the atom. Such a collective response, or atomic plasmon,¹⁹ is anticipated to be favored in the outer subshells of high- Z materials for which the correlation energy becomes a more substantial fraction of the total electronic energy.^{4,20} The coherent motion envisaged has a counterpart in nuclear matter known as the giant dipole,²¹ although giant multipoles higher than the dipole are known.²²

All aspects of the experimental findings can be unified if an important mode of nonlinear coupling involves a direct multiquantum interaction with an atomic shell which undergoes a collective response. In this picture, it would follow naturally that the shell structure of the material would be reflected as an important property governing the coupling to the radiation field. Collective inner-shell responses have been discussed in relation to processes of single-photon ionization.²³ It is generally found that in cases for which the electronic correlations are important, the single-particle spectrum is very greatly altered, leading to a collectively enhanced many-electron pro-

cess. In this regard, the xenon $4d^{10}$ shell^{24,25} and the lanthanides²⁶ have been studied extensively. Recent analyses of collective responses in atomic and molecular systems have been given by Brandt and co-workers,²⁷⁻²⁹ Wendin,^{14,16,24} and Amusia and co-workers.^{15,30} The results of our current studies simply indicate a nonlinear analog of this basic electronic mechanism. In the present experiments, the implication of the d -shell electrons seems particularly strong given the sharp change in behavior seen between Ar and Kr. Naturally, f electrons³¹ would be expected to behave similarly, a consideration that clearly motivates study of the lanthanide sequence. Finally, the spatial dependence of the self-consistent field experienced by the atom²³ is expected to give rise to a complex Z dependence of the atomic response, an aspect that may be related to the relatively low value of maximum energy indicated in Fig. 1(b) for Hg.

In summary, studies examining the nonlinear coupling of intense ultraviolet radiation to atomic systems, spanning the atomic number range $Z=2$ to $Z=92$, reveal several important characteristics of this interaction. It is concluded that the conventional treatments of multiquantum ionization do not correspond to our experimental findings for high- Z materials. The essential findings are (1) an unexpectedly large amplitude for collision-free coupling, (2) a strong enhancement in the coupling strength for the heavy elements, and (3) the inference, based on the atomic-number dependence and the anomalous coupling strength, that a collective motion of d and f shells may play an important role in these phenomena. With this physical picture, selectivity in the population of excited ionic states is expected on the basis of photoelectron studies.³²

Support for these studies was provided by the U. S. Office of Naval Research, the U. S. Air Force Office of Scientific Research through Grant No. AFOSR-79-0130, the National Science Foundation through Grant No. PHY81-16636, and the Avionics Laboratory, U. S. Air Force Wright Aeronautical Laboratories, Wright Patterson Air Force Base, Ohio. Fruitful discussions concerning atomic ionization energies with R. L. Carman and the skillful assistance of J. Wright and M. Scaggs are gratefully acknowledged.

A. L'Huillier, L. A. Lompre, G. Mainfray, and C. Manus, Phys. Rev. Lett. 49, 1814 (1982).

- ¹⁷T. S. Luk, H. Pummer, K. Boyer, M. Shahidi, H. Egger, and C. K. Rhodes, in *Excimer Lasers—1982*, edited by C. K. Rhodes, H. Egger, and H. Pummer, AIP Conference Proceedings No. 100 (American Institute of Physics, New York, 1983).
- ¹⁸H. Egger, T. S. Luk, K. Boyer, D. R. Muller, H. Pummer, T. Srinivasan, and C. K. Rhodes, *Appl. Phys. Lett.* **41**, 1032 (1982).
- ¹⁹R. D. Cowan, *The Theory of Atomic Structure and Spectra* (Univ. of California Press, Berkeley, 1981).
- ²⁰T. A. Carlson, C. W. Nestor, Jr., N. Wasserman, and J. D. McDowell, *At. Data* **2**, 63 (1970).
- ²¹F. T. Porter and M. S. Freedman, *J. Phys. Chem. Ref. Data* **7**, 1267 (1978).
- ²²J. Bearden and A. F. Burr, *Rev. Mod. Phys.* **39**, 125 (1967).
- ²³G. L. DePoorter and C. K. Rofer-Depoorter, *Spectrosc. Lett.* **9**, 521 (1975).
- ²⁴R. P. Madden and K. Codling, *Astrophys. J.* **141**, 364 (1965); J. W. Cooper, U. Fano, and F. Prats, *Phys. Rev. Lett.* **10**, 518 (1963); U. Fano, in *Photoionization and Other Probes of Many-Electron Interactions*, edited by F. J. Wuilleumier (Plenum, New York, 1976), p. 11.
- ²⁵K. Codling, R. P. Madden, and D. L. Erderer, *Phys. Rev.* **155**, 26 (1966).
- ²⁶J. A. R. Samson and G. N. Haddad, *Phys. Rev. Lett.* **33**, 875 (1974); J. A. R. Samson, in *Photoionization and Other Probes of Many-Electron Interactions*, edited by F. J. Wuilleumier (Plenum, New York, 1976), p. 419.
- ²⁷F. J. Comes, U. Nielsen, and W. H. E. Schwarz, *J. Chem. Phys.* **58**, 2230 (1973).
- ²⁸D. L. Erderer, *Phys. Rev. Lett.* **13**, 760 (1964).
- ²⁹G. Wendin, *Phys. Lett.* **37A**, 445 (1971).
- ³⁰M. Ya. Amusia, V. K. Ivanov, and L. V. Chernysheva, *Phys. Lett.* **59A**, 191 (1976).
- ³¹G. Wendin, in *Photoionization and Other Probes of Many-Electron Interactions*, edited by F. J. Wuilleumier (Plenum, New York, 1976), p. 61.
- ³²Y. Gontier and M. Trahin, *Phys. Rev.* **172**, 83 (1968).
- ³³H. R. Reiss, *Phys. Rev. A* **1**, 803 (1970), and *Phys. Rev. Lett.* **25**, 1149 (1970), and *Phys. Rev. D* **1**, 3533 (1971), and *Phys. Rev. A* **6**, 817 (1972).
- ³⁴F. Bloch, *Z. Phys.* **91**, 363 (1933).
- ³⁵*Correlation Effects in Atoms and Molecules*, edited by R. Lefebvre and C. Moser, *Advances in Chemical Physics* Vol. 14 (Wiley, New York, 1969); O. Sinanoglu and K. A. Brueckner, *Three Approaches to Electron Correlation in Atoms* (Yale Univ. Press, New Haven, Conn., 1970); A. Hibbert, *Rep. Prog. Phys.* **38**, 1217 (1975); A. W. Weiss, *Adv. At. Mol. Phys.* **9**, 1 (1973).
- ³⁶G. C. Baldwin and G. S. Klaiber, *Phys. Rev.* **71**, 3 (1947), and **73**, 1156 (1948); M. Goldhaber and E. Teller, *Phys. Rev.* **74**, 1046 (1948).
- ³⁷*Giant Multipole Resonances*, edited by F. E. Bertrand (Harwood Academic, London, 1980).
- ³⁸A. Zangwill and P. Soven, *Phys. Rev. A* **21**, 1561 (1980); W. Ekardt and D. B. Tran Thoai, *Phys. Scr.* **26**, 194 (1982).
- ³⁹G. Wendin, *J. Phys. B* **3**, 455, 466 (1970), and **4**, 1080 (1971), and **5**, 110 (1972), and **6**, 42 (1973).
- ⁴⁰D. J. Kennedy and S. T. Manson, *Phys. Rev. A* **5**, 227 (1972); J. B. West, P. R. Woodruff, K. Codling, and R. G. Houlgate, *J. Phys. B* **9**, 407 (1976); G. R. Wight and M. J. Van der Wiel, *J. Phys. B* **10**, 601 (1977); D. M. P. Holland, K. Codling, J. B. West, and G. V. Marr, *J. Phys. B* **12**, 2465 (1979).
- ⁴¹J. P. Connerade and D. H. Tracy, *J. Phys. B* **10**, L235 (1977).
- ⁴²W. Brandt and S. Lundquist, *Phys. Rev.* **132**, 2135 (1963).
- ⁴³W. Brandt, L. Eder, and S. Lundquist, *J. Quant. Spectrosc. Radiat. Transfer* **7**, 185 (1967); G. Wendin and M. Ohno, *Phys. Scr.* **14**, 148 (1976).
- ⁴⁴W. Brandt and S. Lundquist, *J. Quant. Spectrosc. Radiat. Transfer* **7**, 411 (1967).
- ⁴⁵M. Ya. Amusia, N. A. Cherepkov, and L. V. Chernysheva, *Zh. Eksp. Teor. Fiz.* **60**, 160 (1971) [*Sov. Phys. JETP* **33**, 90 (1971)].
- ⁴⁶A. Zangwill and P. Soven, *Phys. Rev. Lett.* **45**, 204 (1980).
- ⁴⁷R. A. Rosenberg, M. G. White, G. Thomson, and D. A. Shirley, *Phys. Rev. Lett.* **43**, 1384 (1979).

T. Srinivasan, H. Egger, T. S. Luk, H. Pummer, and J. K. Rhodes
Department of Physics, University of Illinois at Chicago,
P.O. Box 4348, Chicago, Illinois 60680, U.S.A.

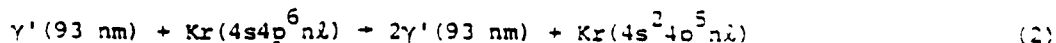
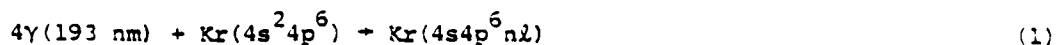
Abstract

Strong, tunable stimulated emission at 93 nm has been observed following four quantum excitation of Kr to $4s4p^6n\lambda$ inner-shell excited configurations using picosecond ArF* (193 nm) radiation.

Discussion

In this paper, the observation of strong, stimulated emission in the extreme ultraviolet following multiphoton excitation of Kr using a 193-nm ArF* laser is reported. The ArF* laser pulse [1], with an output power of 1 GW, 10 psec duration, and 5 cm^{-1} bandwidth, was focussed with a $f = 50 \text{ cm}$ lens into a differentially pumped cell similar to one used for harmonic generation in the extreme ultraviolet [2]. The cell was attached to the entrance slit of a 1 m VUV monochromator (McPherson 225) and the generated XUV radiation was detected by an optical multichannel analyzer (OMA PAR).

With Kr pressures between 100 Torr and 1000 Torr, stimulated emission in krypton at 93 nm is observed. Significantly, this result experimentally establishes the selectivity of multiquantum processes for the excitation of atomic inner-shell states, since the excited level $4s4p^6n\lambda$ is populated by a four quantum process at 193 nm from the ground state $4s^24p^6$ configuration [3]. Overall, the observations can be understood by the reactions



which illustrate the direct excitation step and the subsequent stimulated emission. It appears that $(n\lambda)$ is (4d) and (6s) in these experiments. The 93 nm radiation is moderately tunable, since the autoionization rate of the upper $4s4p^6n\lambda$ level confers a substantial width ($\sim 100 \text{ cm}^{-1}$) on the bandwidth of the system [4]. The tunability has been experimentally demonstrated in this case over a region of $\sim 600 \text{ cm}^{-1}$, a fact which can be explained by the presence of a number of closely spaced lines. Incidentally, the selective promotion of an inner-shell electron in this example reinforces the conclusion derived from earlier studies concerning the influence of the atomic shell structure on the multiquantum coupling strength [5]. The maximum efficiency observed in the initial experiments for conversion to 93 nm from the excitation at 193 nm corresponds to $\sim 10^{-4}$. Latest results indicate that it may be possible to increase the efficiency by one to two

*To be published in Laser Spectroscopy VI. Proc. 6th Intl. Conf., Interlaken (1983), Springer Series in Optical Sciences, edited by H. P. Weber and W. Luthy (Springer-Verlag).

orders of magnitude. To our knowledge, this system represents the first inner-shell transition laser and the shortest wavelength reported for stimulated emission.

Acknowledgements

The authors wish to acknowledge the expert technical assistance of M. J. Scaggs and J. R. Wright. This work was supported by the Office of Naval Research, the Air Force Office of Scientific Research under grant no. AFOSR-79-0130, the National Science Foundation under grant no. PHY81-16626, and the Avionics Laboratory, Air Force Wright Aeronautical Laboratories, Wright Patterson Air Force Base, Ohio.

References

1. H. Egger, T. S. Luk, K. Boyer, D. F. Muller, H. Pummer, T. Srinivasan, C. K. Rhodes: Appl. Phys. Lett. 41, 1032 (1982)
2. H. Egger, R. T. Hawkins, J. Bokor, H. Pummer, M. Rothschild, C. K. Rhodes: Opt. Lett. 5, 282 (1980)
3. K. Codling, R. P. Madden: J. Res. Natl. Bur. Std. 76A, 1 (1972)
4. D. L. Ederer: Phys. Rev. A4, 2263 (1971)
5. T. S. Luk, H. Pummer, K. Boyer, M. Shahidi, H. Egger, C. K. Rhodes: "Anomalous collision-free multiple ionization of atoms with intense picosecond ultraviolet radiation", Phys. Rev. Lett. (to be published)

Vacuum Ultraviolet and Extreme Ultraviolet Generation with Excimer Lasers *

C. K. RHODES

Department of Physics, University of Illinois at Chicago
P.O. Box 4348, Chicago, Illinois 60680, U.S.A.

Abstract

High spectral brightness rare gas halogen (RGH) sources can be used to generate coherent extreme ultraviolet radiation by either harmonic generation mechanisms or direct multiquantum excitation of appropriate gain media. In order to demonstrate the basic characteristics of these two approaches, recent comparative measurements have been made. With the use of a 4 GW 193 nm (ArF*) system operating at a pulse duration of ~ 10 ps, harmonic generation has been studied in several atomic and molecular media and used to generate ~ 20 kW at 64.3 nm and ~ 200 W at 38.6 nm. In addition, stimulated emission in molecular hydrogen, on both the Lyman and Werner bands excited by two quantum absorption at 193 nm, has resulted in the generation of radiation as short as 117.6 nm at an efficiency on conversion approaching one percent. It has been concluded that the latter method is superior for the generation of short wavelength radiation. Extension of these results to both shorter wavelengths and higher power levels requires an extended study of the basic character of high order nonlinear processes in the ultraviolet. Recent studies of collision-free multiply-charged ion production with irradiation at 193 nm point to an anomalously strong coupling to high Z materials, with processes involving as many as 99 quanta being observed. These findings strongly suggest that the direct excitation of inversions by appropriate multiquantum processes in the region below 100 nm in certain atomic systems can be generated with existing laser instrumentation. This report discusses (1) the properties of stimulated emission in H_2 , (2) the findings arising from the studies of multiply-charged ion production, and (3) the observation of intense, tunable stimulated emission at 93 nm with 193 nm radiation from inner-shell excited $4s4p^6nl$ configurations of krypton excited by a four quantum process.

*Invited presentation at Laser 83 Opto-Elektronik, 6th International Congress, Munich, 27 June - 1 July, 1983.

Discussion

A. Stimulated emission in hydrogen

Intense vacuum ultraviolet stimulated emission in molecular hydrogen, on both the Lyman and Werner bands, following excitation by two quantum absorption at 193 nm on the $X^1\Sigma_g^+ \leftarrow E,F^1\Sigma_g^+$ transition, has been observed. The shortest wavelength seen in the stimulated spectrum was 117.6 nm corresponding to the $C^1\Pi_u \leftarrow X^1\Sigma_g^+$ (2-5) Q(1) transition which appears to be inverted with a mechanism involving electron collisions. The maximum energy observed in the strongest stimulated line was ~ 100 eV, a value corresponding to an energy conversion efficiency of $\sim 0.5\%$. The pulse duration of the stimulated emission is estimated from collisional data to be ~ 10 ps, a figure indicating a maximum converted vacuum ultraviolet power of ~ 10 MW.

Table I contains the transitions and corresponding wavelengths observed [1] and Fig. 1 illustrates the general pattern of emission observed.

B. Collisionless multiquantum ionization of atoms

Recent progress in the generation of coherent high intensity vacuum ultraviolet and extreme ultraviolet radiation has stimulated interest in the study of the production of highly stripped and excited ions by multiquantum processes [2,3]. We report herein results of experiments examining processes of the type



for which observed values of N and q range as high as 99 and 10, respectively.

The experimental arrangement used to detect the production of highly ionized species consists of a double focussing electrostatic energy analyzer (Comstock) which, in the present experiment, is operated as a time-of-flight mass spectrometer (Fig. 2). The energy analyzer is positioned in a vacuum vessel which is continuously evacuated to a background pressure of $\sim 10^{-7}$ Torr. Materials to be investigated are introduced into the vacuum container at pressures of typically $\sim 10^{-6}$ Torr. The 193 nm ArF* laser [4] beam (~ 10 ps, ~ 4 GW) is focussed by a $f = 50$ cm lens in front of the energy analyzer's entrance iris resulting in intensities of $\sim 10^{14}$ W/cm². Ions formed in the focal region are collected into the analyzer with an extraction field



Fig. 1. Stimulated emission from H_2 following $E, F \leftarrow X(2-0) O(3)$ two-photon excitation with 2 ArF^* (193 nm) quanta. For the $E, F \leftarrow C$ transition, see text.

Transition	Wavelength Å		Excited X+E,F transition	Transition	Wavelength Å		Excited X+E,F transition
	Present work	Previous work [1,2]			Present work	Previous work [1,2]	
E → B				E → B			
0-0 P(1)	11210	11159.1		2-1 P(3)	8370	8369.23	
B → X				2-0 P(3)	7544.1	7544.06	
0-3 R(0)	1275.2	1274.6		B → X			
0-3 P(2)	1280	1279.5	0+0	1-6 P(4)	1440.9	1440.7	0+0
0-4 R(0)	1333.6	1333.5	0(0)	1-6 R(2)	1428.6	1428.9	0+0
0-4 P(2)	1339	1338.6		1-7 P(4)	1499.6	1499.6	
0-5 R(0)	1394.4	1393.7		1-7 R(2)	1487.6	1487.7	
0-5 P(2)	1399.8	1399		1-8 P(4)	1557.4	1557.6	
0-6 R(0)	1455.5	1454.9		1-8 R(2)	1545.4	1545.7	
0-6 P(2)	1460.9	1460.2		C → X			
				2-5 O(2)	1176.3	1176.8	
E → B	Not measured			E → B			
B → X				2-2 P(4)	9222	9222.04	
1-6 P(3)	1435.7	1436.2		B → X			
1-7 R(1)	1486.1	1486.2	0+2	1-8 P(5)	1531.5	1531.7	0+0
1-7 P(3)	1494.7	1495.2	0(1)	2-9 R(3)	1570.3	1571.4	0+0
1-8 R(1)	1544.4	1544.9		2-9 P(5)	1564.9	1565.6	
1-8 P(3)	1552.9	1553.4		C → X			
C → X				2-5 O(3)	1177.7	1178.3	
2-5 O(1)	1175.4	1175.8					

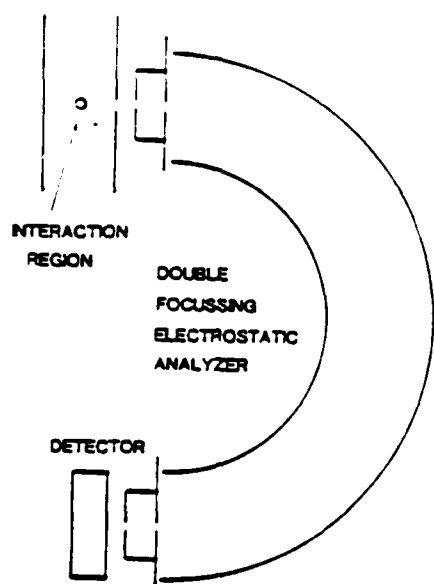


Fig. 2. Experimental system used in ion detection

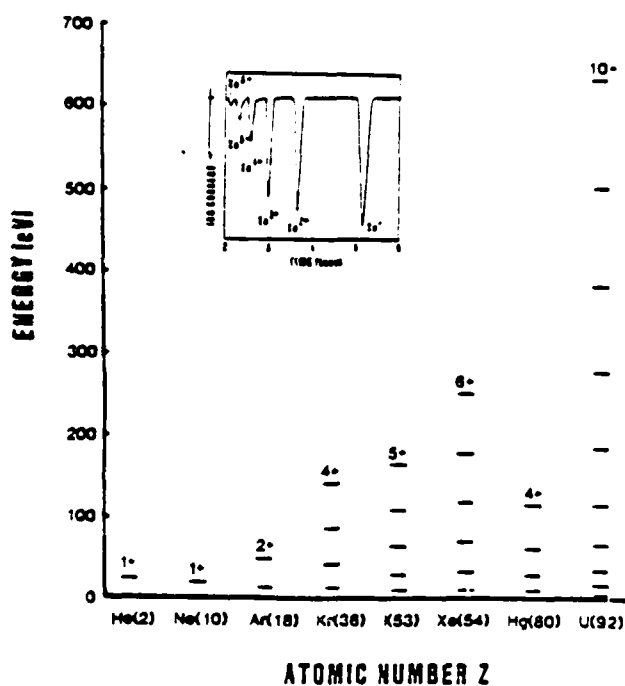


Fig. 3. Data concerning multiple ionization of atoms with 193 nm irradiation at $2 \times 10^{-4} \text{ W/cm}^2$. Plot of total ionization energies of the observed charge states as a function of atomic number (Z). Inset: Typical time-of-flight ion current signal for xenon

of 1000 V cm and detected with a microchannel plate at the exit of the energy analyzer. The observed ionic charge states together with a typical time-of-flight spectrum for Xe are given in Fig. 3.

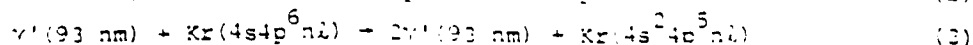
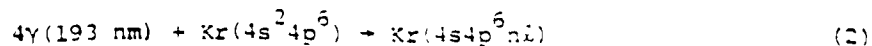
The experimental data display two unusual features. First, the magnitude of the total energy which can be communicated to the atomic system is unexpectedly large, especially for high Z materials. The total energy investment of ~ 633 eV, a value equivalent to 99 quanta, needed to generate U^{10+} from the neutral atom represents the highest energy value reported for a collision-free nonlinear process. The removal of the tenth electron from uranium, which requires ~ 133 eV if viewed as an independent process, requires a minimum of 31 quanta. Second, the ionic distributions do not fall off rapidly towards higher ionic states as one would expect if stepwise multiphoton ionization were to dominate the coupling.

It is concluded that the conventional treatments of multiquantum ionization do not correspond to our experimental findings for high-Z materials. Moreover, the data strongly indicate that the shell structure of the atom is an important physical property governing the strength of the coupling. In order to consolidate the observations into a single physical picture, a mode of interaction involving radiative coupling to a collective motion of an atomic shell is proposed [5].

C. Stimulated emission at 93 nm in multiquantum excited krypton

Strong, stimulated emission in the extreme ultraviolet following multiphoton excitation of Kr using a 193-nm ArF* laser has been observed. The ArF* laser pulse [4], with an output power of 1 GW, 10 ps duration, and 5 cm^{-1} bandwidth, was focussed with a $f = 50$ cm lens into a differentially pumped cell similar to one used for harmonic generation in the extreme ultraviolet [6]. The cell was attached to the entrance slit of a 1 m VUV monochromator (McPherson 225) and the generated XUV radiation was detected by an optical multichannel analyzer (OMA PAR).

With Kr pressures between 100 Torr and 1000 Torr, stimulated emission in krypton at 93 nm is observed. Significantly, this result experimentally establishes the selectivity of multiquantum processes for the excitation of atomic inner-shell states, since the excited level $4s4p^6nl$ is populated by a four quantum process at 193 nm from the ground state $4s^24p^6$ configuration [7]. Overall, the observations can be understood by the reactions



which illustrate the direct excitation step and the subsequent stimulated emission. It appears that (nl) is (4d) and (6s) in these experiments. The 93 nm radiation is moderately tunable, since the autoionization rate of the upper $4s4p^6nl$ level confers a substantial width ($\sim 100\text{ cm}^{-1}$) on the bandwidth of the system [8]. The tunability

has been experimentally demonstrated in this case over a region of $\sim 100 \text{ nm}^2$, a fact which can be explained by the presence of a number of closely spaced lines. Incidentally, the selective promotion of an inner-shell electron in this example reinforces the conclusion derived from earlier studies concerning the influence of the atomic shell structure on the multi-quantum coupling strength [5]. The maximum efficiency observed in the initial experiments for conversion to 93 nm from the excitation at 193 nm corresponds to $\sim 10^{-4}$. Latest results indicate that it may be possible to increase the efficiency by one to two orders of magnitude. To our knowledge, this system represents the first inner-shell transition laser and the shortest wavelength reported for stimulated emission.

Conclusions

On account of the unusual spectral brightness available from RGH media, particularly picosecond systems, it seems clear that major implications for short wavelength production are present. Given the scaling characteristics of RGH systems, at least the 1 TW range, the feasibility of a laboratory scale coherent source operating at kilovolt quantum energies is strongly implied.

Acknowledgements

The author wishes to acknowledge the expert technical assistance of M. J. Scaggs and J. R. Wright in addition to numerous fruitful discussions with K. Boyer, H. Egger, T. S. Luk, H. Pummer, M. Shahidi, and T. Srinivasan. This work was supported by the Office of Naval Research, the Air Force Office of Scientific Research under grant no. AFOSR-79-0130, the National Science Foundation under grant no. PHY81-16626, and the Avionics Laboratory, Air Force Wright Aeronautical Laboratories, Wright Patterson Air Force Base, Ohio.

References

1. H. Pummer, H. Egger, T. S. Luk, T. Srinivasan, C. K. Rhodes: "Vacuum ultra-violet stimulated emission from two-photon excited molecular hydrogen", Phys. Rev. A (in press)
2. A. L'Huillier, L. A. Lompre, G. Mainfray, C. Manus: Phys. Rev. Lett. 48, 1614 (1982)
3. T. S. Luk, H. Pummer, K. Boyer, M. Shahidi, H. Egger, C. K. Rhodes: In AIP Conference Proceedings, Vol. 100, Excimer Lasers - 1983, ed. by H. Egger, H. Pummer, C. K. Rhodes (American Institute of Physics, New York, 1983)
4. H. Egger, T. S. Luk, K. Boyer, D. F. Muller, H. Pummer, T. Srinivasan, C. K. Rhodes: Appl. Phys. Lett. 41, 1032 (1982)
5. T. S. Luk, H. Pummer, K. Boyer, M. Shahidi, H. Egger, C. K. Rhodes: "Anomalous collision-free multiple ionization of atoms with intense picosecond ultraviolet radiation", Phys. Rev. Lett. (in press)
6. H. Egger, R. T. Hawkins, J. Bokor, H. Pummer, M. Rothschild, C. K. Rhodes: Opt. Lett. 5, 292 (1980)
7. K. Codling, R. P. Madden: J. Res. Natl. Bur. Std. 76A, 1 (1972); K. Codling, R. P. Madden: Phys. Rev. A 4, 3261 (1971)
8. D. L. Ederer: Phys. Rev. A 4, 3263 (1971)

II. DIRECT NUCLEAR-PUMPED LASERS:

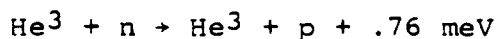
(PRELIMINARY THOUGHTS)

M. O . SCULLY

The first nuclear-pumped lasers had relatively low energies and seemed to hold little promise for high power applications. This is somewhat surprising since the amount of energy available in the nuclear fissioning process is so high. The reason for this low efficiency is quite clear when one realizes that although the energies involved in nuclear processes are high, the nuclear cross sections are smaller than atomic by many orders of magnitude. This argument is sketched at the end of this note.

However, recent work in the area of nuclear pumped-lasers, phase locked laser arrays, and gaseous reactors, suggests that these considerations should be updated and the question of possible high power nuclear-pumped lasers considered afresh.

In this regard we note that in recent work involving He^3 , the reaction



gives a stored energy of $\sim 1 \text{ kw/cm}^3$. This involves lasing argon at $1.8 \text{ } \mu\text{m}$ with a reactor pulse time of $130 \text{ } \mu\text{s}$ and a peak flux of $4.3 \times 10^{16} \text{ neutrons/sec cm}^2$.

If this could be extended to a cw reactor having a flux of on the order of 10^{14} , dimensions of approximately $1 \times 1 \times 3 \text{ meters}$, we would have a megawatt nuclear-pumped laser device.

More interesting, however, is the possibility of a U_{235} fission-fragment pumped laser in which case we would have a 150 MeV per fission event available to excite the medium. If we simply assume (optimistically) that the energy available from the fission fragment goes to pump some as yet to be specified lasing species, we could anticipate increasing the laser power output by a factor of

approximately 150 over that obtained via He^3 . Hence we would now have roughly 100 kilowatts of laser power emitted per liter of lasant material. This would then suggest a 100 megawatt device associated with a nuclear-pumped laser having the dimensions mentioned above.

Naturally there are problems with this extrapolation. For example, UF_6 , a logical vehicle for the uranium is a strong absorber in most regions of the spectrum and deactivator of the excited species. One might consider using a metallic uranium lining in many small "tubes" containing a lasing medium (Figure 1) as per the suggestion of McCarther, et al.[1] In fact, as in Table 3, page 57 of that report, a 2,000 megawatt reactor translates (he hopes) into a 440 megajoule laser output (as per Table 7 of page 67). [These latter two tables are reproduced in the Appendix for easier reference.]

Thus, it is conceivable that (if one had the right lasing constituents) a megawatt nuclear-pumped laser in the visible or near UV is achievable. We note, however, that the density of inverted atoms and thus the energy stored per cm^3 is much lower in a reactor pumped laser than would be the case in, for example, an electron beam pumped device (from a maximum of 1 to 100 j/cm^3 for the nuclear laser to as much as 10^4 j/cm^3 for electron beam pumping). This in itself is not a killer. A large array of phase-locked lasers could be used in this context and thus compensate for the lower energy density (Figure 2). Furthermore the upper lasant level should be metastable in order to be better matched to the nuclear pumping rate.

Naturally, any judgement of device effectiveness must be weighted in view of other devices and systems which compete with the types of unspecified lasers discussed above. In this regard we note that conversion efficiencies from reactor to electrical power are on the order of 40% and we know that free-electron laser efficiencies approaching 30% are feasible. This would imply an overall nuclear to laser photon efficiency of something on the order of 10%! The flaw in this scheme is the necessity of converting from reactor energy to electrical with the subsequent complexity of hardware and added weight considerations, but it still looks very good to me.

In conclusion I strongly recommend that reactor-based laser systems be considered in light of current presidential directives and that the possibility of direct pumping of an as yet unspecified gas or plasma be considered and compared with the reactor-FEL hybrid both in terms of the technology and in ongoing systems' studies.

- [1] "Concepts for the Construction of Large Reactor-Excited Laser Systems". D. A. McArthur, T. R. Schmidt, J. S. Philbin, and P. B. Tollefsrud, Sandia Laboratory Report SAND 76-0584 (Sept. 1977).

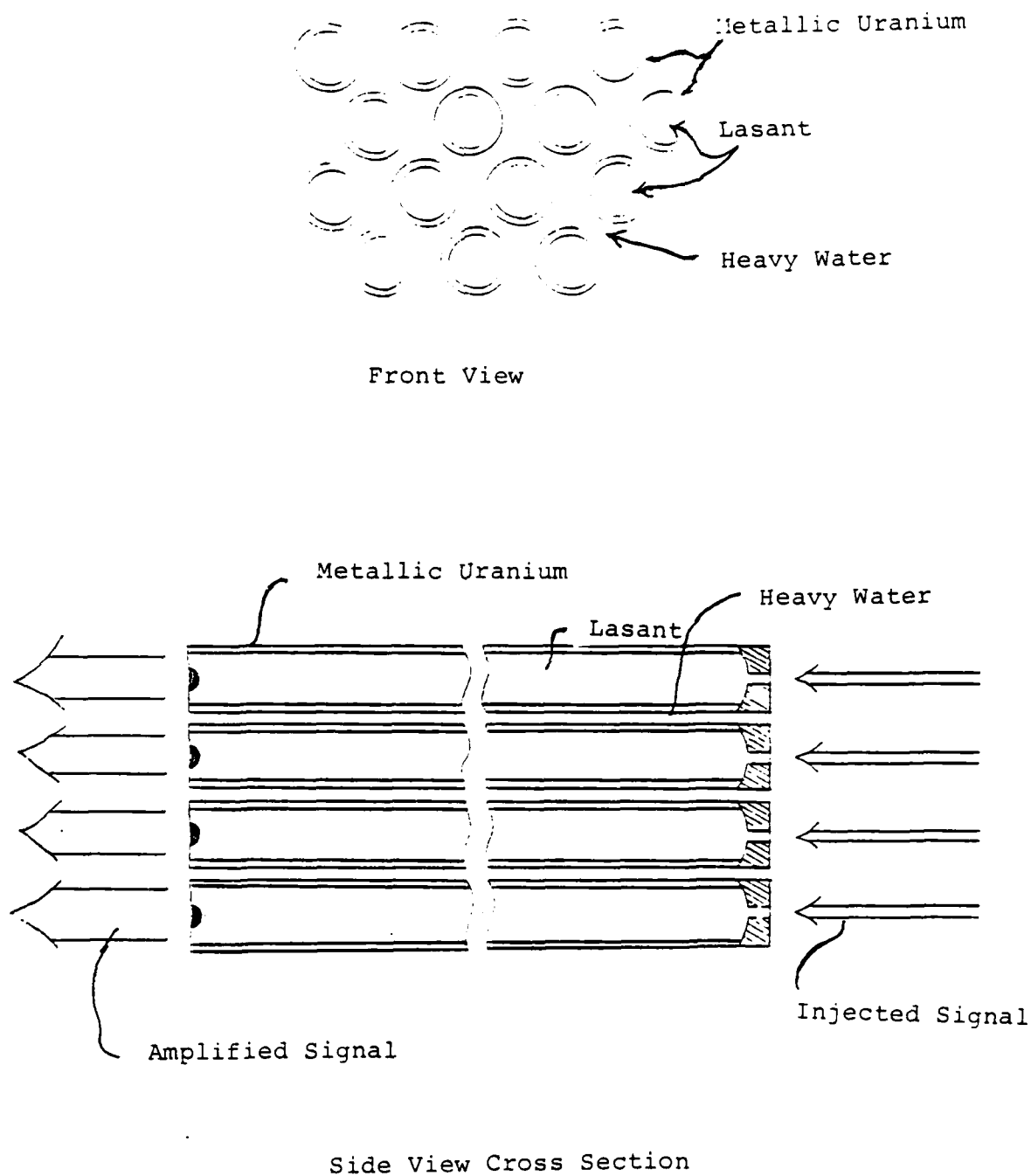


FIGURE 1. Schematic of nuclear-pumped laser.

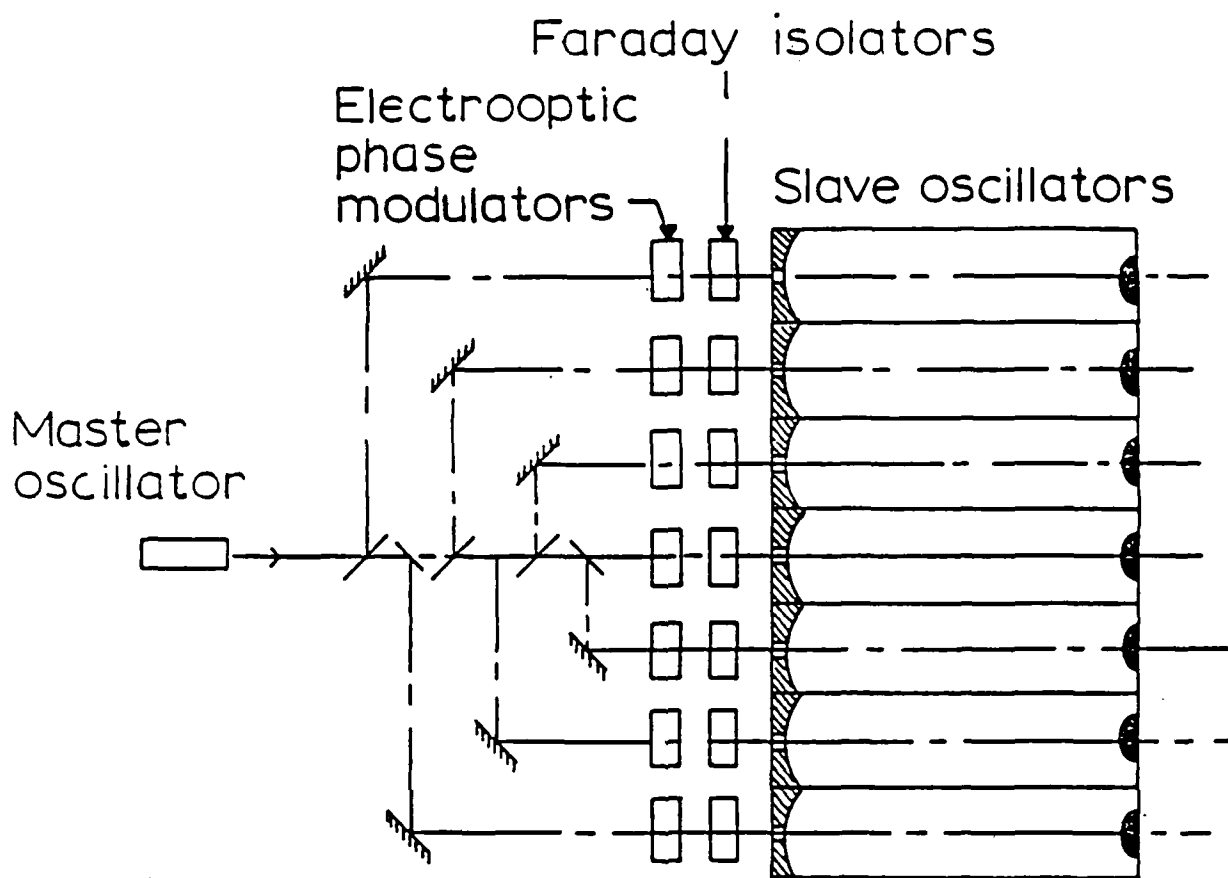


FIGURE 2. Phased Array of Injection Locked Lasers

$$\sigma_{\text{nuc}} \phi_{\text{neutron}} \times \left[\frac{\text{energy released/fission}}{\text{energy per electron ion pair}} \right]$$

$$\ll \sigma_{\text{atom}} \phi_{\text{electron}} \times \left[\frac{\text{energy of electron}}{\text{energy per excitation}} \right]$$

For conceivable systems the nuclear numbers are like

$$10^{-22} \text{ cm}^2 \cdot 10^{15} \frac{\text{neutrons}}{\text{cm}^2 \text{ sec}} \cdot 10^{21} \times \frac{10^7 \text{ ev/fission of U235}}{30 \text{ electron volts/pair}}$$

$$\sim 10^{19} \frac{\text{excited "lasants"}}{\text{cc}} \sim \frac{1 \text{ j}}{\text{cc}}$$

Whereas for electron beam pumped devices this goes like

$$10^{-16} \text{ cm}^2 \cdot 10^{18} \frac{\text{electrons}}{\text{cm}^2 \text{ sec}} \cdot 10^{21} \times \frac{10^2 \text{ ev/electron}}{10 \text{ ev/excited atom}}$$

$$\sim 10^5 \frac{\text{j}}{\text{cc}}$$

Table 1

Comparison of direct nuclear-pumped laser with an
e-beam pumped laser

A frequent objection to the nuclear-pumped laser is the observation that these devices are able to store only a tiny fraction of the inverted population per cubic centimeter that is possible from pumping via, for example, electron beam devices. This is sketched above and is indeed correct. The reason is that nuclear cross-sections are smaller by some six quarters of magnitude than atomic and that nuclear reactor fluxes are likewise a million times smaller than the usual electron fluxes.

While this is true, it is not a complete statement of the problem and neglects, for example, the very attractive feature of a nuclear reactor based laser device in that the energy storage per gram is, of course, a million times larger than the corresponding energy stored in atomic states. Therefore the weight considerations in space and the lifetime of any device based on electronic energy transitions, as compared to nuclear, can come down on the side of the reactor-based devices.

APPENDIX B

TABLE III⁺
 SELF-CRITICAL LASER EXCITER PROPERTIES
 CO/U/BeO SYSTEM

Relative Moderator Volume Fraction	Reactor Radius (M)	Reactor Volume (M ³)	Reactor Mass (10 ³ KG)	Pulse Reactor Energy (MJ)	Temperature Increase** (K)	"SS"* Reactor Power (MW)
1.0	0.58	2.2	2.71	9.5	4.3	552
0.9	0.70	3.1	3.56	14.0	4.8	728
0.8	0.91	4.8	4.86	23.2	5.4	1076
0.7	1.36	10.0	8.71	52.9	6.3	2097
0.6	4.88	117.0	78.10	540.5	5.8	23230

* For operation of 2 seconds duration.

** On a single intense pulse limited by energy deposition in foil coating.

+ Reference [1].

TABLE VII[†]LASER CHARACTERISTICS OF CRITICAL LASER EXCITER
CO/U/BeO SYSTEM

Moderator Volume Fraction	Total Gas Energy (MJ)	Specific Gas Energy (J/l - atm)	Output Density (J/cm ²)	Pulse Laser Output (MJ)	"SS"*** Laser Output (MJ)
1.0	2.0	551	140	1.0	116
0.9	2.9	529	135	1.4	153
0.8	4.9	500	127	2.4	225
0.7	11.0	490	125	5.5	440
0.6	113.0	372	95	56.5	4880

* For beam extraction on one end.

** For peak fission density in foils of 5.04×10^{14} fissions/cm³.

*** For an average core temperature increase of 500 K, without external cooling.

† Reference [1].

LASER DETECTION OF TRACE CONTAMINANTS
IN THE ATMOSPHERE

JOHN WIESENFELD*

JULY 1983

LA JOLLA INSTITUTE
P. O. Box 1434
La Jolla, CA 92038
(619) 454-3581

THIS RESEARCH WAS SPONSORED BY THE
DEFENSE ADVANCED RESEARCH PROJECTS
AGENCY UNDER ARPA ORDER NO.: 3710
CONTRACT NO.: MDA-903-82-C-0376

The views and conclusions contained in this document are those of the authors and should not be interpreted as necessarily representing the official policies either express or implied, of the Defense Advanced Research Projects Agency or the United States Government.

* Associate of the La Jolla Institute

TABLE OF CONTENTS

	<u>Page</u>
Executive Summary	1
I. Introduction	5
II. Spectroscopic Detection of Trace Species Using Lasers.	12
III. Applications of Lasers to Atmospheric Monitoring	26
IV. Concluding Remarks	41
Bibliography	47

Executive Summary

The development of laser-based methods for the detection of trace contaminants in the atmosphere has yielded research tools of great utility. With the introduction of new laser sources, these techniques will become of more general applicability, the eventual goal being the development of a truly 'universal' method for routine characterization of trace species. This report includes an assessment of the current state of research in this field as well as a discussion of potential opportunities for further refinement of newly emerging technologies not yet widely applied to atmospheric measurements.

All methods for atmospheric monitoring of contaminants must contend with the wide variability in such physical characteristics as aerosol content, visibility, and convective activity. While such variability might be of little consequence in certain applications where continuous monitoring is not required, it becomes a matter of intense concern when even intermittent service interruptions are unacceptable. Trace constituents are present even in the pristine atmosphere; when diurnal and meteorological variations in trace composition are convoluted with the potential contamination of this relatively clean environment, the need for high specificity in a monitoring technique is underscored.

An ideal trace contaminant monitor can be imagined as being not only highly selective and sensitive (measurements at or below the ppm level often being desirable) over a wide dynamic range, but also general in scope and capable of providing a rapid, real-time response when a contaminant is detected. Range and azimuthal information are often of critical importance. Operational simplicity is a must for routine operation.

Of the available techniques for remote detection in the troposphere,

Differential Absorption Lidar (DIAL) has been most fully developed. With high sensitivity and ranging capability, this method offers enormous potential for true remote operation. Under ideal conditions, visible/uv probe excitation has enabled the detection of such small molecules as SO_2 , NO_2 , and O_3 . Many other small molecules have been detected in the infrared, although the technique is not so general because intense, continuously tunable infrared sources are not generally available. Further tests of DIAL, especially involving infrared spectroscopy in the fingerprint region, should include evaluation of sensitivity and selectivity under various conditions of atmospheric visibility and aerosol composition. The effectiveness of DIAL in monitoring trace composition in the direction of the sun must also be determined.

Raman spectroscopy was recognized at an early stage in the development of atmospheric sensing methods as having considerable potential for remote characterization of major components and has been successfully applied to the measurement of temperature, etc. Its major limitation is sensitivity, with overlapping weak transitions arising from major constituents overwhelming even strong transitions associated with trace species. No other technique for laser-based contaminant detection is more general than Raman spectroscopy, excitation at a single frequency being required for full analysis. The utility of Raman spectroscopic methods for atmospheric analysis depends critically upon the required level of detection sensitivity, levels much below 1000 ppm being relatively difficult to achieve.

Of the local methods, optoacoustic spectroscopy has demonstrated the greatest potential for sensitive detection of trace materials under atmospheric conditions. Because of the exquisite sensitivity of detection afforded by electret microphones, it has proved possible to monitor absorptions as weak

as 10^{-7} using routinely available laser sources. The development of broadly tunable laser diode array sources of sub-Doppler width radiation may make optoacoustic spectroscopy even more generally applicable to problems of trace contaminant detection.

Both laser induced fluorescence (LIF) and photoionization spectroscopies have been employed for wide-ranging laboratory studies of molecular dynamics in the gas phase. LIF has also been applied to the still somewhat controversial detection of ultra-trace quantities of OH radicals in the troposphere. Significant enhancement in selectivity through spectral simplification may be realized by rotationally cooling analytes in supersonic jets prior to analysis. Laser photoionization is of special interest for it is, in principle, capable of detecting single atoms and molecules. Mass selection of photoionized molecules and fragments makes possible what is, in essence, a multidimensional analysis scheme. As is well recognized from mass spectrometry, scrutiny of fragmentation products makes possible the identification of generic sub-structure components which cannot be recognized by more standard spectroscopic tools. Thus, laser photoionization spectroscopy seems a highly sensitive, especially selective method for trace contaminant detection; its applicability to problems of atmospheric monitoring should be fully explored.

While the feasibility of these various methods for trace analysis have been demonstrated in the laboratory (uniformly) and field (occasionally), relatively little comparative work has been reported. In the near future, trials of these techniques under realistic conditions should be undertaken. Special emphasis should, when appropriate, be placed on ascertaining the reliability of these methods for long-term, uninterrupted analysis. Similarly, increased attention should be paid to refinement pathways, especially with

regard to the potential for development of relatively cost-effective integrated packages containing laser sources, detectors, and even perhaps the necessary signal processing electronics. It would be particularly interesting to analyze entire detection systems rather than individual components with a view toward understanding the relative merits of complex remote sensing techniques vs. multiple installations of simpler local field detection methods under the broad range of conditions which would be encountered in a typical application.

1. Introduction

The detection of complex materials in the atmosphere represents a significant challenge to even the most modern analytical instrumentation.^{1,2} Yet, because of the importance of trace species detection in such diverse areas as environmental protection, geological exploration and national defense, this area has received wide attention from chemists, physicists, and engineers. As a result of the extraordinary sensitivity and selectivity afforded by spectroscopic techniques, these have been most generally exploited in the development of trace species detection both in the laboratory and field.³ Naturally, the continued development of lasers as powerful sources of tunable, monochromatic radiation from the ultraviolet to the infrared makes detection schemes based on spectroscopy even more attractive, especially for remote sensing applications. This report deals with such laser-based techniques for trace species detection in the atmosphere.

1.1 Atmospheric Considerations

The spectroscopic detection of trace species is considerably complicated by the physical characteristics of the atmosphere. At a total pressure of ca. 760 torr, absorption lines are significantly pressure broadened, thus causing loss of spectral resolution. This phenomenon, which is especially serious in the infrared region, makes impossible spectral discriminations that can easily be accomplished in the laboratory at lower pressures. As all spectroscopic techniques depend upon the absorption of light, pressure broadening affects the selectivity of each. Methods involving detection of optical emission following absorption of laser radiation must also contend with the collisional deactivation of excited states accessed by the probe.

As the time between gas kinetic collisions at 760 torr is on the order of 0.3 nsec, on average even the most short-lived electronically excited state will undergo many collisions prior to emission. Collisional quenching of electronically excited states (especially of large molecules) by N_2 and/or O_2 is often very efficient and may be expected to compete most effectively with optical emission. This, of course, can decrease the observed emission signal by orders of magnitude for molecules with not atypical optical lifetimes on the order of 10-100 nsec. Vibrational deactivation of excited states can also compete most effectively with emission; the rate of vibrational deactivation can depend upon the relative humidity because H_2O is an effective partner for vibrational energy transfer. This can greatly complicate quantitative measurements.

With the exception of the natural variability in H_2O , the composition of the major tropospheric constituents, N_2 , O_2 and CO_2 , is essentially constant. This most certainly cannot be said of either the physical characteristics of the troposphere or its minor chemical constituents. Meteorological variability in such attributes as visibility, aerosol content, convective activity, etc., are enormous and conditions for propagation of laser radiation vary accordingly.⁴ Techniques for remote sensing of trace constituents are most strongly impacted by this variability. The significance of this observation depends upon the application. While it would only be a minor inconvenience for geophysical applications, it might represent a profound limitation in situations involving defense against toxic agents on the battlefield. The chemistry of minor components of even the unperturbed troposphere is extraordinarily complex⁵ and the injection of anthropogenic emissions such as NO_x , SO_2 and the hydrocarbons can lead to the development of such undesirable environmental phenomena as

photochemical smog and acid rain. This wide-ranging variability in minor constituents especially O_3 , H_2O_2 , NO_x , and free radicals such as HO_2 and HO greatly complicates the detection of specific trace contaminants for two reasons. Firstly, the presence of sulfates leads to the formation of visibility limiting aerosol particles (i. e., smog when taken to an extreme) of highly uncertain composition. Secondly, spectroscopic transitions which could be associated with specific trace materials in the pristine atmosphere can become totally obscured by interfering lines associated with these highly variable minor constituents that contribute to an ever-changing background. Systematic evaluations of the relative utility of various spectroscopic techniques under widely varying atmospheric conditions have not appeared in the literature.

1.2 Laser technology

An extensive review of laser technology applicable to trace species detection in the atmosphere lies beyond the scope of this work (but see references 4 and 6-9 for recent developments). In Table 1 are listed the important operating characteristics of commonly available laser systems, the output of which spans the spectrum from the ultraviolet to the infrared. Excellent spectral brightness, tunability and stability are available in the visible due to the refinement of the dye laser. Frequency doubling of the dye laser's output extends these characteristics to the ultraviolet, albeit primarily when operating in the pulsed mode, and of course at significantly reduced powers.

In the infrared, high powers and continuous tunability are also available, but not in the same device. Chemical and energy transfer lasers operating with such gain media as CO and CO_2 can provide intense output at discrete

Table 1. A compendium of laser specifications of importance to trace contaminant detection in the atmosphere.
[Source: Laser Focus Buyer's Guide 1977]

Type	Wavelength range (nm)	Peak Power (W)	Average Power (W)	Resolution	Pulse Width
cw dye	380-1000		1-10 W	< 5 MHz	
flash pumped dye	430-800	> 10 MW	5 W	0.001 nm	300 nS
N ₂ pumped dye	360-950	> 100 kW	60 mW	0.001 nm	6 nS
YAG pumped dye	380-1175	5 MW	2 W	0.005 nm	5 nS
excimer pumped dye	350-970	1.5 MW	5 W	0.001 nm	15 nS
CO ₂	9000-11000*	5 MW	10 W		100 nS
multi gas l.r.	2600-11000*	5 MW	1 W		500 nS
diode	3000-30000		5 mW	< 1 MHz	
excimer	193-351*	20 MW	50 W	0.1 nm	15 nS

* discrete frequencies available in this region

frequencies in the spectral regions near 2000 and 1000 cm^{-1} , respectively. The rapid development of the tunable diode laser suggests that this device will play a major role in state-of-the-art detection systems.¹⁰ These are individually tunable over only relatively narrow spectral regions, but the construction of laser diode arrays¹¹ would make it possible to operate these sources over extended spectral regions.

1.3 The ideal trace species detector

While each application will have an associated set of 'ideal' characteristics as a design goal, there probably are several features which would be especially desirable in any trace species detection apparatus. These include:

1. **high sensitivity** for detection of materials which, like such free radicals as OH, are present at densities of 10^6 - 10^7 cm^{-1} , but nonetheless are of critical importance. Similarly high sensitivity can provide an early warning of the presence of a material which is only harmful at higher concentrations;
2. **good selectivity** to permit reliable discrimination between materials with similar spectral characteristics;
3. **wide dynamic range** so that subject materials may be monitored reliably both at ultra-trace and trace levels;
4. **generality** so that a wide variety of materials can be detected using one generic type of apparatus;
5. **directionality** which permits localization and ranging of a particular material. This may be provided by direct remote sensing or the dispersal of multiple sensors;

6. **real-time response** to permit effective decisions and implementation of necessary countermeasures in the case of toxic substances;
7. **convenience**, reliability, and simplicity of operation by technical personnel who are not intimately familiar with the fundamental principles of the instrument's design and function.

The design of an effective trace detection system depends, of course, upon the choice of an appropriate spectroscopic technique as well as the development of sophisticated computational tools to serve in a support role. Limitations associated with the analysis of a stream of physical data may prove more serious than any inherent limits of spectral sensitivity. Indeed, the sensitivity of the more widely studied spectroscopic techniques is typically more than sufficient for the detection of contaminant materials at levels near or above 100-1000 ppm. Of real concern must be the specificity of a detection scheme for particular trace species in the presence of a widely varying background of natural and anthropogenic gases. The requirement of specificity usually imposes extra complexity upon the detection system designed to operate in the 'real' atmosphere, a premium being paid for the need to reject information concerning materials present in higher concentrations than the desired analyte. We will see that Raman spectroscopy, for one, is limited in its practical application for the detection of trace contaminants by the contribution of the major atmospheric components. Clearly, a technique analogous to multidimensional thin-layer chromatography¹² in which more than one attribute of a molecule (in this case, its relative chromatographic response in several solvents) are simultaneously ascertained. An example of such a method applicable to atmospheric monitoring is mass-selective multiphoton ionization spectroscopy¹³ in which a molecule is ionized by resonant interaction with light and then

resolved following mass selection of the ion. Such multidimensional signatures are relatively straightforward to identify and interferences can be kept to a minimum.

2. Spectroscopic detection of trace species using lasers

This section is concerned with the description of generic spectroscopic techniques which may be applied to trace detection. Applications to problems of atmospheric significance will be considered in section 3.

Laser-based detection schemes may be categorized into broad classes. One involves the measurement of light intensity, as in the cases of absorption, fluorescence, or scattering. In the limit of weak signals, the sensitivity of these techniques is limited by collection geometry and detector quantum efficiency. The second group of methods as typified by photoionization and optogalvanic techniques requires the detection of charge. These often offer significant advantages over optically-based methods because the collection efficiency for charged particles is relatively high. In yet another class typified by optoacoustic methods, light absorption is detected by monitoring energy deposition; this is detected by monitoring the pressure (and hence the temperature) variations in a gaseous sample exposed to optical radiation.¹⁴

2.1 Absorption spectroscopy

Both atoms and molecules are routinely detected at trace levels by absorption spectroscopy. The well-known Beer-Lambert law relates the intensity of light, I , transmitted through a sample of length, l , to the initial intensity, I_0 ,

$$I/I_0 = \exp(-\epsilon lc)$$

where ϵ is the cross-section and c is the concentration. At low levels of light absorption, a differential measurement scheme is often employed and

$I = I_0 - \Delta I = I_0 \epsilon lc$. The cross-section varies strongly with the nature of the transition. It is on the order of 10^{-16} cm^2 for a strong absorption in the ultraviolet. As values of $I/I_0 = 10^{-4}$ may routinely be made, a detection

limit of 10^{10} cm^{-3} is easily attained over a pathlength of 1 meter.¹⁵ This represents part-per-billion detection at an ambient pressure of 1 atm.

Differential detection automatically corrects for fluctuations in source intensity, but such methods may become impractical when long pathlengths are being used in order to overcome limitations imposed by small cross-sections in the infrared 'fingerprint' region. A variety of techniques have been introduced to deal with such situations. For example, the probe laser may be frequency modulated so that the output frequency is given by

$$f(t) = f + \delta f \sin \omega_m t$$

where the modulation represents only a small fraction of the absorption line width and ω_m is the modulation frequency. This dithering of the laser frequency introduces an AC component into the transmitted light intensity which then may be detected as a derivative signal.¹⁶ This technique of derivative absorption spectroscopy can reduce the minimum observable absorption by as much as 10^4 .

Further enhancements in detection of weak absorbers may be achieved by introduction of the sample into the cavity of a laser operating near threshold.¹⁷ The output power will display a highly nonlinear dependence upon the intracavity absorption. This technique, while sensitive to absorptions as low as 10^{-5} , suffers from both the need for a homogeneous sample as well as the complex relationship between absorber concentration and laser output.¹⁸ Furthermore, not all laser cavities may be conveniently accessed for sample placement.

Optoacoustic detection was first developed by Alexander Graham Bell.¹⁴ In concept, it is exceptionally simple: Energy absorbed by the sample is transferred to a gas in which, as the result of heating, a pressure pulse is induced. The magnitude of the associated sound signal depends upon the

energy absorbed. Optoacoustic spectroscopy offers special advantages in the infrared region where optical detector noise most often limits trace analysis.

At atmospheric pressure, the deexcitation of sampled molecules and subsequent energy transfer to the bulk gas is expected to be quite efficient, especially following excitation in the infrared. Eventually, the sound wave associated with the thermal excitation can be detected using a sensitive electret microphone.¹⁹ The detection limit depends critically upon such factors as laser power, cell geometry and microphone sensitivity. Interference resulting from absorption of radiation by the windows of the cell must be minimized by the use of acoustic baffles;²⁰ alternatively windowless cells may be used.²¹ Absorption sensitivities of 10^{-9} may be achieved under the most favorable circumstances in which use is made of the phase sensitive detection of the sound wave induced by a chopped laser beam in an acoustically resonant cell.²² This corresponds to a detection limit of 10^7 cm^{-3} or 0.001 ppt for typical infrared transitions!

Another advantage of optoacoustic spectroscopy lies in its wide dynamic range. Two constraints fix the upper end of its useful range. One, the saturation of microphone and detection circuitry can be overcome by use of lower probe power. The other, nonlinear absorption of the laser beam near the input end of the cell, places an approximate limit of 10^6 on the dynamic range.

2.2 Emission spectroscopy

As noted earlier, an excited state populated by the absorption of a photon may, in the absence of collisional deactivation, reemit radiation. Only short-lived excited states will actually emit significant radiation

at atmospheric pressures, thereby limiting applications of this spectroscopy to electronically excited states pumped by visible or ultraviolet radiation. Electronic emission spectra can be diagnostic of the subject species and so may provide qualitative information concerning its identity.

Resonance and non-resonance fluorescence techniques have been widely applied to the detection of metal atoms in the gas phase.²³ In principle, the non-resonant techniques, wherein the atom is pumped to a higher-lying electronically excited state, undergoes collisional deactivation to the lowest-lying excited state and then emits at a longer wavelength than the initial probe, will display the highest sensitivity.²⁴⁻²⁶ Indeed, for favorable cases, e. g., the alkali metals, non-resonance fluorescence detection is capable of a detection limit of ca. 10^4 cm^{-3} . Because of the small volume probed, this suggests that these techniques are capable of detecting a single atom!²⁷ Whether this is so remains a matter of some controversy--to what extent can one ensure that a cell containing an atmosphere of buffer gas is, in fact, saturated with Na vapor at 10^4 cm^{-3} ?

A wide variety of molecular species have been detected using laser-induced fluorescence (LIF), which has become a mainstay of molecular dynamics research.²⁸ A (highly non-inclusive) list of molecular species observed using this method includes C_2 , CH , OH , NH , CN , NH_2 , CH_2 , NO , NCO , $\text{C}_6\text{H}_5\text{CH}_2$, and C_6H_6 . Although LIF is most efficiently applied to detection at low pressures, trace species have been observed at atmospheric pressure and even in luminescent flames.²⁹ The practical limit for detection under high pressure conditions is about 10^6 cm^{-3} .

Identification of larger molecules by fluorescence spectroscopy is complicated by the broad fluorescence excitation and emission spectrum characteristic

of species with so many molecular vibrations. Thus, the spectra of such polynuclear aromatic hydrocarbons as naphthalene, anthracene, and benzpyrene (this last being highly carcinogenic) are very difficult to identify, being relatively featureless broad continua even at low pressures in the gas phase.³⁰ These spectra can be greatly simplified and identification made significantly more straightforward by cooling the molecules to such a low temperature that only the lowest rotational states are populated to any degree.³¹ Thus, at 4 K, even the most congested spectra can clearly be identified. Experimentally, cooling may be achieved by dispersing the molecule in a glass-forming organic matrix in a cryostat.³² Alternatively, large molecules seeded in a light collision partner and expanded through a supersonic jet can be rotationally cooled to a few degrees K.³³ This technique has been extended to hydrocarbons as large as the porphyrins. The fluorescence excitation spectra of molecules eluted from a gas chromatograph can be detected either in a glass or cooled expansion; detection limits near 1 ppb have been established for pyrene in a complex mixture of cigarette tar.³⁴ While the technique of cooling in a glass is not suitable for rapid real-time measurements, the supersonic jet could be used as a source under such circumstances. The problem here would be removal of the heavy gases such as N_2 and O_2 , the presence of which would interfere with efficient rotational cooling of the contaminant molecule. It should be noted that further selectivity enhancement can be obtained in a complex mixture of fluorescent materials through the use of temporal gating which limits observation times to the fluorescence lifetime of the desired analyte.³⁵

The utility of LIF has been recently extended by the development of two-photon excitation methods which permit the detection of such species

as O, S, and the halogens, all of which display one-photon resonances in the vacuum ultraviolet only.^{36,37} Nominal detection limits here are on the order of 10^{12} cm^{-3} . In another approach based on multiphoton excitation, larger molecules which do not fluoresce efficiently at atmospheric pressure are first photodissociated into smaller fragments using a high intensity, high energy ultraviolet laser.³⁸ These photofragments are then detected using standard LIF techniques. There is nothing especially novel about this technique. Indeed, it has been exploited for the study of photodissociation dynamics of small molecules in a number of laboratories. A more generalized method might be based on the decomposition of complex molecules by multiphoton infrared excitation using a high-power CO_2 or Nd/YAG laser, key fragments like NO, CN, PO, etc., then being detected by LIF.

Other techniques involving detection of emission following non-specific excitation of a gas have also been suggested. For example, infrared emission from a laser-excited gas may be dispersed in order to obtain qualitative information concerning trace constituents from spectral signatures. Discriminating against strong background black-body emission would be required. Alternatively, by using a sufficiently intense laser pulse, a plasma may be generated. The spectral profile of the plasma emission may then be monitored^{39,40} in a manner analogous to that of spark source emission spectrometry which has long been used to analyze the trace composition of metal samples. This technique provides a link to those methods which depend upon detection of ionic species in that it would in principle be possible to obtain the mass spectrum of ions produced in the laser-excited plasma. A significant difficulty associated with application of such techniques to atmospheric sampling is the need to maintain a reproducible mechanism for plasma formation

and sampling in the presence of aerosol particulates.

2.3 Photoionization spectroscopy

Mass spectroscopists have for decades used single-photon photoionization as a means of preparing ionized samples for analysis.⁴¹ Because the ionization potentials of most materials of interest lie in the range 7-12 eV, high energy photons with wavelengths in the region 100-180 nm are required to achieve photoionization. Recently, techniques based upon nonlinear mixing have been developed to produce tunable, high intensity laser radiation in the vacuum ultraviolet region.⁴² Typical output powers are ca. 5 kW at a pulse repetition rate of 10 Hz. At such power levels, a target molecule present at the ppm level can readily be detected using a conventional particle multiplier in conjunction with an electrometer. Application of ion counting techniques further enhances the detection sensitivity of the photoionization method to the 1 ppb level and beyond. If the ionization potential of the matrix, i. e., N₂ and O₂ for the atmosphere, is higher than that of the subject species, photoionization provides a key advantage over conventional mass spectroscopy because ionization of the host gas can be completely suppressed.

Direct one-photon photoionization methods do suffer from the instrumental disadvantages of bulk and complexity; both laser-based and conventional sources of vacuum ultraviolet radiation are nontrivial in their operation and even relatively small quadrupole mass filters require ultra-high vacuum pumps, etc. An enormous simplification in experimental complexity can be realized by the exploitation of two-photon ionization techniques.⁴³ In the absence of a resonant real intermediate state, cross sections for two-photon ionization are typically $10^{-49} - 10^{-50} \text{ cm}^4 \text{ sec}^{-1}$. However, if the laser

is tuned to the wavelength of an allowed transition to a real intermediate state at an energy greater than halfway to the ionization potential, population in the intermediate state will rapidly build (in the absence of non-radiative loss processes such as fragmentation), and ionization can be viewed as the sequential, incoherent absorption of two photons for which the overall cross section is much larger. As saturation of the intermediate transition is approached, the sensitivity of two-photon excitation approaches that of VUV one-photon photoionization.¹³

During the course of a laser wavelength scan in two-photon ionization spectroscopy, the source will naturally be in resonance part of the time and out of resonance the rest. If the total ionization signal is monitored under such conditions, it will display a characteristic signature that may, under favorable circumstances, be closely associated with the ordinary absorption spectrum of the subject species. If, as is sometimes the case, the intermediate state is dissociative and so does not build any significant population in the laser field, the fragments may be readily ionizable (as is the case for NO⁴⁴ and probably PO), and the wavelength dependence of the observed ionization efficiency may still be distinctive of a particular molecule, although there will no longer be a simple correspondence with the absorption spectrum of the parent. If the photofragmentation product displays a high ionization potential, this technique will not, in general, be applicable.

Other constraints also limit the range of molecules which may be probed by two-photon photoionization spectroscopy. Commercially available dye lasers do not provide output below 350 nm without recourse to energy inefficient frequency doubling and mixing. Thus, only molecules with ionization potentials below 6.9 eV can be detected in this manner. In addition, because Rydberg

states are most effective as intermediate states for promoting transitions to the ionization continuum,⁴⁵ and as the energy of the lowest such state is limited by the laser wavelength range to be below $28,000\text{ cm}^{-1}$, the maximum ionization potential is further restricted to approximately 5.1 eV. Only a small number of molecules satisfy this requirement. However, it should be remembered that further development of laser frequency upconversion technology may soon relax this restriction considerably.

The utility of photoionization spectroscopy is considerably extended by use of multiphoton excitation, which by definition requires that the subject molecule absorb three or more photons per ion produced. Resonant enhancement greatly increases the magnitude of the ionization cross section and may occur at the absorption of any one or perhaps several photons. As in the case of two-photon ionization, large increases (or perhaps dips if the resonant state is dissociative) in the observed signal occur as the laser frequency is tuned into resonance with the allowed transition to a real intermediate state.⁴⁶ Under favorable circumstances, a characteristic fingerprint spectrum may be observed.

Two problems are associated with multiphoton photoionization spectroscopy. First, at the high laser intensities required to promote the coherent n -photon transitions through virtual states to the real intermediates, (pulsed laser intensities on the order of 10^9 MW cm^{-2} are typical), photofragmentation of parent ions is common.^{47,48} This can obscure the nature of the subject species if mass spectrometric detection is being employed. Second, as in the case of two-photon photoionization, fragmentation of an intermediate real state into neutral molecules of high ionization potential will greatly decrease the overall ion yield. Occasionally, one may take advantage of

this second phenomenon if a large molecule with a high ionization potential can be induced to produce neutral photofragments of low ionization potential. This is analogous to the photofragmentation-LIF scheme discussed in the previous section.³⁸ For example, large phosphate esters can, upon fragmentation, be expected to yield PO radicals which have a large multiphoton ionization cross-section.⁴⁹

The instrumental requirements for two- and multiphoton ionization spectroscopy are relatively modest. Perfectly acceptable signals may be obtained at ppm concentrations by focussing with a short focal length lens the well-collimated output of commercially available dye lasers into a cell outfitted with two electrodes biased by a dc supply. Ordinary electrometers are quite adequate to measure the resulting signal. Mass selective detection can be accomplished quite easily through the use of a time-of-flight mass spectrometer used in conjunction with pulsed excitation. As noted earlier, mass specific detection of ionization products offers a significant enhancement of the selectivity of photoionization spectroscopy for now a multidimensional 'fingerprint' pattern may be obtained,⁵⁰ that corresponding with the resonant interaction of light with matter as well as that arising from the molecular fragmentation pattern of the parent ion. Because the use of mass-selective detection reduces the background ionization signal while not significantly lowering the intensity of the ions collected following photoionization (the result of efficient ion optics), the detection limit can be expected to improve significantly (by as much as several orders of magnitude) if mass selection is implemented, a rare case where detection sensitivity is actually improved through the use of higher resolution methods! The use of time-of-flight mass analysis offers another significant advantage, that of multiplexing,

with all masses being monitored simultaneously. Specific functional groups can be detected simply by monitoring the temporal delays associated with the masses of these fragments.

Optogalvanic spectroscopy also takes advantage of electrical detection of resonance transitions.⁵¹ In this technique, the change in steady-state current in a discharge or flame is measured when the laser output frequency comes into resonance with a transition of an atom or molecule present. The effect of the absorbed energy is to perturb the steady state populations of intermediate species formed in collisional processes that produce and consume ions in the discharge. Such perturbations change the degree of ionization and, hence, the impedance of the discharge. The resulting ac component of the current flow following these perturbations gives rise to the observed optogalvanic effect.

Although the magnitude of the observed impedance change depends upon the discharge mechanism in a complex way,⁵² the technique can be made quite reproducible for a given set of initial conditions, and once calibrated, quantitative analysis of trace species becomes relatively straightforward. Detection limits likewise depend critically on the details of the experimental setup, but sub-ppb levels have been demonstrated for the alkali metals.⁵³ The dynamic range can be as large as 10^5 for metals with low ionization potentials. Both detection limit and dynamic range degrade for metals with higher ionization potentials. Only a few molecular species have been detected using this technique. These include I_2 ⁵⁴ and HCO.⁵⁵

Optogalvanic spectroscopy requires little in the way of complex equipment. Given a stable flame or discharge, it is only necessary to pass a laser beam of moderate intensity through the sample region. Detection can

be accomplished through the use of phase sensitive amplifiers thereby improving the signal quality dramatically. Because it is not necessary to actually ionize the absorbing species, only one-photon transitions need be excited and even infrared excitation can be used to couple laser energy into the plasma. However, large molecules will surely lose their chemical identity in either an electric discharge or flame, so detection will depend on absorption by fragments only. This significantly decreases the specificity of the technique for complex molecules.

2.4 Raman Spectroscopy

Light interacting with molecules is elastically scattered anisotropically in a manner which depends upon the refractive index, the density and the wavelength. Such Rayleigh scattering displays a small cross-section, typically on the order of 10^{-26} cm², but becomes especially important at short wavelength due to a λ^{-4} cross-section dependence. Because Rayleigh scattering is elastic no structural information may be gleaned from this phenomenon.

Small particulates and the atmospheric aerosol scatter radiation with far larger cross-section than do individual molecules. First treated quantitatively by Mie, this phenomenon may be directly related (especially in the visible and infrared regions where, because of its λ^{-1} dependence, it dominates Rayleigh scattering) to atmospheric visibility. The quantitative nature of this relationship is still being explored.⁵⁶ The wavelength dependence of the Mie scattering cross-section, which may reach 10^{-8} cm² when the diameter of the particulate matter approximates the wavelength of the scattered radiation, is well understood and is, of course, of primary importance to the characterization of DIAL measurements in the free atmosphere.

Inelastic Raman scattering is a spectroscopic tool of great utility because the frequency shift, Δ , observed following scattering via absorption to a virtual state is characteristic of the species present.⁵⁷ This phenomenon presents the spectroscopist with a powerful technique for monitoring a wide variety of gaseous molecules; no resonance is required. However, because the cross-section for Raman scattering is relatively low, ca. 10^{-28} cm², wide exploitation of this technique awaited the development of the laser as a high intensity source of monochromatic radiation. Indeed, because there is no requirement for resonant interaction between probe and scatterer, high power lasers such as Nd/YAG serve as general sources for detection of all molecules. The cross-section for Raman scattering does increase by 10^5 - 10^6 if excitation is carried out at or near resonance between electronic states. Interferences arising from fluorescence are then encountered; these can be mitigated by the use of suitable short-pulse lasers and gating electronics which can temporally discriminate against relatively long-lived fluorescence.⁵⁸

Raman scattering results in excitations corresponding to the $\Delta J = 0, \pm 1$ transitions with $\Delta v = 0, \pm 1$. The S and O sidebands associated with $\Delta J = +2$ and -2 respectively are far weaker than the central, normally unresolved Q band, the frequency shift of which, Δv , is characteristic of the species being excited. Trace species detection can be greatly complicated by the presence of weak S and O transitions arising from major components obscuring the main Q band of the minor constituents. It has been suggested that the pure rotational Raman spectra arising from the $\Delta v = 0$ transition might be analyzed using a Fabry-Perot interferometer. Such an arrangement would have the advantage of high resolution and greatly enhanced throughput when compared to the double (and even triple) monochromators required to obtain the necessary

resolution of the Raman signal and rejection of the inelastically scattered radiation.^{59,60}

Spectroscopic probes based upon coherent interaction of probe radiation with molecules have been developed to characterize the composition and local temperature of small molecules. Of these, Coherent anti-Stokes Raman Spectroscopy (CARS), which is governed by the 3rd order electric susceptibility, $\chi^{(3)}$, is the most important.⁶¹ Pump laser output at ω_1 is mixed with that of a tunable laser at ω_2 , yielding coherent anti-Stokes radiation at $2\omega_1 - \omega_2$. Detection of the output beam can occur remotely from the test region and may be accomplished even in the presence of high-level luminescence, as in flames.⁶² However, interferences arising from the presence of nonresonant background susceptibility are encountered. These may be minimized through careful selection of pump, probe, and detector polarization orientations.⁶³

Ordinarily, CARS measurements are made by scanning the probe laser over the range of spectral interest. By utilizing a broad band probe laser and detecting the generated coherent signal with an Optical Multichannel Analyzer, spectra may be obtained in a relatively brief time.⁶⁴ In principle, single-shot spectra are made possible by the multiplexing advantage associated with such an apparatus. In general, long sample pathlengths in CARS measurements are not useful, the observed signal being the integral of scattering by all of the constituents present. Hence, the desired minor constituent scattering signal would still be overwhelmed by that of the major components. Nonetheless, CARS and related coherent scattering techniques such as BOXCARS have been successfully exploited as important probes of various combustion systems in which Mie scattering by particulates and spontaneous luminescence posed potentially serious interferences.

3. Application of lasers to atmospheric monitoring

Having presented an introduction to laser-based, spectroscopic methods for detection of trace species in gases, we go on to consider their application in the atmosphere. In doing so, it is desirable to first classify detection schemes with regard to their generic mode of operation. They are:

Laboratory All of the techniques which may be applied to atmospheric monitoring were originally developed for laboratory studies. Here, it is possible to deal with relatively clean, simple mixtures free of particulate matter, etc. Problems arising from atmospheric turbulence are absent so long as closed cells are used. Measurements made at low ambient pressure avoid complications that arise as the result of undesirable pressure broadening and excited state deactivation.

Field Techniques which are capable of the characterization of complex mixtures may be applied to the detection of trace species in the atmosphere local to the sampling site. Such field methods must be capable of dealing with the many trace constituents that may be present in the real world, preferably by being sufficiently specific so that the instrumentation will respond to the subject species alone. Laboratory techniques that have been applied to flames are usually capable of being adapted to field atmospheric measurements. For the purpose of the present discussion, it is assumed that field measurements allow real-time monitoring of trace contaminants; methods which depend upon 'grab' sampling and subsequent analysis in the laboratory are not considered to fall in this category.

Remote Methods which permit the characterization of atmospheric composition over a distance scale of kilometers are, of course, highly desirable. Such measurements may be characterized as being either single- or double-

ended depending on whether some type of device, e.g., a detector or retroreflector, must be situated remotely from the base station. Some methods are, in a sense, pseudosingle-ended because they rely on the presence of some physical reflector of the probe radiation such as a topological feature (e. g., shrubbery) or aerosol scatterers. Remote methods are by their nature the most difficult to implement as they must deal with such problematical variables as scattering, turbulence, refraction, etc. Also, because of fundamental limitations on the propagation of light, no remote sensing technique may depend upon multiple photon excitation of subject species.

Within the context of these general classes we may now go on to discuss those techniques which have been proposed and/or developed for trace species detection in the atmosphere. Special emphasis will be placed on case studies which illustrate the problems associated with making measurements in the real world, because it is often practical constraints and not fundamental physical limitations which prevent that general applicability of specific techniques to problems of atmospheric importance.

It would probably not be unwise to reiterate some of the difficulties associated with detection of trace species in the atmosphere. As mentioned in section 1.1, all spectroscopic techniques, regardless of the mode of operation, must contend with the loss of resolution associated with pressure broadening and with excited state deactivation processes. In addition all remote sensing technologies must also contend with the meteorological variables such as fog, haze, precipitation, etc., which conspire to limit long-range visibility. Atmospheric turbulence arising from thermal instabilities can wreak havoc on any remote sensing technique. Methods involving beam expansion and suitable

placement of transmitter and reflector can serve to minimize, but not eliminate, such problems. Also, a detection 'blind spot', for example in the direction of the sun, might well limit the utility of a particular technique for certain applications. Clearly, these factors must be weighed against the mission requirements for trace contaminant monitoring in a given application.

Although a spectroscopic technique should, in principle, be capable of identifying specific molecular contaminants, it may be sufficient (or perhaps even desirable) in some applications to provide identification of some specific functional moiety or subgroup (e. g., the PO group which is characteristic of some insecticides and nerve gas agents). This may be accomplished by use of a technique involving dissociation of the parent molecule by a high energy beam of electrons (as in the case of routine mass spectroscopy) or photons. If more than one photon is required in order to achieve photodissociation some specificity may be associated with resonant enhancement of multiphoton processes. Once again, additional complexity will be introduced if separate sources are required for excitation and detection. This may be avoided if, for example, one high energy, high intensity laser such as ArF not only photodissociates the parent molecule but also pumps the photofragment to an electronically excited state which then emits at a characteristic wavelength.³⁸ Such fragmentation patterns may then serve as markers of contaminants containing specific subgroups.

Derivatization provides an alternative method for subgroup identification in analytical chemistry. Here one takes advantage of a chemical reaction involving all molecules containing a specific functional moiety (e. g., ketones, aldehydes, phosphates, etc.) and some reagent to yield a product with known spectroscopic properties. Examples of such methods abound in organic qualitative

analysis; the reaction of phenylhydrazine with organic unknowns to produce brightly colored hydrazone derivatives was, prior to the development of routine NMR and mass spectral analysis, a high point of undergraduate chemistry laboratories. More recently, chemists have reacted non-volatile materials with silanes to yield derivatives with sufficiently high vapor pressure to permit gas chromatographic analysis at relatively low temperatures.⁶⁵ Clever application of known chemical reaction mechanisms may lead to the development of derivatization methods in which contaminants of a particular type might, for example, undergo reaction with specific reagents to yield highly fluorescent, easily detected products. Whether such techniques could be applied to real-time characterization of trace materials remains an open question.

3.1 Absorption spectroscopy

Because of its directness, absorption spectroscopy has been extensively applied to the detection of trace species in the atmosphere. Measurements can be carried out directly in the atmosphere (thereby yielding an integrated path intensity) or in a long pathlength multiple reflection cell. An active retroreflector offers the best efficiency in terms of intensity, but it must be physically placed at some remote site. Passive reflection from topographic features (e. g., a hill side or tree) or the atmospheric aerosol (Mie scattering) offers true remote operation and the capacity for obtaining range information, but at the cost of lower sensitivity and potentially significant performance variability.

Because only few molecules display sharp, easily identifiable electronic absorption spectra (SO_2 , NO_2 , and the aromatic hydrocarbons being notable examples) detection of characteristic absorptions is usually carried out

in the infrared. The diode laser is an especially useful source of tunable radiation for such measurements; it is easily tunable over narrow frequency ranges and so may be conveniently configured for derivative spectroscopy. Because intensity requirements are not especially stringent in experiments involving detection of actively reflected probe beams, low power sources are acceptable.

Several systems have been described which detect trace gases in the atmosphere using absorption techniques. A variety of minor atmospheric constituents including SO_2 , O_3 , N_2O , NH_3 , and PAN were detected; absorptions as weak as 10^{-7} m^{-1} could be observed.⁶⁶ Both CO and SO_2 have been detected in a long pathlength White cell with a limit of 0.1 ppb for SO_2 and 0.3 ppt for CO.⁶⁷ Another important atmospheric contaminant is H_2SO_4 ; it is present in the plume of fossil fuel-fired power plants and contributes to acid precipitation. A tunable diode-based spectrometer using active retroreflectors has been used to monitor such emissions.⁶⁸ Because absorption at 880 cm^{-1} is a factor of 9 stronger than at 962 cm^{-1} , a differential method was developed to minimize interference by ambient CO_2 and H_2O . The detection sensitivity of this spectrometer for H_2SO_4 was reported as 1 ppb-m.

Molecular lasers such as CO and CO_2 , which can provide output on a variety of vibrotational transitions, have also been used as source probes for trace constituent monitoring. In principle, it is possible to analyze a mixture of N substances for which the absorption cross sections are known at N different wavelengths by measuring the total absorption at these wavelengths. In practice, this is rarely the case because even minor background absorption by unknown materials or the slightest experimental error makes the inversion from absorption to density for weak absorbers essentially impossible. However, limited studies

of this type have been carried out and it has been possible to detect O_3 , N_2O , CO , and CH_4 in this manner.⁶⁹ Complex mixtures have been resolved through the use of a carefully stabilized CO_2 laser.^{70,71} A particularly elegant approach to infrared absorption measurements may be applied to molecules possessing a permanent dipole moment. Modulated Stark spectral shifting of the absorption spectrum has permitted the detection of vinyl chloride in the presence of other major and minor atmospheric constituents.⁷²

The optoacoustic effect has been exploited for the field detection of trace constituents. Some time ago, Patel utilized a spin-flip Raman source for detection of NO by optoacoustic techniques.^{73,74} That this is a viable detection method for field applications was amply demonstrated by measurements of stratospheric NO using a balloon-borne apparatus. Other studies have involved the use of discrete-frequency lasers. For example CO/CO_2 laser-based optoacoustic spectroscopy in the infrared has permitted the detection of such materials as isotopically substituted water and phosgene, the detection limit for the latter having been estimated as 0.1 ppm.⁷⁵ Very recent optoacoustic studies using a CO_2 laser have permitted the detection of the nerve gas GB with an estimated limit of 10 ppb.⁷⁶ Further exploitation of the optoacoustic technique will no doubt result from the continued development of the laser diode, especially when constructed in switchable arrays.¹¹ The combination of such a broadly and easily tuned source with the data acquisition speed and 'intelligence' of an integrated microcomputer system could make this an exceptionally attractive technique for field measurements. Indeed, it would be possible through the use of two-way fiber optic communication to utilize one laser source with a network of remote sensors to provide area coverage that would normally not be available with a single spectrometer.

Differential Absorption Lidar (DIAL) measurements of trace components in the atmosphere were first described in the mid 1960's and early 1970's.⁷⁷ Basically, DIAL makes use of a co-located pulsed laser probe and receiver/telescope arrangement with which the backscattering of the laser pulse from particles and molecules may be determined with adequate temporal resolution to permit range information to be obtained. By utilizing a laser which can be operated both on and off of a molecular resonance and measuring the temporal profiles of the backscattered beam, absorption profiles can be inferred. This, in turn, yields the density distribution of trace molecules in, for example, a plume or cloud. With the notable exception of H_2O , DIAL does not, in general, have sufficient sensitivity to monitor ambient concentrations of trace constituents in the unpolluted troposphere.

An impressive variety of molecular species have been detected using DIAL (see Table 2 for a listing of field studies). Most measurements made to date have involved detection of enhanced concentrations in tanks or plumes, or along roadways. Among the species monitored in this way were O_3 , SO_2 , NO_2 , C_2H_4 , CH_4 , and HCl . Mobile apparatus mounted in vans or on aircraft are currently being developed and actively tested. One of the most elegant studies reported to date involved resolution of NO_2 in the atmosphere above a large industrial city; detection of NO_2 to a level of 0.4 ppm was accomplished by monitoring the Mie scattered return of a tunable dye laser pulse.^{78,79} A point source of NO_2 emission (a chemical factory) could be discerned in this study.

Sensitive detection of SO_2 (25 ppb) and NO_2 (above a 2 ppb background) in a power plant plume has also been demonstrated, with a range of 2 km being achieved for the SO_2 using a frequency-doubled dye laser source.⁸⁰ Infrared

Table 2. Selected DIAL measurements of trace species under field conditions.
 [Source: E. V. Browell, Topical Meeting on Optical Techniques
 for Remote Probing of the Atmosphere, Incline Village, NV (January,
 1983) Paper TuB2-1.]

Gas	Wavelength Region (nm)	Test System	Reference
O ₃	9500	Aircraft	Appl. Opt., 20, 545 (1981)
	290	Mobile*	Monterey Rem. Sense. Workshop
	290	Aircraft*	Appl. Opt., 22, 522 (1983)
SO ₂	300	Mobile*	Appl. Opt., 18, 2998 (1979)
	300	Mobile	Appl. Opt., 22, 522 (1983)
	300	Mobile*	Monterey Rem. Sense. Workshop
NO ₂	460	Mobile*	Appl. Phys., 3, 115 (1974)
	440	Mobile*	Appl. Phys., 4, 181 (1974)
			Appl. Opt., 18, 2998 (1979)
C ₂ H ₄	10000	Mobile*	Monterey Rem. Sense. Workshop
SF ₆	10000	Aircraft	Monterey Rem. Sense. Workshop

* Range resolved

Note: 'Monterey Rem. Sense. Workshop' refers to the Proceedings of
 the Workshop on Optical and Laser Remote Sensing, Monterey,
 CA (February 1982).

DIAL measurements of HCl, CH₄, and N₂O using a DF laser have been reported with detection sensitivities better than 1 ppm.⁸¹ Recent publications have dealt with the remote sensing of hydrazine derivatives using a CO₂ laser source⁸² as well as an airborne DIAL system for the measurement of O₃ and aerosol profiles.⁸³ A tunable optical parametric oscillator has been used as a source for DIAL measurements of CO and SO₂.^{84,85}

While DIAL appears to be an exceptionally sensitive remote probe of atmospheric composition, it does not seem to have been tested under a variety of meteorological conditions. Because of the nature of the technique, it would appear that such considerations would greatly affect its operation, as would the position of the sun relative to the laser/telescope location. Whether such constraints are of significance in a particular application is problematical.

3.2 Fluorescence spectroscopy

Laser-induced fluorescence detection of atmospheric constituents present in trace quantities is, in general, limited to efficient emitters with short (less than 100 nsec) optical lifetimes. Typically, LIF becomes more practical at higher altitudes where the mean collision rate between excited species and ambient quenchers is slow with respect to that of spontaneous emission. Remote LIDAR sensing from the ground by LIF of sodium and potassium atoms in the mesosphere has been reported^{86,87} and the association between these species and meteoric sources established.

Because of its crucial importance to the chemistry of the troposphere, the OH radical has been the subject of intense interest. Several groups have detected OH at atmospheric pressure using LIF in the middle ultraviolet-

let.^{38,89} Considerable controversy still surrounds these measurements because quantitative analysis requires that multiple sources of interference be properly accounted for.^{90,91} These include photochemical production of OH as the result of ambient O₃ photolysis by the probe laser followed by reaction of the product electronically excited oxygen atoms with H₂O during the lifetime of the laser pulse, as well as aerosol scattering by particles in the probe volume. The use of picosecond lasers or exceptionally large excitation volumes would significantly reduce some of these problems, but others remain. Recently, XeCl excimer lasers which can be tuned to an intense OH absorption at 308 nm have been developed to carry out LIDAR measurements of hydroxyl radicals in the upper atmosphere.⁶ While it has been suggested that the nominal LIF detection limit for OH is on the order of 10^6 cm^{-3} , this, too, is in some doubt.

Another, far less specific fluorescence field probe of atmospheric composition is initiated by the breakdown of an air sample using the focused output of a high-power Nd/YAG laser. Emission arising from trace constituents can indeed be observed; the detection of diisopropylmethyl phosphonate by monitoring of the P I and P II emission lines in a laser-induced plasma can be accomplished in the laboratory with a detection limit of 15 ppm.³⁹ Chlorine-containing materials can be detected at 60 ppm. This technique offers several apparent advantages including generality and respectable sensitivity. Because this is, in effect, discharge excitation, problems long associated with such analytical methods arise here, too. These include matrix effects (the system response to a particular analyte depends on the associated concentration of other species such as H₂O) and irreproducibility in spark generation associated with temporal and spatial variations in the laser beam output. Special problems

will arise if particulate matter is present as the result of beam wandering and movement. The practicality of laser-induced spark emission spectroscopy in the field remains to be proven.

3.3 Photoionization spectroscopy

Because photoionization spectroscopy using laser sources has only recently been developed, its application to systems at atmospheric pressure has been minimal to date. It now seems clear, however, that resonance enhanced MPI techniques present significant advantages when compared to other detection schemes such as LIF. At easily attained laser powers, collisional deactivation of most real (and certainly all virtual) intermediate states does not compete effectively with absorption of further photons which result in ionization. Thus, at high pressures, no significant decrease in observed ionization is expected. The application of MPI to detection of trace species in the atmosphere is limited to field measurements, remote determinations being made impossible by the need to achieve sufficiently high laser fluxes and to sample ion formation at the test site.

The reported applications of MPI to systems at atmospheric pressure have involved flames. In particular, NO has been observed in an ordinary Bunsen burner flame using two-photon enhanced, three-photon ionization.⁹² This experiment is, of course, facilitated by the relatively low ionization potential and large cross-section characteristic of the nitric oxide molecule.⁴⁴ Nonetheless, it was possible to utilize the observed vibrational population distribution of NO to estimate the temperature in the oxidative region of the flame. Recently, observation of atomic oxygen in flames has been reported.⁹³ This two-photon resonant, three-photon ionization process required excitation

of the $3^3P_J \leftarrow 3^2P_{0,1,2}$ two-photon allowed transition at ca. 226 nm. In a related study, this two-photon resonant multiphoton ionization has been used to monitor the distribution of spin-orbit levels in $O(2^3P_J)$ following photodissociation of O_3 in the Hartley band continuum near 226 nm.⁹⁴ Such tunable far UV radiation is now routinely available through the use of nonlinear frequency doubling and mixing techniques. In principle, it would be possible to estimate both the density of atomic oxygen and its electronic temperature, the latter through measurement of the relative population of the easily resolved J levels of the 2^3P state. It would appear that this technique may be significantly more sensitive at atmospheric pressure than the two-photon induced LIF measurements which are strongly affected by collisional quenching of the electronically excited 3^3P_J state.³⁶

A wide selection of gases have been detected using MPI.⁴⁵ These include the aforementioned NO and O as well as such simple molecules as N_2 , O_2 , and NO_2 , all of considerable atmospheric importance, aromatics such as benzene, toluene, and naphthalene, and even much larger molecules such as the porphyrins.⁹⁵ Because the primary thrust of the experimental studies making use of MPI techniques has been the elucidation of molecular dynamics, much emphasis has been placed on the detection of subject molecules in defined quantum states. The enormous sensitivity of laser ionization techniques (single-atom detection has been demonstrated⁹⁶) makes state-resolved detection of even these large molecules feasible.

Finally, the MPI technique has further been exploited in the detection of electronically excited, optically metastable species including $CO(A^3\Pi)$ ⁹⁷ and $O_2(a^1\Delta)$.⁹⁸ These have been observed following laser photolysis of source molecules and in a flowing discharge afterglow. Once again, the resolution

afforded by the use of a narrow bandwidth excitation source when taken in conjunction with the application of mass discrimination of ionization products make MPI an extraordinarily sensitive, highly selective method for detection of trace species under a wide range of experimental conditions. The application of this technique to the field characterization of complex materials in the atmosphere awaits further development.

3.4 Raman Spectroscopy

The application of Raman spectroscopy to atmospheric sensing has long been attractive for several reasons. Firstly, because the inelastic frequency shift associated with Raman scattering does not depend upon the wavelength of the excitation source (although the cross-section certainly does), a single laser can be utilized to probe all molecules being studied, a single spectral scan yielding quantitative information on the density of each molecule relative to N_2 . Secondly, both the inherent narrow Raman linewidth and short temporal profile permit discrimination against spontaneous fluorescence, blackbody background radiation and elastic scattering processes. Finally, excellent spatial resolution can be obtained through the use of the common LIDAR configuration for detection of backscatter intensity. As noted earlier, the main (and often compelling) disadvantage of Raman spectroscopy which limits its application to trace detection of atmospheric materials is the low cross-section combined with the overlap of O- and S-branch Raman scattering by the major atmospheric constituents, N_2 , O_2 , H_2O , and CO_2 .

Early applications of Raman spectroscopy to atmospheric problems involved measurement of major components. Thus, studies of the O_2/N_2 ratio were suggested as early as 1970,⁹⁹ and direct measurement of the rotational population dis-

tribution characterizing N_2 (and hence its temperature) by observation of the pure rotational Raman scattering of this molecule was reported in 1975.¹⁰⁰ Unfortunately, this measurement is rather insensitive to the temperature and extraordinary measures must be taken to minimize interference by the elastically scattered return signal. Raman techniques are still actively being exploited for the remote sensing of atmospheric properties such as temperature, major constituent composition, humidity, etc.

Somewhat more problematical are applications of Raman spectroscopy to the detection of trace species in the atmosphere. The low cross-section and major constituent interferences noted earlier mitigate against routine detection of contaminant species. Thus, it has proved possible to sense SO_2 and kerosene in a controlled plume at a range of 200 m by detecting the Raman backscatter of a 2 J Ruby laser pulse using a 1 m, f6.8 telescope.¹⁰¹ Other measurements of SO_2 in power plant plumes have been reported with sensitivities down to 100 ppm at ranges to 200 m.¹⁰² Inspection of the results obtained to date suggests that routine remote detection of contaminants by Raman spectroscopy much below the 1% level is not especially promising, especially when compared to the already available DIAL and fluorescence LIDAR methods. Recently, development of remote sensing capabilities has certainly emphasized these latter techniques.

Field determination of trace species in the atmosphere by Raman spectroscopy offers many of the advantages outlined above while avoiding the sensitivity problems that become so acute in remote sensing. For example, detection of trace CH_4 in room air has been demonstrated at levels of 2-4 ppm (signal to noise ratio: 20/1) using spontaneous Raman scattering of uv KrF excimer laser pulses at 248 nm.¹⁰³ Remote detection of inelastic backscatter at

these short wavelengths cannot be accomplished because of interferences by elastic scattering and ozone absorption. CARS measurements in flames are now a well-recognized technique for characterization of composition and temperature.⁶² Whether CARS, which is experimentally quite complex, involving the use of two lasers, polarization optics, and synchronously scanned detectors (or a multichannel analyzer), will be applied to atmospheric measurements is still open to question. Workers at LASL have utilized time-resolved CARS to detect O_2 in its $^3\Sigma$ and $^1\Delta$ states following O_3 photolysis in the ultraviolet and visible regions.¹⁰⁴ The state-resolved spectra which are obtained reveal considerable information concerning the photodissociation dynamics of this atmospherically critical triatomic. Inspection of the experimental results suggests that good spectra can be obtained at pressures near 1 torr, with the detection limit for O_2 being perhaps on the order of 10 ppm, although in these experiments, the composition of the test gas is quite simple and tightly controlled. Clearly, Raman spectroscopic methods with their generality and specificity are potentially useful for atmospheric characterization, although sensitivity constraints probably limit their application to plumes and other regions of relatively high concentration.

4. Concluding remarks

There can be little doubt that laser-based spectroscopic probes of atmospheric composition have become valuable tools of no small practical importance to chemists, physicists, and engineers. To what extent any of these tools can be applied to a specific task depends upon the associated requirements for selectivity, sensitivity, etc. Great effort is currently being expended on the refinement of DIAL and LIDAR which are capable of remote sensing of trace species. To what extent (and in what roles) should alternative contaminant monitoring schemes be similarly developed?

4.1 Operational Characteristics

Having reviewed the fundamental physics and atmospheric applications of a variety of spectroscopic techniques for trace contaminant detection, it would be useful to assess the performance of these methods (Table 3) with regard to the criteria presented for the 'ideal' detector in section 1.3:

Sensitivity With the notable exception of Raman techniques all of the spectroscopic tools discussed here seem quite capable of trace detection at or below the ppm level. Absorption (including DIAL and optoacoustic spectroscopy), LIDAR, and photoionization methods are all especially sensitive, the last being, at least in principle, capable of single atom/molecule detection. The practical limit for Raman detection is at least two orders of magnitude higher than that of these other techniques.

Selectivity In general, infrared spectroscopy throughout the fingerprint region offers far greater promise of specific detection of trace contaminants in complex mixtures, when compared to ultraviolet spectra which are generally relatively broad. Notable exceptions have been studied, including

Table 3. Summary of detection system capabilities with regard to 'ideal' detection system described in Section 1.3.

Method	Sensitivity	Selectivity	Dynamic range	Generality	Directionality	Real time response	Convenience
DIAL (ir)	+	+	7	+	++	++	7
DIAL (uv)	++	0	7	+	++	++	7
LIDAR	++	+	+	+	++	++	7
Optoacoustic	++	++	++	+	0	0	+
Fluorescence (rotational cooling)	++	++	0	+	+	+	0
laser excited plasma	+	+	7	+	+	+	+
Photoionization	++	++	+	+	+	0	+
Optogalvanic	+	7	7	+	0	+	0
Raman	+	+	+	+	++	++	+

Estimates of performance characteristics

- ++ Especially good
- +
- 0 Desirable
- 0 Neutral
- Undesirable
- 7 Unknown

SO₂, NO₂, and O₃. Large molecules are especially difficult to characterize unless their spectrum includes a strong feature not present in the ambient background. Rotational cooling and synchronous detection schemes provide real promise for the simplification of large molecule LIF spectra if the added experimental complexity is not of overriding concern. DIAL measurements in the infrared are complicated by the need to obtain a comparison signal off of absorption resonance. While this may be possible to provide under ideal conditions, no sufficiently high power source of broadly tunable infrared radiation is available (with the possible exception of high pressure CO₂ lasers) to make such schemes routine. Detection of specific trace contaminants in complex mixtures by Raman spectroscopy seems feasible, if strong features (and relatively high concentrations) are present. Because of the two-dimensional nature of laser photoionization spectroscopy with mass selective detection, this technique is potentially highly selective even in quite complex mixtures. The support of further efforts to establish performance criteria for system selectivity under realistic conditions seems most justified.

Dynamic range The dynamic range of absorption and Raman techniques seems excellent, being on the order of at least 10⁵. All fluorescence methods can be prone to self-trapping of radiation at sufficiently high concentrations. Photoionization methods should display a relatively good dynamic range, although as-yet unexplored space charge and detector saturation effects may play a role at high concentrations.

Generality As noted in the body of this report, Raman spectra may be obtained for virtually all molecules using a single laser frequency. This cannot be said of any other technique. Absorption spectra in the

infrared are generally quite characteristic of at least a generic type of molecule making optoacoustic and DIAL methods relatively straightforward. Fluorescence spectroscopy is much more limited as only relatively few molecules possess electronically excited states with high emission quantum yields (i. e., states which do not undergo radiationless processes to yield the ground state) and lifetimes sufficiently short not to undergo collisional quenching by major atmospheric constituents.

Directionality Only LIDAR, DIAL, and Raman methods yield range and azimuthal information. Other techniques can provide such data only to the extent to which multiple sensors can be conveniently deployed in the field. Because of problems associated with the generation of overlapping Raman spectra of major constituents, the range of this technique is probably somewhat limited.

Real-time response Sampling methods limit the real-time response of all local, field techniques because some provision must be made to introduce the analyte into the detection apparatus. This would certainly be of concern if a long pathlength cell of high internal volume were used for an absorption measurement. Small dead volume sampling schemes can be devised, however, and neither optoacoustic spectroscopy nor rotational cooling methods require that large samples be rapidly taken. All remote methods provide essentially instantaneous sampling of the environment.

Convenience By their nature, all remote sensing techniques for trace contamination require considerable experimental complexity and sophistication. Whether it will be possible to make such methods routinely available to non-researchers is not yet obvious. Local methods seem to offer greater promise for routine application by non-experts, with

the possible development of integrated laser source, sample chamber, and detection electronics packages for optoacoustic methods using tunable diode lasers seeming quite exciting. Local field measurements of atmospheric composition have long been carried out using more conventional methods and similar approaches to laser-based techniques seems quite feasible.

This clearly represents only a cursory overview of laser-based techniques for trace contaminant characterization, but the observations made concerning specific attributes of these methods are based on reported (and to some extent inferred) limitations of each type of measurement. None can presently be considered a truly 'universal' approach.

4.2 Programmatic considerations

The results obtained to date are impressive, but it is not clear to what extent a balanced development program is currently under way. Thus, while remote sensing techniques offer the most spectacular promise under ideal circumstances, their utility for all applications under wide-ranging meteorological conditions has not been demonstrated, at least in the open literature. Proven field techniques such as optoacoustic spectroscopy which have already been demonstrated in atmospheric sensing applications and for which the development of low power, tunable laser diode sources would represent a major boon, should be further explored. Microminiaturization of laser/sensor modules would make their installation over a wide range of remote sites relatively straightforward and cost effective.¹⁰⁵ Similarly, the still developing method of multiphoton photoionization spectroscopy should be carefully monitored and atmospheric applications encouraged. Here, too, is a technique with great sensitivity and specificity, which, when viewed in the light of its

inherent simplicity, may well be most attractive for atmospheric detection of contaminant species.

Because so many competitive techniques have been developed for use in contaminant monitoring, it now seems appropriate for comparative studies of detection sensitivity and specificity to be undertaken. To date no such tests have been reported. Of special importance will be the evaluation of different methods under conditions which are less than ideal. No laser-based method for trace analysis in the atmosphere is currently used routinely in any but research environments. As noted elsewhere in this document, some applications critically require continuous operation under all meteorological and environmental conditions. Which (if any) of the laser-based techniques developed to date admit of such strenuous requirements?

Not previously discussed in this document are the problems of data reduction and decision making based on the flood of information made available by these extraordinary spectroscopic techniques. This problem will be greatly exacerbated under conditions where rapid, real-time decisions must be reached based on spectroscopic data. How will such decisions be made? What rate of 'false alarms' is acceptable? What rate of misidentifications can be tolerated? To what extent is the extraordinary sensitivity of a particular technique offset by its response selectivity? Clearly, each application has associated with it a unique set of answers to these questions. Under circumstances in which action must quickly be taken, some sort of decision support system must be devised to carry out the necessary data analysis. Further development of 'expert systems' for spectral analysis seems clearly warranted, for the interpretation of massive data streams that may ultimately limit the application of laser-based detection techniques to real-time problems.

Bibliography

1. N. Omenetto and J. D. Winefordner, *CRC Crit. Rev. Anal. Chem.*, **13**, 59 (1981).
2. Analytical Laser Spectroscopy, Ed. N. Omenetto, Wiley: New York (1979).
3. Optical and Remote Sensing, Ed. D. K. Killinger and A. Mooradian, Springer-Verlag: Berlin (1983).
4. R. M. Measures, in Reference 2, p. 295.
5. J. A. Logan, M. J. Prather, S. C. Wofsy, and M. B. McElroy, *J. Geophys. Res.*, **86**, 7210 (1981).
6. J. B. Landenslager, I. S. McDermid, and Th. J. Pacala, in Reference 3, p.236.
7. R. L. Byer, T. Kane, J. Eggleston, and S. Y. Long, in Reference 3, p. 245.
8. A. Mooradian, P. F. Moulton, and N. Menyuk, in Reference 3, p. 257.
9. T. Srinivasan, H. Egger, T. S. Luk, H. Pummer, and C. K. Rhodes, in Reference 3, p. 269.
10. R. S. Eng, J. F. Butler, and K. J. Linden, *Opt. Eng.*, **19**, 945 (1980).
11. E. Garmire, LaJolla Institute Report LJI-R-82-217 (1982).
12. F. L. J. Sixma and H. Wynberg, A Manual of Physical Methods in Organic Chemistry, Wiley: New York (1964) p. 48.
13. V. S. Antonov and V. S. Letokhov, *Appl. Phys.*, **24**, 89 (1981).
14. First described by A. G. Bell, *Proc. Am. Assoc. Adv. Sci.*, **29**, 115 (1880).
15. C. K. N. Patel, *Science*, **202**, 157 (1978).
16. E. D. Hinkley, R. T. Ku, and P. L. Kelley, in Laser Monitoring of the Atmosphere, Ed. E. D. Hinkley, Springer-Verlag:New York (1976) p. 238.
17. N. C. Peterson, M. J. Kurylo, W. Braun, A. M. Bass, and R. A. Keller, *J. Opt. Soc. Amer.*, **61**, 746 (1971).
18. G. O. Brink, *Opt. Commun.*, **12**, 123 (1980).
19. C. K. N. Patel, *Phy. Rev. Lett.*, **28**, 649 (1972).
20. C. F. Dewey, Jr., *Opt. Eng.*, **13**, 483 (1974).

21. P. O. F. Helander, Linköping Studies in Science and Technology, 90, Linköping University (1983).
22. C. K. N. Patel and R. J. Kerl, Appl. Phys. Lett., 30, 578 (1977).
23. N. Omenetto and J. D. Winefordner in Reference 2, p. 167.
24. S. Mayo, R. A. Keller, J. C. Travis, and R. B. Green, J. Appl. Phys., 47, 4012 (1976).
25. J. A. Gelbwachs, C.F. Klein, and J.E. Wessel, IEEE J. Quantum. Electron. 13, No. 9, 11D (1977).
26. M. S. Epstein, S. Bayer, J. Bradshaw, E. Voightman, and J. D. Winefordner, Spectrochim. Acta, 35B, 233 (1980).
27. C. Th. J. Alkemade, Appl. Spectrosc., 35, 1 (1981).
28. For a review of early work, see Zare and Dagdigian, Science, 185, 739 (1974).
29. Laser Probes for Combustion Chemistry, Ed. D. R. Crosley, ACS Ser. 134 (1980).
30. J. P. Byrne and I. G. Ross, Aust. J. Chem., 24, 1107 (1971).
31. J. M. Hayes and G. J. Small, Anal. Chem., 55, 565A (1983).
32. J. C. Brown, J. A. Duncanson, and G. J. Small, Anal. Chem., 52, 1711 (1980).
33. D. H. Levy, Ann. Rev. Phys. Chem., 31, 197 (1980).
34. J. C. Brown, M. C. Edelson, and G. J. Small, Anal. Chem., 50, 1394 (1978).
35. R. E. Russo and G. M. Hieftje, Anal. Chim. Acta, 134, 13 (1982).
36. W. K. Bischel, B. E. Perry, and D. R. Crosley, Appl. Opt., 21, 1419 (1982).
37. W. Heaven, T. A. Miller, R. R. Freeman, J. C. White, and J. Bokor, Chem. Phys. Lett., 86, 458 (1982).
38. M. O. Rodgers, K. Asai, and D. D. Davis, Appl. Opt., 19, 3597 (1980).
39. T. R. Loree and L. J. Radziemski, Plasma Chem. Plasma Process., 1, 271 (1981).
40. L. J. Radziemski and T. R. Loree, Plasma Chem. Plasma Process., 1, 281 (1981).

41. C. A. McDowell in Mass Spectrometry, C. A. McDowell, Ed., McGraw Hill: New York (1963) p. 506.
42. R. Wallenstein, *Opt. Comm.*, **33**, 119 (1980).
43. S. V. Andreev, V. S. Antonov, I. N. Knyazev, and V. S. Letokhov, *Chem. Phys. Lett.*, **45**, 166 (1977).
44. M. Asscher, W. L. Guthrie, T.-H. Lin and G. A. Samorjai, *Phys. Rev. Lett.*, **49**, 76 (1982).
45. P. M. Johnson and C. E. Otis, *Ann. Rev. Phys. Chem.*, **32**, 139 (1981).
46. G. J. Fisanick, T. S. Eichelberger, B. A. Heath, and M. B. Robin, *J. Chem. Phys.*, **72**, 5571 (1980).
47. U. Boesl, H. J. Neusser, and E. W. Schlag, *J. Chem. Phys.*, **72**, 4327 (1980).
48. J. P. Reilly and K. L. Kompa, *J. Chem. Phys.*, **73**, 5468 (1980).
49. K. C. Smyth and W. G. Mallard, *J. Chem. Phys.*, **77**, 1779 (1982).
50. R. V. Ambartzumian and V.S. Letokhov, *Appl. Opt.*, **11**, 354 (1972).
51. C. R. Webster and C. T. Rettner, *Laser Focus*, **19**, 41 (Feb. 1983).
52. J. C. Travis, P. K. Schenck, G. C. Turk, and W. G. Mallard, *Anal. Chem.*, **51**, 1516 (1979).
53. G. C. Turk, J. C. Travis, J. R. DeVoe, and T. C. O'Haver, *Anal. Chem.*, **51**, 1890 (1979).
54. C. T. Rettner, C. R. Webster and R. N. Zare, *J. Phys. Chem.*, **85**, 1105 (1981).
55. R. Vasudev and R. N. Zare, *Bull. Am. Phys. Soc.* (Jan. 1982).
56. B. G. Schuster, *Opt. Quant. Electron.*, **7**, 215 (1975).
57. M. C. Tobin, Laser Raman Spectroscopy, Wiley: New York (1971).
58. J. M. Harris, R.W. Chrisman, F. E. Lytle, and R. S. Tobias, *Anal. Chem.*, **48**, 1937 (1976).
59. J. J. Barrett, in Laser Raman Gas Diagnostics, Ed. M. Lapp and C. M. Penney, Plenum: New York (1974) p. 191.
60. W. M. H. Smith, *Opto-Electronics*, **4**, 161 (1972).
61. J. W. Nibler and G. V. Knighten in Raman Spectroscopy of Gases and Liquids,

- Ed. A. Webber, Springer-Verlag: Berlin (1979).
62. R. J. Hall and A. C. Eckbreth, *Opt. Eng.*, **20**, 494 (1981).
 63. A. C. Eckbreth and R. J. Hall, *Combust. Sci. Tech.*, **25**, 175 (1981).
 64. W. B. Roh, P. W. Schreiber, and J. P. E. Taran, *Appl. Phys. Lett.*, **29**, 174 (1976).
 65. J. S. Fritz and G. H. Schenck, Jr., Quantitative Analytical Chemistry, 3rd Ed., Allyn and Bacon: Boston (1974) p. 396.
 66. J. Reid, M. J. Shewchun, B. K. Garside, and E. A. Ballik, *Appl. Opt.*, **17**, 300 (1978).
 67. J. Reid, M. J. Shewchun, B. K. Garside, and E. A. Ballik, *Opt. Eng.*, **17**, 56 (1978).
 68. R. S. Eng, A. W. Mantz, and T. R. Todd, *Appl. Opt.*, **18**, 3438 (1979).
 69. B. M. Golden and E. S. Yeung, *Anal. Chem.*, **47**, 2132 (1975).
 70. B. D. Green and J. I. Steinfeld, *Appl. Opt.*, **15**, 1688 (1976).
 71. B. D. Green and J. I. Steinfeld, *Environ. Sci. Technol.*, **10**, 1134 (1976).
 72. D. M. Sweger and J. C. Travis, *Appl. Spectrosc.*, **33**, 46 (1979).
 73. C. K. N. Patel, E. G. Burkhardt, and C. A. Lambert, *Science*, **184**, 1173 (1974).
 74. E. G. Burkhardt, C. A. Lambert, and C. K. N. Patel, *Science*, **183**, 1111 (1975).
 75. W. Schnell and G. Fisher, *Opt. Lett.*, **2**, 67 (1978).
 76. G. P. Quigley, L. J. Radziemski, R. K. Sander, and A. Hartford, Jr., LANL Report LA-UR-81-3364 (1981).
 77. For early work see R. T. H. Collins and P. B. Russell, in Laser Monitoring of the Atmosphere, Ed. E. D. Hinckley, Springer-Verlag: New York (1976) p. 71.
 78. K. W. Roth, U. Brinkmann, and H. Walther, *Appl. Phys.*, **3**, 115 (1974).
 79. K. W. Roth, U. Brinkmann, and H. Walther, *Appl. Phys.*, **4**, 181 (1974).
 80. K. Fredriksson, B. Galle, K. Nystrom, and S. Svanberg, *Appl. Opt.*, **18**, 2998 (1979).
 81. E. R. Murray, J. E. Van der Laan, and J. G. Hawley, *Appl. Opt.*, **15**, 3140

(1976).

82. N. Menyuk, D. K. Killinger, and W. E. DeFeo, *Appl. Opt.*, **21**, 2275 (1982).
83. E. V. Browell, A. F. Carter, S. T. Shipley, R. J. Allen, C. F. Butler, M. N. Mayo, J. H. Siviter, Jr., and W. M. Hall, *Appl. Opt.*, **22**, 522 (1983).
84. T. Hennigsen, M. Garbuny, and R. L. Byer, *Appl. Phys.*, **24**, 242 (1974).
85. R. A. Baumgartner and R. L. Byer, *Opt. Lett.*, **2**, 163 (1978).
86. R. D. Hake, Jr., D. E. Arnold, D. W. Jackson, W. E. Evans, R. A. Long, and R. B. Ficklin, *J. Geophys. Res.*, **77**, 6839 (1972).
87. F. Felix, W. Keenlside, G. Kent, and M. C. W. Stanford, *Nature*, **246**, 345 (1973).
88. D. D. Davis, W. S. Heaps, D. Philen, M. Rodgers, T. McGee, A. Nelson, and A. J. Moriarty, *Rev. Sci. Instrum.*, **50**, 1505 (1979).
89. C. C. Wang, L. I. Davis, Jr., and P. M. Selzer, *J. Geophys. Res.*, **86**, 1181 (1981).
90. T. M. Hard, R. J. O'Brien, and T. B. Cook, *J. Appl. Phys.*, **51**, 3459 (1980).
91. G. Ortgies, K.H. Gericke, and F. J. Comes, *Z. Naturforsch.*, **36a**, 177 (1981).
92. B. H. Rockney, T. A. Cool, and E. R. Grant, *Chem. Phys. Lett.*, **87**, 141 (1982).
93. J. E. M. Goldsmith, *J. Chem. Phys.*, **78**, 1610 (1983).
94. G. D. Greenblatt, A. R. Sivaram, and J. R. Wiesenfeld, work in progress.
95. S. E. Luetwyler, U. Even and J. Jortner, *Chem. Phys. Lett.*, **86**, 439 (1982).
96. G. S. Hurst, M. G. Payne, S. D. Kramer, and J. P. Young, *Rev. Mod. Phys.*, **51**, 767 (1979).
97. R. L. Whetten, K.-J. Fu, and E. R. Grant, personal communication.
98. P. L. Houston, W. Marinelli, A. R. Sivaram, and J. R. Wiesenfeld, work in progress.
99. R. L. Schwiesow and V. E. Derr, *J. Geophys. Res.*, **75**, 1629 (1970).
100. J. Cooney, *Appl. Opt.*, **14**, 270 (1975).

101. T. Hirschfeld, E. R. Schildkraut, H. Tannenbaum, and D. Tannenbaum, Appl. Phys. Lett., 22, 38 (1973).
102. H. P. DeLong, Opt. Eng., 13, 5 (1974).
103. P. J. Hargis, Jr., SPIE, 286, 139 (1981).
104. J. J. Valentini, Chem. Phys. Lett., 96, 395 (1983).
105. See for example H. Inaba in Reference 3, p. 288 for a discussion of a fiber optic linked remote sensing scheme.